6-1-1994

Optimization of the heat pumping capacity of a thermoelectric heat pump

David A. Heavner

OPTIMIZATION OF THE HEAT PUMPING CAPACITY OF A THERMOELECTRIC HEAT PUMP

by

DAVID A. HEAVNER

A thesis submitted in partial fulfillment
of the requirements for the degree of
Master of Science in Mechanical Engineering

Approved by:

Prof. Shirish P. Mulay
(Thesis Advisor)

Prof. Robert Hefner

Prof. Satish Kandlikar

Prof. Charles Haines
(Department Head)

Department of Mechanical Engineering
College of Engineering
Rochester Institute of Technology
June, 1994

PERMISSION GRANTED:

I, David A. Heavner, hereby grant permission to the Wallace Memorial Library of the Rochester Institute of Technology to reproduce my thesis entitled "Optimization of the Heat Pumping Capacity of a Thermoelectric Heat Pump" in whole or in part. Any reproduction will not be for commercial use or profit.

June 22, 1994

David A. Heavner

PERMISSION GRANTED:

I, David A. Heavner, hereby grant permission to the Wallace Memorial Library of the Rochester Institute of Technology to reproduce my thesis entitled "Optimization of the Heat Pumping Capacity of a Thermoelectric Heat Pump" in whole or in part. Any reproduction will not be for commercial use or profit.

June 22, 1994

David A. Heavner

Abstract:

A steady state model of a thermoelectric heat pump fitted with pin fin heat exchange surfaces is developed from the equations governing the operation of a thermoelectric device and pressure drop/ heat transfer correlations for staggered tube banks in cross flow. The model computes current draw, heat pumped at the cold side, heat rejected at the hot side, hot and cold side exhaust temperatures, and hot and cold side pin base temperatures when given the following parameters: ambient temperature, thermoelectric geometry factor, number of thermocouple junctions, input voltage, pin diameter, pin height, transverse pin stagger, longitudinal pin stagger, contact resistance between the thermoelectric modules and the heat exchange surfaces, and fan performance curves for the hot and cold sides. Results of a FIDAP numerical model of a 4 row heated pin system are presented and compared to the heat transfer and pressure drop correlations chosen for use in the model. Nine tests were run with a working thermoelectric heat pump unit under various air flow and voltage input to collect data for the purpose of comparison with the model. Using empirically determined contact resistance values, the model predicted Q_C (heat pumped from the cold side) values that agreed with experiment within about 10%, Q_H (heat rejected from the hot side) values that agreed with experiment within about 5%, and current draw values that agreed with experiment within about 5%. Further examination of the contact resistance values suggested the presence of an undesirable air gap at the heat sink/thermoelectric module interface. The presence of this air gap was confirmed by examining the contact patterns left on pressure sensitive films that were placed between the thermoelectric modules and the heat sinks. An optimization exercise was performed with the model in an effort to maximize Q_C. Pin geometry was varied to achieve minimum values of heat sink thermal resistance for both the hot and cold side heat exchange surfaces. Using these minimized thermal resistance values, input voltage, thermoelectric geometry factor, and number of thermocouple junctions were varied to achieve maximum Q_C. Using the empirically determined thermal contact resistance values, a 29% increase in Q_C was achieved over the stock case. The model predicted a 79% improvement over the stock case when utilizing thermal contact resistance values corresponding to the elimination of the air gaps at the thermoelectric module/heat sink interfaces.

TABLE OF CONTENTS

Page

LIST OF TABLES

LIST OF FIGURES

Figure Page

Figure Page

Figure Page

Figure Page

LIST OF SYMBOLS

B_x x-component of fluid body force
B_y y-component of fluid body force
c_P heat capacity (J/kg-K)
D cylinder diameter (mm)
E electrical potential (volts)
f friction factor
$flow_{min}$ lower bound of volumetric flow rate being considered during present iteration of bisection method (CFM)
$flow_{max}$ lower bound of volumetric flow rate being considered during present iteration of bisection method (CFM)
$flow_{bar}$ average of $flow_{min}$ and $flow_{max}$ (CFM)
G geometry factor (area/length) of thermoelectric semiconductor element (m)
h convective heat transfer coefficient (W/m^2-K)
I electrical current (amperes)
I_{bar} average of I_{min} and I_{max} (amps)
I_{min} lower bound of current being considered during present iteration of bisection method (amps)
Imax upper bound of current being considered during present iteration of bisection method (amps)
k_{air} thermal conductivity of air (W/m-K)
k_{pin} thermal conductivity of pin (W/m-K)
K thermoelectric module thermal conductance (W/cm-K)
L length of pin in pin bank (mm)
M number of pins in a row of a pin fin base
N number of thermoelectric thermocouple junctions in heat pump assembly
N_r number of rows of pins on a pin fin base
Nu Nusselt number
ΔP pressure drop (inches of H_2O)
P_L nondimensional longitudinal stagger
Pr Prandtl number
Pr_w Prandtl number at cylinder wall
P_T nondimensional transverse stagger
P^* nondimensional pressure
Q_a heat rejected from a pin fin surface calculated via mass flow rate, heat capacity, and temperature drop (watts)
Q_b heat rejected from a pin fin surface calculated via log mean temperature difference method (watts)
$Q_{b,act}$ Q_b corrected for pin efficiency (watts)
Q_C heat flow into the thermoelectric cold side (watts)
Q_{Cbar} average of Q_{Cmin} and Q_{Cmax} (watts)
Q_{Cmin} lower bound of Q_C being considered during present iteration of bisection method (watts)

Q_{Cmax}	upper bound of Q_C being considered during present iteration of bisection method (watts)
Q_H	heat flow out of the thermoelectric hot side (watts)
q	heat flow (watts)
q''	heat flux (watts/m^2)
q''^*	nondimensional heat flux
q_τ	Thompson heat (watts/m)
R	electrical resistance (ohms)
R_{IC}	thermal contact resistance between cold side pin fin base and thermoelectric module (°C/W)
R_{IH}	thermal contact resistance between hot side pin fin base and thermoelectric module (°C/W)
R_{PC}	thermal resistance of cold side pin fin bank (°C/W)
R_{PH}	thermal resistance of hot side pin fin bank (°C/W)
$Re_{,D}$	Reynolds number with pin diameter as characteristic length
$R_{D,max}$	Reynolds number associated with the maximum velocity found in a pin fin array
R_{th}	thermal resistance (°C/W)
S_L	longitudinal stagger of pin fin array (mm)
S_T	transverse stagger of pin fin array (mm)
T	temperature (°C)
T_b	base temperature of pin bank (°C)
T_c	cold side thermoelectric temperature (°C)
T_h	hot side thermoelectric temperature (°C)
T_{high}	upper bound of exhaust temperature being considered during present iteration of bisection method (°C)
$T_{i,ex}$	exhaust temperature corresponding to point i (°C)
$T_{i,amb}$	ambient temperature at the moment $T_{i,ex}$ was measured (°C)
T_{in}	temperature of air at intake side of heat exchanger (°C)
T_{low}	lower bound of exhaust temperature being considered during present iteration of bisection method (°C)
T_{out}	temperature of air at exhaust side of heat exchanger (°C)
$T_{out,est}$	average of T_{high} and T_{low}, estimated exhaust temperature (°C)
T_w	temperature of pin wall (°C)
T_0	temperature of intake air flowing over cold pin fin bank (°C)
T_1	temperature of cold side pin fin base (°C)
T_2	temperature at cold side of thermoelectric module (°C)
T_3	temperature at hot side of thermoelectric module (°C)
T_4	temperature of hot side pin fin base (°C)
T_5	temperature of intake air flowing over hot pin fin bank (°C)
T^*	nondimensional temperature
T_∞	fluid temperature at infinity (°C)
ΔT	temperature difference (°C)

ΔT_{LM}	log mean temperature difference (°C)
$\bar{T}$	absolute temperature of thermoelectric module (K)
U	fluid velocity at infinity (m/s)
u	x–component of velocity (m/s)
u^*	nondimensional x–component of velocity (m/s)
V	electrical potential (volts)
V_{max}	maximum air velocity in pin fin bank (m/s)
$\dot{V}$	volumetric air flow (CFM)
v	y–component of velocity (m/s)
v^*	nondimensional y–component of velocity (m/s)
x^*	nondimensional x coordinate
y^*	nondimensional y coordinate
α	Seebeck coefficient (volts/ K)
Φ	Peltier coefficient (volts)
η	fin efficiency
μ	fluid viscosity (N s/m^2)
μ_w	fluid viscosity (N s/m^2) at the cylinder wall
ϱ	electrical resistivity (ohm cm) or mass density (kg/m^3)
τ	Thompson coefficient (volts/ K)
$\aleph$	pressure drop correlation correction factor
∇	gradient operator ($\partial/\partial x\,\hat{i} + \partial/\partial y\,\hat{j} + \partial/\partial z\,\hat{k}$)

CHAPTER 1

INTRODUCTION

1.1 Basic Characteristics of Thermoelectric Modules

A Peltier thermoelectric module is a solid state electrical device capable of both heating and cooling. The devices are small, lightweight, have no moving parts, and are therefore quite reliable. In applications where small amounts of heat must be moved, these devices are often chosen over a more traditional refrigeration system consisting of a compressor, expansion valve, evaporator, and condenser. They are found in commercial, scientific, and military applications.

The performance of a thermoelectric module is governed by four thermodynamic principles. The first of these four is the Peltier effect, which describes the absorption or release of thermal energy at the junctions of dissimilar conductors in a thermocouple circuit. This is diagrammed in Figure 1.1. A flow of heat q is observed leaving junction 1 where conductors A and B are joined and a flow of heat q′ is observed exiting junction 2. The heat flow q is given by

$$q = \Phi I \tag{1.1}$$

where Φ is the Peltier coefficient of the conductor pair and I is the current.

The second principle is the Seebeck effect, which describes the operation of a thermocouple circuit. As shown in Figure 1.2, if a temperature difference is imposed on two thermocouple junctions, a voltage potential E will be generated. The voltage developed is given by

$$E = \alpha\ (T_1 - T_2) \tag{1.2}$$

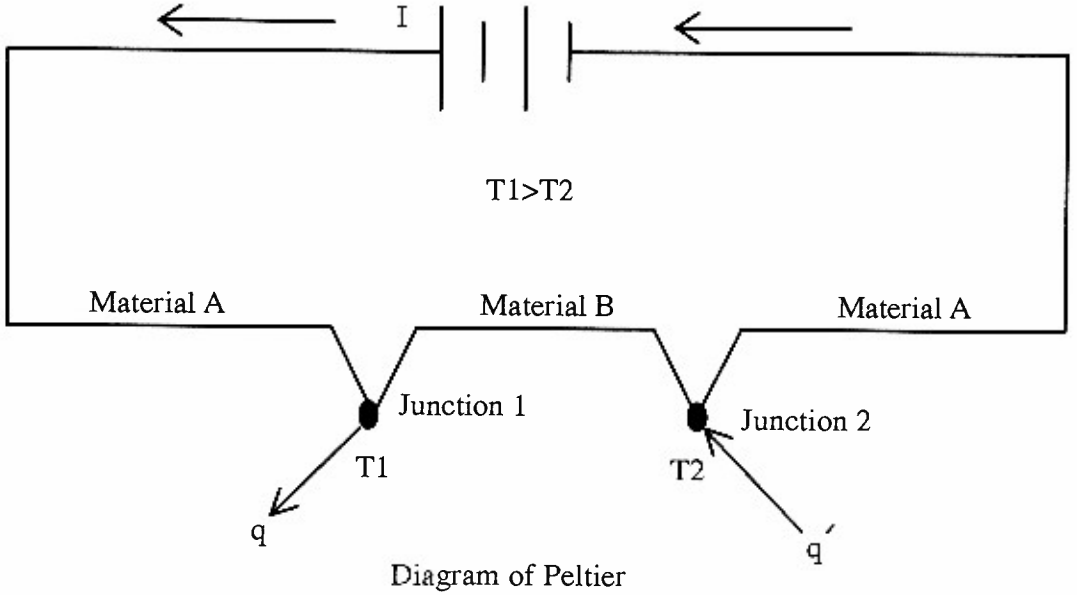

Diagram of Peltier Effect

Figure 1.1

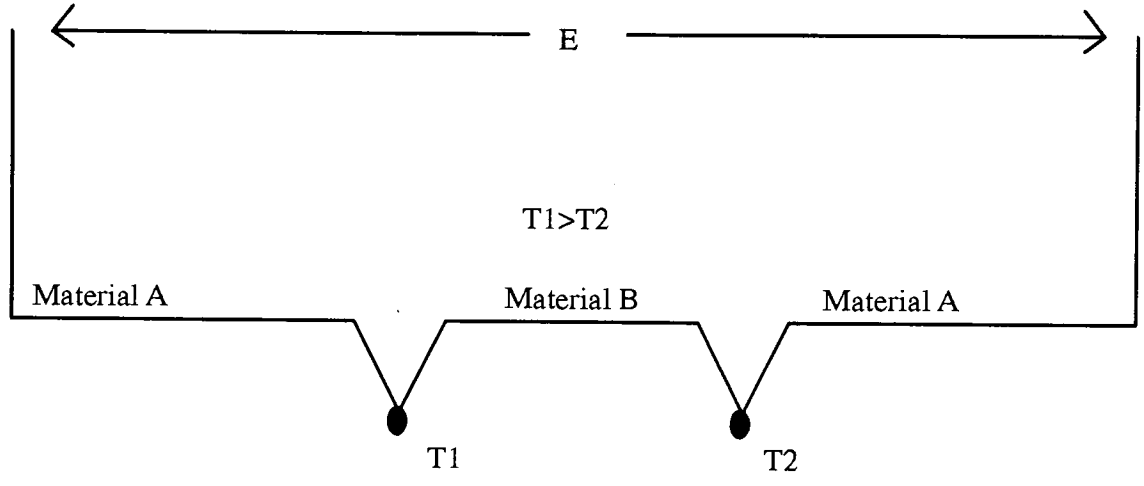

Diagram of
Seebeck Effect

Figure 1.2

where α is the Seebeck coefficient and is a function of the absolute temperatures of the thermocouple junctions.

The third principle is Joule heating, which occurs when a current is passed through an electrical resistance. The heat produced is given by

$$q = I^2R \tag{1.3}$$

where R is the electrical resistance in ohms and I is the current in amperes.

The fourth governing principle is the Thompson effect, which describes a heating effect that occurs when a current is passed through a thermocouple conductor which has imposed upon it a temperature gradient. The effect is described mathematically by

$$q_\tau = \tau I \frac{dT}{dx} \tag{1.4}$$

where τ is the Thompson coefficient and dT /dx is the temperature gradient along the conductor.

The construction of a practical thermoelectric module is illustrated in cross section by Figure 1.3. P and N doped semiconductor elements (typically bismuth telluride) are joined by the conductive bridge elements as shown. The bridge elements, in turn, are bonded to a ceramic plate which acts as an electrical insulator, a thermal conductor, and a structural member.

As current is passed through the device in the direction shown, electrons pass from P–elements to N–elements on side 2 only. This constitutes a transition from a low energy state to a high energy state, and heat is absorbed from side 2 as a result. Side 2 in this instance is referred to as the "cold side" of the thermoelectric device. On the other hand, electrons pass from N–elements into P–elements on side 1, and this constitutes a high–to–low energy transition. As a result of this energy transition, heat is released at side 1. Side 1 is referred

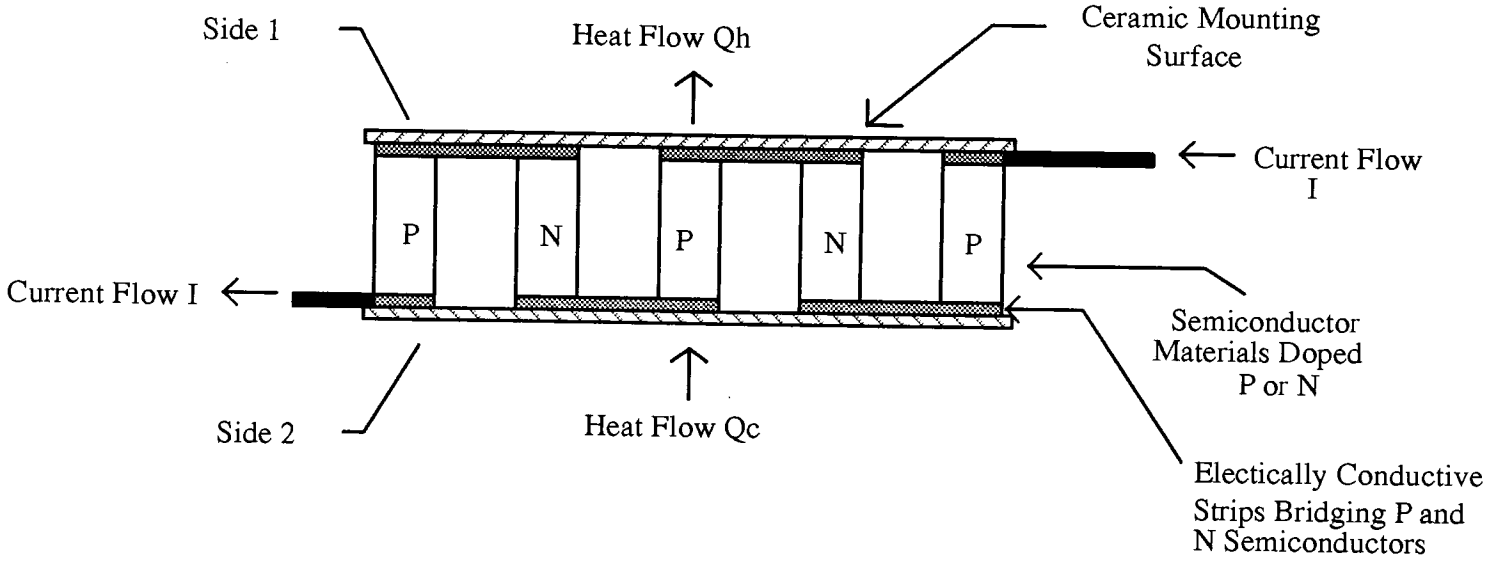

Thermoelectric Module
in Cross Section

Figure 1.3

to as the "hot side". This absorption and release of thermal energy is the Peltier effect previously described. Hereafter, Q_C will used to refer to heat flow into the cold side of the device and Q_H will be used to refer to heat flow from the hot side of the device.

This situation is completely reversed by passing current through the device in the direction opposite of that shown in Figure 1.3. Heat is absorbed at side 1 and rejected at side 2. This aspect of thermoelectric devices is a benefit should a particular application require both heating and cooling. By reversing the direction of current flow, the refrigeration effect can replaced by heating.

The heat pumping action of the thermoelectric device is affected by several factors. One such factor is the conduction of heat through the semiconductor material from hot side to cold side. This is simply Fourier's law of heat conduction given by

$$q'' = -k\nabla T \tag{1.5}$$

where q'' is the heat flux, k is the thermal conductivity of the semiconductor material, T is the temperature, and ∇ is the gradient operator.

Joule heating further reduces the heat pumping effectiveness of the thermoelectric module as does the Thompson effect. In fact, enough current can be passed through the thermoelectric module so that resistive heating dominates the Peltier effect and the net result is that heat is rejected from both the cold side and the hot side.

The equations that describe the overall performance of a thermoelectric device follow. Melcor, Inc. (1993) gives the relationship between driving voltage and current flow through the device as

$$E = 2N[I\varrho/G + \alpha\Delta T] \tag{1.6}$$

where E is the driving voltage, N is the number of P–N junctions, I is the current in amperes, ϱ is the resistivity in ohm–cm, G is the area divided by the length of thermoelectric element in cm (typically referred to as the geometry factor), α is the Seebeck coefficient in volts/K, and ΔT is the temperature difference between hot and cold sides ($T_h - T_c$) in K. The heat pumped by the device at the cold surface is given by

$$Q_C = 2N[\alpha I T_c - I^2\varrho/(2G) - K\Delta TG] \quad (1.7)$$

where Q_C is the heat pumped in watts at the cold side, T_c is the cold side temperature in K, and N, α, I, ϱ, and G have the same definitions as used in equation (1.6).

1.2 Practical Considerations of Thermoelectric Heat Pump Design

The thermoelectric module must be coupled to a hot and a cold side heat exchange surface before any substantial amount of heat may be moved through the cold side of the device. These surfaces may be as simple as extruded heat sink stock or more complex, such as a cold plate utilizing a liquid as a heat exchange media.

The coupling of the heat exchange surfaces to the thermoelectric module's cold and hot side surfaces is critical for effective heat transfer performance. A first requirement is that the heat exchange surfaces be flat. A specification of .001 inches flatness per inch of surface is a typical recommendation by thermoelectric module manufacturers. Some thermoelectric modules are manufactured with tinned surfaces so that they may be soldered to a copper heat exchange surface. Other coupling techniques include permanently bonding the thermoelectric module to the heat exchange surfaces with conductive epoxy adhesive or mechanically clamping the device between the heat exchange surfaces which have been previously coated with a thin film of a thermal grease.

The relative performance of a particular interface method may be understood by examining its thermal resistivity. Still air (which would correspond to a dry heat sink to thermoelectric device interface) has a thermal resistivity (ϱ) of 30.5 °C-m/ W. Thermal greases typically have a resistivity of 1.4 °C-m/ W, while thermally conductive epoxies have a resistivity value of 1.2 °C-m/ W. Soft solder (63% tin, 37% lead) joints have a resistivity as low as 0.2 °C-m/ W. Even though the resistivity of solder is quite low, a thicker film of it is typically required to bond the thermoelectric module to the heat sink surface in comparison to thermal greases and epoxies. The performance benefits of solder over thermal grease or epoxy are therefore not as great as the differences in thermal resistivity might suggest. Permanent bonding techniques such as solder or adhesives also suffer the drawback of inducing stress to the thermoelectric module because the coefficient of thermal expansion of the thermoelectric module rarely matches that of the heat sink material. Thermal greases allow some relative motion to occur between the thermoelectric module and the heat sink surfaces to occur, thus relieving many stresses as they build up in the heat pump assembly.

A final consideration in choosing an interface method should be whether or not it is desirable to be able to remove a thermoelectric module for service. Solder and thermal epoxy make the thermoelectric module/heat exchange surface assembly very difficult and expensive to disassemble, whereas the thermal grease approach makes even field service a possibility.

It is important to note that poor thermal coupling of the thermoelectric device to its heat exchange surfaces does not only affect heat pumping performance, but may lead to device failure. Improper coupling, especially to the hot side heat exchange surface, may result in overheating to the extent that the thermoelectric device will unsolder itself internally, resulting in an open circuit condition.

The design of the thermoelectric heat pump must also take into account the possibility that water could condense on the cold side surfaces and ultimately end up in the thermoelectric module itself. This situation will result in galvanic action within the thermoelectric module which may degrade performance or cause failure due to short circuiting. A hermetic seal as shown in Figure 1.4 is often used in the design to keep condensate away from critical areas. This seal, if made from a low density foam material, may also double as a thermal barrier between hot and cold side heat exchange surfaces should these surfaces overhang the footprint of the thermoelectric module. This situation is also depicted in Figure 1.4.

1.3 Description of Heat Pump Analyzed in this Work

The heat pump to be considered in the following analysis is an assembly used in an application where modest amounts of heat (approximately 50 watts) must be pumped for the purpose of cooling an insulated container. The insulated container is divided into two compartments. There is a medium humidity compartment kept at approximately 33% RH and a low humidity compartment kept at approximately 15% RH. A setpoint temperature of 22.2 °C is maintained in both compartments. The maximum allowable ambient temperature is 30 °C.

The features of the heat pump assembly are detailed in Figure 1.5. A total of six thermoelectric modules are utilized in the assembly, all of which are manufactured by Melcor Corp. of Trenton, NJ. As shown, four of the modules are Models CP1.4-127-045L (N=127, G=.17) and the remaining two modules are Models CP1.4-071-045L (N=71, G=.17). Appendix A gives an example of a thermoelectric data sheet along with an example of the nomenclature used by Melcor to describe a thermoelectric module. The thermoelectric modules are coupled to hot and cold heat sink interfaces via a thin film of

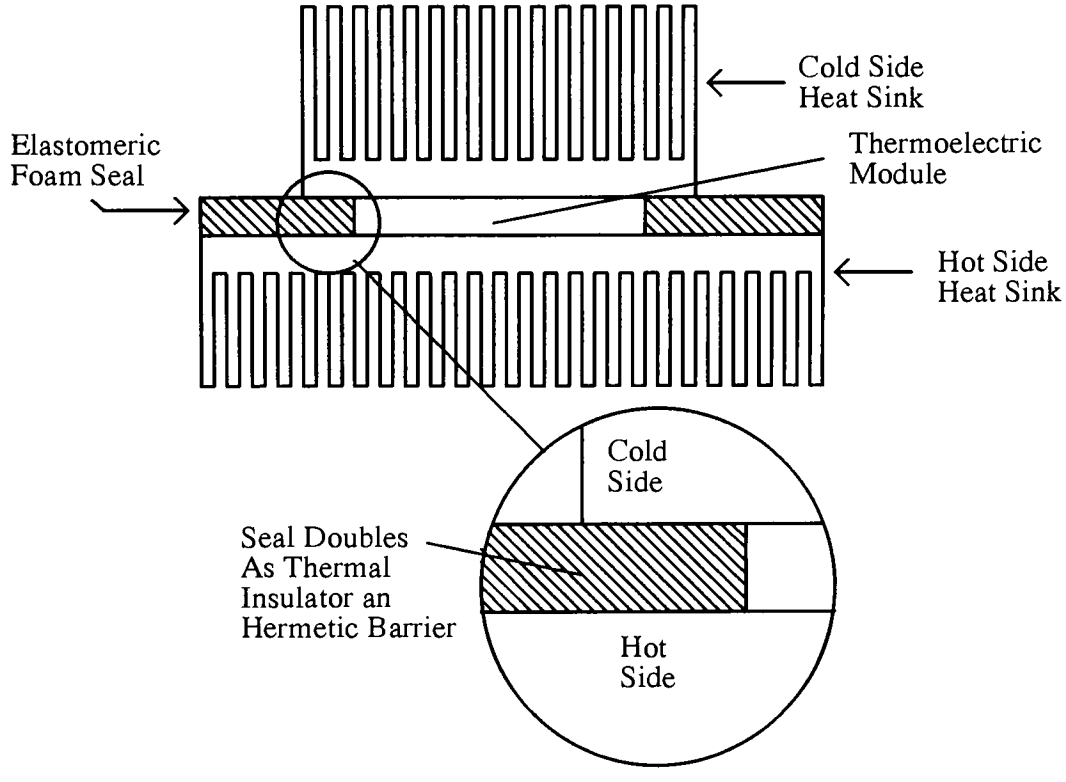

Hermetic Sealing Technique for a Thermoelectric Module

Figure 1.4

thermal joint compound (Wakefield type 120) and clamped in place by two fasteners per device. The hot and cold heat sinks are a pin fin design and are plaster cast in aluminum alloy 356 T-6, which has a thermal conductivity of 153 W/m-K. Three of the cold side pin fin castings (those designated "outer" in Figure 1.5) are utilized to cool the medium humidity compartment. The other three cold side casting (those designated "inner") are used to cool the low humidity compartment. The inner and outer banks of cold side pin fins are separated by a hermetic sealing wall which is a feature of the insulated container. Air is passed over the inner and outer cold side pin banks by two separate tubeaxial fans. The cold side heat sinks each have 39 pins, with the pins having heights of 53.09 mm and average diameters of 3.97 mm (there is a slight taper to the pin as a casting consideration). The heat sinks have a staggered configuration which is shown in Figure 1.6, with S_L (longitudinal stagger dimension) = 5.49 mm and S_T (transverse stagger dimension) = 10.32 mm . The width of these heat sinks is 57.66 mm and the length of the heat sink is 40 mm. There is one thermoelectric module associated with each cold side heat sink. The hot side pin fin heat sink is also cast from 356 T-6 aluminum alloy and has pins with the same height and average diameter, but a different staggered pattern which is shown in Figure 1.7 (S_L = 7.00 mm and S_T = 14.00 mm). The area of this heat sink is 35,588 mm^2 and is populated by 318 pins. It is important to note that the hot side heat sink is not purely rectangular, but actually sweeps out a slight radius.

There are a few final comments to be made about the thermoelectric heat pump described above. First, the system as designed operates at relatively low Reynolds numbers with respect to pin diameter ($Re_D < 1000$ for both the hot and cold side pins). A final consideration is that it would be undesirable to implement a fan system having the capability to generate large pressures differences across the cold side pins. The humidity within the

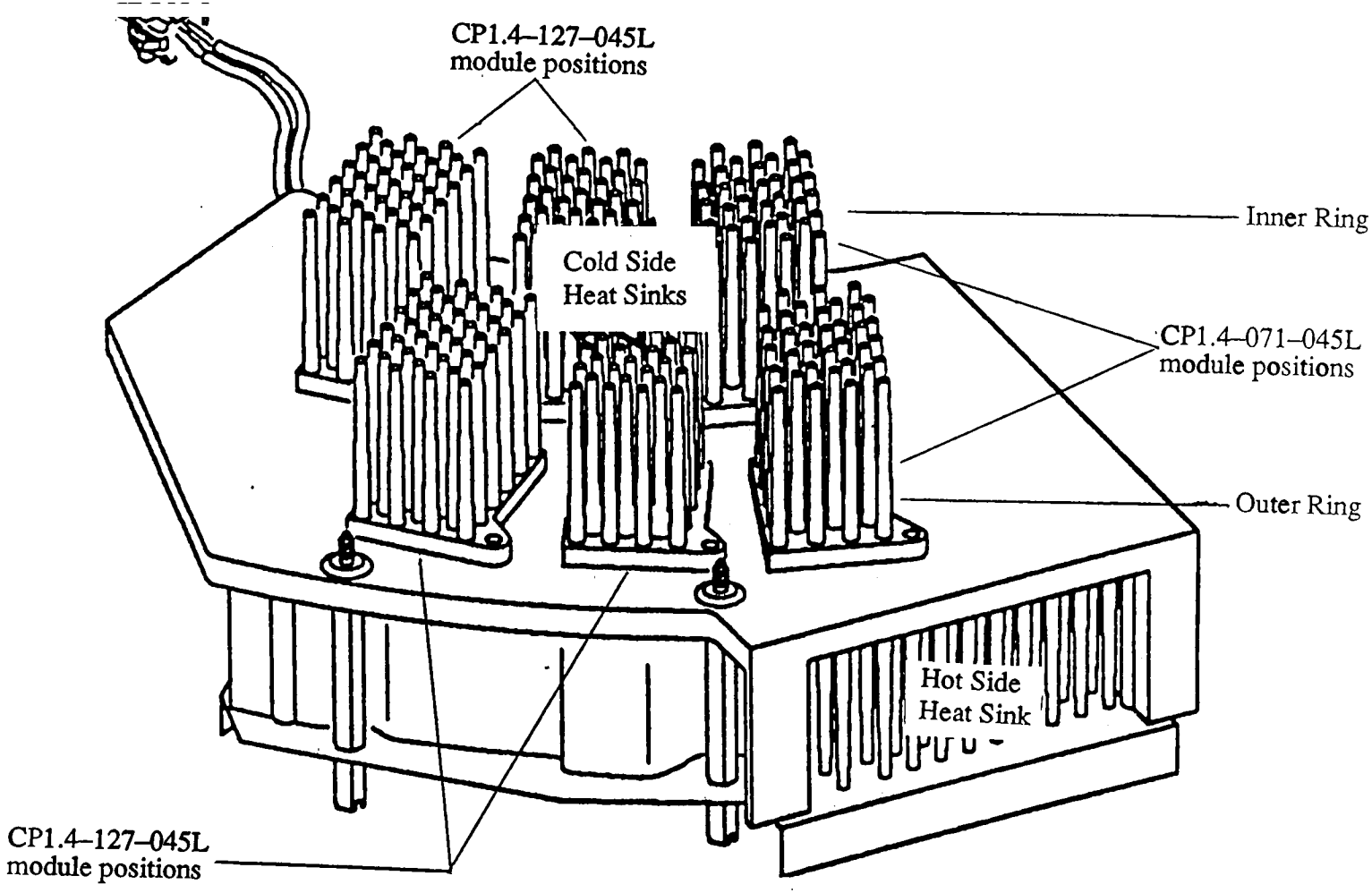

Diagram of Thermoelectric Heat Pump
Analyzed in this Work

Figure 1.5

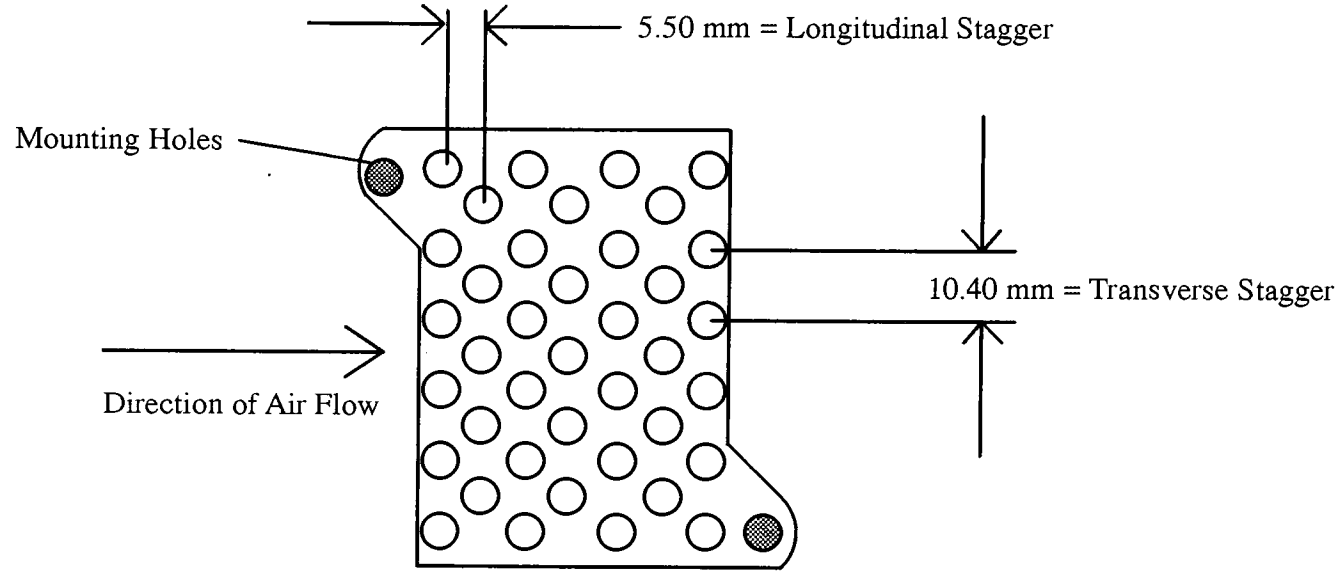

Cold Side Pin Fin Configuration

Figure 1.6

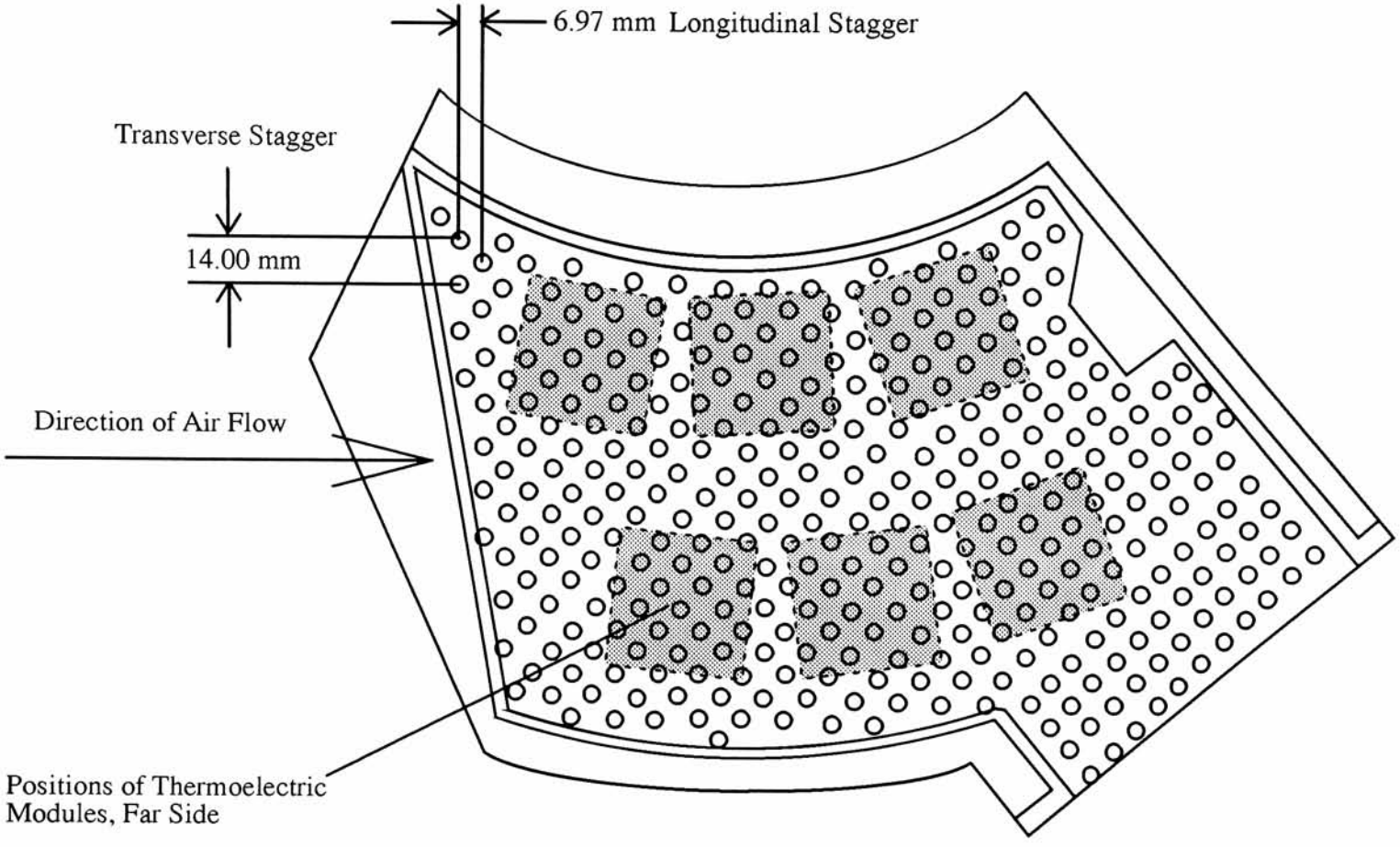

Hot Side Pin Fin Configuration
Figure 1.7

insulated container is controlled via desiccants or saturated salt solutions. Large pressure differences with respect to ambient act to drive air infiltration though gasketed seams in the enclosure which reduces the effective life of the desiccants or salt solutions, and this drives more frequent replacement intervals.

The goal of this thesis is to maximize the cooling capacity of the heat pump described above. To accomplish this goal, a heat thermoelectric pump simulation model is developed from analytical and empirical equations. In this model, pin fin geometry and details of thermoelectric module implementation are considered to be variable quantities. The predictive capability of this model (which actually consists of three computer programs) is demonstrated by comparison with experimental data as well as with data from an FEA fluid dynamics package. Finally, the model is exercised through an appropriate range of pin fin and thermoelectric module variables in an attempt to maximize the heat pumped at the cold side of the device. Recommendations are presented that detail the combination of these variables that produce the best performance.

CHAPTER 2

LITERATURE REVIEW

The purpose of this literature review is to identify sources of information concerning components of the heat pump system described in Chapter 1. There was an effort to identify pertinent information regarding single or banks of heated pins/cylinders in cross flow, thermoelectric module characteristics, and any literature describing modeling or optimization techniques of thermoelectric heat pump systems.

Frank (1993) describes at a very general level of detail a program that had been developed to model thermoelectric module performance. The article also briefly mentions a companion program that was developed to predict flow and heat transfer characteristics of finned heat sinks. A comparison of predicted versus test results revealed quite good correlation. Heat load errors were within 5%, current draw errors were within .1 amp, exhaust air temperature errors were within .6 °C, and average heat sink temperature errors were within 1.0 °C. The article indicates that measured values of thermal resistance for the heat sinks were used for this analysis rather than calculated values from the companion program. Calculated values of thermal contact resistance between thermoelectric modules and heat sinks were used based on manufacturer's performance data of the specific interface compounds used. Results of a design study are also presented.

A substantial body of literature was discovered concerning heat transfer of single heated cylinders in cross flow, but much less for banks of cylinders in cross flow. It was found that most of the literature was not pertinent to this study because of the relatively low range of Reynolds number ($Re_D < 1000$) under consideration. For instance, it was quite

common to find literature that discussed cylinders in cross flow conditions having $Re_D >$ 10000, and occasionally $Re_D > 100000$.

Perhaps one of the most useful pieces of literature encountered concerning the general topic of heat transfer from single cylinders or banks of cylinders in cross flow was an article by Morgan (1975). Not only was this a very comprehensive source of information regarding the general topic of free and forced heat transfer from cylinders, but was also a very good source of references, with 254 cited. The literature on this topic dates back to the late 1800's where there was apparently considerable interest in understanding heat transfer of single cylinders as it pertained to hot wire annemometry and heating of electrical power transmission lines. Heat transfer characteristics of banks of tubes were of interest to those primarily involved with heat exchangers associated with the power generation industry.

Morgan (1975) presents correlation data from 75 different sources as part of his study of heat transfer of single cylinders in cross flow (in cases where the original author had presented only raw data, Morgan developed correlations). Eight of the more recent of these correlations were used as checks for the FIDAP numerical results obtained in Chapter 4 of this paper.

There is a much smaller body of work which pertains to some of the theoretical aspects of heat transfer from heated cylinders in cross flow. Zhukauskas (1972), for instance, presents the following relationship for the calculation of the local heat transfer coefficient under laminar conditions near the front stagnation point of a heated tube in air

$$Nu_x = [.9450-.7696(x/D)^2-.3478(x/D)^4]Re^{.5} \qquad (2.1)$$

where x is circumferential distance from the front stagnation point. This relationship was developed from boundary layer theory and is also used as a comparison for the numerical

results obtained in Chapter 4.

Zhukauskas (1972) presents the most recent heat transfer and pressure drop correlations to be used for banks of tubes or pins with Reynolds numbers as low as 100 as well as correction factors that allow the correlations to be used for shallow banks banks of tubes or pins (less than 20 rows). These equations and correction factors form the basis of the computer program COPT.FOR and HOPT.FOR (Cold Optimizer and Hot Optimizer) that are discussed in Chapter 3. Zhukauskas (1972) does point out, however, that the available experimental data for banks of tubes in cross flow for $100 < Re_D < 1000$ is rather scarce. Omohundro (1949), Bergelin (1950), and Bergelin (1952) are some of the few original authors that have investigated heat transfer and pressure drop over banks of tubes at low Reynolds number conditions.

Many texts and articles describe the theory and governing equations for thermoelectric heat pump modules. Guyer (1989) and Threlkeld (1970) provide general descriptions of thermoelectric cooling. Materials Electronic Products Corporation (1993) of Trenton, NJ (Melcor) provided the thermoelectric module performance formulae and the temperature dependent material properties used in the development of the FORTRAN program HP.FOR.

CHAPTER 3

ANALYTICAL MODEL OF THERMOELECTRIC HEAT PUMP SYSTEM

3.1 Description of Model

Figure 3.1 is an illustration of a pin fin/thermoelectric heat pump model. A quantity of heat Q_C is extracted from an air stream flowing over the cold side pin fins. This is brought about by the temperature difference between node 1 and node 0 acting though the thermal resistance of the cold side pin fins, R_{PC}. Q_C must also move across the junction of the cold side pin fins and the thermoelectric module. The thermal contact resistance between the cold pin base and the thermoelectric module, R_{IC}, is encountered at this point, which gives rise to the temperature difference between node 2 and node 1. Q_C is absorbed by the cold side of the thermoelectric module. Q_C plus the Joule heating of the thermoelectric module is rejected at the hot side (node 3) and crosses the junction of module and hot side pin fin where this energy is finally passed to the hot side air stream. The temperature difference between nodes 4 and 3 drives this energy across the hot side thermoelectric module/pin fin thermal resistance, R_{IH}. The temperature difference between nodes 5 and 4 act to reject energy from the hot side pin fins to the hot side air stream through the hot side pin fin thermal resistance R_{PH}. Equations 1.6 and 1.7 describe the relationships between the voltage drop E, the current I, the temperature drop T_3-T_2, the heat pumped Q_C, the number of thermocouple junctions N, and the geometry factor G of the thermoelectric modules(s).

The model described above was developed in the form of three computer programs. The first two programs, HOPT.FOR and COPT.FOR (which are nearly identical), can be used to calculate the thermal resistance of hot and cold side pin fins/fan systems,

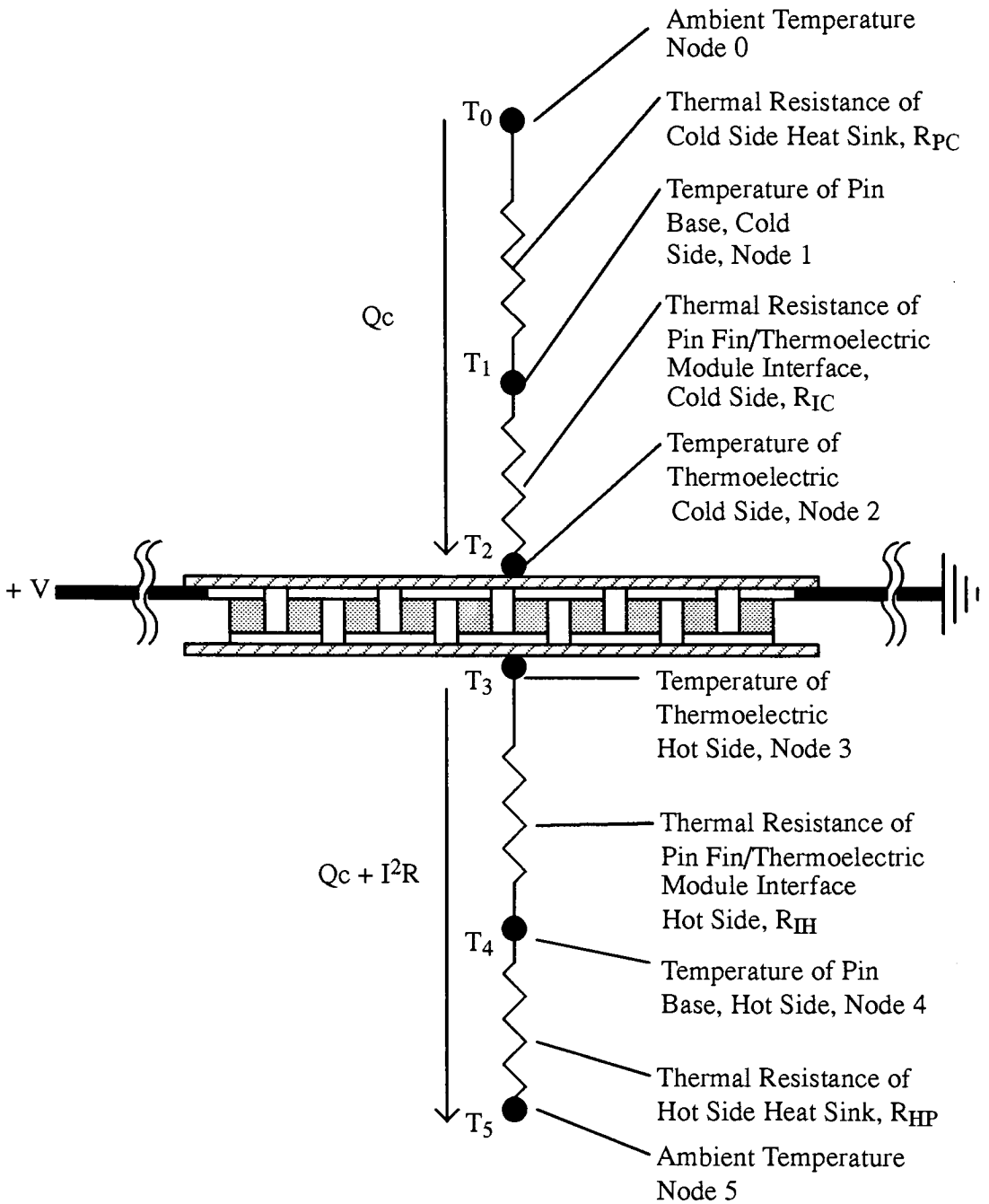

Diagram of Pin Fin/Thermoelectric Heat Pump Model

Figure 3.1

respectively. A listing of HOPT.FOR is given in Appendix B. The subtle differences between the two programs will be discussed shortly. Both take as input the pressure versus flow curve of the fan system in question, the heat sink area available in terms of width and length to be populated with pins, geometry information concerning the pins and pin layout (transverse stagger S_T, longitudinal stagger S_L, pin diameter D, and pin height L), the thermal conductivity of the pin fin heat sink material, and finally an estimate of the pin base temperature. The output of the program is the thermal resistance of the heat sink in terms of °C/W. Once calculated, the pin fin thermal resistance information is used as input to a program titled HP.FOR (listing given in Appendix C) along with a calculated or an experimentally derived value for the thermoelectric module/pin fin thermal interface resistances (R_{IC} and R_{IH}), the total number N of thermoelectric thermocouple junctions present, the geometry factor G, the driving voltage V, and the ambient temperature (T_0 and T_5). The output of HP.FOR is the amount of heat pumped at the cold and hot sides (Q_C and Q_H), the current draw I of the system, and the nodal temperatures T_1 through T_4 as shown in Figure 3.1. In practice, it is found that a few iterations of each program are required to model a given heat pump system because of the initial estimate of pin base temperature required by HOPT.FOR and COPT.FOR. That is, once results are obtained from HP.FOR, the appropriate node temperatures are used to repredict hot and cold side thermal resistances which are again used as inputs to HP.FOR. This process is continued until an acceptable level of convergence is obtained. It is found, however, that an initial estimate of pin base temperature within a few °C will typically yield pin fin thermal resistance values within a few percent of the value obtained after a few iterations. Convergence is rapidly obtained.

HOPT.FOR, COPT.FOR, and HP.FOR are intended to be general purpose design tools that allow an engineer to quickly evaluate the effects of pin fin geometry, heat sink

material, fan performance, and various combinations of thermoelectric modules on the overall performance of a thermoelectric heat pump system. The programs are rather idealistic in several important aspects. First, heat sinks are considered only as rectangular banks of staggered pins. The rectangular constraint arises from the availability of applicable flow and heat transfer correlations. The second constraint of the model is that a multiple thermoelectric module system can be analyzed only if all modules are constructed of identically sized semiconductor elements. For example, a system containing two thermoelectric modules having identically sized semiconductor elements placed on common heat sinks could be analyzed. A similar analysis could not be done using HOPT.FOR, COPT.FOR, and HP.FOR if the two thermoelectric modules had different geometry factors, however. A third constraint is that the model assumes a staggered configuration for both the hot and cold side pin fin banks. Furthermore, HOPT.FOR and COPT.FOR assume a constant pin base temperature across the hot and cold side, respectively. Depending of the system being modeled, this may not be a good assumption. For example, a high output heat pump system having many thermoelectric modules populating a heat sink surface may give rise to substantially different module-to-module hot side temperatures. Since thermoelectric module performance is temperature dependent and the model assumes a constant pin base temperature, this may result in prediction errors of unacceptable magnitude. Finally, all thermoelectric modules are depicted as being wired in a series fashion.

3.2 Pin Fin Thermal Resistance Calculations

The thermal resistances of the hot and cold side pin fins, R_{HP} and R_{CP} respectively, are a function of the particular fan performance curves which drive the air flow across the two pin banks, the geometry of the pin fins banks (pin diameter, pin height, transverse stagger, and longitudinal stagger), pin fin materials, and fluid properties. Two particular

correlations describing pressure drop across a pin fin bank were examined. The first correlation (Zhukauskas, 1972) gives the pressure drop across a staggered bank of tubes by

$$\Delta p = N\aleph\left(\frac{\varrho V_{max}^2}{2}\right)f \tag{3.1}$$

where N is the number of rows of tubes, $\aleph$ is a correction factor given by Figure 3.2, ϱ is the fluid density, f is a friction factor also given by Figure 3.2, and V_{max} is given by

$$\begin{aligned} V_{max} &= \frac{V_\infty\ S_T}{S_T - D} \qquad \text{for} \quad S_D > \frac{S_T + D}{2} \\ V_{max} &= \frac{V_\infty\ S_T}{2(S_D - D)} \qquad \text{for} \quad S_D < \frac{S_T + D}{2} \end{aligned} \tag{3.2}$$

V_∞ can be calculated by dividing the volumetric flow rate of air through a duct by the cross sectional area of that duct. Figure 3.3 defines S_T, S_D, S_L, and D. Note that for Figure 3.2, P_L and P_T are nondimensional longitudinal and transverse staggers and are given by

$$\begin{aligned} P_L &= \frac{S_L}{D} \\ P_T &= \frac{S_T}{D} \end{aligned} \tag{3.3}$$

and $Re_{D,max}$ is given by

$$Re_{D,max} = \frac{\varrho V_{max} D}{\mu} \tag{3.4}$$

where ϱ is the mass density of air and μ is the viscosity of air.

For the purposes of developing a computer program to determine the thermal resistance of a pin fin heat sink, correlations were developed for the friction factor f and the correction factor $\aleph$ from the information contained in Figure 3.2. The following piecewise approximation was developed for $\aleph$:

$$\begin{gathered} \aleph = 1 \text{ for } P_T/P_L \leq 1.17 \\ \aleph = (-.0006556 * Re_{max} + 1.2655) * \log_{10}((P_T/P_L) - .17) + 1 \\ \text{for } P_T/P_L > 1.17. \end{gathered} \tag{3.5}$$

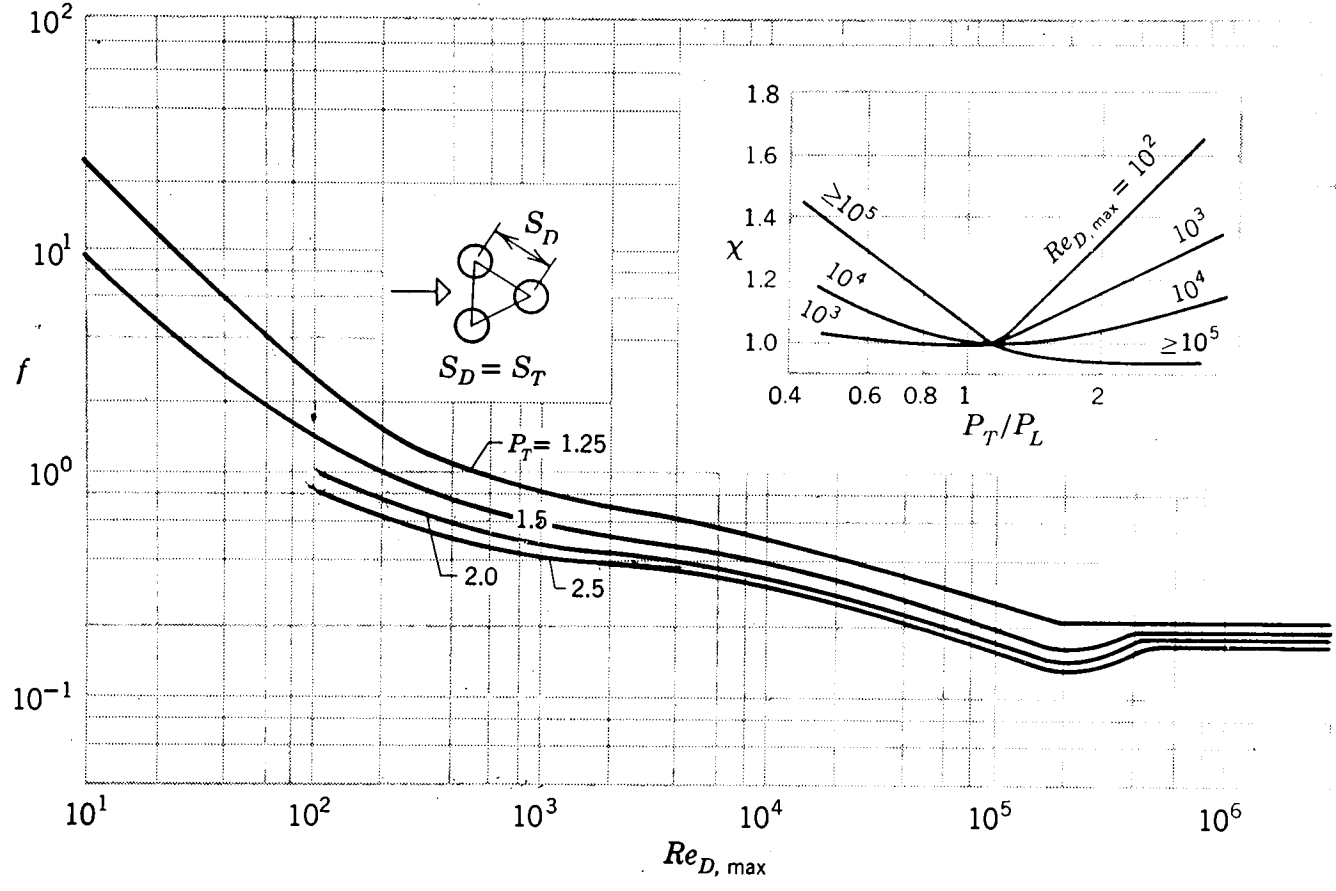

Friction Factor f and Correction Factor χ for a
Staggered Bank of Pins, Incropera and DeWitt (1981)
Figure 3.2

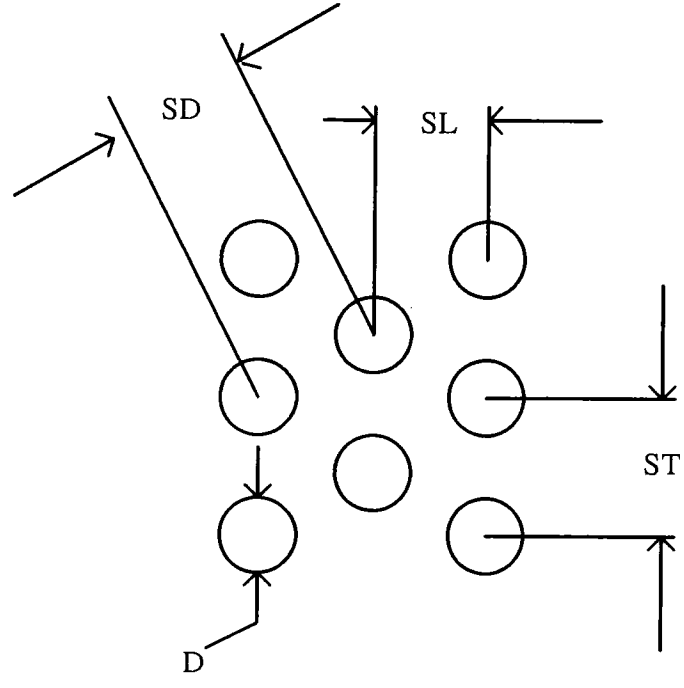

Diagram of ST, SD, and D for a Staggered Pin Bank
Figure 3.3

For $Re_{D,max} < 200$, the friction factor f was approximated by the relationships that follow. For $1.25 < P_T < 1.5$,

$$f = A1 - (A1 - A2) * (P_T - 1.25)/.25$$

where

$$A1 = 2.692-(2.692-1.557) * (Re_{D,max}-100)/100$$
$$A2 = 1.462-(1.462-.9844) * (Re_{D,max}-100)/100 \quad (3.6)$$

For $1.5 \leq P_T \leq 2$

$$f = A1 - (A1 - A2) * (P_T - 1.5)/.5$$

where

$$A1 = 1.462-(1.462-.9844) * (Re_{D,max}-100)/100 \quad (3.7)$$
$$A2 = 1-(1-.734) * (Re_{D,max}-100)/100$$

For $P_T > 2$,

$$f = A1 - (A1 - A2) * (P_T - 2)/.5$$

where

$$A1 = 1-(1-.734) * (Re_{D,max}-100)/100 \quad (3.8)$$
$$A2 = .801-(.801-.614) * (Re_{D,max}-100)/100$$

For $200 \leq Re_{max} \leq 1000$, the following relationships were used:

$$f = A * \exp(-.0042 * Re_{D,max}) + B$$

where for $1.25 < P_T < 1.5$,

$$A = 1.8 - (1.8 - .96) * (P_T - 1.25)/.25$$
$$B = .78 - (.78 - .57) * (P_T - 1.25)/.25$$

for $1.5 \leq P_T < 2$, (3.9)

$$A = .96 - (.96 - .6) * (P_T - 1.5)/.5$$
$$B = .57 - (.57 - .475) * (P_T - 1.5)/1.5$$

and for $P_T \geq 2$,

$$A = .6 - (.6 - .46) * (P_T - 2)/.5$$
$$B = .475 - (.475 - .415) * (P_T - 2)/.5$$

A second correlation for pressure drop across a bank of tubes or pins (Guyer, 1989) is given by

$$\Delta P = f\ N\ \left(\frac{\varrho V_{max}^2}{2}\right)\left(\frac{\mu_w}{\mu}\right)^{0.14} \quad (3.10)$$

where N is the number of pin rows, ϱ is the fluid mass density, μ_w is the fluid viscosity at the tube or pin wall, μ is the fluid viscosity of the main fluid stream, and f is a friction factor given by

$$f = [1.0 + (.472/((S_T/D)-1.0)^{1.08})\ ]Re_{D,max}^{-0.16} \qquad (3.11)$$

Figure 3.4 shows the algorithm used to determine flow rate and pressure drop across a bank of pin fins when given a particular pressure versus flow curve for a fan system. A bisection method is employed which first bounds the solution by taking the maximum flow rate ($flow_{max}$) to be that of the unrestricted system flow and the minimum flow rate ($flow_{min}$) to be zero. The pressure drop of the pin fin bank at the average of $flow_{max}$ and $flow_{min}$ ($flow_{avg}$) is computed using the appropriate selections of equations 3.1 though 3.11. The operating pressure of the fan system at $flow_{avg}$ is also calculated from the system pressure versus flow curve. If the absolute difference between $flow_{min}$ and $flow_{max}$ is less than a specified tolerance (.0001 CFM was used), the routine terminates and returns the current pressure drop and $flow_{avg}$ as the system operating pressure and flow rate. If this difference is greater than the specified tolerance, the solution boundaries are redefined using $flow_{avg}$ as $flow_{max}$ if the calculated pin bank pressure drop is greater than the fan system operating pressure. If the calculated pin bank pressure drop is less than the fan system operating pressure, the problem boundaries are redefined by setting $flow_{min}$ equal to $flow_{avg}$. The algorithm is allowed to loop in this manner until the tolerance criterion is satisfied.

Zhukauskas (1972) gives the Nusselt number of a staggered bank of pin fins as

$$Nu = C * Re_{D,max}^{n} Pr^{.36} * \left(\frac{Pr}{Pr_w} \right)^{.25}$$

where

$$C = .35 * \left(\frac{S_T}{S_L} \right)^{.2} \text{ and } n = .6 \text{ for } S_T < 2S_L \qquad (3.12)$$

and

$$C = .4 \text{ and } n = .6 \text{ for } S_T > 2S_L$$

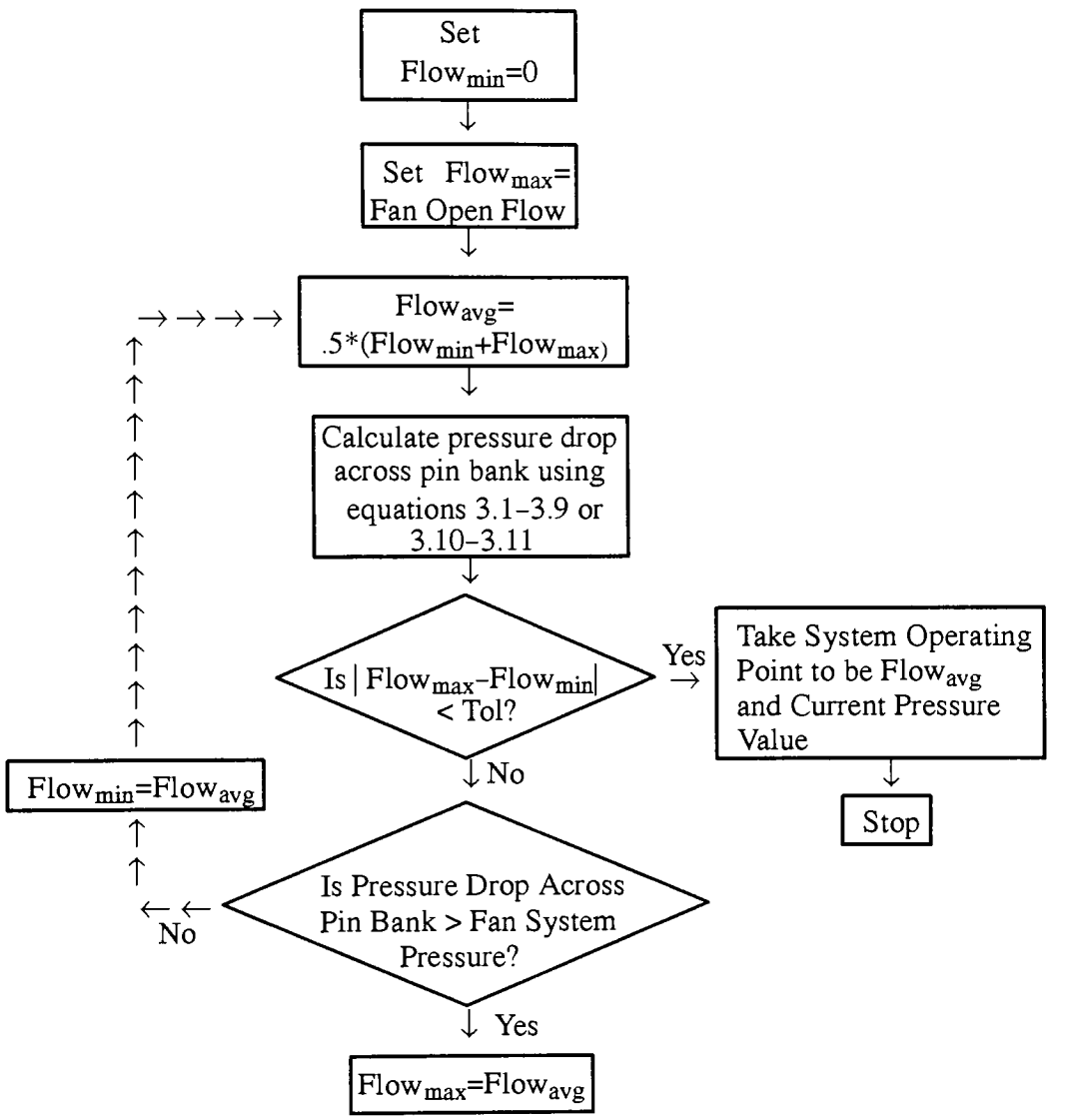

Algorithm to Determine Pressure and Flow of
Pin Fin/Fan System
Figure 3.4

These equations are good for $100 \leq Re_{max} \leq 2 \times 10^5$ in banks of pins having 20 or more rows. Figure 3.5 is used to correct the results of equation 3.12 where less than 20 rows of pin are encountered. All fluid properties are evaluated at T_∞ except Pr_w . $Re_{D,max}$ is given by equation 3.4. The concept of log mean temperature difference and conservation of energy is used to calculate the overall heat transfer rate from a bank of pins. If the temperature entering a bank of pin fins is at temperature T_{in} and exits at temperature T_{out}, the overall heat transfer rate from an energy balance stand point is given by

$$Q_a = \dot{m}\, C_p\, (\, T_{out} - T_{in}) \tag{3.13}$$

where $\dot{m}$ and C_p are the mass flow rate and the heat capacity of the fluid in question. The heat transfer rate is also given by Guyer (1989) as

$$Q_b = (\frac{Nu\ *\ k}{D}\ )NM\pi DL(\Delta T)_{LM} \tag{3.14}$$

where Nu is the Nusselt number computed with equation 3.12, k is the thermal conductivity of the fluid, D is the pin diameter, N is the number of pin rows, M is the number of pins per row, and L is the pin length. ΔT_{LM} is given by

$$\Delta T_{LM} = \frac{(T_w - T_{in}) - (T_w - T_{out})}{\ln[(T_w - T_{in})/(T_w - T_{out})]} \tag{3.15}$$

where T_{in} is the fluid intake temperature, T_{out} is the fluid exhaust temperature, and T_w is the temperature of the pin wall. However, since the pins have a finite thermal conductivity k_{pin}, equation 3.14 must be corrected with respect to fin efficiency η, where

$$\eta = \frac{Q_{actual}}{Q_{ideal}} \tag{3.16}$$

For a cylindrical pin fin,

$$\eta = \frac{\tanh(ml)}{ml} \tag{3.17}$$

$$m = \sqrt{\frac{4h}{k_{pin}D}}$$

$$h = \frac{Nu * k_{air}}{D} \qquad \text{(3.17 cont'd.)}$$

Thus, correcting equation 3.14 for fin efficiency gives the result

$$Q_{b,act} = \eta\, Q_b \qquad (3.18)$$

The programs HOPT.FOR and COPT.FOR request the user for the ambient air temperature which is equal to the fluid intake temperature T_{in}. The program also prompts the user for an estimate of pin base temperature as described in section 3.1. This information bounds the problem. In the case of a cold side pin fin bank (COPT.FOR), the lowest possible temperature (T_{low}) that the exhaust air (T_{out}) could achieve is that of the pin temperature, T_w. The highest possible temperature that the exhaust air could achieve is that of the fluid intake temperature T_{in} ($T_{high.}$). In the case of a hot side pin fin bank (HOPT.FOR), the boundaries are modified slightly. The lowest possible temperature of T_{out} is T_{in} (T_{low}) and the highest possible temperature achievable is T_w (T_{high}). In either case, the program makes an initial estimate of the exhaust temperature to be

$$T_{out\,est.} = .5 * (T_{high} + T_{low}) \qquad (3.19)$$

Fluid (air) properties are evaluated at T_∞, which is T_{in} via linear interpolation of data points at 250 K, 300 K, and 350 K.

Both HOPT.FOR and COPT.FOR evaluate the volumetric flow rate of the pin fin/fan system via the method described in Figure 3.4. The mass flow rate is calculated by

$$\dot{m} = \varrho * \dot{V} \qquad (3.20)$$

where $\dot{V}$ is the volumetric flow rate and ϱ is the fluid density. Q_a and $Q_{b,act}$ are then calculated with equations 3.13 and 3.18 using the estimate of $T_{out,est.}$ as given in equation

3.19. If Q_a is found to be less than $Q_{b,act}$ in the case of a cold side pin fin bank, then the problem is rebounded by setting

$$T_{low} = T_{out,est.} \tag{3.21}$$

then

$$T_{out,est.} = .5 * (T_{low} + T_{high}) \tag{3.22}$$

If Q_a is greater than $Q_{b,act}$, then the problem is rebounded by setting

$$T_{high} = T_{out,est.} \tag{3.23}$$

then

$$T_{out,est.} = .5 * (T_{low} + T_{high}) \tag{3.24}$$

Note that if a hot side pin fin bank is being analyzed, equations 3.21 and 3.23 are swapped to correctly rebound the problem. Q_a and $Q_{b,act}$ are then calculated using the latest value of $T_{out,est}$. This bisection method of solution is continued until the absolute difference of Q_a and $Q_{b,act}$ is less than a specified tolerance value, which was taken to be .01 watts. At this point, both HOPT.FOR and COPT.FOR calculate the thermal resistance of the pin fin system by

$$R_{th} = |T_w - T_1|/Q_a \tag{3.25}$$

Figure 3.6 is a diagram of the algorithm for a cold side pin fin bank (COPT.FOR). HOPT.FOR differs only in the single aspect described above.

The value of R_{th} calculated by either HOPT.FOR or COPT.FOR changes slightly as one varies estimates of pin base temperature. The variations are caused by slight variations in flow rate (temperature dependent viscosity is used in equation 3.4 to calculate $Re_{D,max}$) and heat transfer rate caused by the temperature dependence of air which the programs take into account. Again, when the programs are used in conjunction with the routine described in section 3.3, convergence (matching node temperatures) is readily achieved in a few iterations.

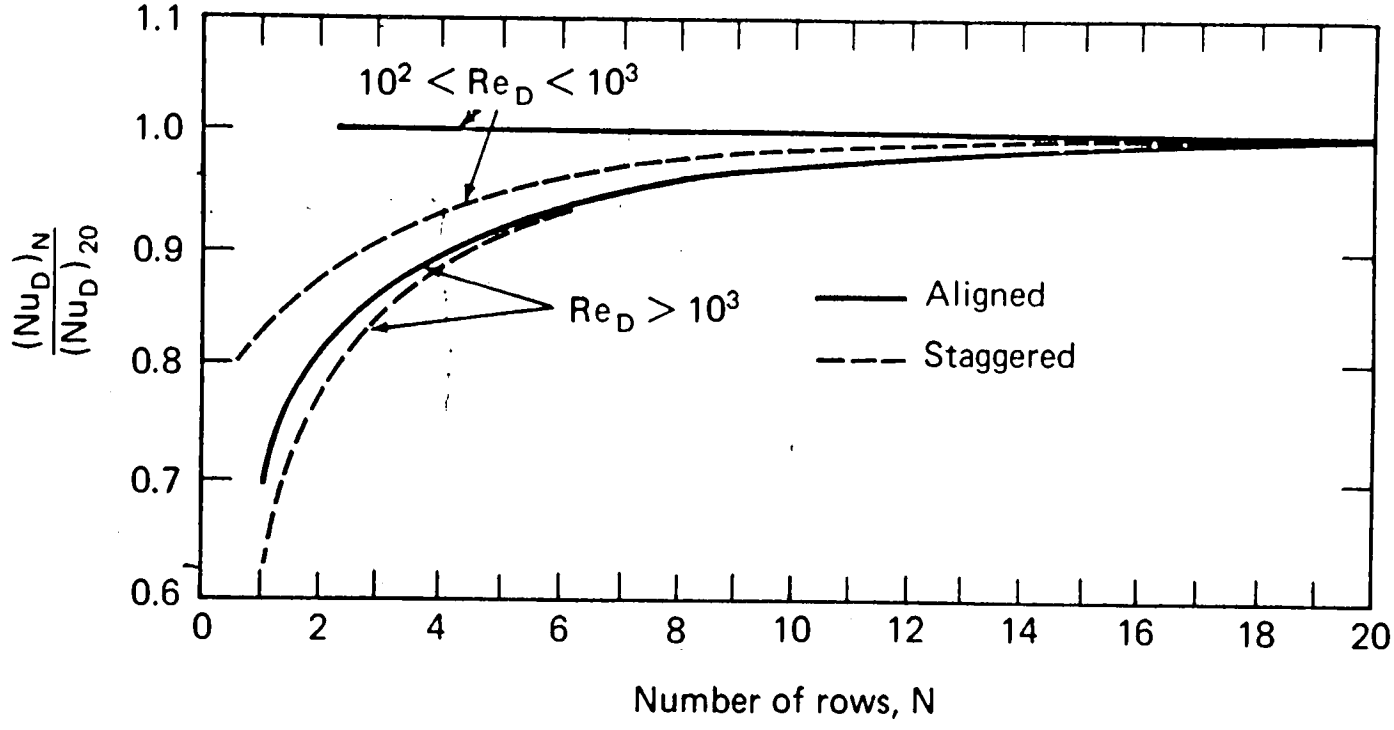

Correction factor used with equation 3.25 when number of rows is less than 20, Guyer (1989)

Figure 3.5

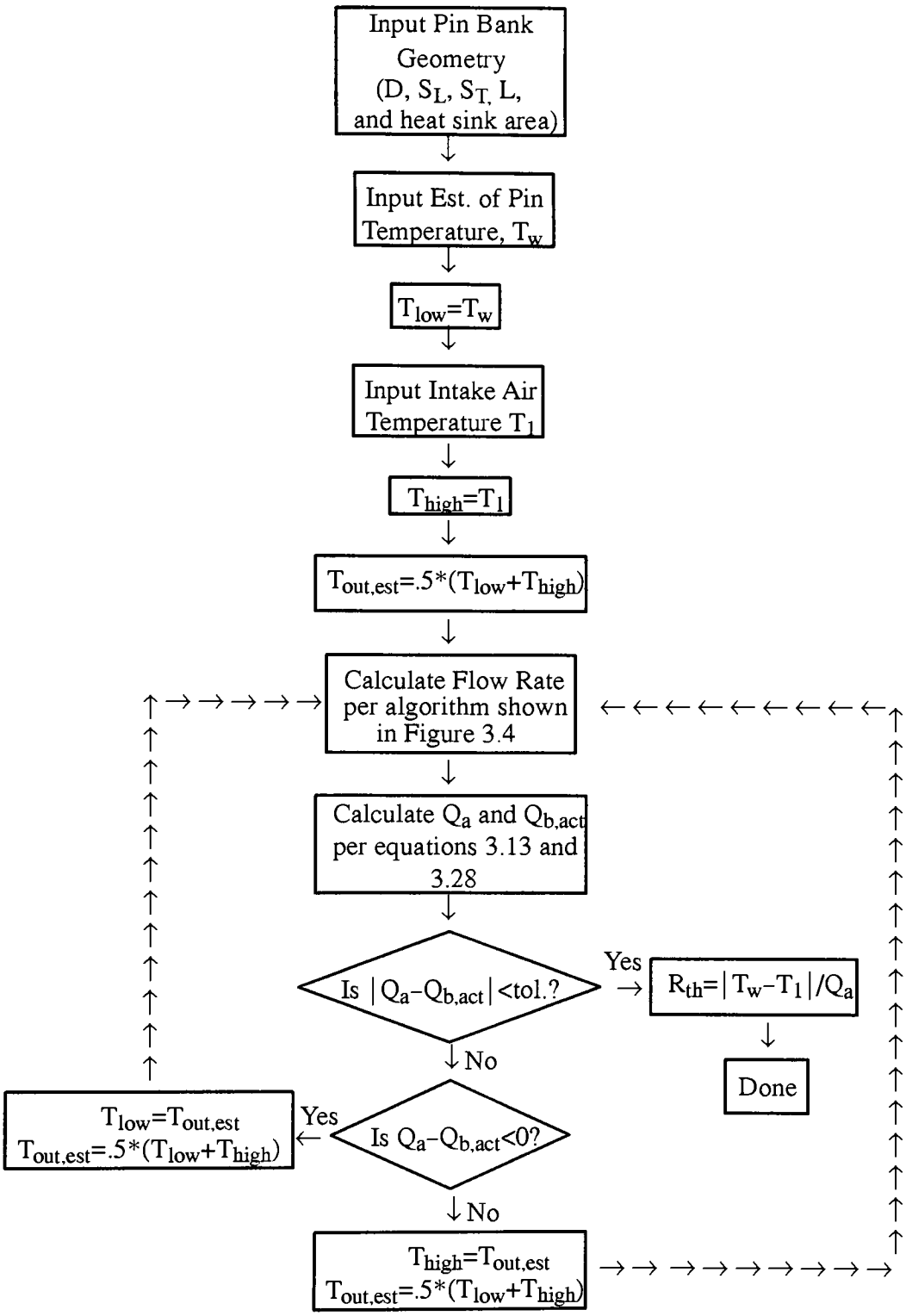

COPT.FOR Algorithm
Figure 3.6

3.3 Method to Compute Thermoelectric Module Performance

Referring to Figure 3.1, the following nodal equations can be written. For node 1,

$$T_1 = T_0 - Q_C * R_{PC} \tag{3.26}$$

For node 2,

$$T_2 = T_1 - Q_C * R_{IC} \tag{3.27}$$

For node 4,

$$T_4 = T_5 + R_{PH} * (Q_C + I * E) \tag{3.28}$$

And for node 3,

$$T_3 = T_4 + R_{IH} * (Q_C + I * E) \tag{3.29}$$

Noting that T_2 is the cold side temperature and that $T_3 - T_2$ is ΔT, and substituting this into equation 1.7, the cold side heat pumped by this particular system is given by

$$Q_C = 2N[\alpha\ I\ T_2 - I^2\varrho/2G - K(T_3-T_2)\ G] \tag{3.30}$$

where N is the number of thermocouple junctions, α is the Seebeck coefficient, I is the current flow, ϱ is the resistivity, G is the thermoelectric element geometry factor (area/length), and K is the device thermal conductance. Solving equation 1.6 for the current I and again noting that $T_3 - T_2$ is ΔT gives

$$I = (E/2N - \alpha(T_3-T_2))G/\varrho \tag{3.31}$$

where E is the voltage applied to the device and N, α, ϱ, G, and K have the definitions as in equation 3.30. Melcor Corp. (1993) whose thermoelectric modules were used in the heat pump that is the subject of this work, gives the following relationships for α, ϱ, and K as a function of the average absolute module temperature:

$$\begin{aligned} \alpha &= (\alpha_0 + \alpha_1\overline{T} + \alpha_2\overline{T}^2) \times 10^{-9} \\ \alpha_0 &= 22224.0\ \text{volts/K} \\ \alpha_1 &= 930.6\ \text{volts/K}^2 \\ \alpha_2 &= -.9905\ \text{volts/K}^3 \end{aligned} \tag{3.32}$$

$$\varrho = (\varrho_0 + \varrho_1\overline{T} + \varrho_2\overline{T}^2) \times 10^{-8}\ \text{ohm-cm} \tag{3.33}$$

$$\varrho_0 = 5112 \text{ ohm cm}$$

$$\varrho_1 = 163.4 \text{ ohm cm/K}$$

$$\varrho_2 = .6279 \text{ ohm cm/K}^2$$

$$K = (K_0 + K_1\overline{T} + K_2\overline{T}^2) \times 10^{-6} \text{ watt/cm-K} \tag{3.34}$$

$$K_0 = 62605 \text{ watt/cm-K}$$

$$K_1 = -277.7 \text{ watt/cm-K}^2$$

$$K_2 = .4131 \text{ watt/cm-K}^3$$

$$\overline{T} = .5 * (T_h + T_c) = .5 * (T_3 + T_4) \tag{3.35}$$

The system of equations 3.26 through 3.35 was solved using a program entitled HP.FOR (see Appendix C) which used a method of bisection to solve for unknowns. The inputs required by HP.FOR are the ambient temperature (T_0 and T_5), the cold side pin fin and interface resistances R_{PC} and R_{IC}, the hot side pin fin and interface resistances R_{PH} and R_{IH}, the driving voltage E, the number of thermoelectric module thermocouple junctions N, the maximum possible current draw of the system, the maximum possible heat pumped Q_C of the system, and the geometry factor G of the thermoelectric modules. The maximum system current draw and the maximum possible heat pumped values are simply rough estimates that may be obtained by examining the performance data of the thermoelectric module manufacturer. The program outputs are the current draw I, the nodal temperatures T_1 through T_4, the cold side heat pumped Q_C, and the hot side heat pumped Q_H.

HP.FOR actually employs two nested bisection algorithms to solve for the current draw I and the heat pumped Q_C of the system. The heat pumped by the system is first bounded by establishing that $Q_{Cmin} = 0$ and that Q_{Cmax} is whatever the maximum possible system heat pumping capacity has been estimated to be. It is best to err on the large side of

Q_{Cmax} to ensure that the solution is indeed bounded by Q_{Cmin} and Q_{Cmax}. A variable Q_{Cbar} is then created and initialized as

$$Q_{Cbar} = .5 * (Q_{Cmin} + Q_{Cmax}) \tag{3.36}$$

In a similar fashion, the system current draw is bounded by establishing that $I_{min}=0$ and I_{max} is a suitably large estimate of the upper bounds of system current draw. A variable I_{bar} is created and initialized to

$$I_{bar} = .5 * (I_{min} + I_{max}) \tag{3.37}$$

Based on these initial estimates of system current draw and heat pumped, the program solves equations 3.26 through 3.29 to obtain an initial estimate of the cold side temperature T_2 and the hot side temperature T_3. The average estimated temperature of the thermoelectric module is then calculated and then values for α, ϱ, and K are calculated from equations 3.32 through 3.35. Equation 3.31 is then solved to give a value of system current draw. If $I_{bar} - I$ is less than zero, the problem is rebounded by taking I_{min} equal to I_{bar}. If $I_{bar} - I$ is greater than zero, the problem is rebounded by taking I_{max} equal to I_{bar}. A convergence test is then applied to examine if the absolute difference between I_{min} and I_{max} is less than a tolerance value (in this case .000001 amps). If this is not the case, I_{bar} is recalculated, the hot and cold sides are recalculated, and finally equation 3.31 reevaluated so that $I_{bar} - I$ may be once again examined for absolute error. This process loop continues until an acceptable error in $|I_{bar} - I|$ is obtained. What has been achieved to this point is an accurate estimate of current associated with a crude estimate of Q_C. Now a better estimate of Q_C must be made.

At this point, equation 3.30 may be evaluated for Q_C based on the nodal temperatures T_2 and T_3 obtained from Q_{Cbar}, which is the estimated value of Q_C. HP.FOR evaluates the

quantity $|Q_{Cbar} - Q_C|$ to see if it is below a tolerance value (taken to be .0001 watts). If the expression is less than the tolerance value, HP.FOR terminates and returns the most recent values of Q_{Cbar}, I_{bar}, and the nodal temperatures T_1 through T_4. If an unacceptable error still exists in $|Q_{Cbar} - Q_{Csys}|$, the problem is rebounded in the following manner:

$$\begin{aligned} &\text{If } Q_{Cbar}-Q_C > 0, \text{ then} \\ &\quad Q_{Cmax} = Q_{Cbar} \\ &\quad \text{else} \\ &\quad Q_{Cmin} = Q_{Cbar} \end{aligned} \tag{3.38}$$

With the new boundaries of Q_C established, HP.FOR again calculates Q_{Cbar}, goes though the bisection method to establish a current draw based on the new value of Q_{Cbar}, and reexamines the error in $|Q_{Cbar} - Q_{Csys}|$. This process continues until an acceptable error in $|Q_{Cbar} - Q_C|$ is achieved. Figures 3.7a and 3.7b detail the algorithm of the FORTRAN program HP.FOR. Section 6.3 contains the results of many runs of HP.FOR that were performed as part of the process meant to maximize the heat pumped by the system.

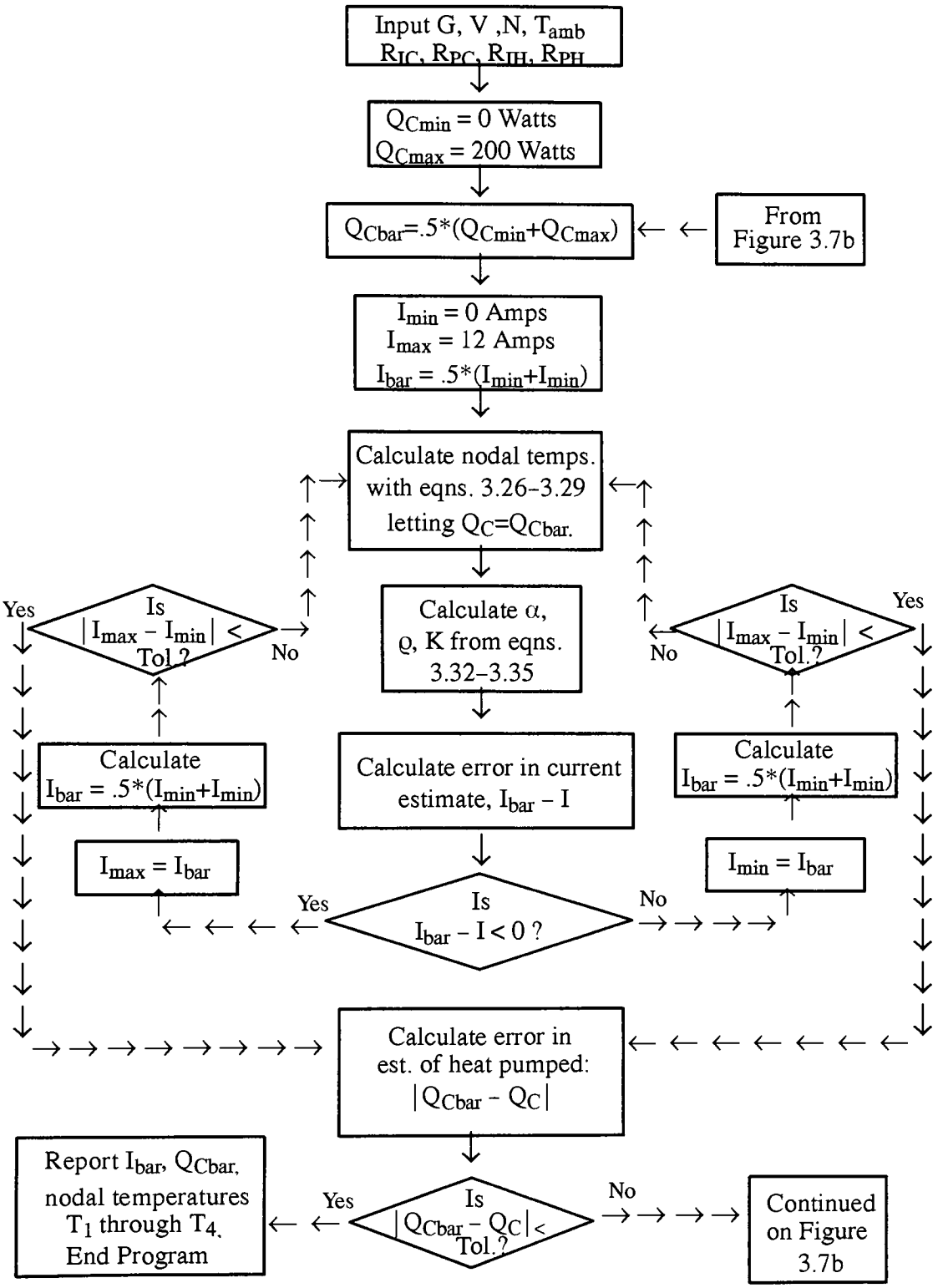

Flow Chart of HP.FOR (1 of 2 pages)
Figure 3.7

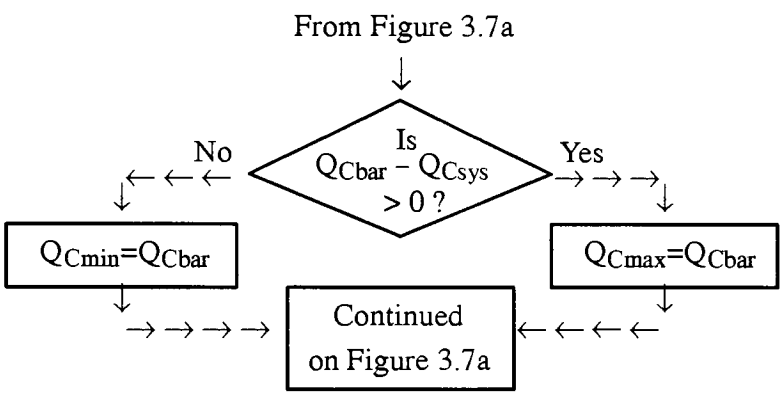

Flow Chart of HP.FOR (continued)
Page 2 of 2
Figure 3.7

CHAPTER 4

NUMERICAL MODEL OF PIN FIN HEAT EXCHANGE SURFACE

4.1 Governing Equations of Fluid Dynamics and Heat Transfer for a Cylinder in Cross Flow

Fox (1978) gives the momentum equations for incompressible flow and invariant viscosity properties in the x and y directions as

$$\varrho \left(\frac{\partial u}{\partial t} + u\frac{\partial u}{\partial x} + v\frac{\partial u}{\partial y} + w\frac{\partial u}{\partial y}\right) = \varrho B_x - \frac{\partial p}{\partial x} + \mu\left(\frac{\partial^2 u}{\partial x^2} + \frac{\partial^2 u}{\partial y^2} + \frac{\partial^2 u}{\partial z^2}\right) \quad (4.1)$$

and

$$\varrho \left(\frac{\partial v}{\partial t} + u\frac{\partial v}{\partial x} + v\frac{\partial v}{\partial y} + w\frac{\partial v}{\partial y}\right) = \varrho B_y - \frac{\partial p}{\partial y} + \mu\left(\frac{\partial^2 v}{\partial x^2} + \frac{\partial^2 v}{\partial y^2} + \frac{\partial^2 v}{\partial z^2}\right) \quad (4.2)$$

where ϱ is the fluid mass density, u is the x component of fluid velocity, v is the y-component of fluid velocity, μ is the fluid viscosity, p is the fluid pressure, and B_x and B_y are the x and y components of body force. Under steady state conditions, negligible body forces, and no variation in the z direction, equations 4.1 and 4.2 become

$$\varrho \left(u\frac{\partial u}{\partial x} + v\frac{\partial u}{\partial y}\right) = -\frac{\partial p}{\partial x} + \mu\left(\frac{\partial^2 u}{\partial x^2} + \frac{\partial^2 u}{\partial y^2}\right) \quad (4.3)$$

and

$$\varrho \left(u\frac{\partial v}{\partial x} + v\frac{\partial v}{\partial y}\right) = -\frac{\partial p}{\partial y} + \mu\left(\frac{\partial^2 v}{\partial x^2} + \frac{\partial^2 v}{\partial y^2}\right) \quad (4.4)$$

Under conditions of constant fluid density and no viscous dissipation, Bermeister (1983) gives the energy equation as

$$\varrho\, c_p \left(\frac{\partial T}{\partial t} + u\frac{\partial T}{\partial x} + v\frac{\partial T}{\partial y} + v\frac{\partial T}{\partial y}\right) = k\left(\frac{\partial^2 T}{\partial x^2} + \frac{\partial^2 T}{\partial y^2} + \frac{\partial^2 T}{\partial z^2}\right) \quad (4.5)$$

where c_p is the fluid heat capacity, T is the temperature, k is the thermal conductivity, and the same definitions for ϱ, u, and v found in equations 4.1 and 4.2 also hold in equation 4.5. Under steady state conditions and with no variation in the z direction, equation 4.5 becomes

$$\varrho\, c\, (u\frac{\partial T}{\partial x} + v\frac{\partial T}{\partial y}) = k\, (\frac{\partial^2 T}{\partial x^2} + \frac{\partial^2 T}{\partial y^2}) \tag{4.6}$$

Finally, the continuity equation in two dimensions under steady, incompressible flow conditions is given by

$$\frac{\partial u}{\partial x} + \frac{\partial v}{\partial y} = 0 \tag{4.7}$$

A wide class of fluid/thermal problems can be easily studied by working with the appropriate nondimensionalized forms of the governing equations. These specialized forms of equations 4.3, 4.4, 4.6, and 4.7 will be derived and discussed at this time. The following quantities are defined as characteristic parameters of the problem:

$$D = \text{cylinder diameter} \tag{4.8}$$

$$U = \text{air inlet velocity} \tag{4.9}$$

$$T_w = \text{cylinder wall temperature} \tag{4.10}$$

$$T_\infty = \text{air inlet temperature} \tag{4.11}$$

From these, the following nondimensional parameters may be created:

$$u^* = \frac{u}{U} \tag{4.12}$$

$$v^* = \frac{v}{U} \tag{4.13}$$

$$x^* = \frac{x}{D} \tag{4.14}$$

$$y^* = \frac{y}{D} \tag{4.15}$$

$$T^* = \frac{(T-T_\infty)}{(T_w-T_\infty)} \tag{4.16}$$

$$p^* = \frac{p}{\varrho U^2} \tag{4.17}$$

$$Re_D = \frac{\varrho UD}{\mu} \tag{4.18}$$

$$Pr = \frac{\mu c}{k} \tag{4.19}$$

$$Nu = \frac{hD}{k} \tag{4.20}$$

A nondimensionalized version of the x-momentum equation may be created by first dividing equation 4.3 by ϱ which gives

$$\left(u \frac{\partial u}{\partial x} + v \frac{\partial v}{\partial y} \right) = -\frac{\partial (p/\varrho)}{\partial x} + \frac{\mu}{\varrho} \left(\frac{\partial^2 u}{\partial x^2} + \frac{\partial^2 v}{\partial y^2} \right) \tag{4.21}$$

Equation 4.21 is now divided by U^2 which gives

$$\frac{u}{U} \frac{\partial}{\partial x} \left(\frac{u}{U} \right) + \frac{v}{U} \frac{\partial}{\partial y} \left(\frac{v}{U} \right) = -\frac{\partial}{\partial x} \left(\frac{p}{\varrho U^2} \right) + \frac{\mu}{\varrho U^2} \left(\frac{\partial^2 u}{\partial x^2} + \frac{\partial^2 v}{\partial y^2} \right) \tag{4.22}$$

Equations 4.14 and 4.15 are rearranged to give the following expressions:

$$x^* D = x \tag{4.23}$$

$$y^* D = y \tag{4.24}$$

The differential of equations 4.23 and 4.24 is now taken which gives

$$D \, \partial x^* = \partial x \tag{4.25}$$

$$D \, \partial y^* = \partial y \tag{4.26}$$

A similar operation is performed on equations 4.12 and 4.13 to give

$$U \, \partial u^* = \partial u \tag{4.27}$$

$$U \, \partial v^* = \partial v \tag{4.28}$$

Equations 4.25, 4.26, 4.27, and 4.28 are substituted into equation 4.22 and simplified with equation 4.17 to give

$$\frac{u^*}{D} \frac{\partial u^*}{\partial x^*} + \frac{v^*}{D} \frac{\partial u^*}{\delta y^*} = -\frac{1}{D} \frac{\partial p^*}{\partial x^*} + \frac{\mu}{\varrho U D^2} \left(\frac{\partial^2 u^*}{\partial x^{*2}} + \frac{\partial^2 u^*}{\partial y^{*2}} \right) \tag{4.29}$$

Equation 4.29 is now multiplied by D to give

$$u^* \frac{\partial u^*}{\partial x^*} + v^* \frac{\partial v^*}{\partial y^*} = -\frac{\partial p^*}{\partial x^*} + \frac{\mu}{\varrho D U} \left(\frac{\partial^2 u^*}{\partial x^{*2}} + \frac{\partial^2 u^*}{\partial y^{*2}} \right) \tag{4.30}$$

Finally, the definition of the Reynolds number (Re_D) is applied per equation 4.18 to give the nondimensionalized form of the x-momentum equation, which is

$$u^* \frac{\partial u^*}{\partial x^*} + v^* \frac{\partial u^*}{\partial y^*} = -\frac{\partial p^*}{\partial x^*} + \frac{1}{Re_D} \left(\frac{\partial^2 u^*}{\partial x^{*2}} + \frac{\partial^2 u^*}{\partial y^{*2}} \right) \quad (4.31)$$

The nondimensional y-momentum equation, which follows, may be created by a similar approach:

$$u^* \frac{\partial v^*}{\partial x^*} + v^* \frac{\partial v^*}{\partial y^*} = -\frac{\partial p^*}{\partial y^*} + \frac{1}{Re_D} \left(\frac{\partial^2 v^*}{\partial x^{*2}} + \frac{\partial^2 v^*}{\partial y^{*2}} \right) \quad (4.32)$$

To create the nondimensional form of the energy equation, the differential of equation 4.16 is taken and the result rearranged to give

$$(T_w - T_\infty)\, \partial T^* = \partial T \quad (4.33)$$

Equation 4.33 is substituted into equation 4.6 to give

$$\varrho\, c\, (T_w - T_\infty) \left(u \frac{\partial T^*}{\partial x} + v \frac{\partial T^*}{\partial y} \right) = k\, (T_w - T_\infty) \left(\frac{\partial}{\partial x} \left(\frac{\partial T^*}{\partial x} \right) + \frac{\partial}{\partial y} \left(\frac{\partial T^*}{\partial y} \right) \right) \quad (4.34)$$

The quantity $(T_w - T\infty)$ is canceled from both sides of equation 4.34 to give

$$\left(\varrho\, c \left(u \frac{\partial T^*}{\partial x} + v \frac{\partial T^*}{\partial y} \right) = k \left(\frac{\partial}{\partial x} \left(\frac{\partial T^*}{\partial x} \right) + \frac{\partial}{\partial y} \left(\frac{T^*}{\partial y} \right) \right) \right. \quad (4.35)$$

Equations 4.25 and 4.26 are substituted into Equation 4.35 to give

$$\frac{\varrho\, c}{D} \left(u \frac{\partial T^*}{\partial x^*} + v \frac{\partial T^*}{\partial y^*} \right) = \frac{k}{D^2} \left(\frac{\partial^2 T^*}{\partial x^{*2}} + \frac{\partial^2 T^*}{\partial y^{*2}} \right) \quad (4.36)$$

The left side of Equation 4.36 is now multiplied and divided by U to give equation 4.37

$$\frac{\varrho\, c\, U}{D} \left(\frac{u}{U} \frac{\partial T^*}{\partial x^*} + \frac{v}{U} \frac{\partial T^*}{\partial y^*} \right) = \frac{k}{D^2} \left(\frac{\partial^2 T^*}{\partial x^*} + \frac{\partial^2 T^*}{\partial y^*} \right) \quad (4.37)$$

Equation 4.37 is now simplified with equations 4.14 and 4.15 and rearrange to give

$$\frac{\mu\, c}{k} \frac{D\, U\, \varrho}{\mu} \left(u^* \frac{\partial T^*}{\partial x^*} + v^* \frac{\partial T^*}{\partial y^*} \right) = \frac{\partial^2 T^*}{\partial x^{*2}} + \frac{\partial^2 T^*}{\partial y^{*2}} \quad (4.38)$$

Finally, equation 4.38 is simplified by the definitions of the Prandtl and Reynolds numbers provided by equations 4.19 and 4.20 to give the nondimensionalized form of the energy equation, which is

$$\Pr \mathrm{Re}_D\left(u^* \frac{\partial T^*}{\partial x^*} + v^* \frac{\partial T^*}{\partial y^*}\right) = \frac{\partial^2 T^*}{\partial x^{*2}} + \frac{\partial^2 T^*}{\partial y^{*2}} \tag{4.39}$$

The nondimensional form of the continuity equation can now be obtained. Both sides of equation 4.7 are divided by U to yield

$$\frac{\partial}{\partial x}\left(\frac{u}{U}\right) + \frac{\partial}{\partial y}\left(\frac{v}{U}\right) = 0 \tag{4.40}$$

Equations 4.25 and 4.26 are substituted into equation 4.40 to give

$$\frac{\partial}{D\partial x^*}\left(\frac{u}{U}\right) + \frac{\partial}{D\partial y^*}\left(\frac{v}{U}\right) = 0 \tag{4.41}$$

Equation 4.41 is then multiplied by D and simplified per equations 4.27 and 4.28 to give the nondimensional form of the continuity equation, which is

$$\frac{\partial u^*}{\partial x^*} + \frac{\partial v^*}{\partial y^*} = 0 \tag{4.42}$$

By comparing terms of the dimensionless (equations 4.31, 4.32, 4.39 and 4.42) to the dimensional forms of the governing equations (4.3, 4.4, 4.6, and 4.7), the following transformations must be performed to a particular problem to take it from the dimensional to the nondimensional realm:

$$\varrho = 1 \text{ (from the momentum equation)} \tag{4.43}$$

$$\mu = 1/\mathrm{Re} \text{ (from the momentum equation)} \tag{4.44}$$

$$c_p = \mathrm{Re}_D^* \Pr \text{ (from the energy balance equation)} \tag{4.45}$$

$$k = 1 \text{ (from the energy balance equation)} \tag{4.46}$$

The heat flux from a heated or cooled cylinder in cross flow may be examined in nondimensional terms as well. In dimensional terms, heat flux is given by

$$q'' = h\,(T_w - T_\infty) \tag{4.47}$$

where T_w is the temperature of the cylinder wall, T_∞ is the ambient temperature of the fluid moving over the cylinder, and h is the local convective heat transfer coefficient. At the surface of the heated cylinder (assuming 2-D conditions), the heat flux is also given by

$$q'' = -k\nabla T = -k\left(\frac{\partial T}{\partial x}\hat{i} + \frac{\partial T}{\partial y}\hat{j}\right) \tag{4.48}$$

Equation 4.48 may be rewritten in terms of T^*, x^*, and y^* with the use of equations 4.25, 4.26, and 4.33 to obtain

$$q'' = -\frac{k\,(T_w - T_\infty)}{D}\left(\frac{\partial T^*}{\partial x^*}\hat{i} + \frac{\partial T^*}{\partial y^*}\hat{j}\right) = -\frac{k\,(T_w - T_\infty)}{D}\nabla T^* \tag{4.49}$$

The quantity ∇T^* is the nondimensional temperature gradient of the system and may be also thought of as the nondimensional heat flux, which will be called q''^*. Thus,

$$q'' = -k\,\frac{(T_w - T_\infty)}{D}\,q''^* \tag{4.50}$$

Equation 4.47 may now be substituted into equation 4.50 to yield

$$h\,(T_w - T_\infty) = -\frac{k}{D}(T_1 - T_0)q''^* \tag{4.51}$$

Finally, if equation 4.51 is now solved for q''^* and the definition of the Nusselt number from equation 4.20 is employed, the following equation is obtained:

$$q''^* = -\frac{hD}{k} = -Nu \tag{4.52}$$

Therefore, if the problem is nondimensionalized in the method previously described, the convective heat transfer coefficient of the system is equivalent in magnitude to the Nusselt number of the system. Conveniently, the Nusselt number is the most common means encountered in the literature of quantifying thermal performance of heated pin or tube bank systems in a wide variety of fluid flow conditions.

4.2 Single Cylinder in Cross Flow

Before constructing a FIDAP model of a complex array of heated pins or cylinders in a fluid cross flow, variations on a simple model consisting of a single heated pin in cross flow were constructed and solved. This single pin configuration has been studied quite extensively, both from a theoretical and an experimental standpoint. It therefore offers a very

good opportunity to evaluate FIDAP's prediction accuracy as well as its sensitivity to various modeling parameters. An understanding of these parameters will assist in the creation, debug, and verification of a model of an array of heated cylinders in fluid cross flow.

Figure 4.1 shows the mesh design which was the basis for the parameter sensitivity study. The problem was evaluated in the nondimensionalized form described in section 4.1. Specifically, the cylinder has a dimensionless diameter of 1.0 per equation 4.14 and 4.15 with a dimensionless surface temperature of +1.0 units per equation 4.16. The mesh boundaries extend from -16 to +20 diameters in the x-direction and from -7 to +7 diameters in the y-direction. The center of the cylinder resides at coordinates (0,0). There is a flow of fluid entering the left vertical boundary of the model with a dimensionless x-velocity of 1.0 units per equation 4.12, a dimensionless y-velocity of 0.0 per equation 4.13, and a dimensionless temperature of 0. The upper and lower horizontal model boundaries are defined to have a dimensionless fluid velocities of 1.0 in the x-direction and 0 in the y-direction. These boundaries represent distances from the cylinder in the y-direction beyond which the fluid flow is undisturbed by the presence of the cylinder. There is a no-slip boundary condition enforced on the cylinder surface (i.e., x-velocity is 0 and y-velocity is 0). All sensitivity studies were performed with a flow over the cylinder of $Re_D = 100$ and the fluid was taken to be air. These constraints in turn define the viscosity to be .01 and the specific heat to be 70.7 per equations 4.44 and 4.45 (air is taken to be at 300° K, therefore $c = Re * Pr = 100 * .707 = 70.7$). The thermal conductivity and density of air are defined to be equal to 1 by equations 4.43 and 4.46. There are a total of 448 elements in this basis model.

The solution of this basic model yielded a Nusselt number of 4.205. The following is a description of the various plots obtained from the model which are included in the

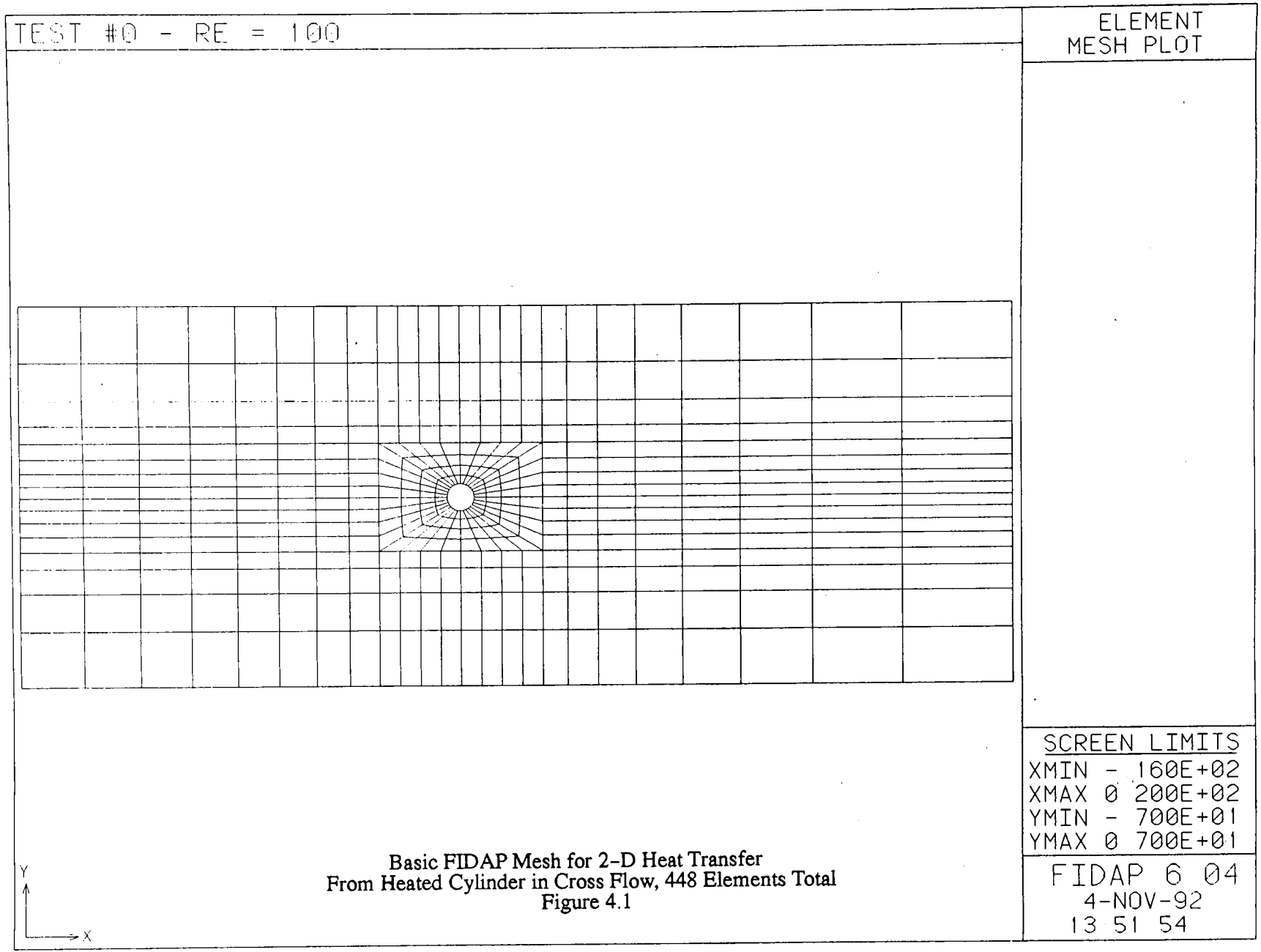

Basic FIDAP Mesh for 2-D Heat Transfer
From Heated Cylinder in Cross Flow, 448 Elements Total
Figure 4.1

following figures:

1. Temperature contour plot showing T^* from 0 to 1, Figure 4.2.
2. Temperature contour plot showing T^* from 0 to 1 with a close up view of the cylinder, Figure 4.3.
3. Temperature contour plot showing T^* from -.0474 to 0, Figure 4.4.
4. Temperature contour plot showing location of minimum values of T^*, Figure 4.5.
5. Plot of heat flux versus position around the cylinder, Figure 4.6.
6. Vector plot of heat flux, Figure 4.7.
7. Streamline contour plot, Figure 4.8.
8. Contour plot of P^*, Figure 4.9.
9. Contour plot of P^* showing close up view of the cylinder, Figure 4.10.
10. Velocity vector plot, Figure 4.11.

Figures 4.4 and 4.5 are especially noteworthy. These plots show the presence of nondimensional temperatures in the flow field significantly less than that of the incoming flow, a physical impossibility. Anomalies of this type are indicative of a finer mesh being required in certain areas of the model.

The Nusselt number of 4.205 obtained at $Re_D = 100$ is low by about 20% according to most modern references. Morgan (1975) has studied the results and/or correlations of approximately 75 authors that have investigated the heat transfer from a single heated cylinder in crossflow. Table 4.1 details several applicable correlations evaluated at $Re_D = 100$ (and above) for purposes of comparison, all of which were a part of the study. An

SENSIVITIY TEST #0 - RE = 100

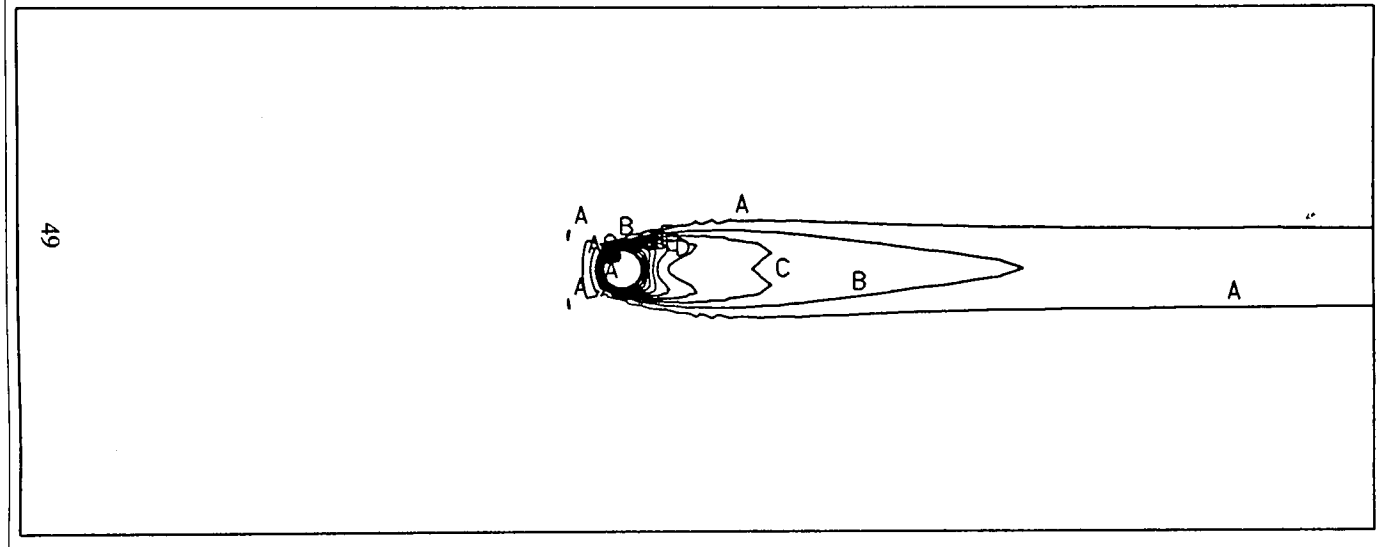

Contour Plot of T^* from 0 to 1
Obtained from Basic Model
Figure 4.2

Y
X

TEMPERATURE
CONTOUR PLOT

LEGEND

A - 0.5000E-01
B - 0.1500E+00
C - 0.2500E+00
D - 0.3500E+00
E - 0.4500E+00
F - 0.5500E+00
G - 0.6500E+00
H - 0.7500E+00
I - 0.8500E+00
J - 0.9500E+00

MINIMUM
-0 47420E-01
MAXIMUM
0 10000E+01

SCREEN LIMITS
XMIN - 160E+02
XMAX 0 200E+02
YMIN - 700E+01
YMAX 0 700E+01

FIDAP 6 04
7-DEC-92
13 21 19

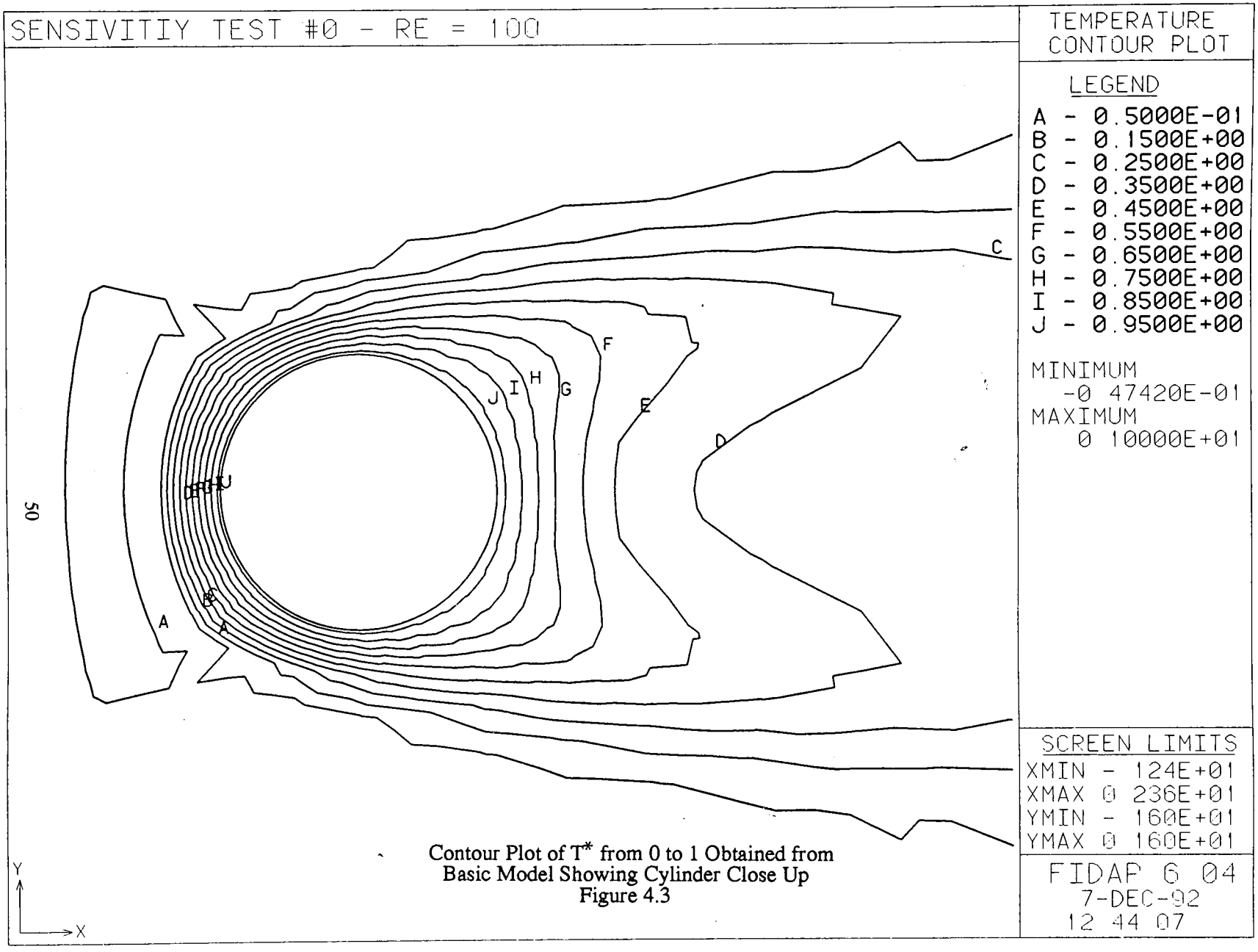

Contour Plot of T* from 0 to 1 Obtained from Basic Model Showing Cylinder Close Up
Figure 4.3

SENSIVITIY TEST #0 - RE = 100

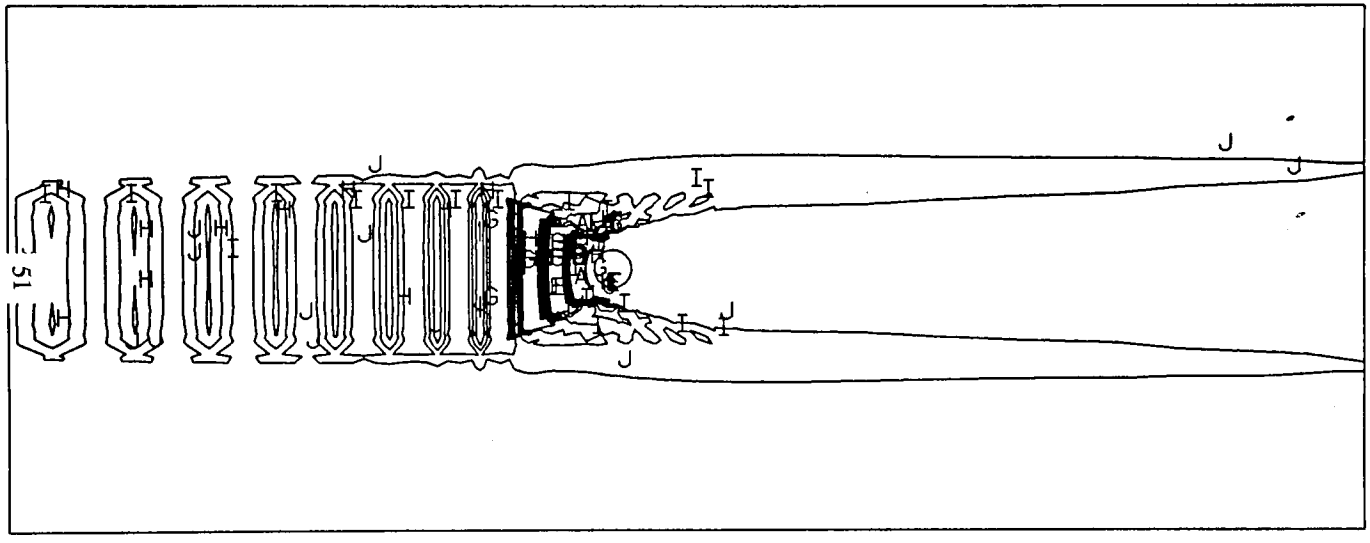

TEMPERATURE CONTOUR PLOT

LEGEND

A - -.4465E-01
B - -.3995E-01
C - -.3525E-01
D - -.3055E-01
E - -.2585E-01
F - -.2115E-01
G - -.1645E-01
H - -.1175E-01
I - -.7050E-02
J - -.2350E-02

MINIMUM
-0 47420E-01
MAXIMUM
0 10000E+01

SCREEN LIMITS
XMIN - 160E+02
XMAX 0 200E+02
YMIN - 700E+01
YMAX 0 700E+01

FIDAP 6 04
7-DEC-92
12 27 16

Contour Plot of T^* from -.0474 to 0
Obtained from Basic Model
Figure 4.4

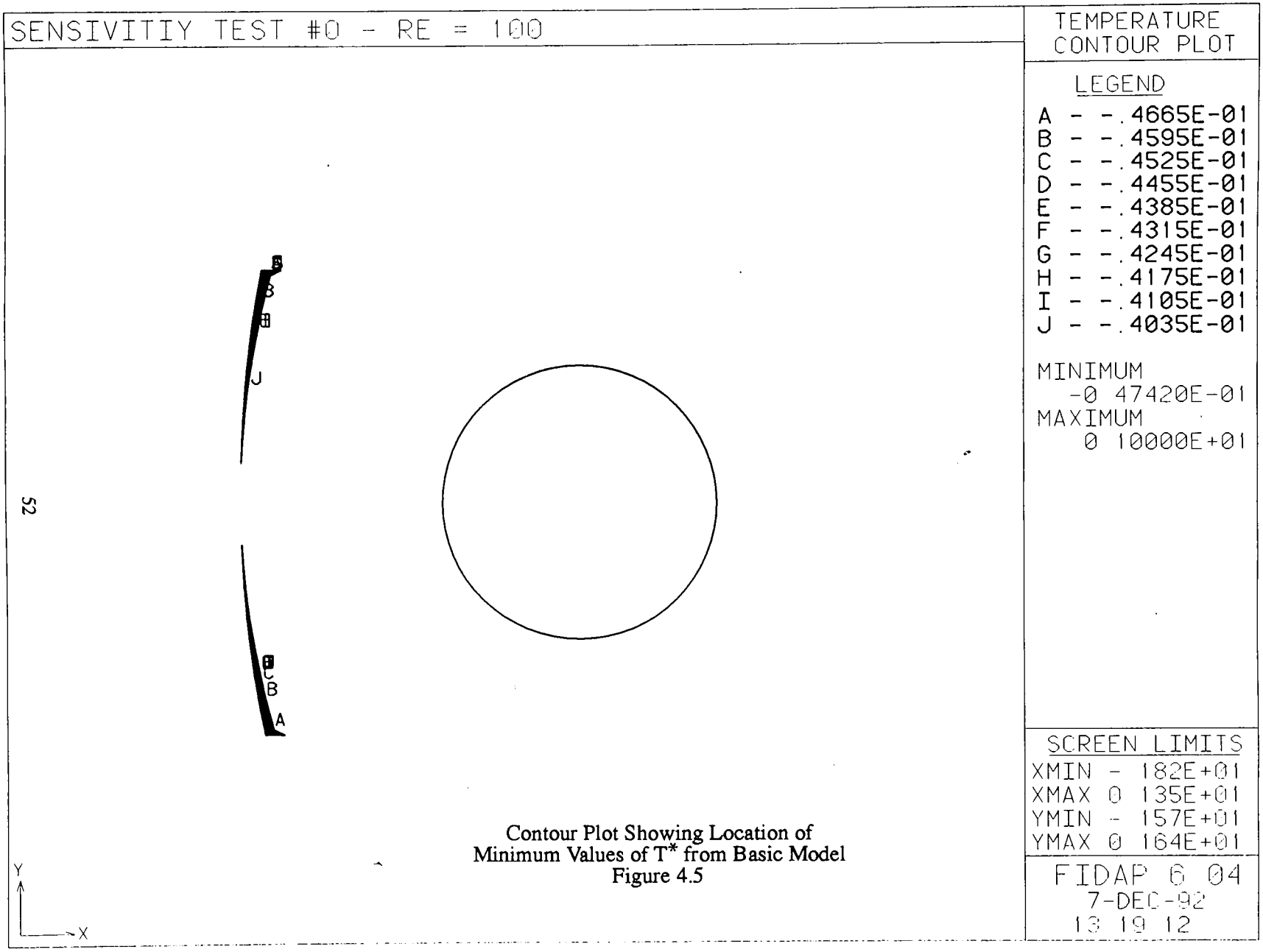

Contour Plot Showing Location of
Minimum Values of T^* from Basic Model
Figure 4.5

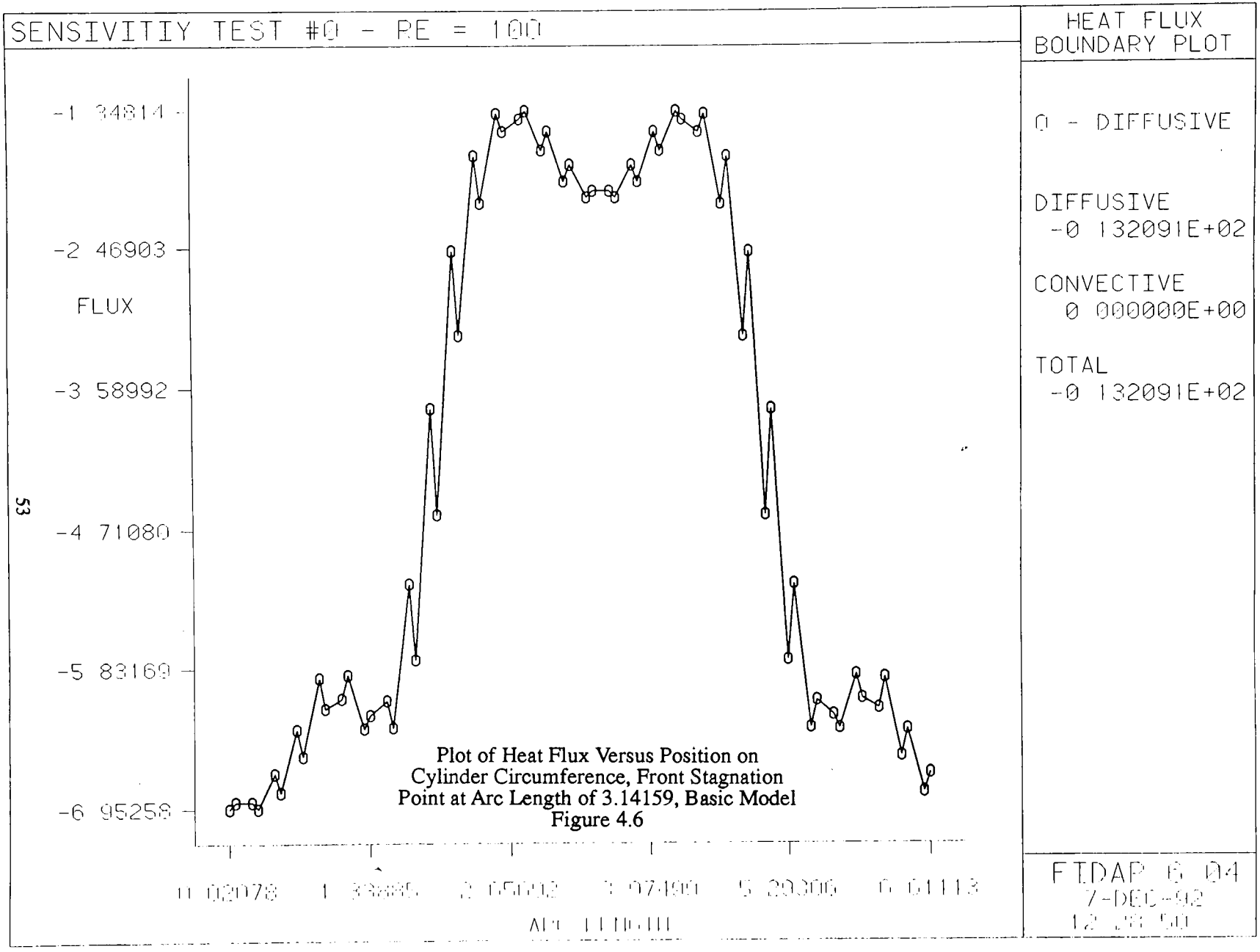

Plot of Heat Flux Versus Position on Cylinder Circumference, Front Stagnation Point at Arc Length of 3.14159, Basic Model
Figure 4.6

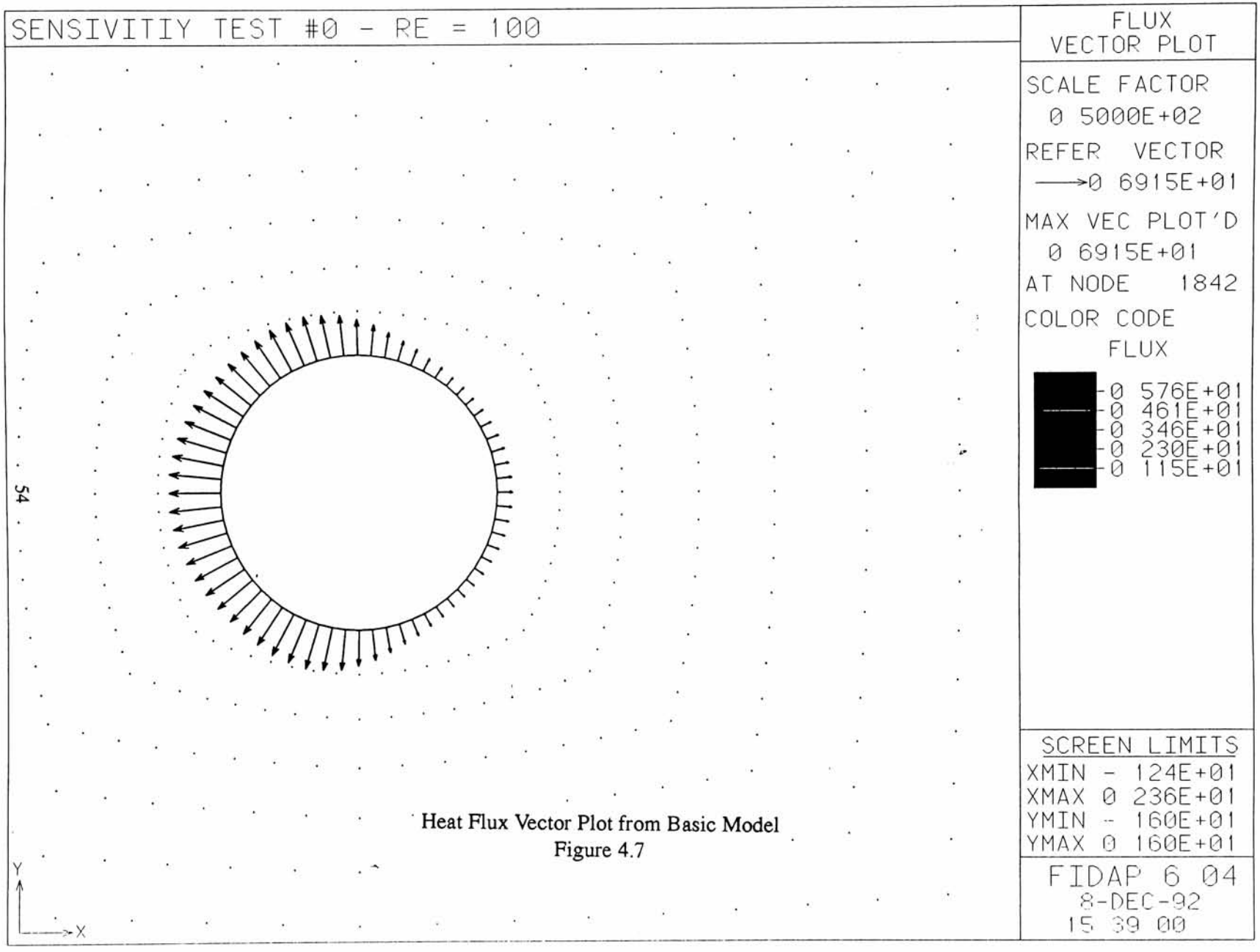

Heat Flux Vector Plot from Basic Model
Figure 4.7

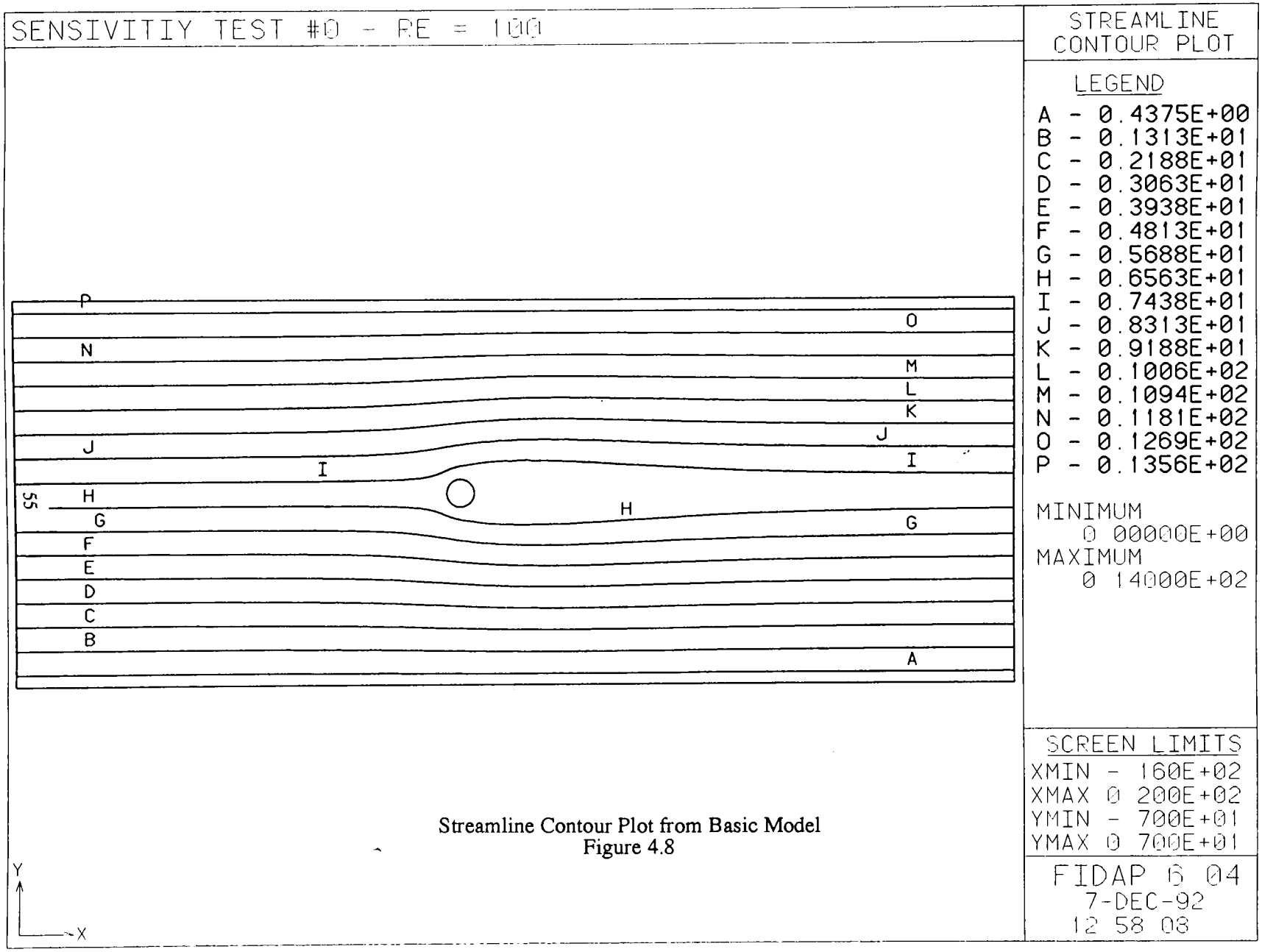

Streamline Contour Plot from Basic Model
Figure 4.8

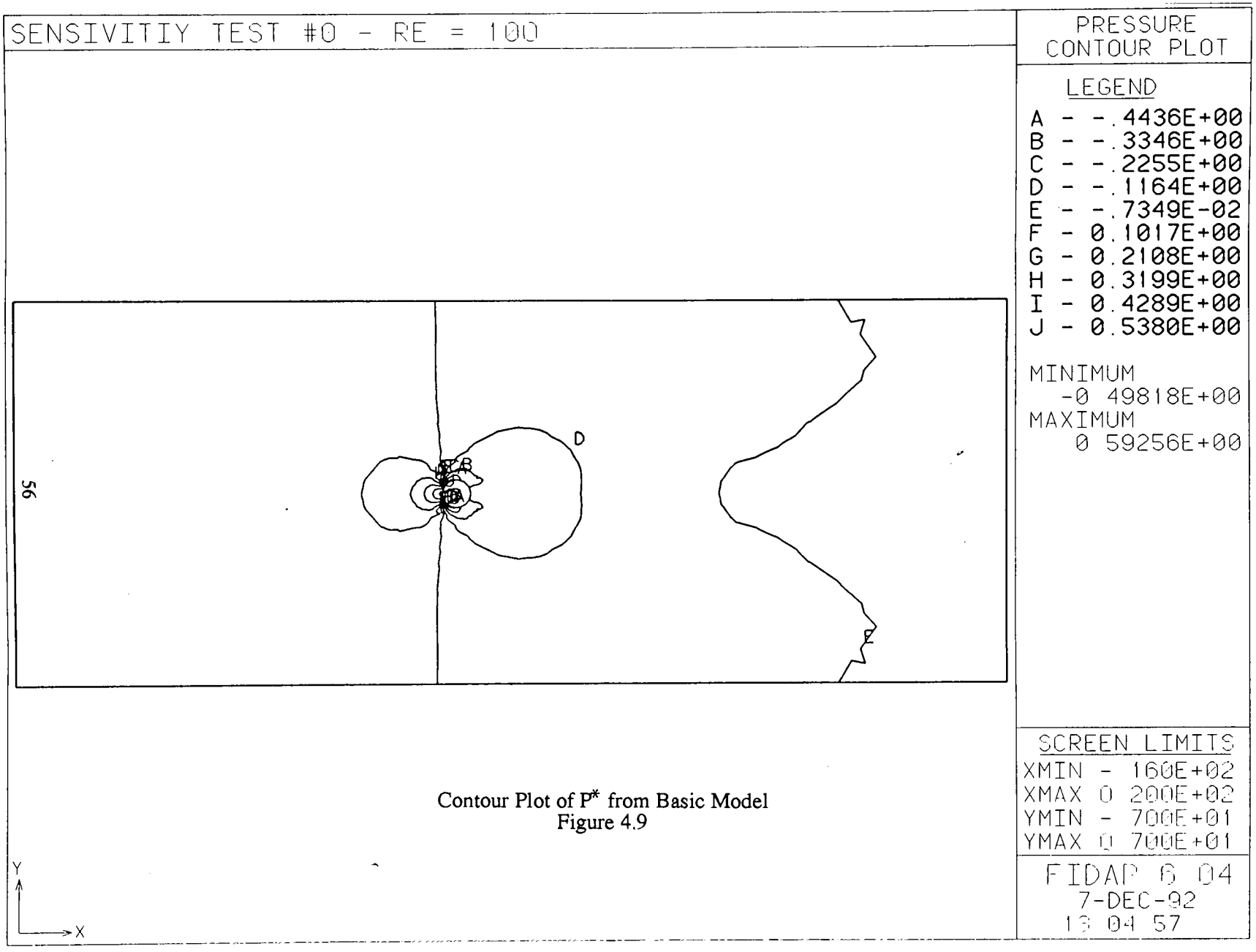

Contour Plot of P* from Basic Model
Figure 4.9

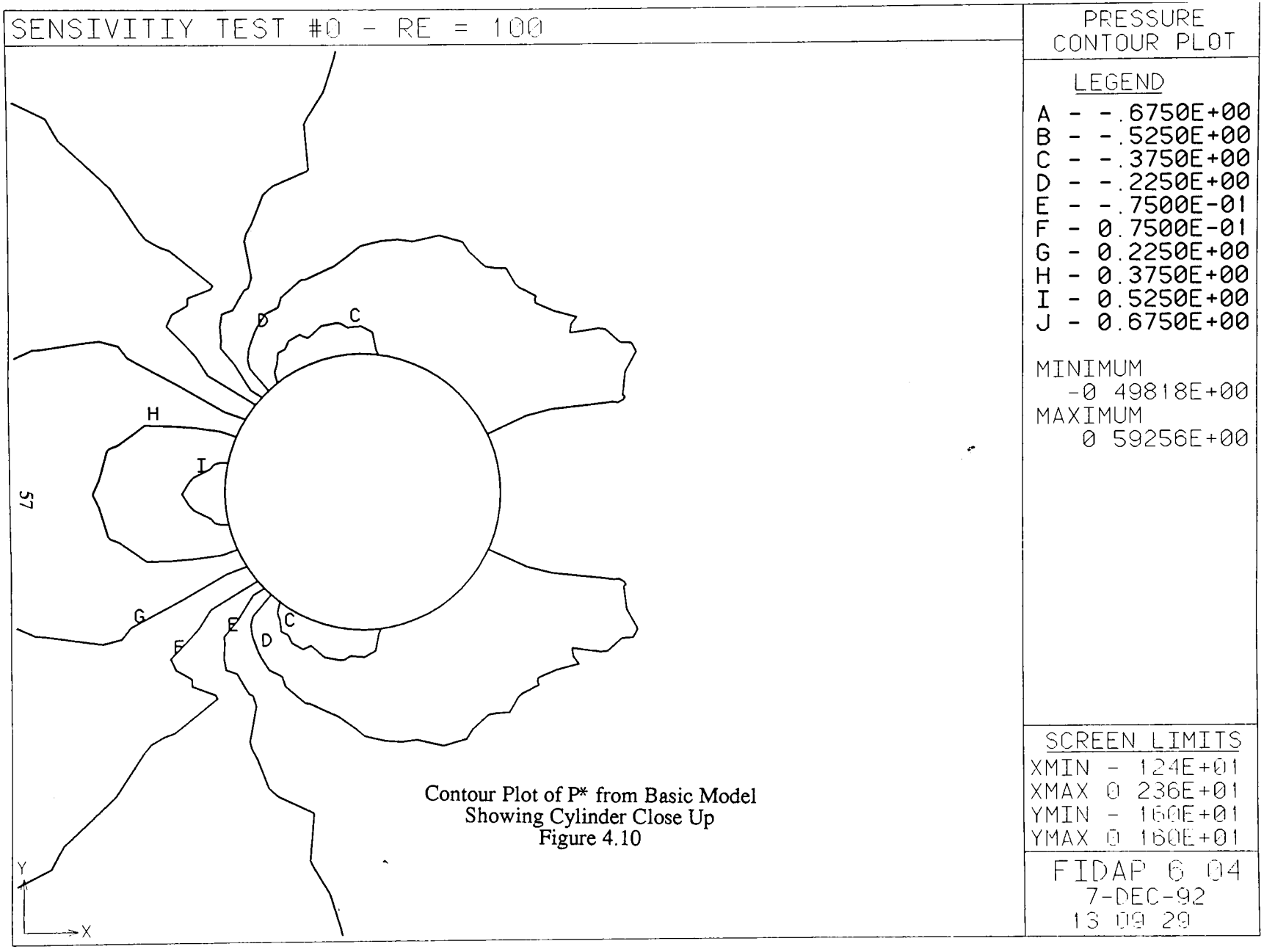

Contour Plot of P* from Basic Model
Showing Cylinder Close Up
Figure 4.10

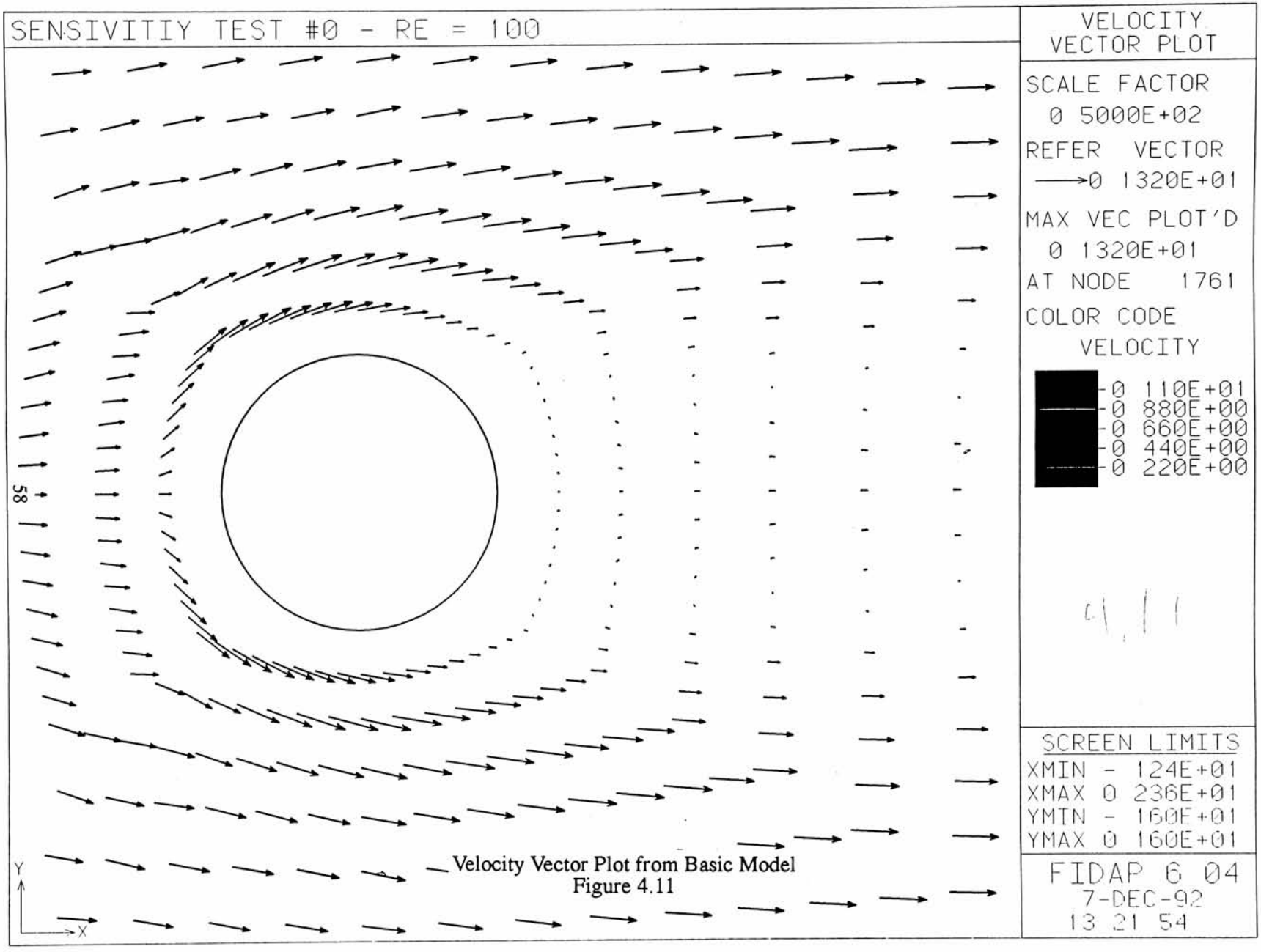

Velocity Vector Plot from Basic Model
Figure 4.11

appropriate correlation was developed by Morgan (1975) where noted if the original researcher did not develop an equation to fit his data set.

The results of Table 4.1 originate from correlations having the form

$$Nu = C + D * Re_D^n * Pr^p \tag{4.53}$$

where C, D, n, and p are constants which vary from author to author. Morgan (1975) notes that, depending on Reynolds number, the experimentally determined values of Nusselt number differ from 10% to 29% from author to author and the results of the various correlations across their respective ranges of Reynolds number vary between 10% and 46% across the literature reviewed. It is stated that the differences are due to experimental anomalies arising from the use of various cylinder length-to-diameter ratios, the effects of wind tunnel free stream turbulence, and the different wind tunnel geometries used by the various researchers. The last entry in Table 4.1 reflects the results of a correlation developed by Morgan (1975) which takes into account the magnitude of these errors and is said to have a maximum uncertainty of +/- 5%.

Table 4.2 lists the various sensitivity studies that were performed on the basic single pin model to understand how mesh density, boundary conditions, and convergence criteria affect the predicted Nusselt number. The resulting pressure, temperature, velocity, streamline and heat flux plots were examined for each of the studies for anomalies (such as instances of T^* less than zero) which may indicate a poorly constructed model.

Studies 1 through 5 shown in Table 4.2 investigated the effects of increasing mesh density in various regions of the model. The only mesh refinement that played a significant role (that is, greater than a 1% change in the predicted value of Nusselt number) in the performance of the model was that of increasing concentric density around the cylinder.

Table 4.1–Comparison of Nusselt Number Predicted by FIDAP versus Correlations by Various Authors Cited by Morgan (1975) for a Single Heated Cylinder in Cross Flow Across a Range of Reynolds Numbers

Re	FIDAP (refined model)	Eckert & Soehngren (1952)	Zhukauskas (1972)	Krall & Eckert (1973)	Wylie & Lalas (1973)	Hilpert (1933)	Morgan (1975)
100	5.21	5.23	4.53	5.32	5.07	5.26	5.10
200	7.27	7.22	6.27	7.32	6.98	7.26	7.07
300	8.86	8.74	7.59	8.82	8.41	8.77	8.56
350	9.52	9.41	8.16	9.47	9.03	9.43	9.20
400	10.10	10.03	8.69	10.07	9.60	10.03	9.80
450	10.61	10.61	9.18	10.63	10.13	10.60	10.36

Table 4.2–Sensitivity Studies performed on Basic Single Pin Model

Study Number	Comments (all changes are with respect to basic model, study number 1)	Predicted Nusselt Number
1	Basic model, 448 elements	4.21
2	Double mesh density concentric to cylinder, 576 elements	5.21
3	Quadruple mesh density concentric to cylinder, 704 elements	5.24
4	Increase mesh density directly in front of cylinder	4.18
5	Increase mesh density above and below cylinder	4.20
6	Set du/dy = 0 and dv/dx = 0 at upper and lower boundaries	4.21
7	Double mesh density concentric to cylinder and change convergence criteria from .001 to .0001	5.25
8	Decrease mesh granularity around cylinder circumference from 32 divisions to 24 divisions	5.22
9	Study 2 mesh run at $Re_D = 200$	7.27
10	Study 2 mesh run at $Re_D = 300$	8.86
11	Study 2 mesh run at $Re_D = 350$	9.52
12	Study 2 mesh run at $Re_D = 400$	10.10
13	Study 2 mesh run at $Re_D = 450$	10.61

Figure 4.12 shows such a mesh that has two times the density in the region around the cylinder than that of Figure 4.1. The predicted value of Nusselt number at $Re_D = 100$ of this particular mesh was 5.214. This agrees quite well with the majority of the results listed in Table 4.1 and differs from Morgan's (1975) correlation by only 2.2%. Any attempts to further refine the mesh in this manner did not significantly affect the predicted value of Nusselt number (that is, much less than 1% change in results) at $Re_D = 100$.

Figures 4.13 through 4.22 are a series of FIDAP plots from the refined model depicted in Figure 4.12. These plots are the same series shown for the basic model in Figures 4.2 through 4.11. An examination of Figures 4.3 and 4.14 shows that the geometry of the temperature contours produced by the refined model is much less erratic than that produced by the basic model. The tighter packing of the temperature contour lines around the stagnation point of the cylinder in the refined model is indicative of a greater predicted heat flux. Increasing the concentric mesh density around the cylinder, as was done in Figure 4.12, allowed a more accurate evaluation of this large temperature gradient and the resulting heat flux. It was found through additional experimentation that making the mesh somewhat courser circumferential as shown in Figure 4.23 also produced nearly identical results at $Re_D = 100$, giving a Nusselt number of 5.215.

The validity of the FIDAP model may also be checked against theoretical calculations for heat flux around a heated cylinder in crossflow. Zukauskas (1972) gives the following equation derived from boundary layer theory to describe the local heat transfer from the front portions of a cylinder:

$$Nu = [.9450-.7696 * (x/D)] * Re_D \qquad (4.54)$$

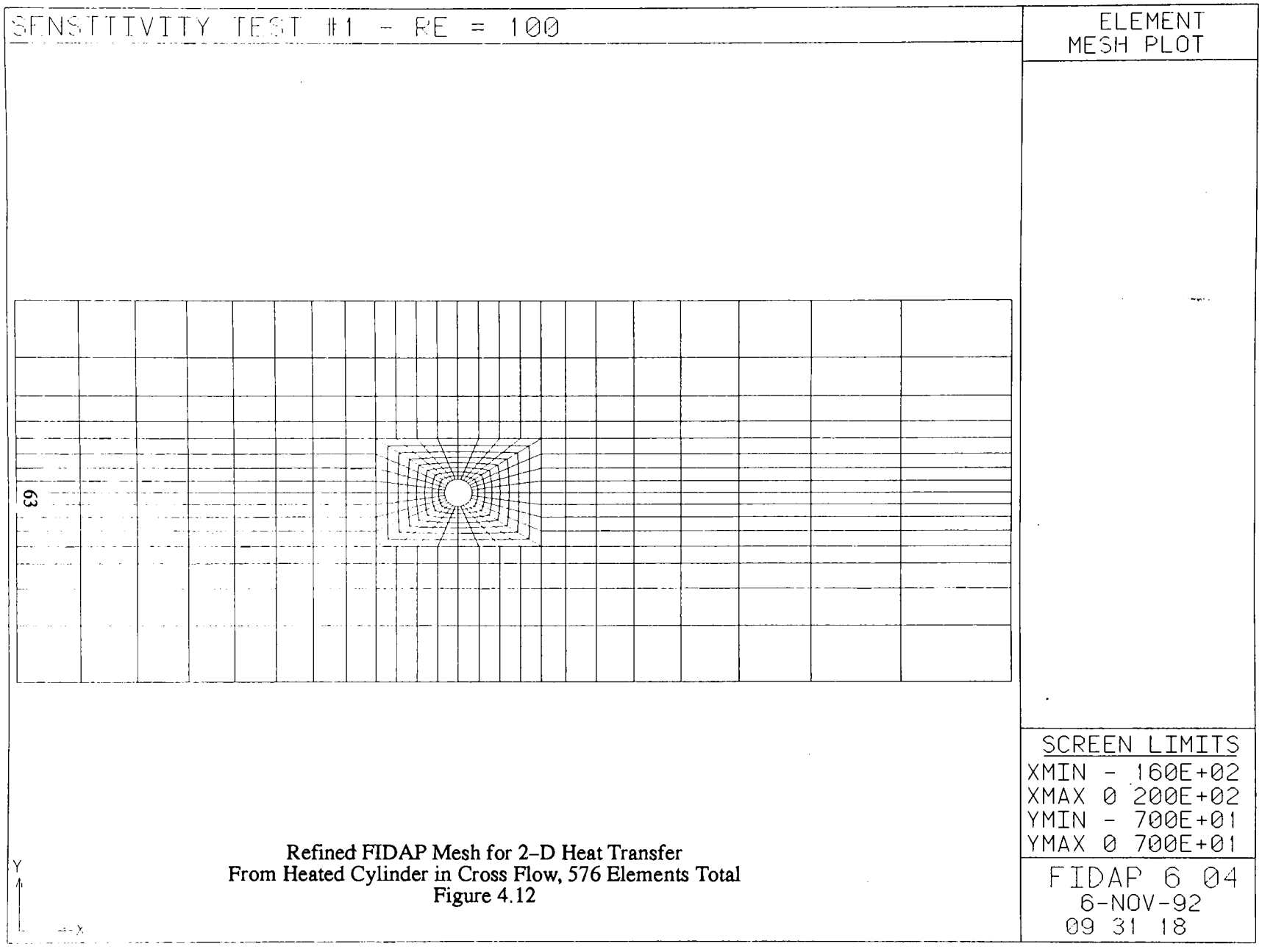

Refined FIDAP Mesh for 2-D Heat Transfer
From Heated Cylinder in Cross Flow, 576 Elements Total
Figure 4.12

SENSITIVITY TEST #1 - RE = 100

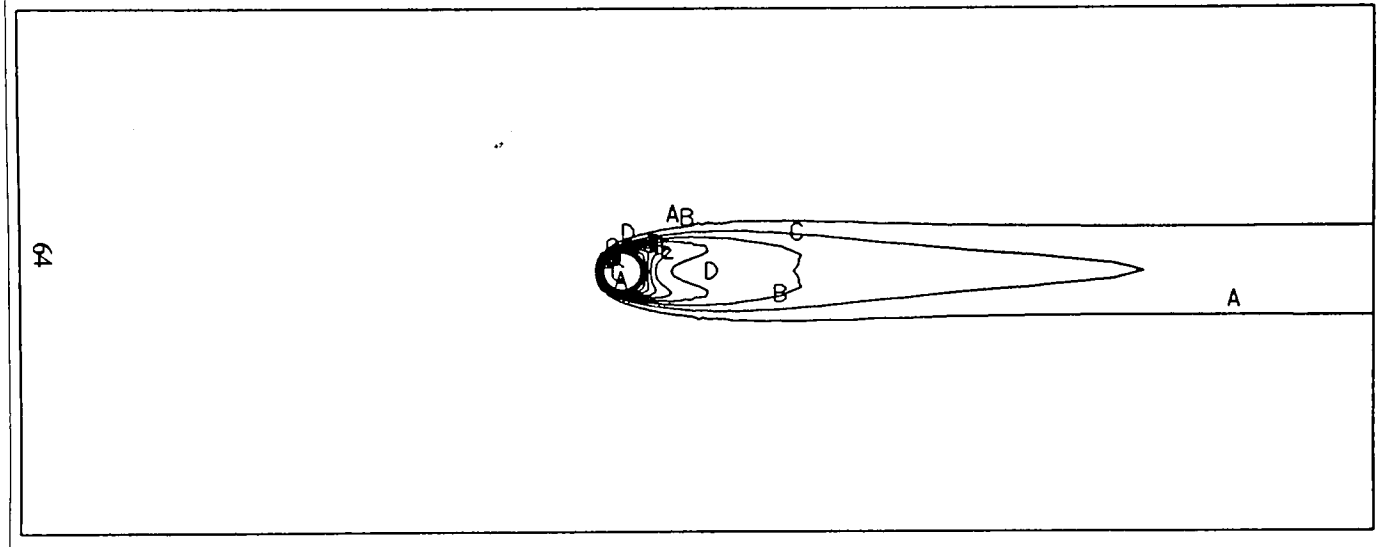

TEMPERATURE CONTOUR PLOT

LEGEND

A - 0.5000E-01
B - 0.1500E+00
C - 0.2500E+00
D - 0.3500E+00
E - 0.4500E+00
F - 0.5500E+00
G - 0.6500E+00
H - 0.7500E+00
I - 0.8500E+00
J - 0.9500E+00

MINIMUM
-0 32442E-02
MAXIMUM
0 10000E+01

SCREEN LIMITS
XMIN - 160E+02
XMAX 0 200E+02
YMIN - 700E+01
YMAX 0 700E+01

FIDAP 6 04
7-DEC-92
22 09 04

Contour Plot of T^* from 0 to 1
Obtained from Refined Model
Figure 4.13

Y
X

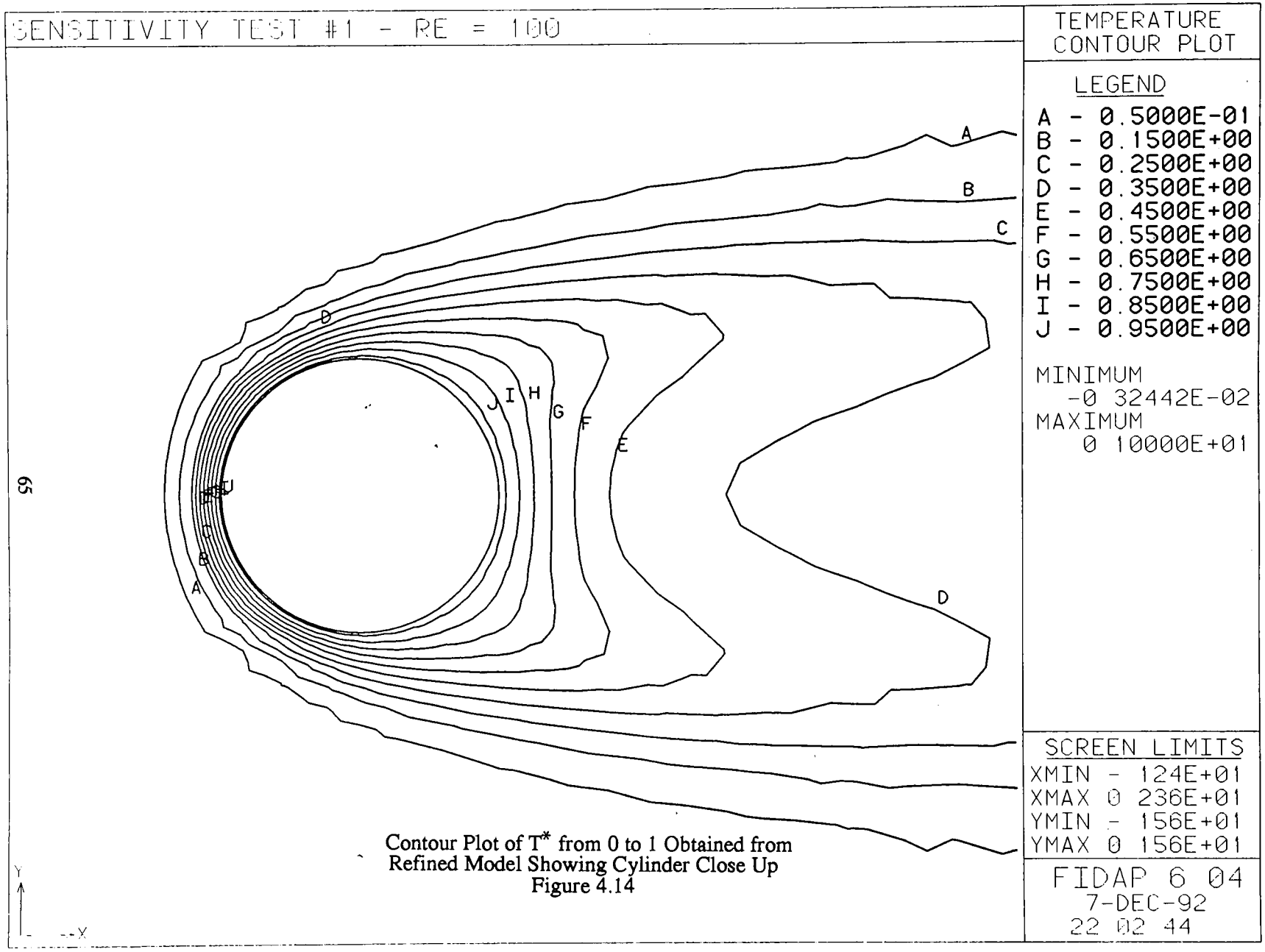

Contour Plot of T* from 0 to 1 Obtained from Refined Model Showing Cylinder Close Up
Figure 4.14

SENSITIVITY TEST #1 - RE = 100

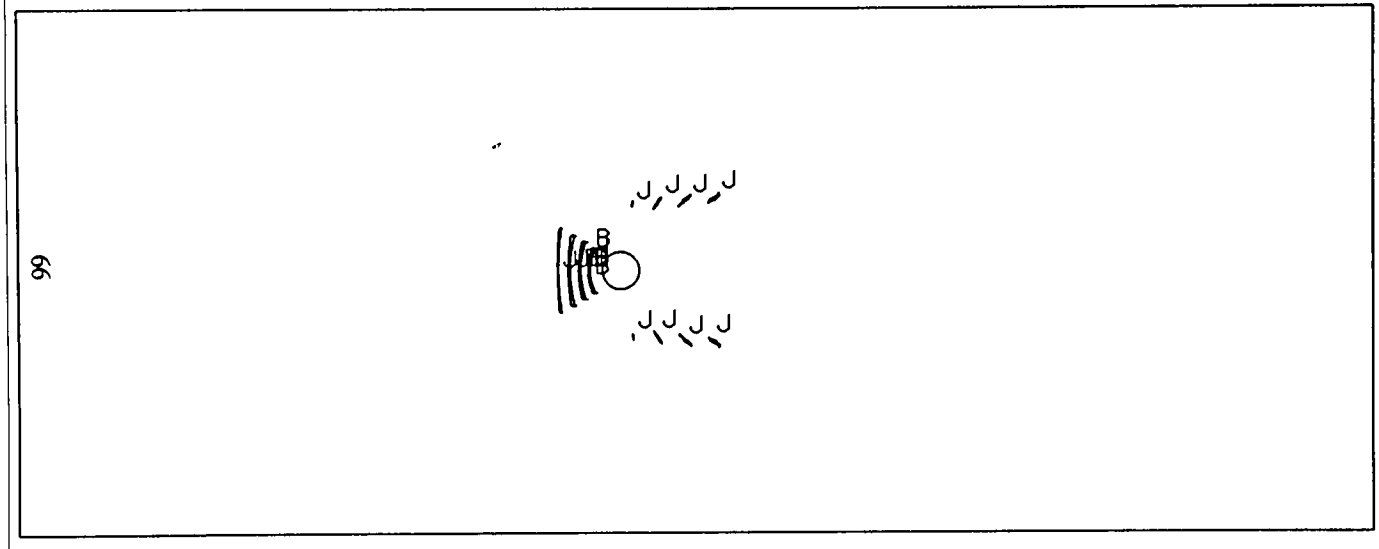

TEMPERATURE CONTOUR PLOT

LEGEND

A - -.3040E-02
B - -.2720E-02
C - -.2400E-02
D - -.2080E-02
E - -.1760E-02
F - -.1440E-02
G - -.1120E-02
H - -.8000E-03
I - -.4800E-03
J - -.1600E-03

MINIMUM
-0 32442E-02
MAXIMUM
0 10000E+01

SCREEN LIMITS
XMIN - 160E+02
XMAX 0 200E+02
YMIN - 700E+01
YMAX 0 700E+01

FIDAP 6 04
7-DEC-92
22 18 13

Contour Plot of T *from -.00304 to 0
Obtained from Refined Model
Figure 4.15

Y
X

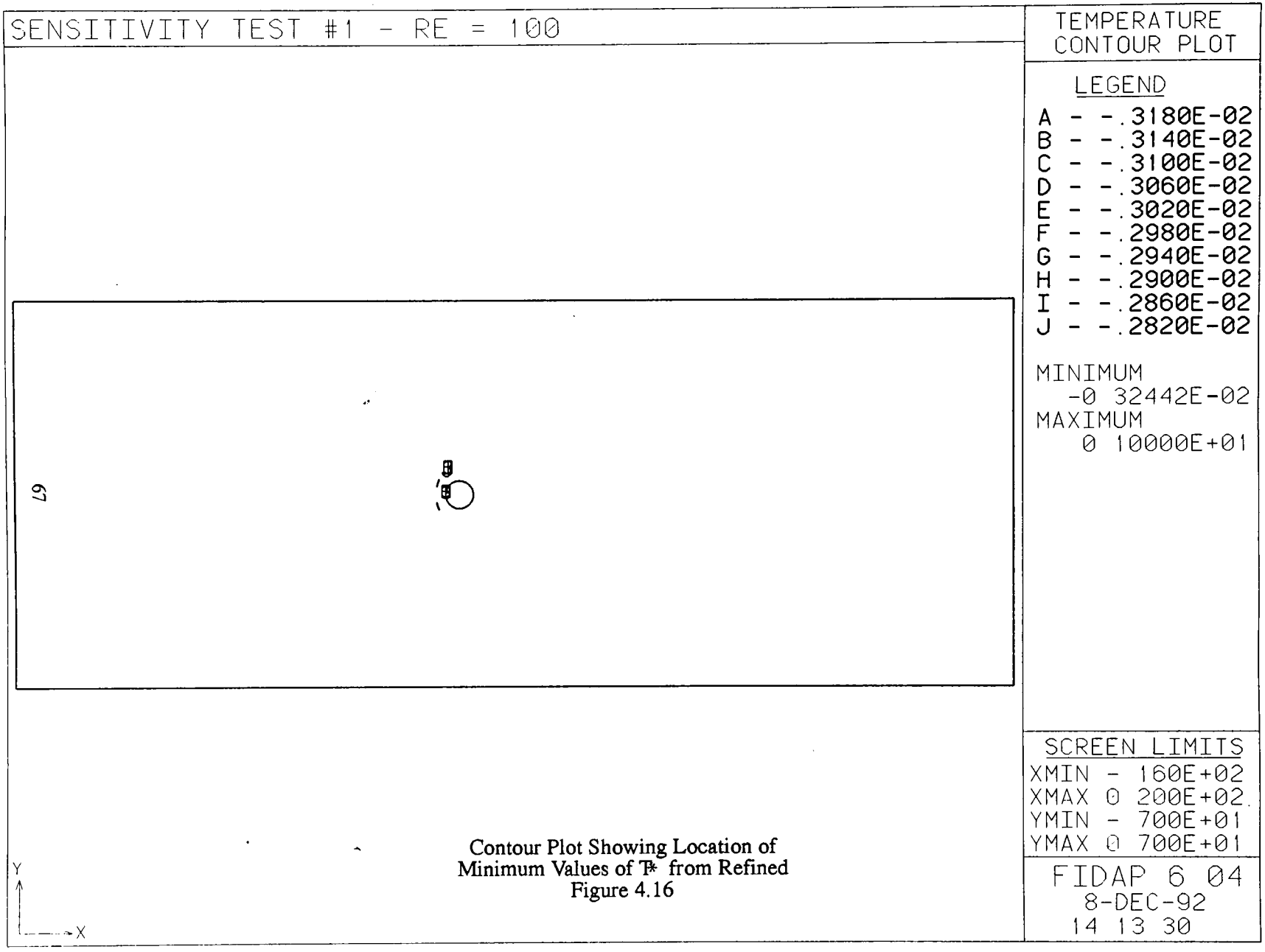

Contour Plot Showing Location of Minimum Values of T* from Refined
Figure 4.16

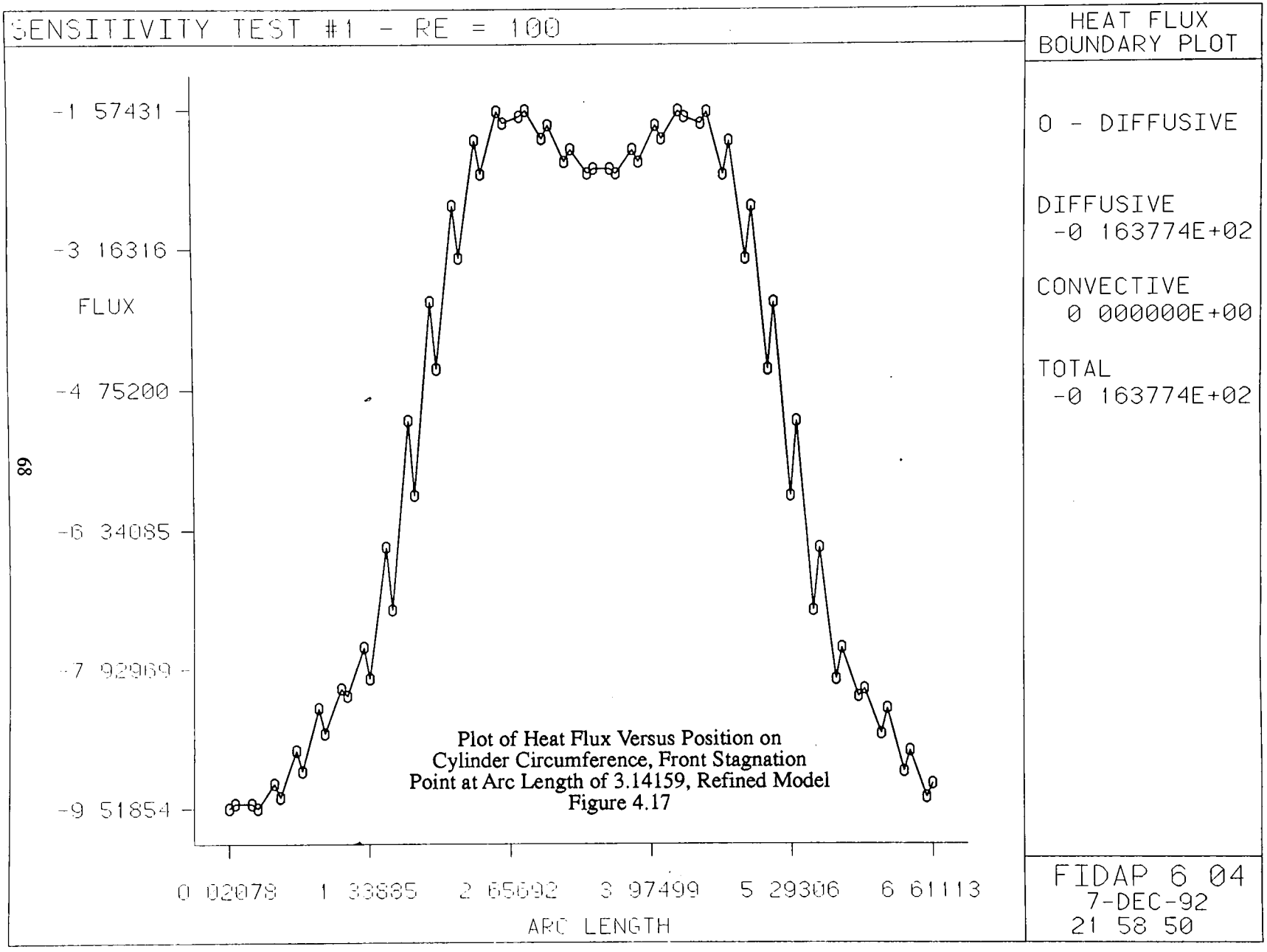

Plot of Heat Flux Versus Position on Cylinder Circumference, Front Stagnation Point at Arc Length of 3.14159, Refined Model
Figure 4.17

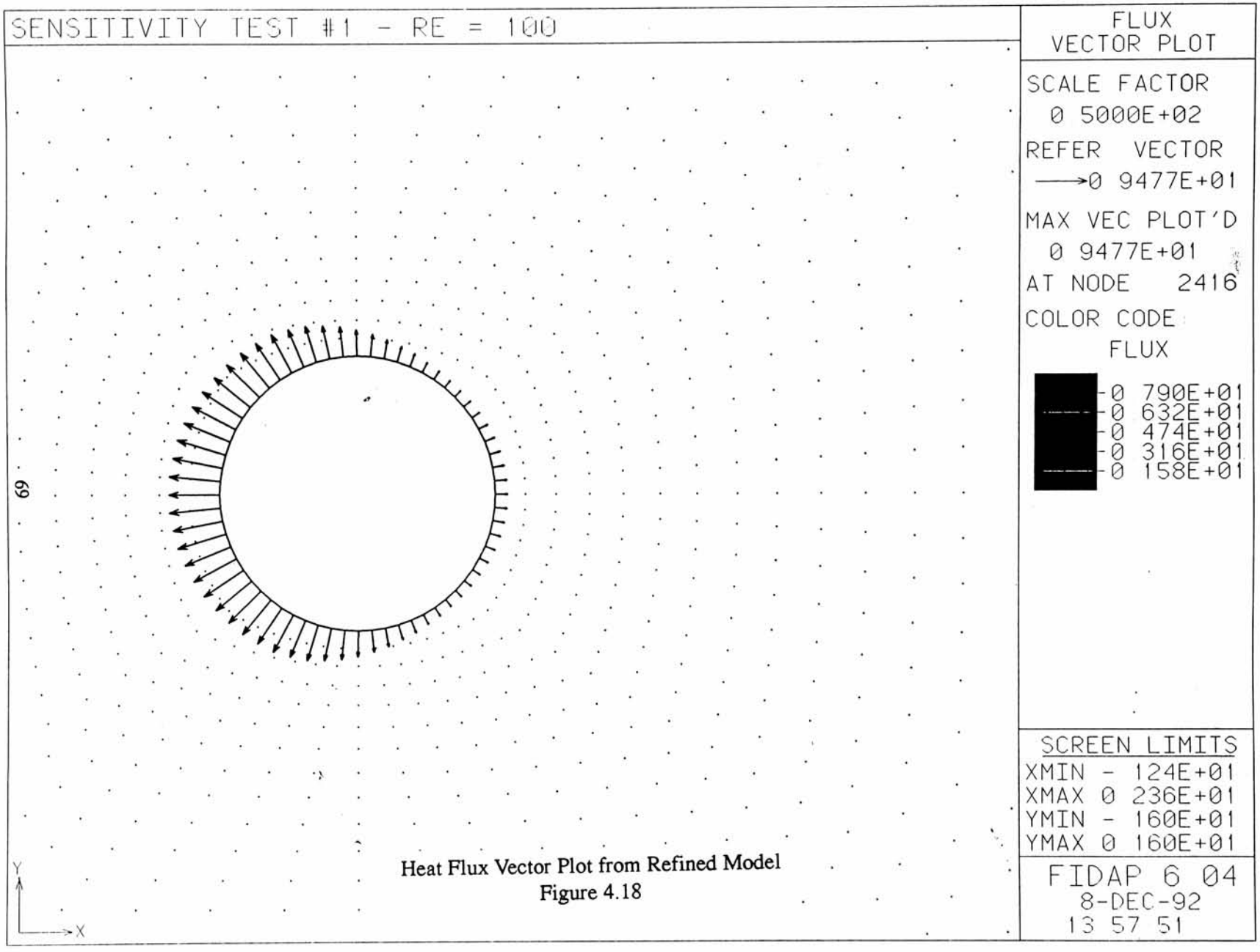

Heat Flux Vector Plot from Refined Model
Figure 4.18

SENSITIVITY TEST #1 - RE = 100

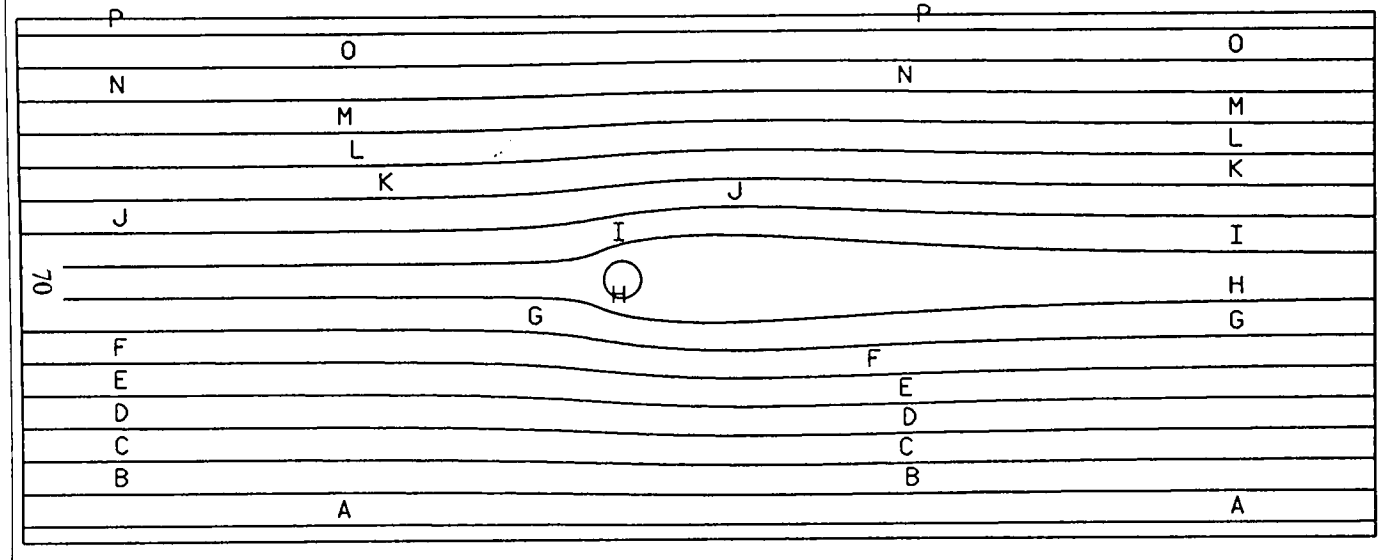

STREAMLINE CONTOUR PLOT

LEGEND

A - 0.4375E+00
B - 0.1313E+01
C - 0.2188E+01
D - 0.3063E+01
E - 0.3938E+01
F - 0.4813E+01
G - 0.5688E+01
H - 0.6563E+01
I - 0.7438E+01
J - 0.8313E+01
K - 0.9188E+01
L - 0.1006E+02
M - 0.1094E+02
N - 0.1181E+02
O - 0.1269E+02
P - 0.1356E+02

MINIMUM
0 00000E+00
MAXIMUM
0 14000E+02

SCREEN LIMITS

XMIN - 160E+02
XMAX 0 200E+02
YMIN - 700E+01
YMAX 0 700E+01

FIDAP 6 04
7-DEC-92
22 09 22

Y
X

Streamline Contour Plot from Refined Model
Figure 4.19

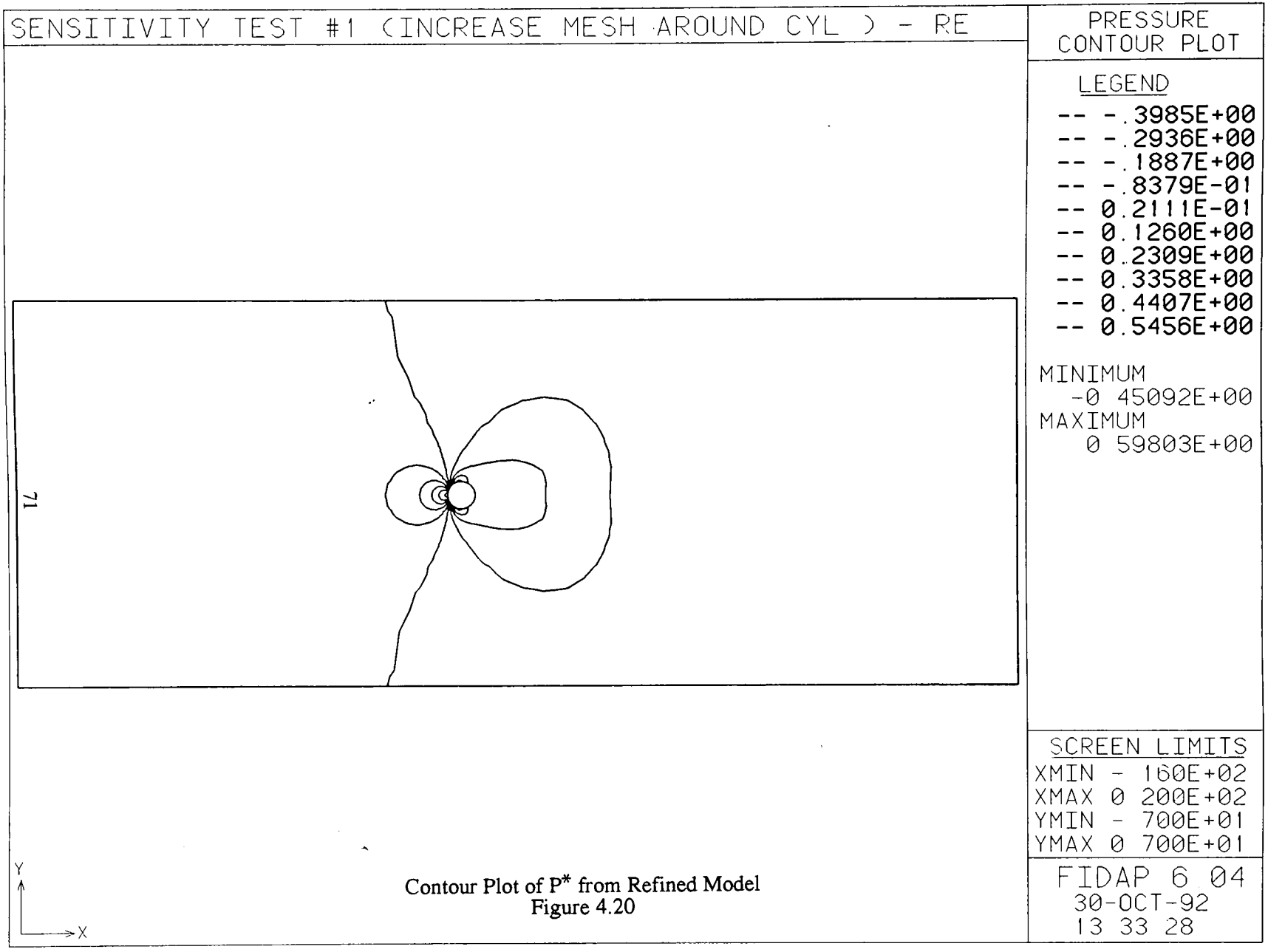

Contour Plot of P* from Refined Model
Figure 4.20

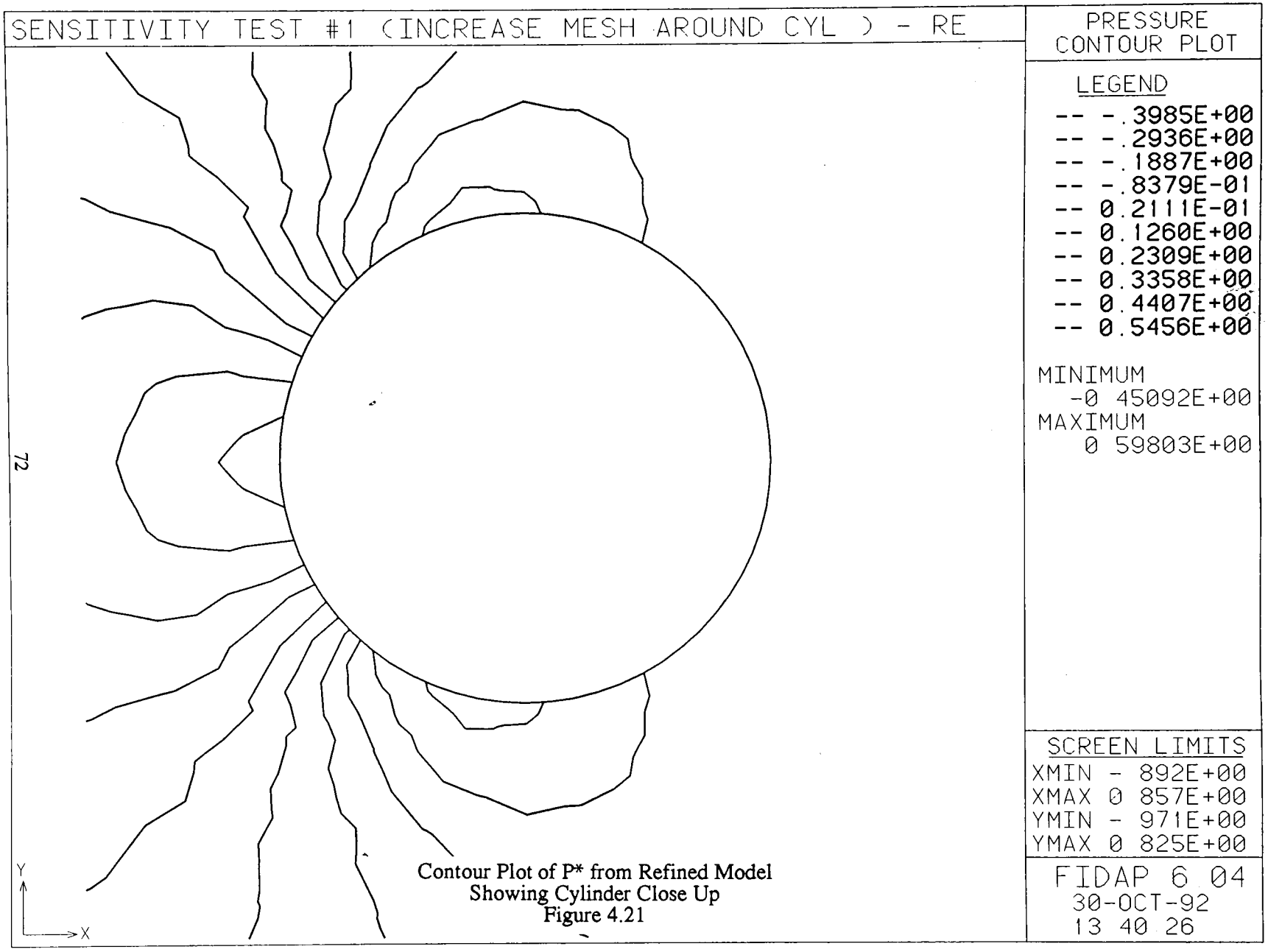

Contour Plot of P* from Refined Model
Showing Cylinder Close Up
Figure 4.21

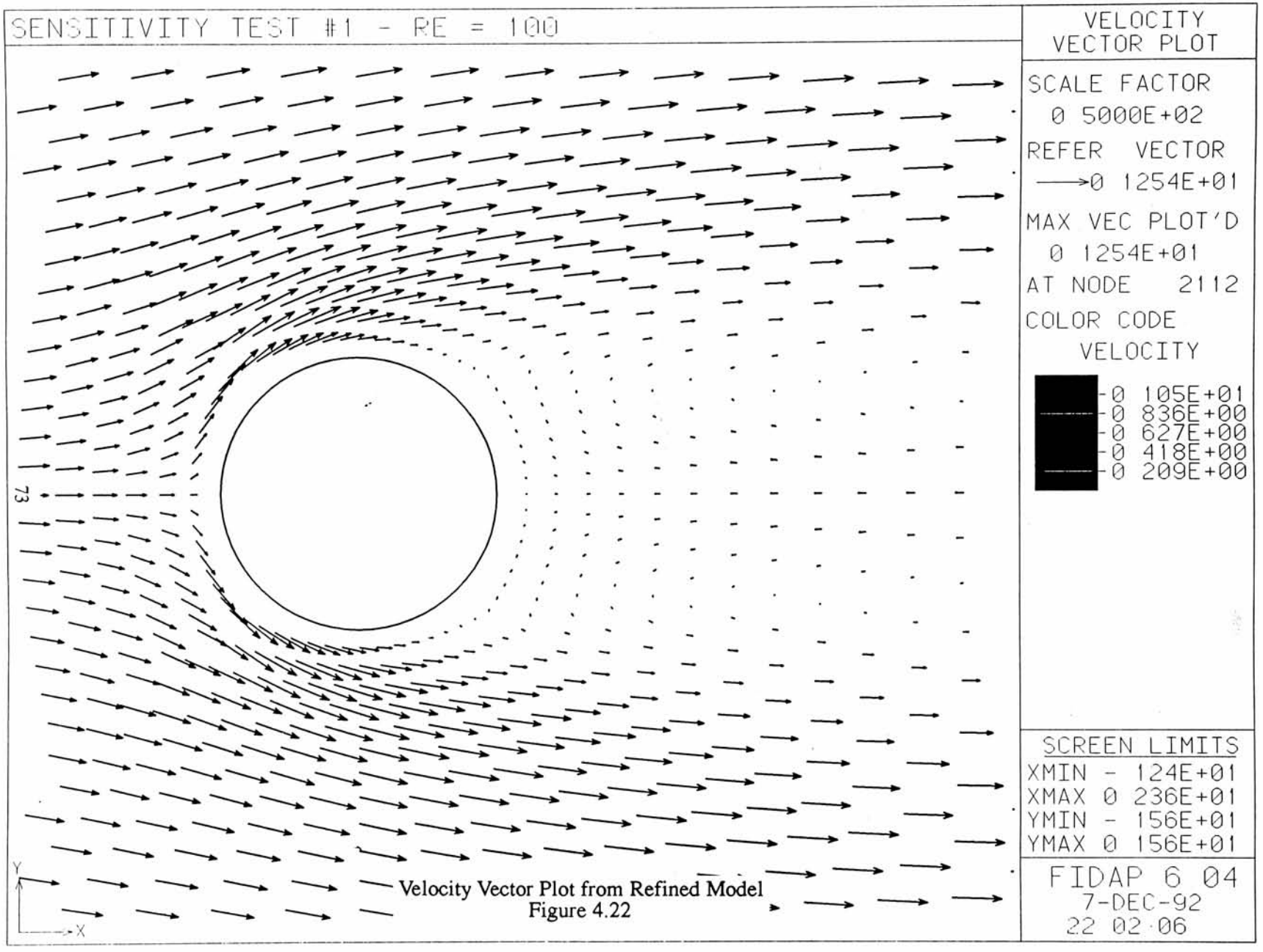

Velocity Vector Plot from Refined Model
Figure 4.22

where x is the circumferential distance around the cylinder measured from the stagnation point and D is the cylinder diameter. At the stagnation point, x = 0, so for Re_D = 100,

$$Nu = [.9450] * 100 = 9.450 \quad (4.55)$$

FIDAP computes the local Nusselt number at the stagnation point of a cylinder utilizing the mesh of Figure 4.12 to be 9.849, which agrees with the theoretical value to within 4.1%.

The effects of boundary condition constraints on the refined mesh were also studied. As a first case, du/dy and dv/dy were both set to zero at the upper and lower horizontal model boundaries. In a second case, an additional constraint of zero heat flux (dT/dy = 0) on those same boundaries was added. Neither of these changes produced a significant difference in predicted Nusselt number from the model.

Finally, the convergence criteria was tightened to understand how this may affect the Nusselt number predicted by the model. The particular solver used in these studies was FIDAP's successive substitution solver. This solver utilizes a root mean square evaluation of all the independent problem variables (in this case pressure, x-velocity, y-velocity, and temperature) over all the equations constituting the global matrix and verifies that the relative change of this RMS norm from one iteration to the next is less than a certain tolerance. The recommended (and default) value for this tolerance is .001. A single run of the model was performed with this tolerance set to .0001. The change to the predicted Nusselt number was very small (<< 1%). The default convergence criteria established by FIDAP appears to be adequate for good results from this model at Reynolds values of 100.

Attempts were also made to run the single pin model at higher values of Reynolds number. Because of memory limitations on the computer system used to run FIDAP, models could not contain more than about 700 elements when using the successive substitution

SENSITIVITY TEST #8 - RE = 100

ELEMENT
MESH PLOT

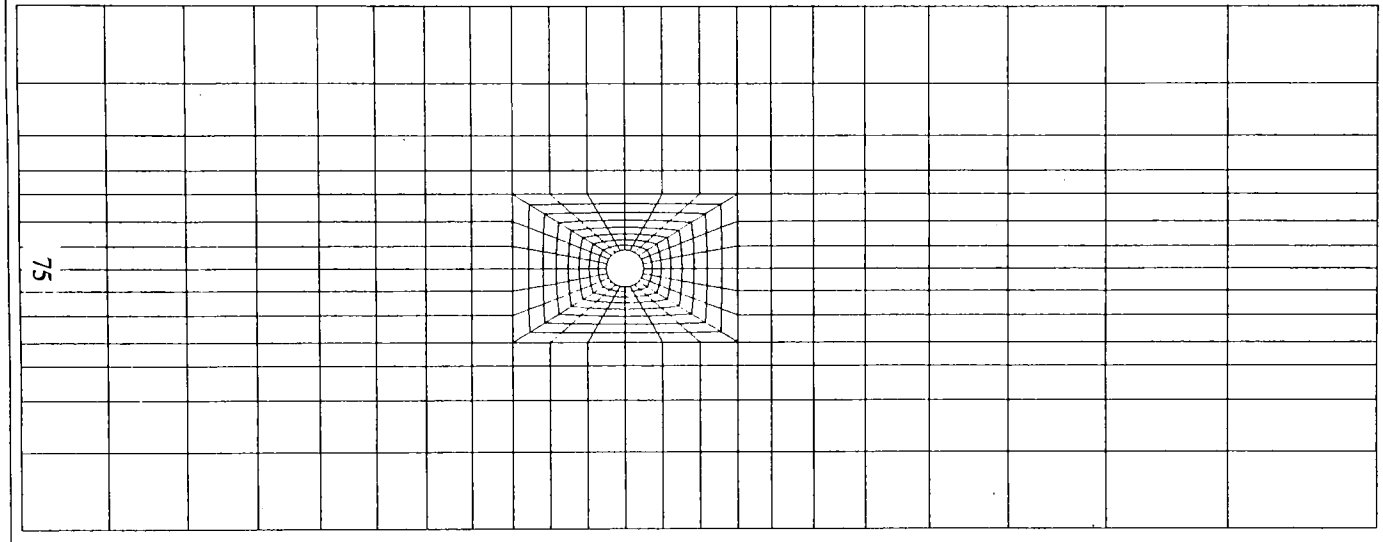

SCREEN LIMITS
XMIN - 160E+02
XMAX 0 200E+02
YMIN - 700E+01
YMAX 0 700E+01

FIDAP 6 04
11-DEC-92
15 31 10

Y
X

FIDAP Mesh with Fewer Elements Circumferentially Around Cylinder, 464 Elements Total
Figure 4.23

solve. This proved to be a crucial factor in running a model at higher Reynolds number conditions. It was found that convergence could not be achieved much above Re=450. The predicted Nusselt numbers from these FIDAP runs is presented in Figure 4.24 as well as in Table 4.1 along with Nusselt numbers computed from a variety of correlations. Extremely good agreement with the correlations of Eckert and Soehngren (1952) and Krall and Eckert (1973) was obtained with errors amounting to 2% or less over the range of Reynolds numbers studied. The correlation of Zhukauskas (1972) had the poorest agreement, typically being about 14% low on predicted Nusselt number when compared to FIDAP results.

Attempts were made to run a tighter meshed model using FIDAP's segregated solver which works with less memory, but at the cost of a much slower speed. It was discovered, however, that the segregated solver did not converge nearly as well as the successive substitution solver, even at lower values of Reynolds number. The successive substitution solver was used in all subsequent studies for this reason.

4.3 Multiple Staggered Cylinders in Cross Flow

A FIDAP model depicting 4 rows of staggered heated cylinders in cross flow was constructed and nondimensionalized in a manner similar to that described for a single cylinder in Section 4.2. 4 rows were chosen as a basis for study because this is the smallest cylinder bank that the equations for Nusselt number and pressure drop presented in Chapter 3 are applicable to. Because of the approximate 700 element model limitation imposed by computer memory available to FIDAP, no more than 4 rows of cylinders could be reasonably meshed. As a consequence, it was not possible to study the affects of mesh density on model performance. This dictated that the model be carefully constructed based on the findings of the single pin model sensitivity studies. For instance, the findings in Section 4.2 dictate that

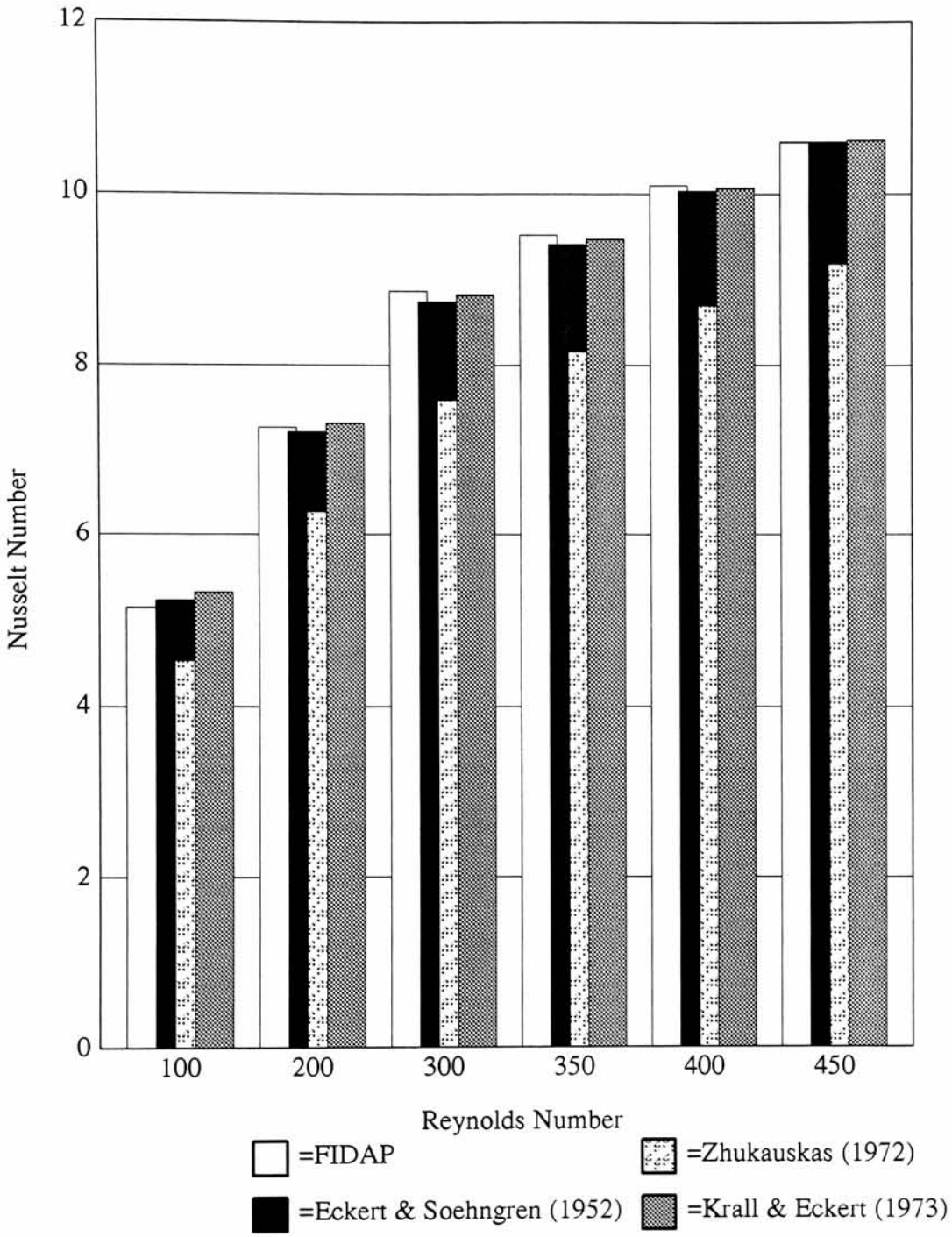

Comparison of Nusselt Number Predicted by FIDAP versus Correlations by Various Authors for a Single Heated Cylinder in Cross Flow Across a Range of Reynolds Numbers (page 1 of 2)

Figure 4.24

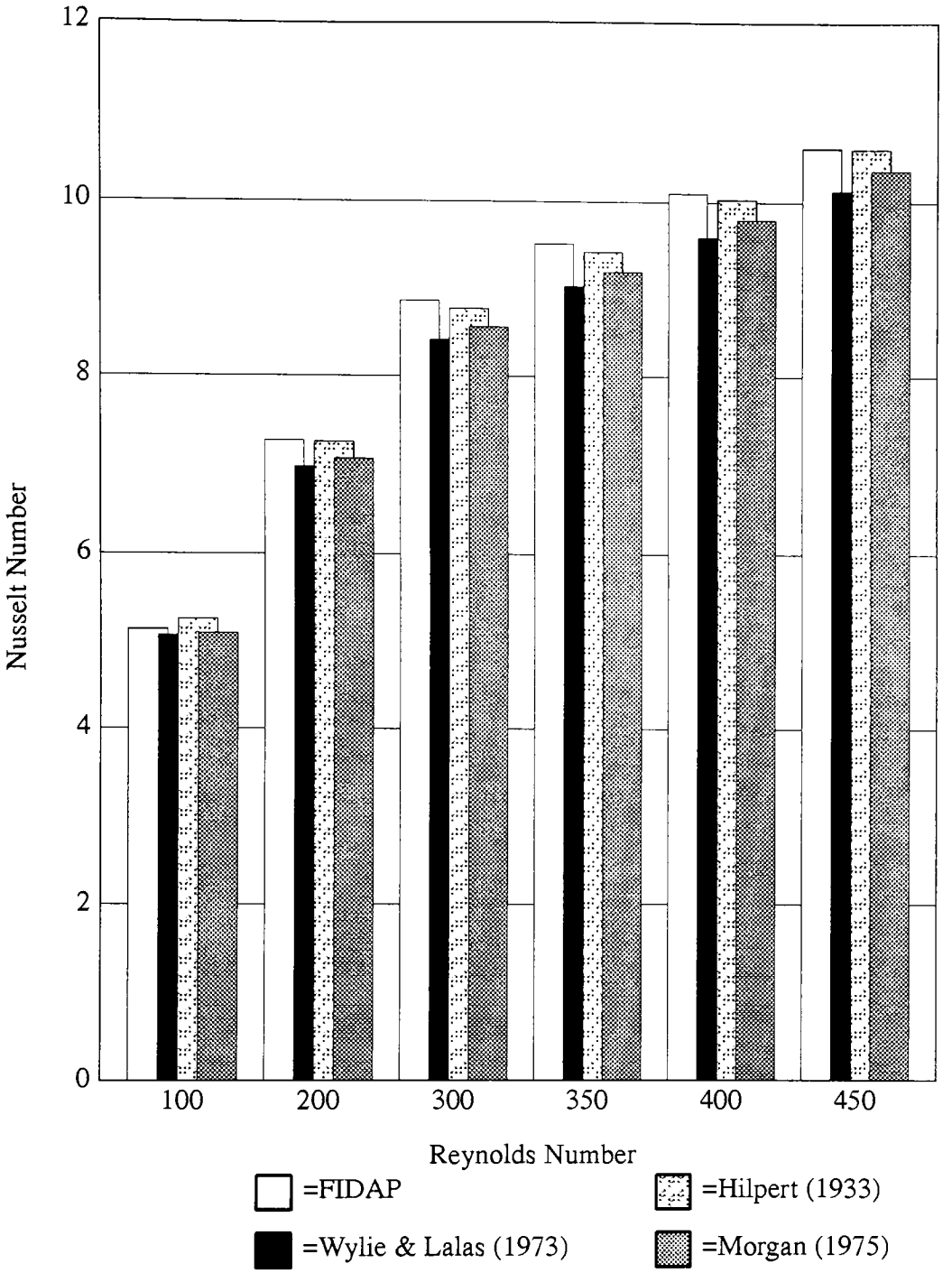

Comparison of Nusselt Number Predicted by FIDAP versus Correlations by Various Authors for a Single Heated Cylinder in Cross Flow Across a Range of Reynolds Numbers (page 2 of 2)

Figure 4.24 (continued)

very thin elements in the radial direction near the surfaces of the cylinders are required to accurately predict heat flux.

The determination of the Nusselt number of the pin bank predicted by FIDAP was more involved than simply noting the average predicted nondimensional heat flux which is equal in magnitude to the Nusselt number for the single pin studies presented in Section 4.2. Since heat flux from a heated pin bank is determined in part from the log mean temperature difference of the system with respect to ambient per equation 3.14, it was necessary to determine the average nondimensional temperature leaving the pin bank of the FIDAP model in question. The predicted heat flux from the FIDAP model was used as input into equation 3.13, which describes the temperature rise of a given mass flow rate of fluid acted upon by a known heat flux. This temperature rise was used to calculate the log mean temperature of the system from equation 3.15. Finally, the log mean temperature difference and the heat flux predicted by FIDAP was used in equation 3.14 to predict the Nusselt number of the pin bank system.

Two cases are presented, the first being a model of a 4 row staggered heated cylinder bank having nondimensional transverse and longitudinal staggers (P_T and P_L) equal to 2, and a second being a model of a 4 row staggered heated cylinder bank having a nondimensional transverse stagger $P_T = 1.3$ and a nondimensional longitudinal stagger $P_L = 2$. The meshes associated with these two models are presented in Figures 4.25 and 4.38, respectively. Temperature, streamline, heat flux, and pressure plots for $Re_D = 100$ are found in Figures 4.26 through 4.37 for the $P_T = 2/P_L = 2$ case and in Figures 4.39 through 4.50 for the $P_T = 1.3/P_L = 2$ case.

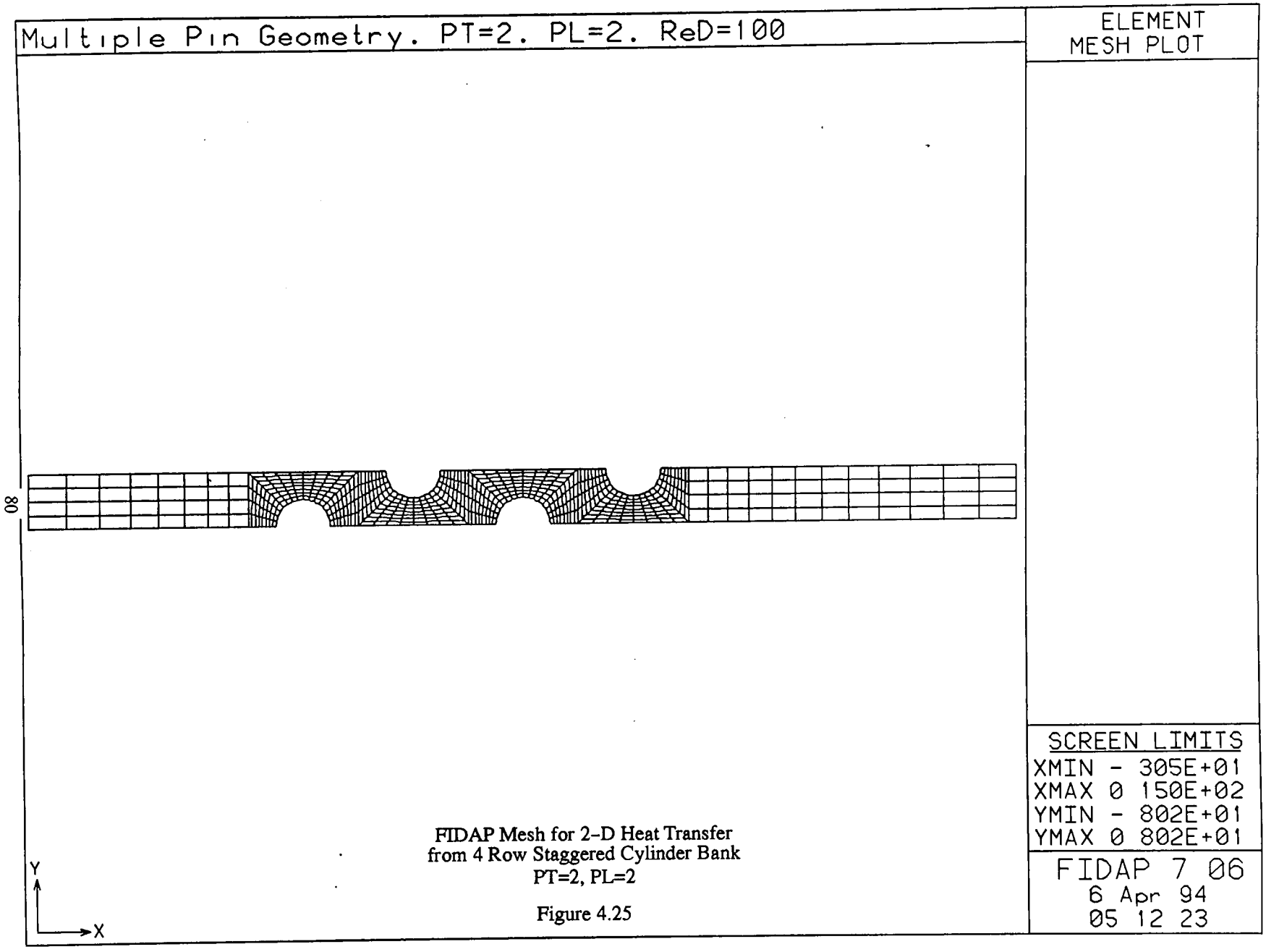

FIDAP Mesh for 2-D Heat Transfer
from 4 Row Staggered Cylinder Bank
PT=2, PL=2

Figure 4.25

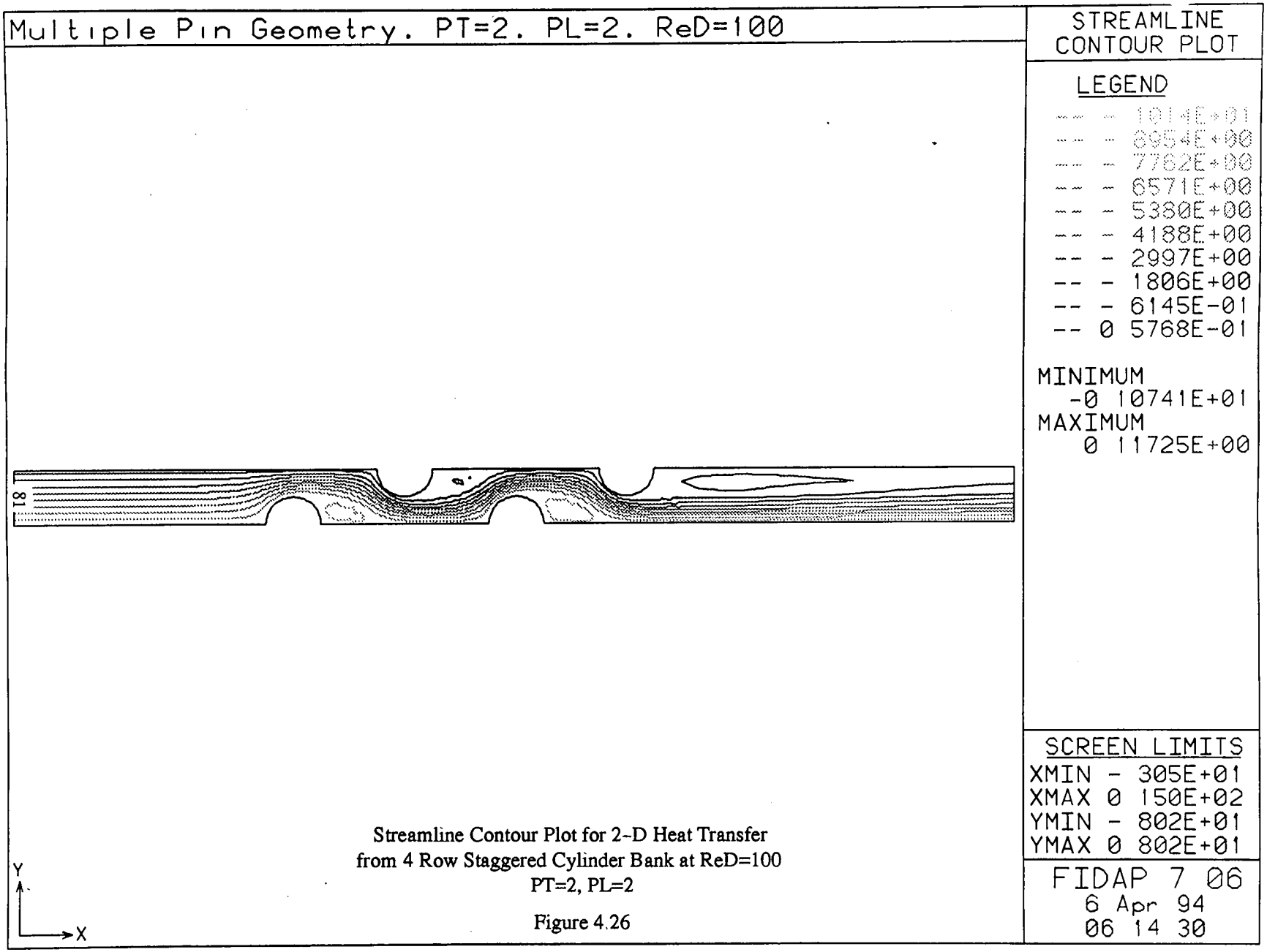

Streamline Contour Plot for 2-D Heat Transfer
from 4 Row Staggered Cylinder Bank at ReD=100
PT=2, PL=2

Figure 4.26

Multiple Pin Geometry. PT=2. PL=2. ReD=100

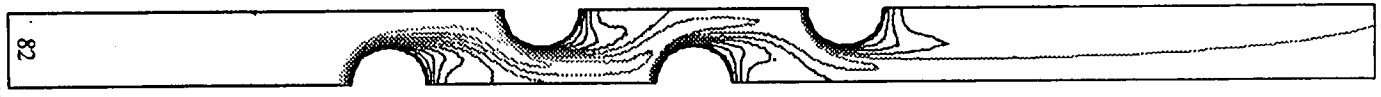

TEMPERATURE CONTOUR PLOT

LEGEND

-- 0 4991E-01
-- 0 1498E+00
-- 0 2499E+00
-- 0 3499E+00
-- 0 4499E+00
-- 0 5499E+00
-- 0 6499E+00
-- 0 7500E+00
-- 0 8500E+00
-- 0 9500E+00

MINIMUM
-0 19932E-03
MAXIMUM
0 10000E+01

SCREEN LIMITS
XMIN - 305E+01
XMAX 0 150E+02
YMIN - 802E+01
YMAX 0 802E+01

FIDAP 7 06
6 Apr 94
06 00 26

Contour Plot of T* for 2–D Heat Transfer
from 4 Row Staggered Cylinder Bank at ReD=100
PT=2, PL=2

Figure 4.27

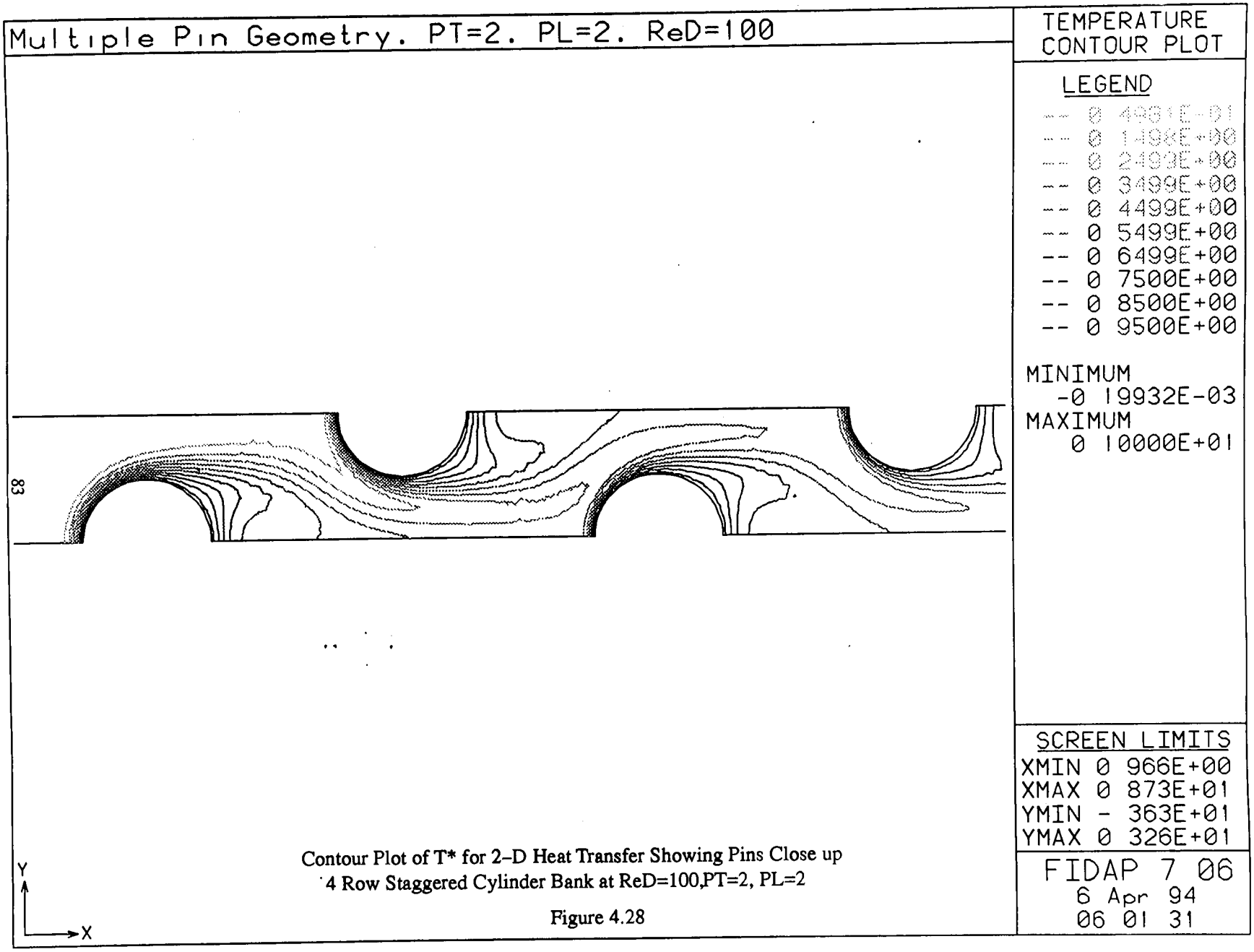

Contour Plot of T* for 2–D Heat Transfer Showing Pins Close up
4 Row Staggered Cylinder Bank at ReD=100,PT=2, PL=2

Figure 4.28

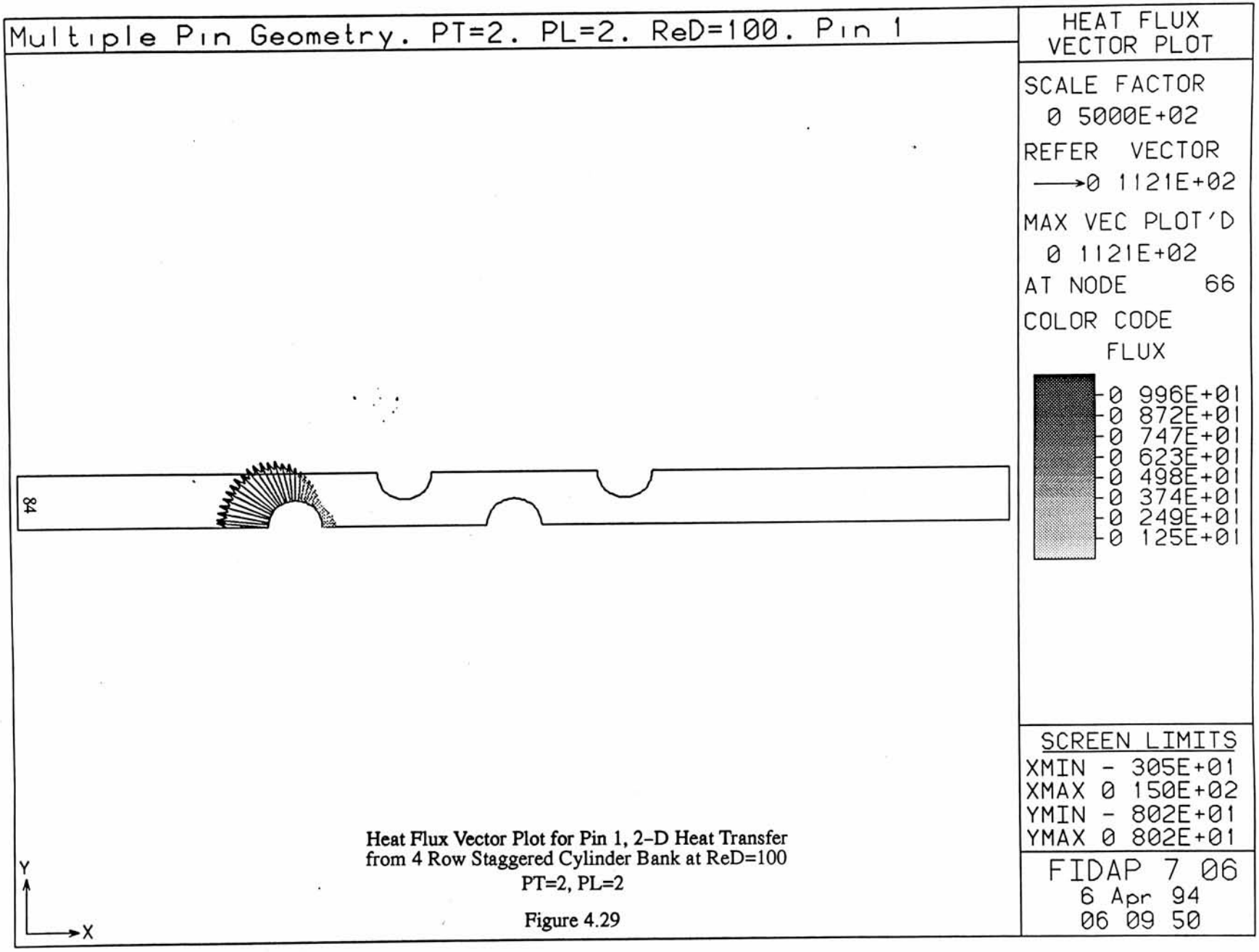

Heat Flux Vector Plot for Pin 1, 2-D Heat Transfer from 4 Row Staggered Cylinder Bank at ReD=100
PT=2, PL=2

Figure 4.29

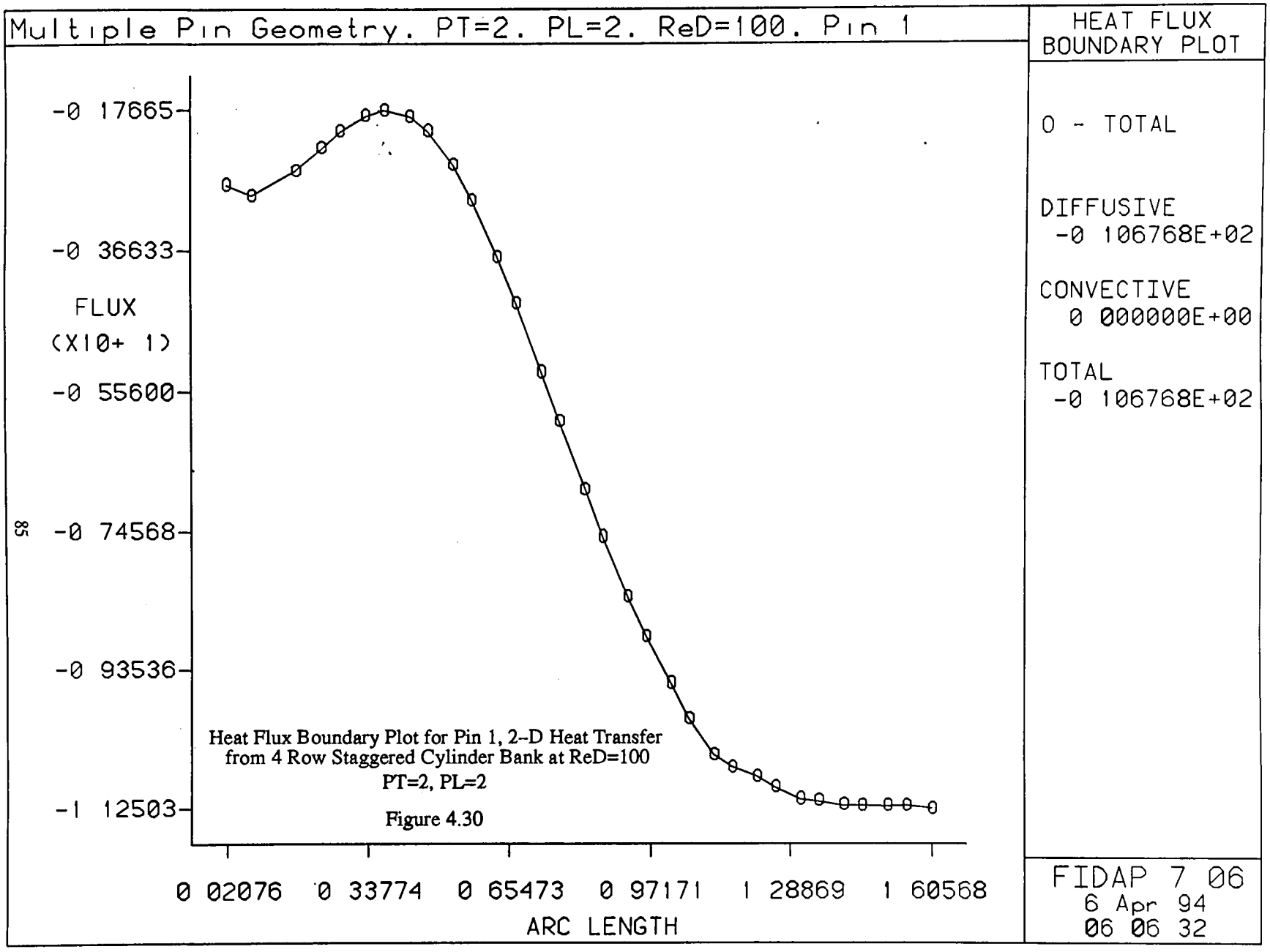

Heat Flux Boundary Plot for Pin 1, 2-D Heat Transfer from 4 Row Staggered Cylinder Bank at ReD=100
PT=2, PL=2

Figure 4.30

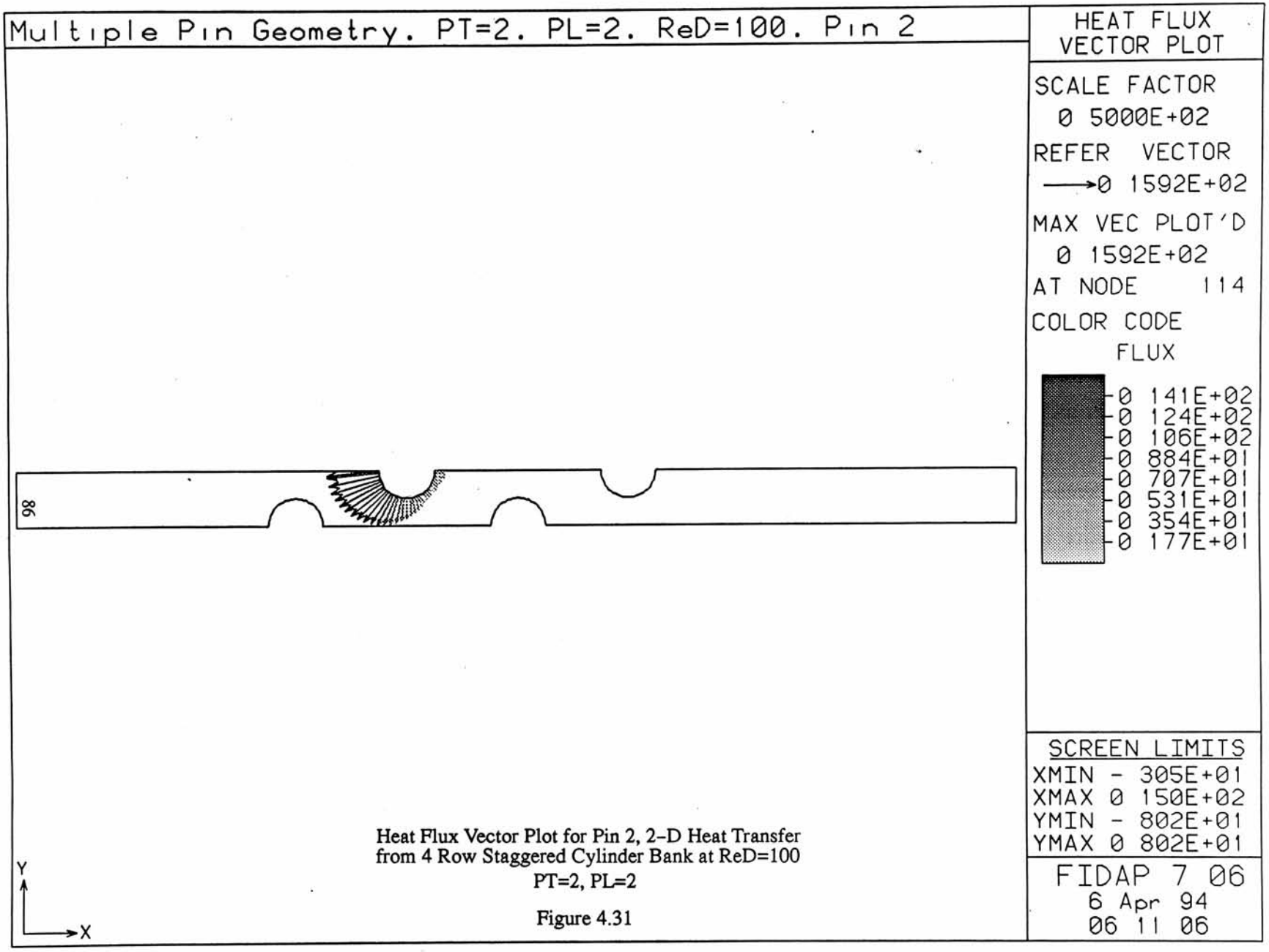

Heat Flux Vector Plot for Pin 2, 2-D Heat Transfer
from 4 Row Staggered Cylinder Bank at ReD=100
PT=2, PL=2

Figure 4.31

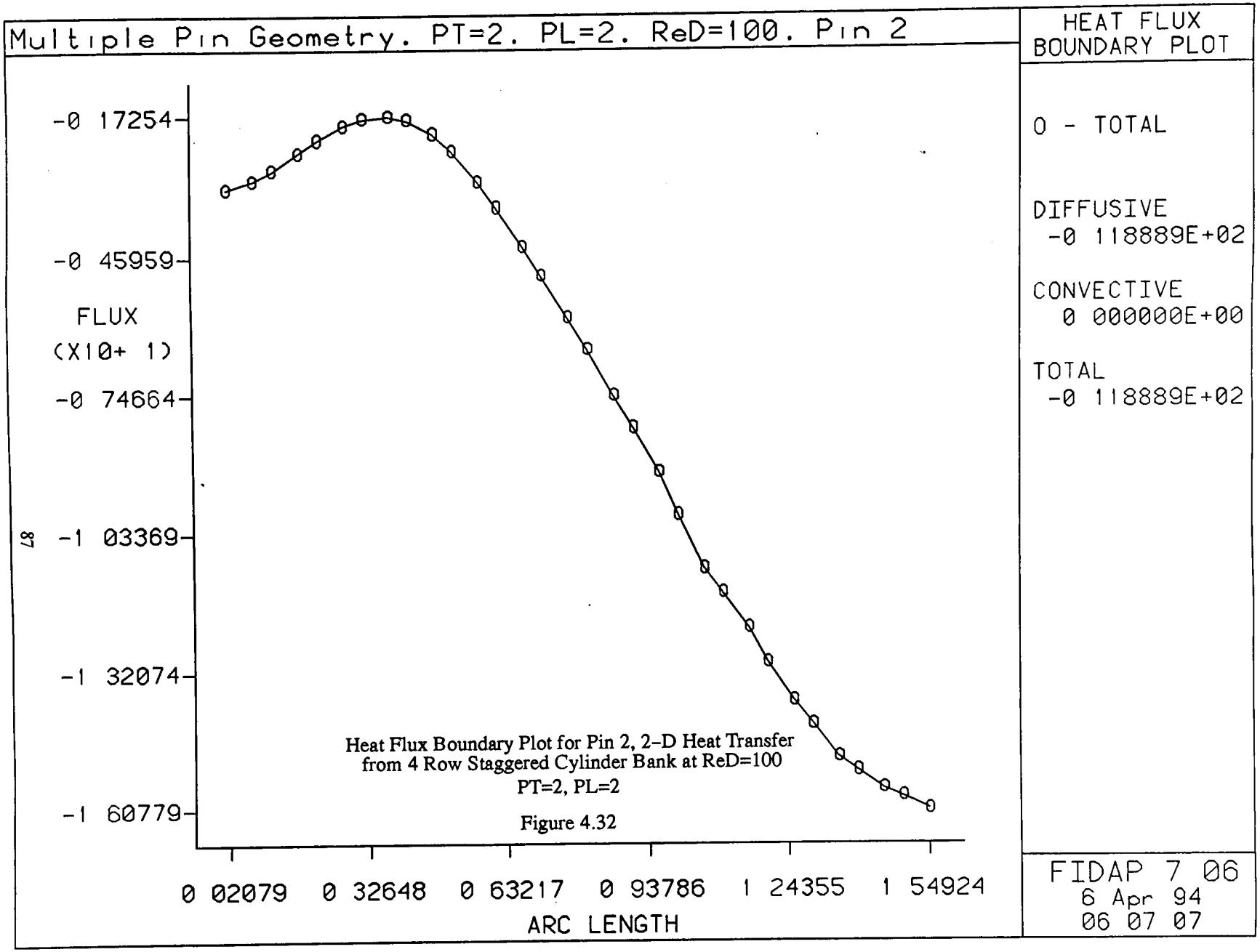

Heat Flux Boundary Plot for Pin 2, 2-D Heat Transfer
from 4 Row Staggered Cylinder Bank at ReD=100
PT=2, PL=2

Figure 4.32

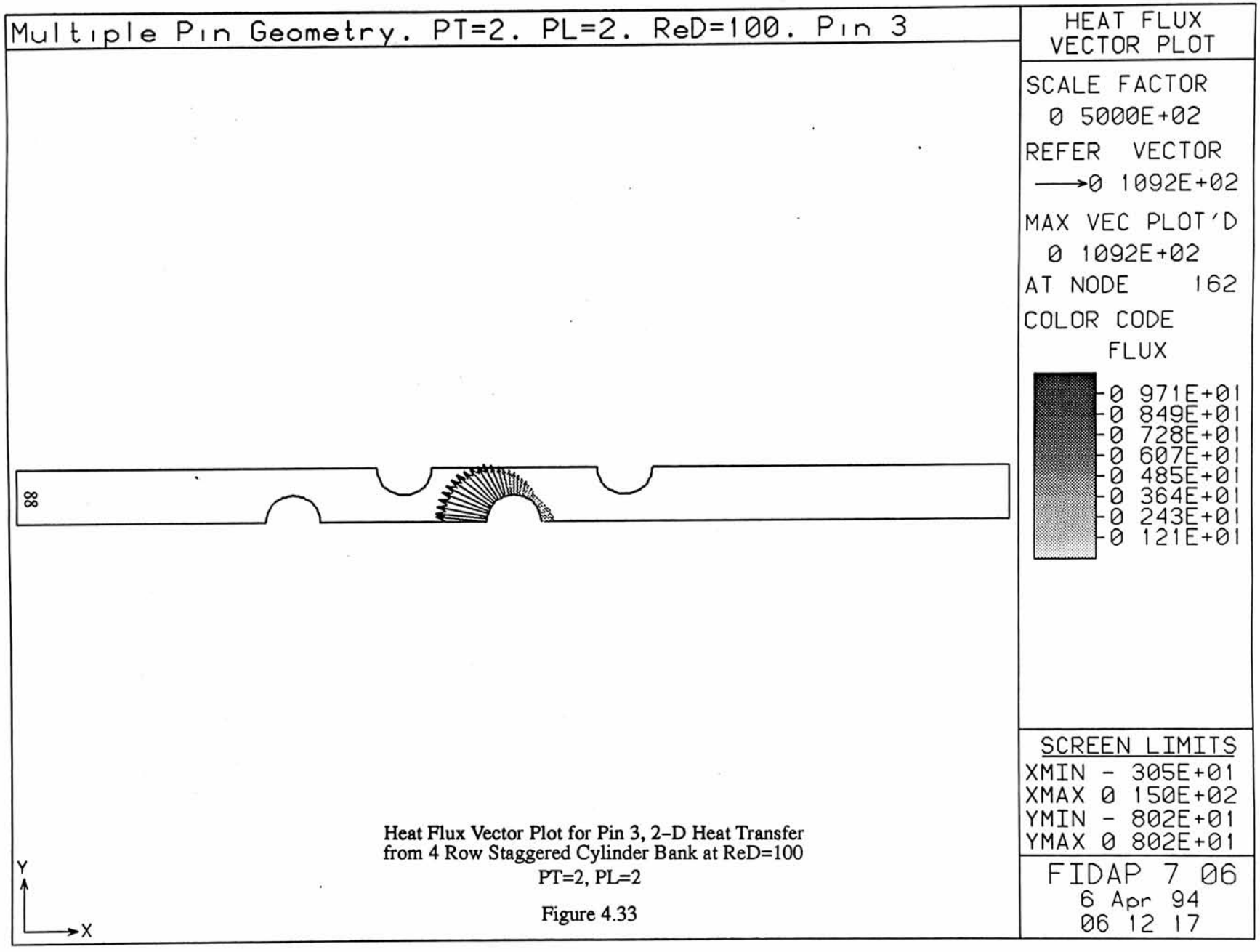

Heat Flux Vector Plot for Pin 3, 2-D Heat Transfer from 4 Row Staggered Cylinder Bank at ReD=100
PT=2, PL=2

Figure 4.33

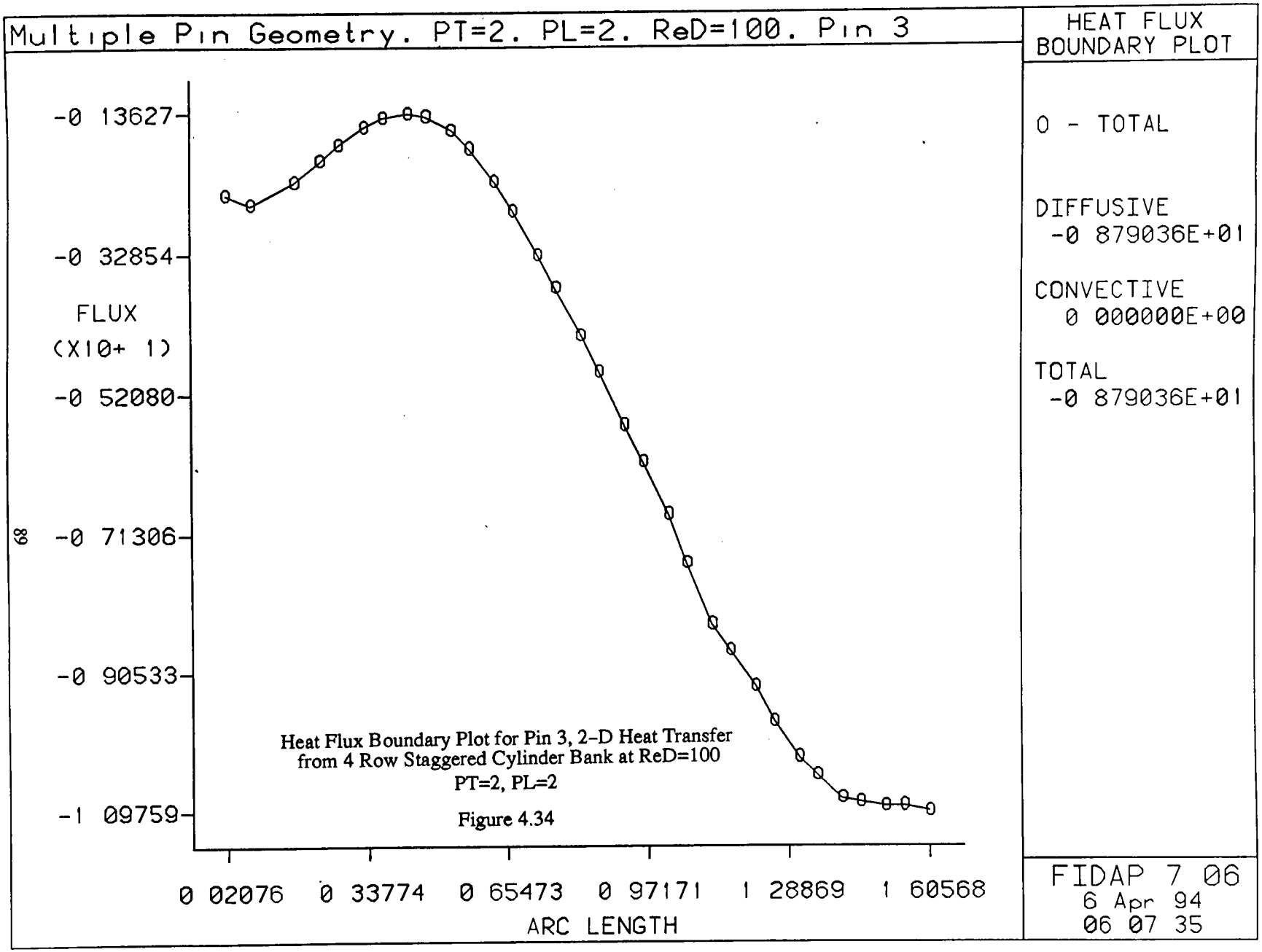

Heat Flux Boundary Plot for Pin 3, 2-D Heat Transfer from 4 Row Staggered Cylinder Bank at ReD=100
PT=2, PL=2

Figure 4.34

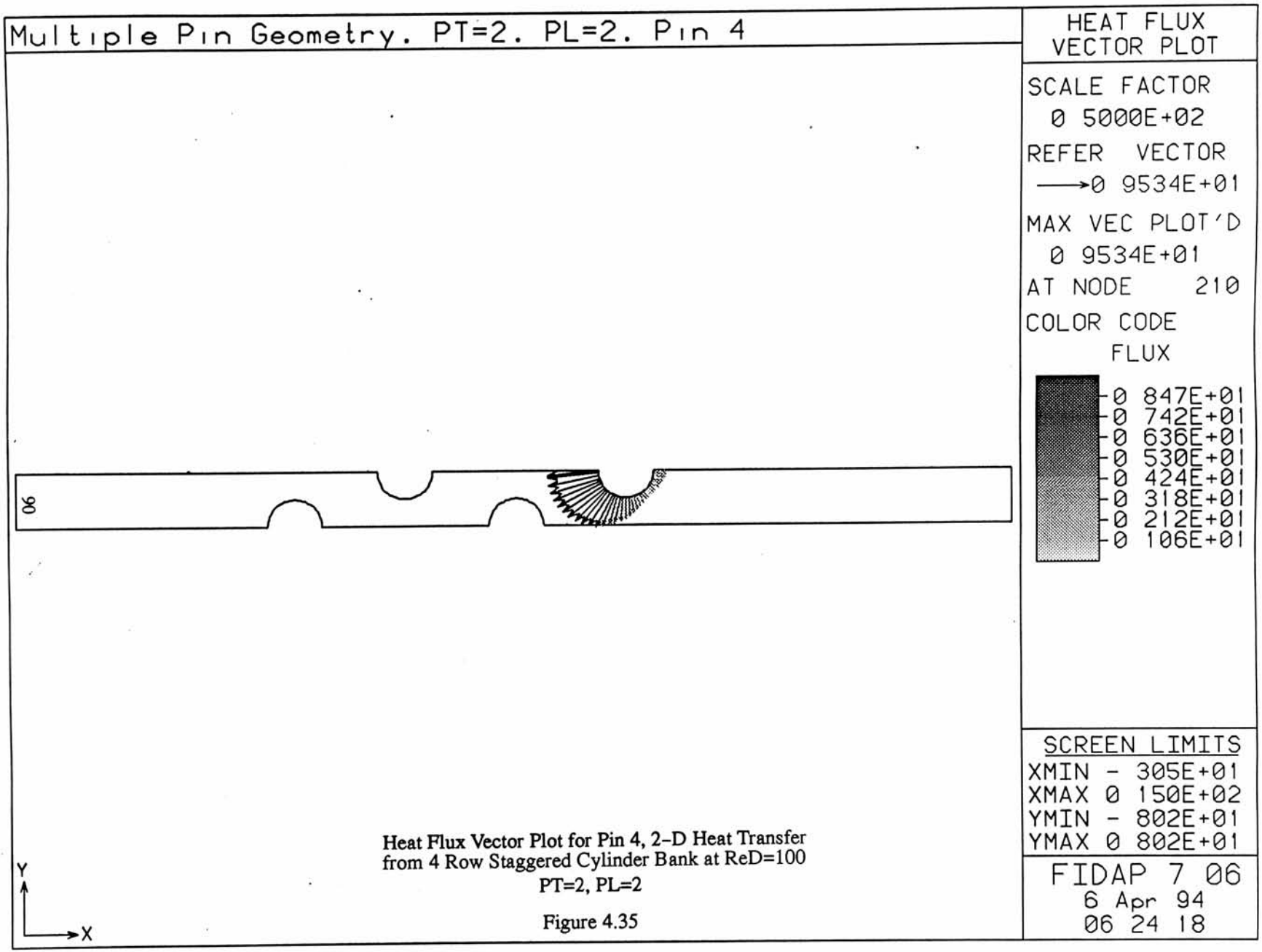

Heat Flux Vector Plot for Pin 4, 2-D Heat Transfer from 4 Row Staggered Cylinder Bank at ReD=100 PT=2, PL=2

Figure 4.35

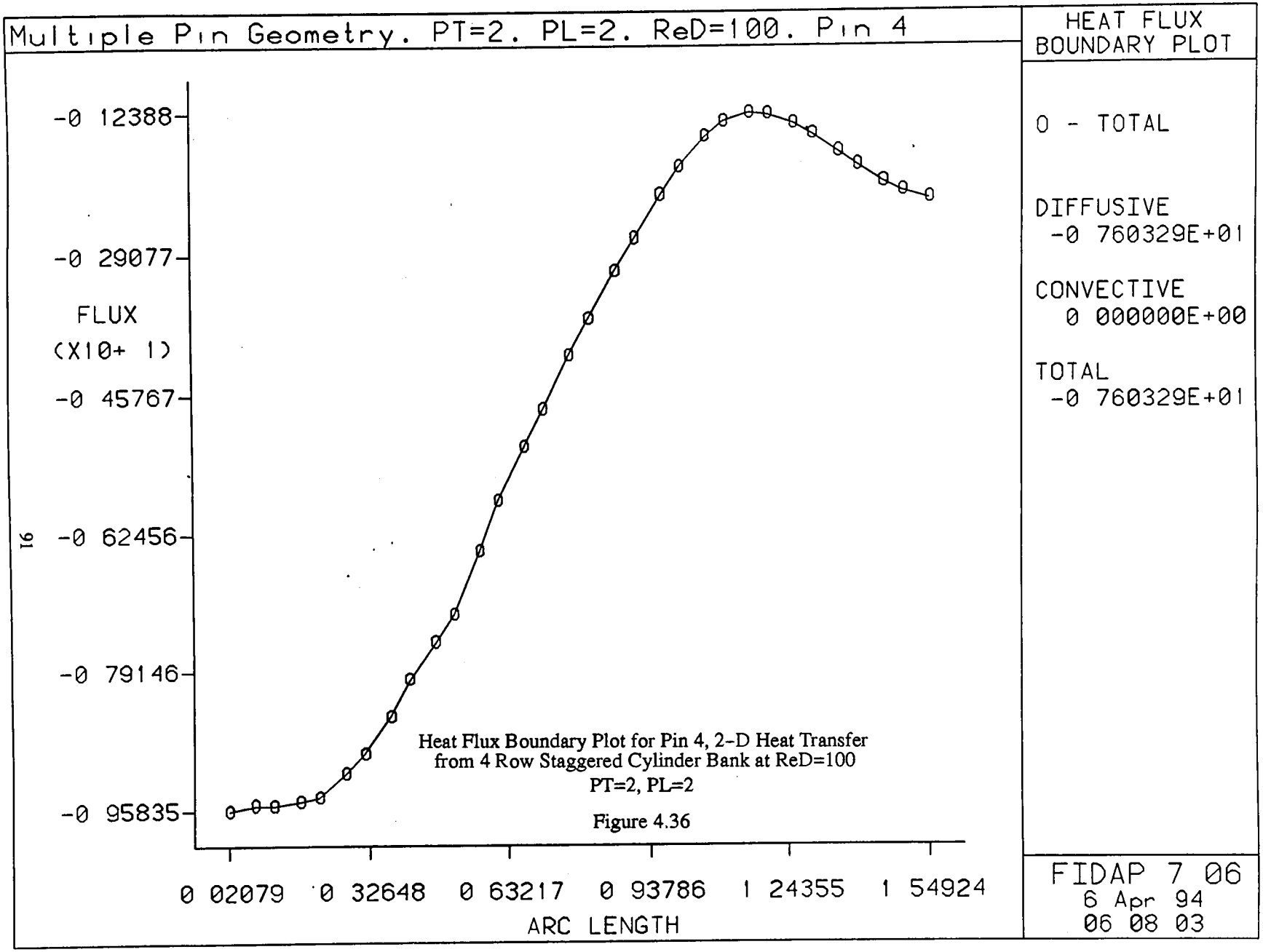

Heat Flux Boundary Plot for Pin 4, 2-D Heat Transfer from 4 Row Staggered Cylinder Bank at ReD=100 PT=2, PL=2

Figure 4.36

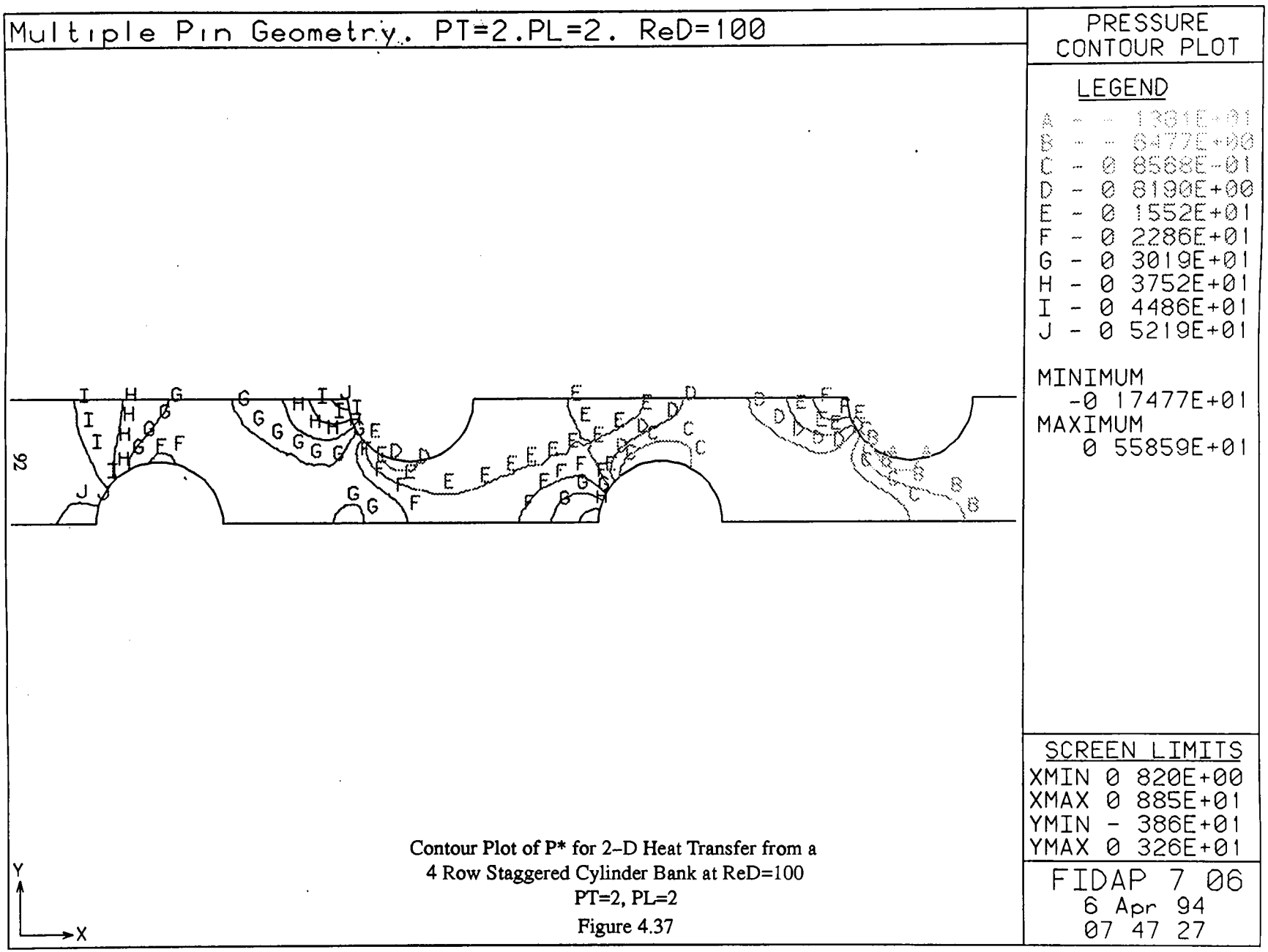

Contour Plot of P* for 2-D Heat Transfer from a
4 Row Staggered Cylinder Bank at ReD=100
PT=2, PL=2
Figure 4.37

Like the single pin models, performance indicators were given by the model's ability to converge as well as the absence of large nondimensional temperatures in the flow field less than zero. It was found, in fact, that nondimensional temperatures of -.03 or less in the flow field usually accompanied difficulties in convergence. The model having the larger transverse stagger ($P_T = 2$) worked well up to Reynolds numbers of 340. The model having the smaller transverse stagger ($P_T = 1.3$) worked well up to only Re = 300. This is explained by the onset of large velocity and temperature gradients at lower values of Reynolds number in comparison to the model having the larger transverse stagger. Tighter meshes would be required to operate these models above these limits.

The results of these multiple pin FIDAP runs are given in Tables 4.3 and 4.4 and in Figures 4.51 through 4.54. Comparisons of predicted Nusselt number and nondimensional pressure drop p* are presented for FIDAP results and the correlations of Chapter 3. FIDAP predicts Nusselt numbers that are about 12% high at the low range of Reynolds numbers studied in comparison to correlation values (equation 3.12) for $P_T = 2$ and $P_L = 2$. Above $Re_D = 200$, the agreement is within about 4%. The trend is quite different for the model having the smaller transverse stagger, however. FIDAP predicts Nusselt numbers that are higher than those given by equation 3.12.. Errors range from 34.3% at $Re_D = 100$ to 14.4% at $Re_D = 300$. For pressure drop predictions, FIDAP predicted values of P* about 17% lower than the results of correlation equations 3.1-3.9 and about 24% lower than equations 3.10-3.11 for $P_T = 1.3$ and $P_L = 2$. For the $P_T = 2$ and $P_L = 2$ case, fairly good agreement between FIDAP and the two correlations for P* was observed at the low end range of Reynolds numbers studied. However, FIDAP predicted P* values approximately 20% higher than the correlations by the time Re_D had reached 340. It is interesting to note that in Figure 4.53, both correlation equations tend toward lower values of P* with higher values

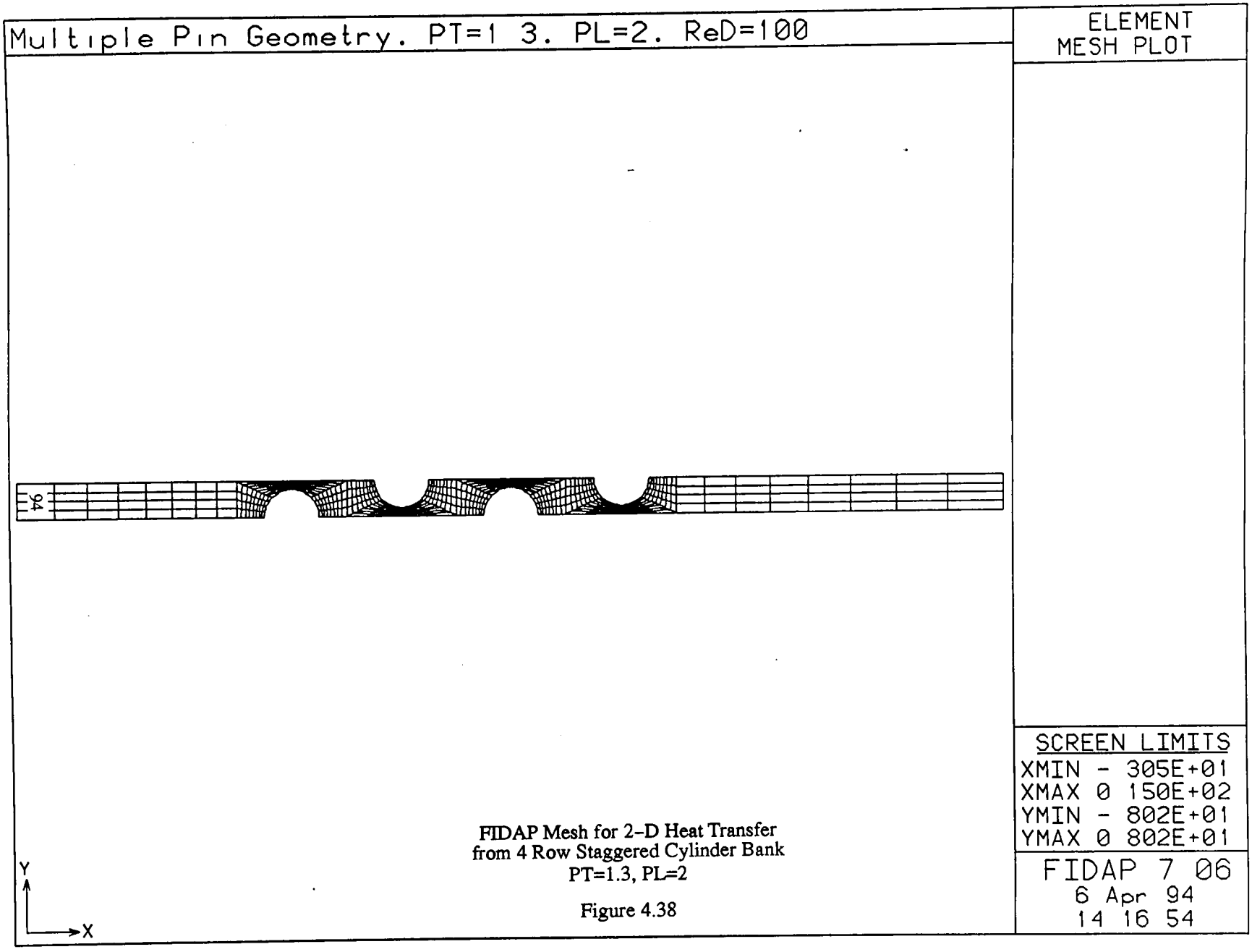

FIDAP Mesh for 2-D Heat Transfer
from 4 Row Staggered Cylinder Bank
PT=1.3, PL=2

Figure 4.38

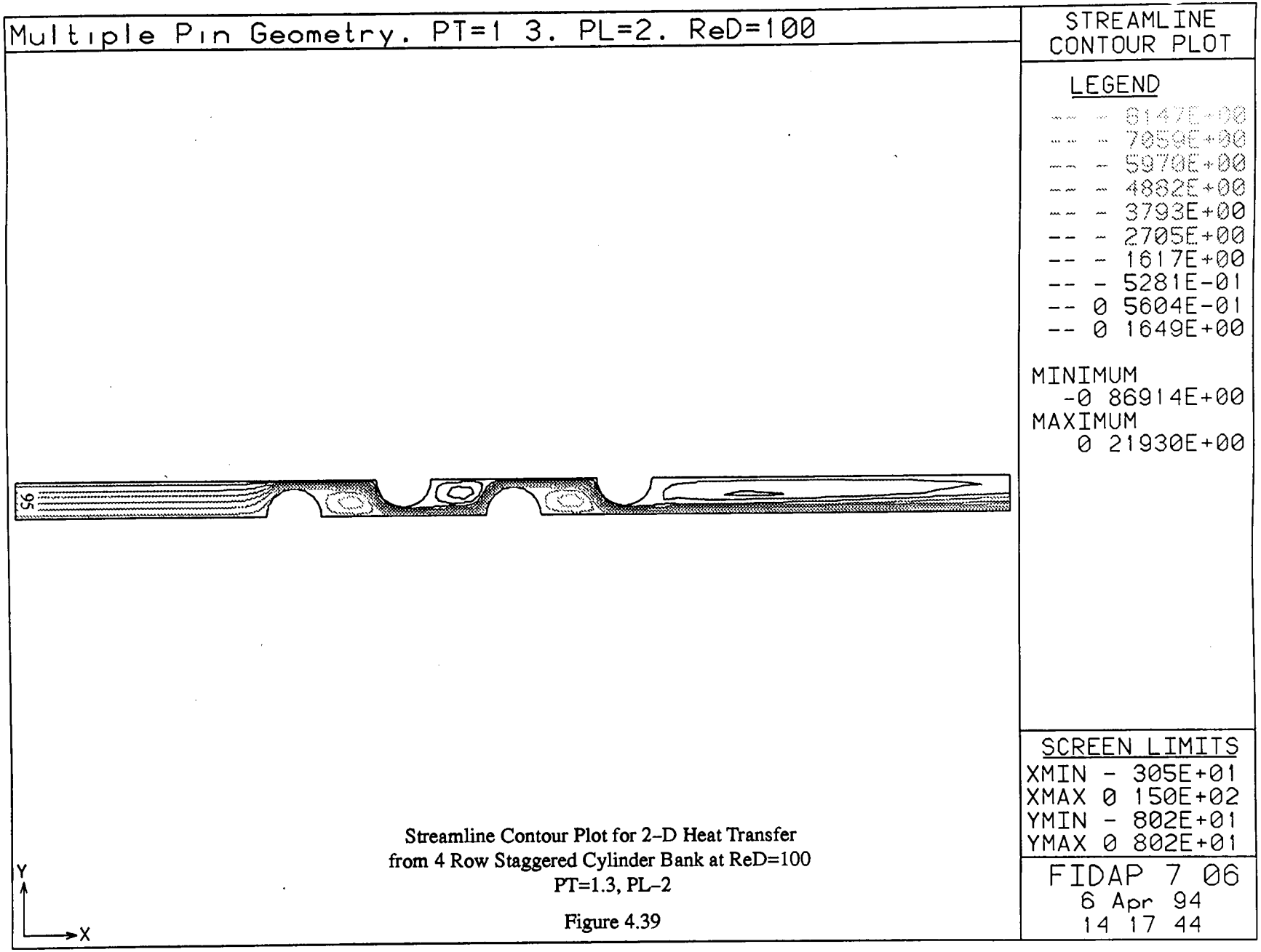

Streamline Contour Plot for 2-D Heat Transfer
from 4 Row Staggered Cylinder Bank at ReD=100
PT=1.3, PL-2

Figure 4.39

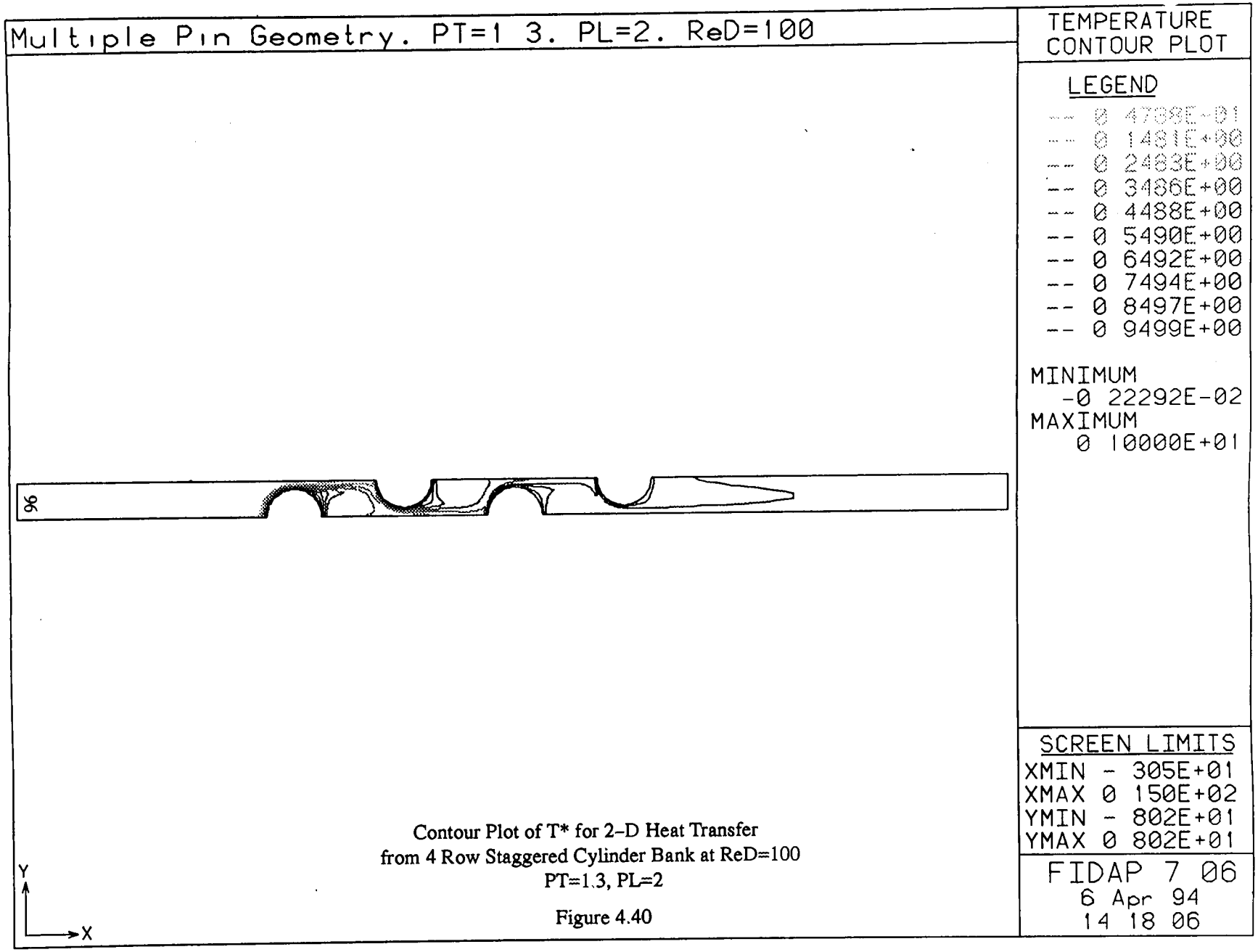

Contour Plot of T* for 2-D Heat Transfer
from 4 Row Staggered Cylinder Bank at ReD=100
PT=1.3, PL=2

Figure 4.40

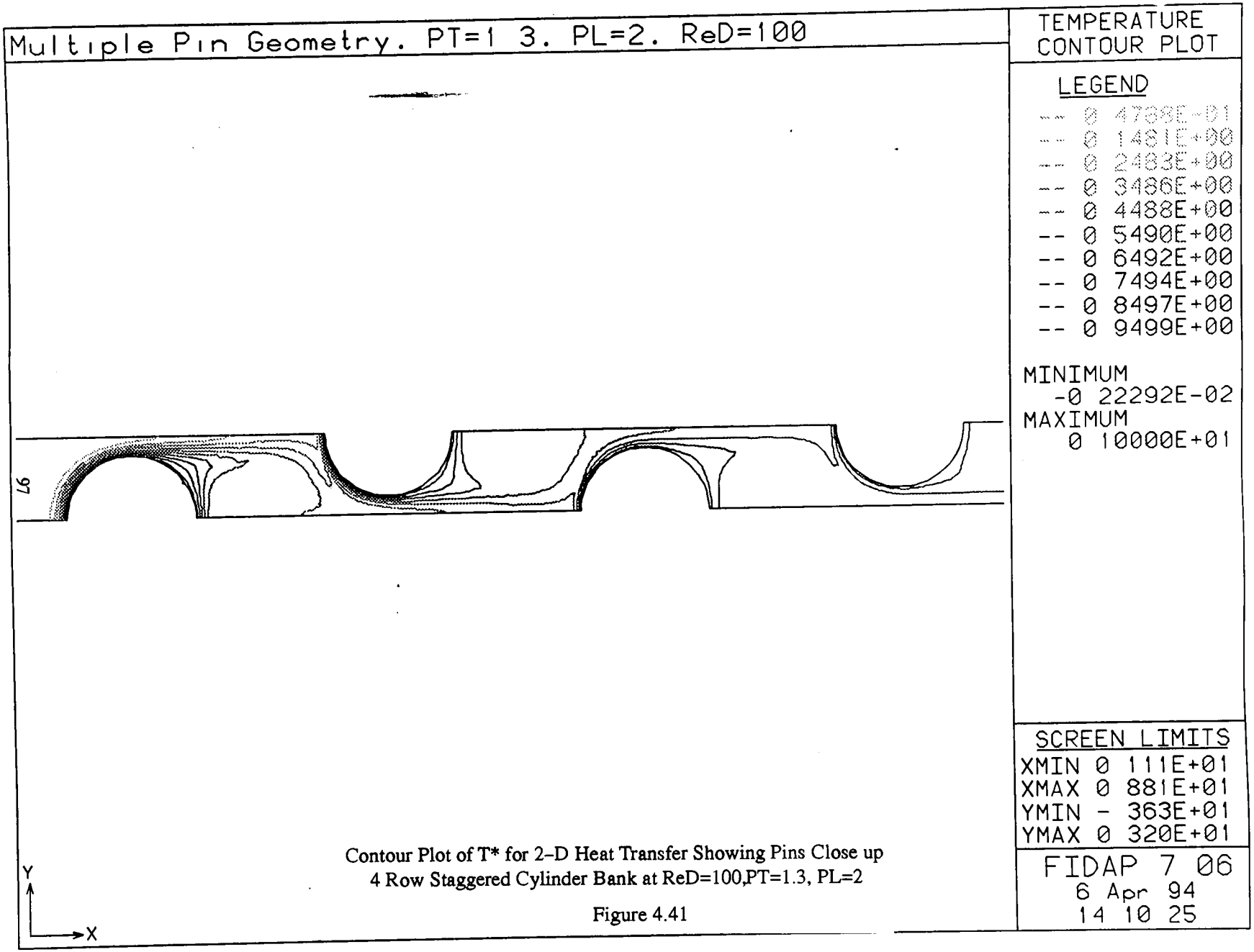

Contour Plot of T* for 2-D Heat Transfer Showing Pins Close up
4 Row Staggered Cylinder Bank at ReD=100,PT=1.3, PL=2

Figure 4.41

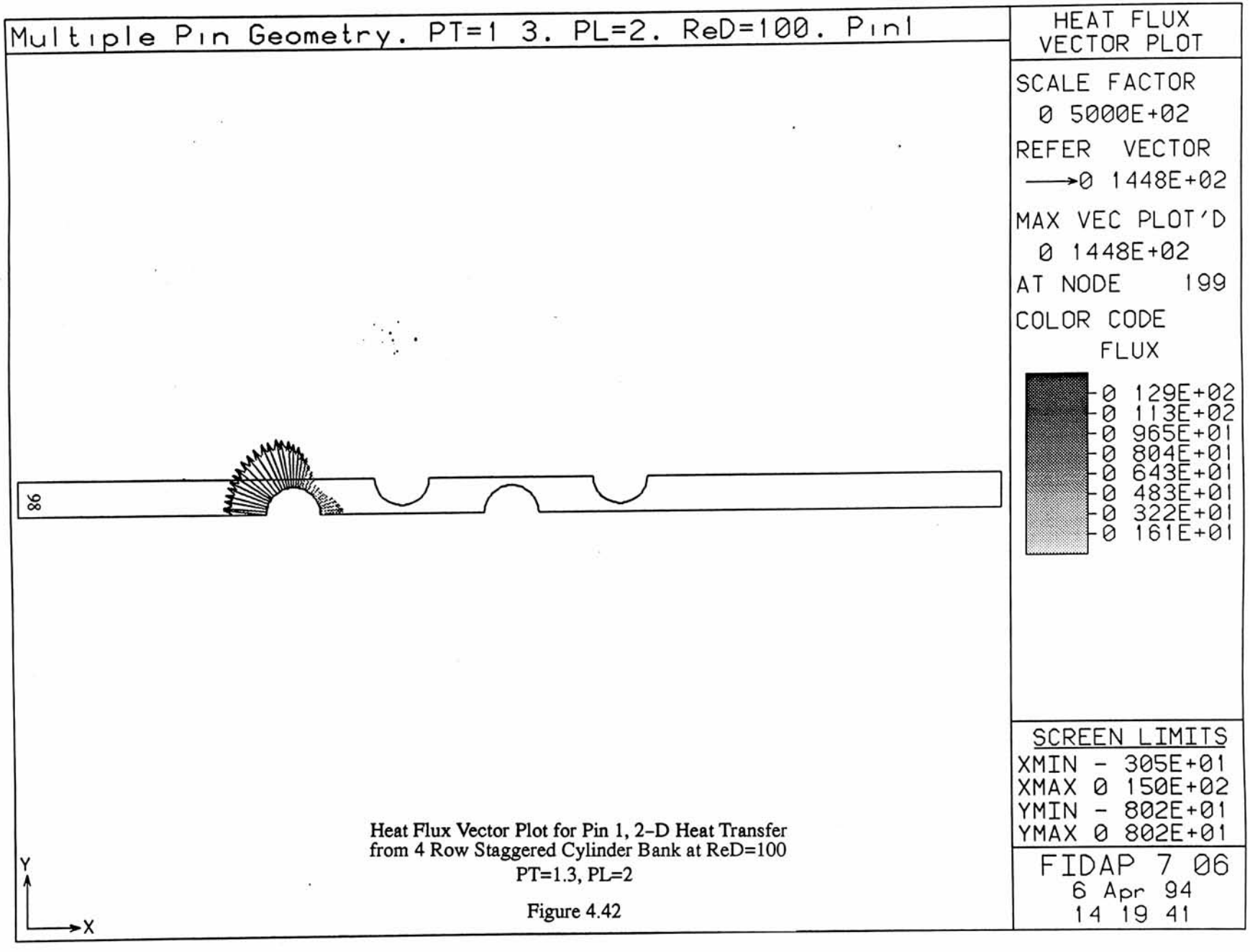

Heat Flux Vector Plot for Pin 1, 2-D Heat Transfer
from 4 Row Staggered Cylinder Bank at ReD=100
PT=1.3, PL=2

Figure 4.42

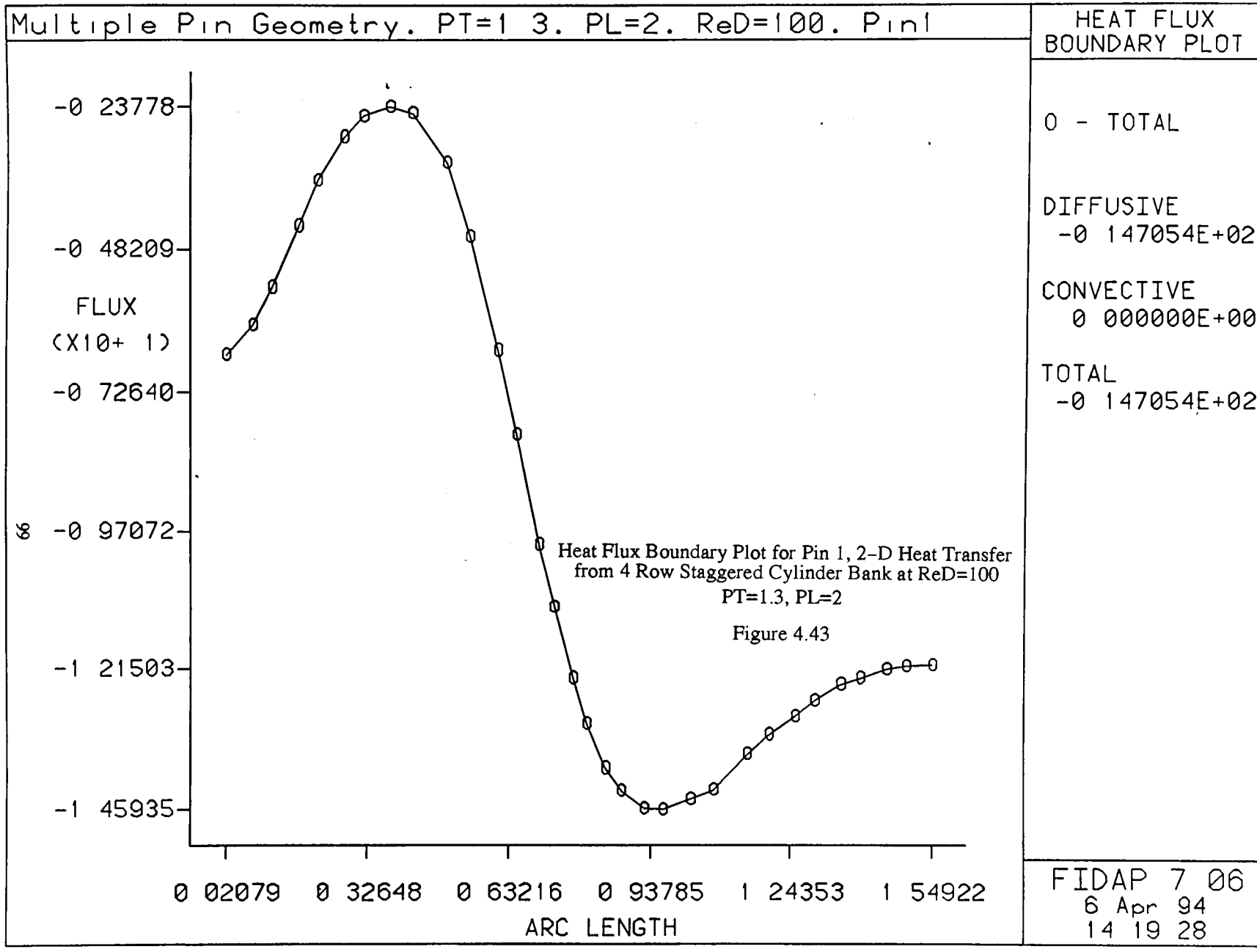

Heat Flux Boundary Plot for Pin 1, 2-D Heat Transfer from 4 Row Staggered Cylinder Bank at ReD=100
PT=1.3, PL=2

Figure 4.43

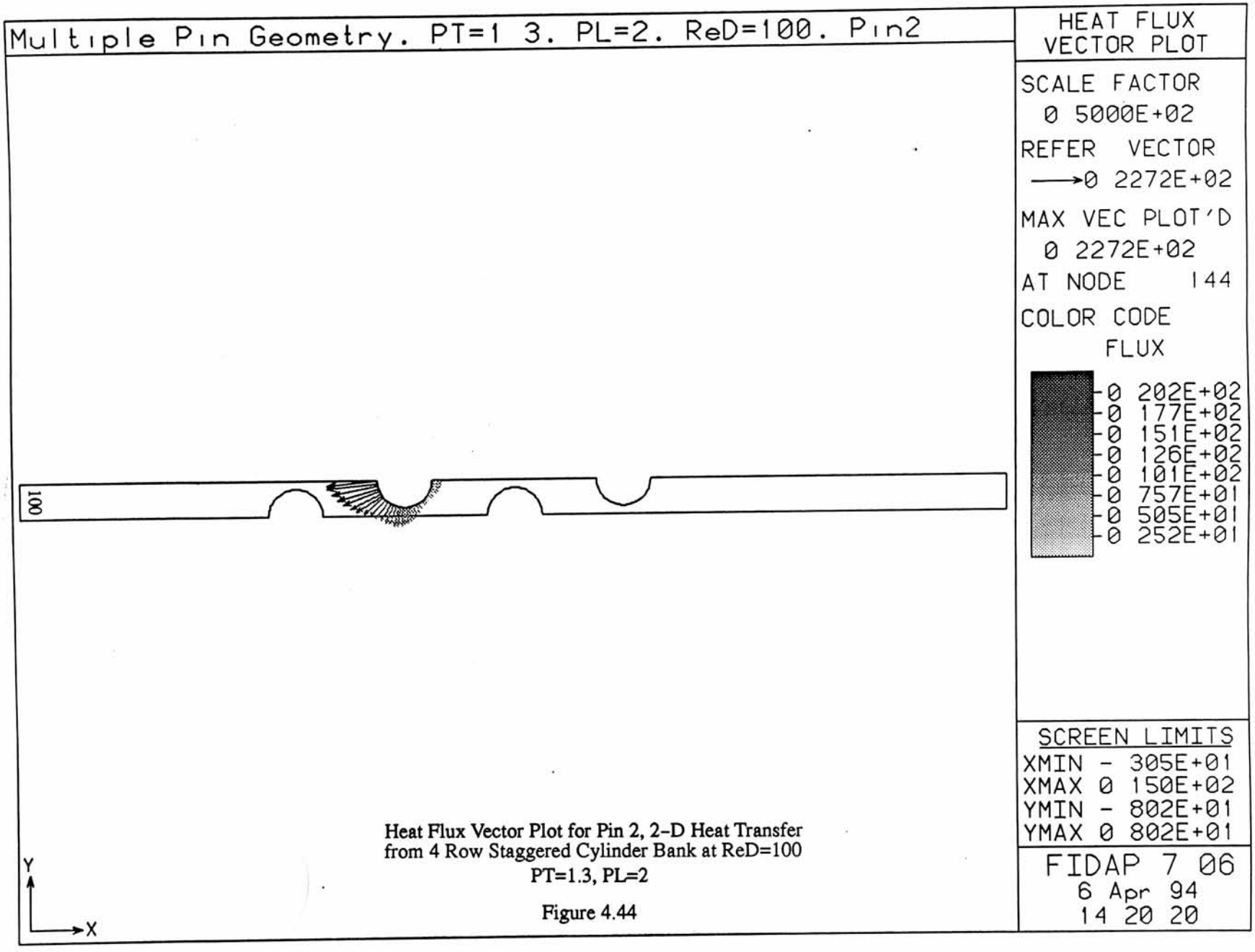

Heat Flux Vector Plot for Pin 2, 2-D Heat Transfer from 4 Row Staggered Cylinder Bank at ReD=100 PT=1.3, PL=2

Figure 4.44

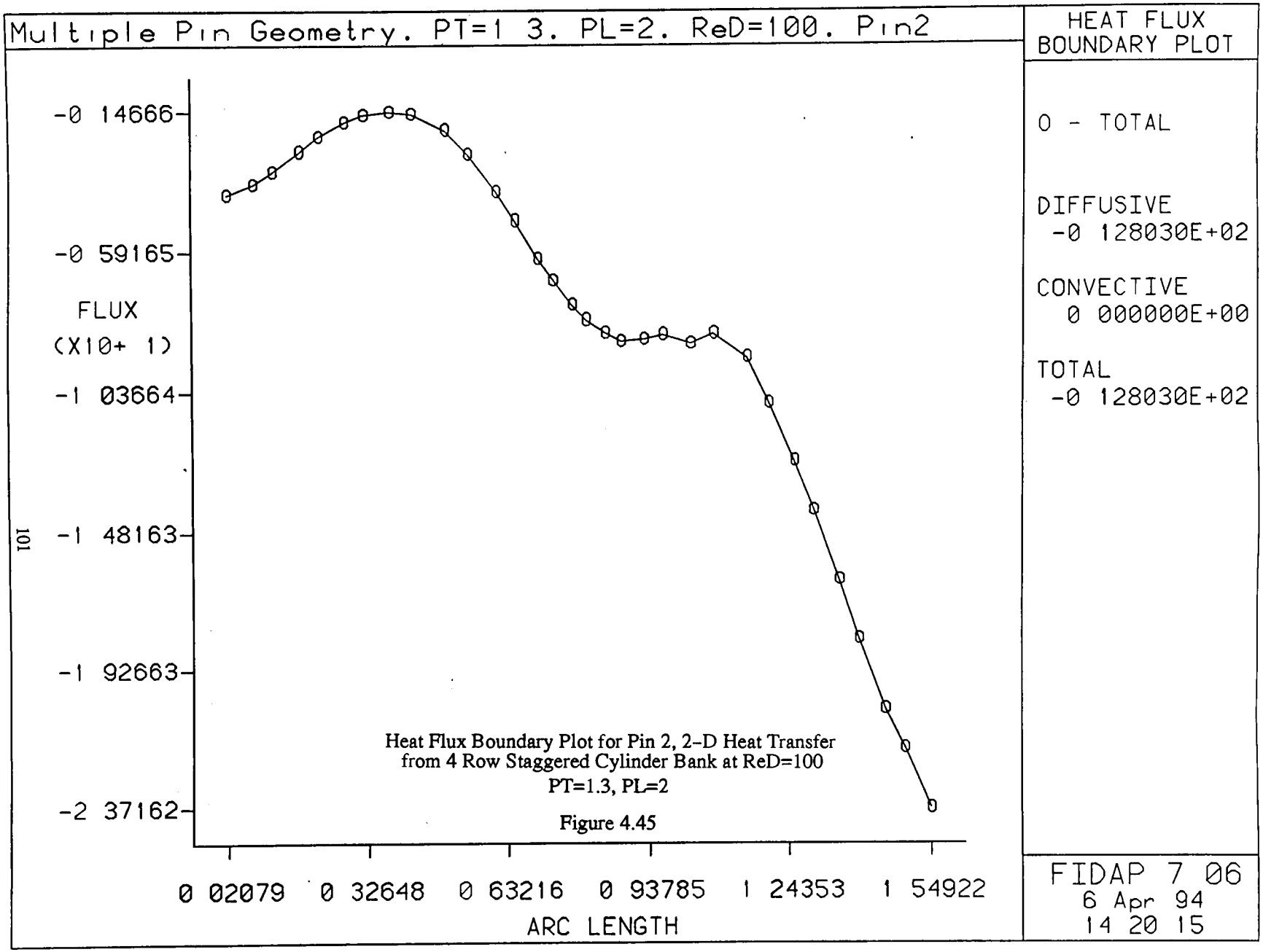

Heat Flux Boundary Plot for Pin 2, 2-D Heat Transfer from 4 Row Staggered Cylinder Bank at ReD=100 PT=1.3, PL=2

Figure 4.45

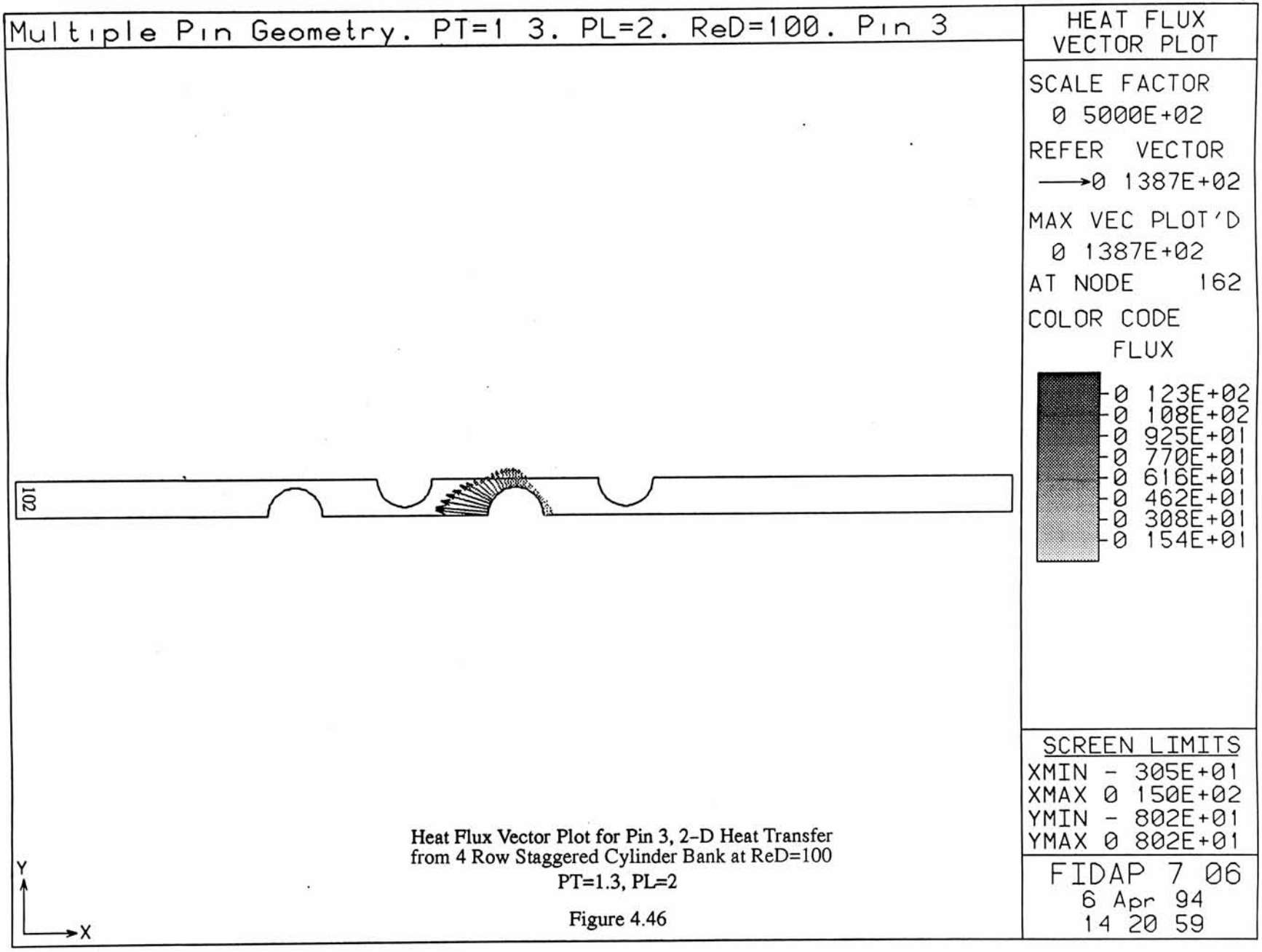

Heat Flux Vector Plot for Pin 3, 2-D Heat Transfer
from 4 Row Staggered Cylinder Bank at ReD=100
PT=1.3, PL=2

Figure 4.46

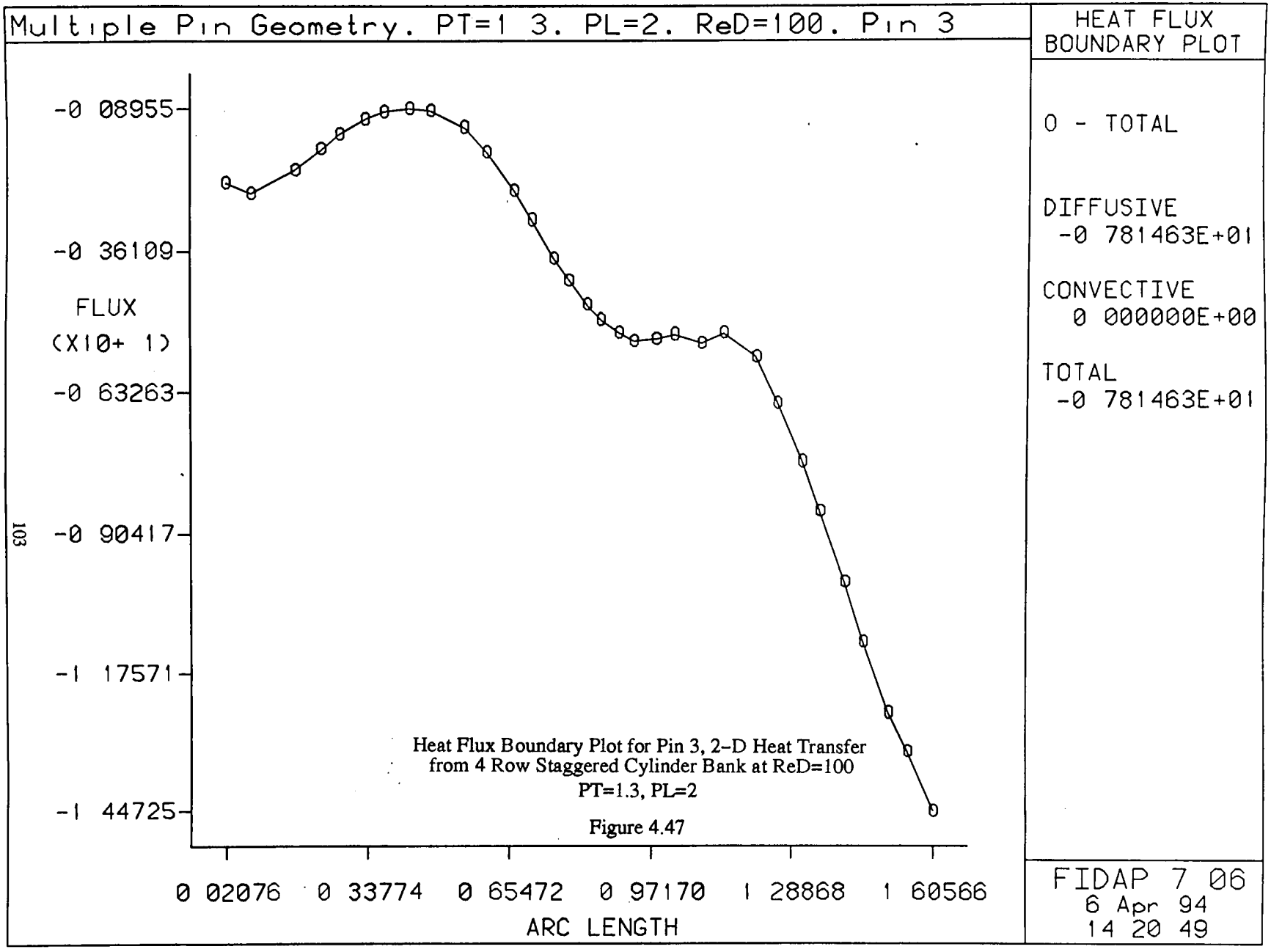

Heat Flux Boundary Plot for Pin 3, 2-D Heat Transfer from 4 Row Staggered Cylinder Bank at ReD=100 PT=1.3, PL=2

Figure 4.47

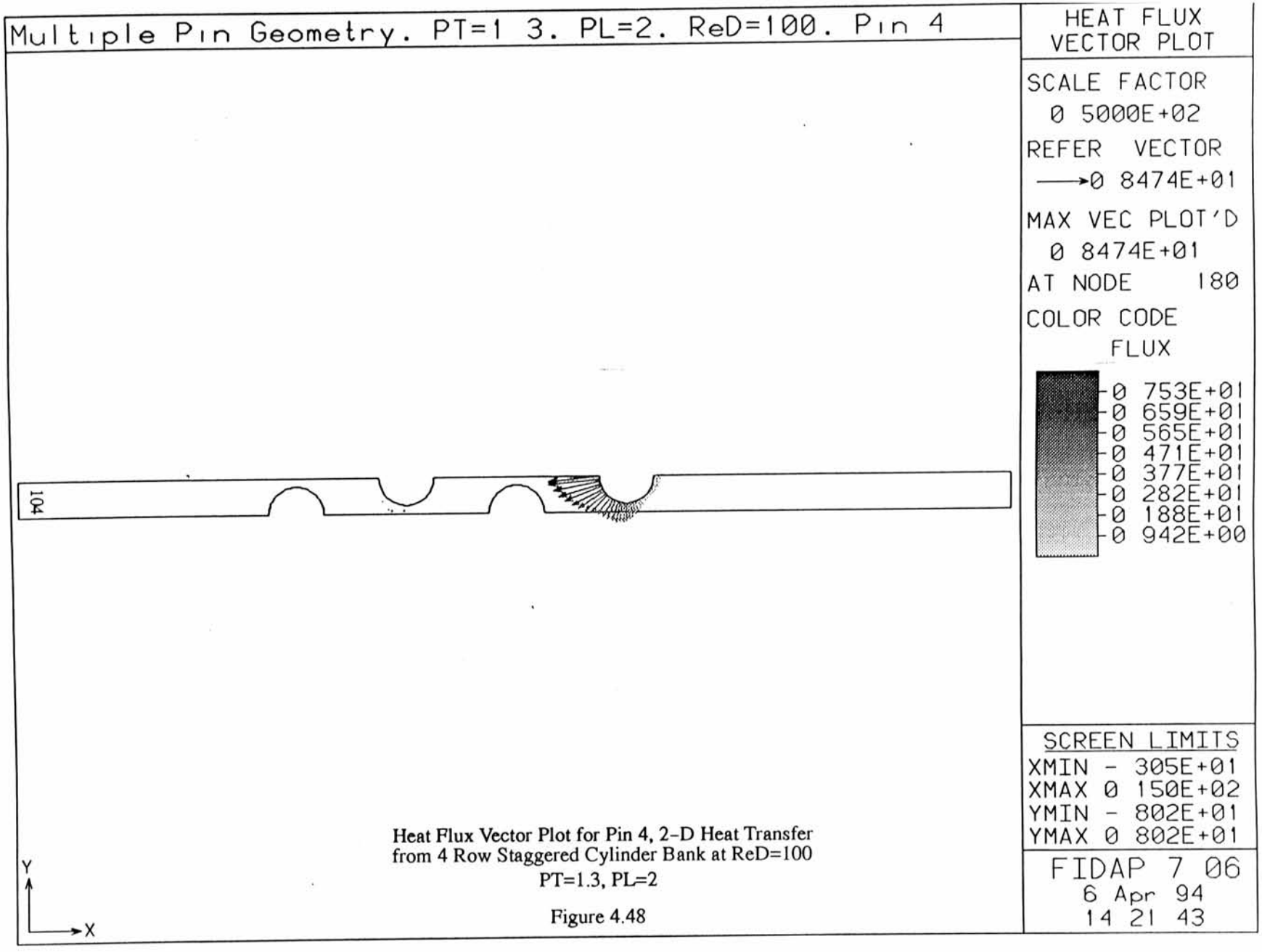

Heat Flux Vector Plot for Pin 4, 2-D Heat Transfer
from 4 Row Staggered Cylinder Bank at ReD=100
PT=1.3, PL=2

Figure 4.48

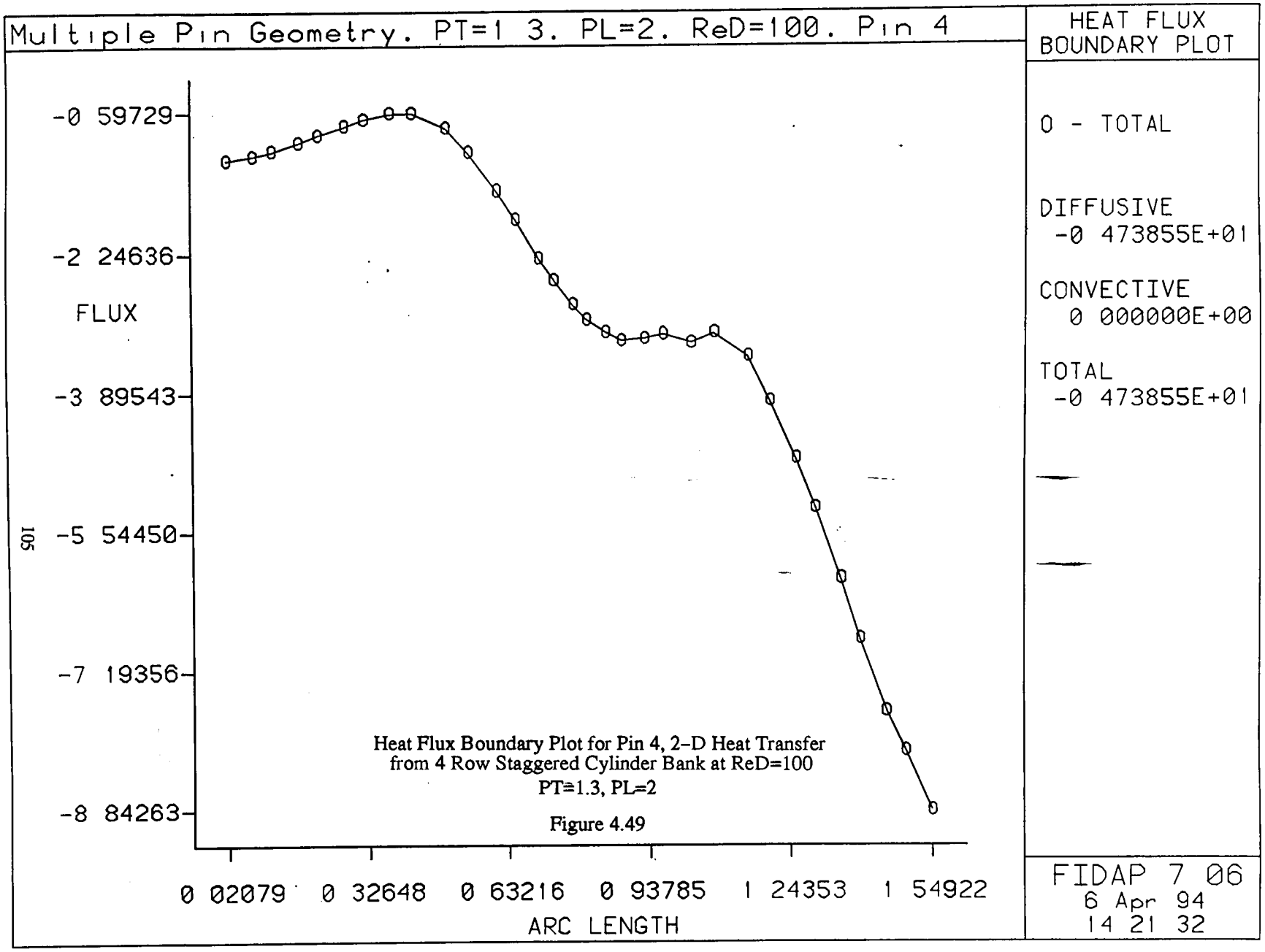

Heat Flux Boundary Plot for Pin 4, 2-D Heat Transfer from 4 Row Staggered Cylinder Bank at ReD=100 PT=1.3, PL=2

Figure 4.49

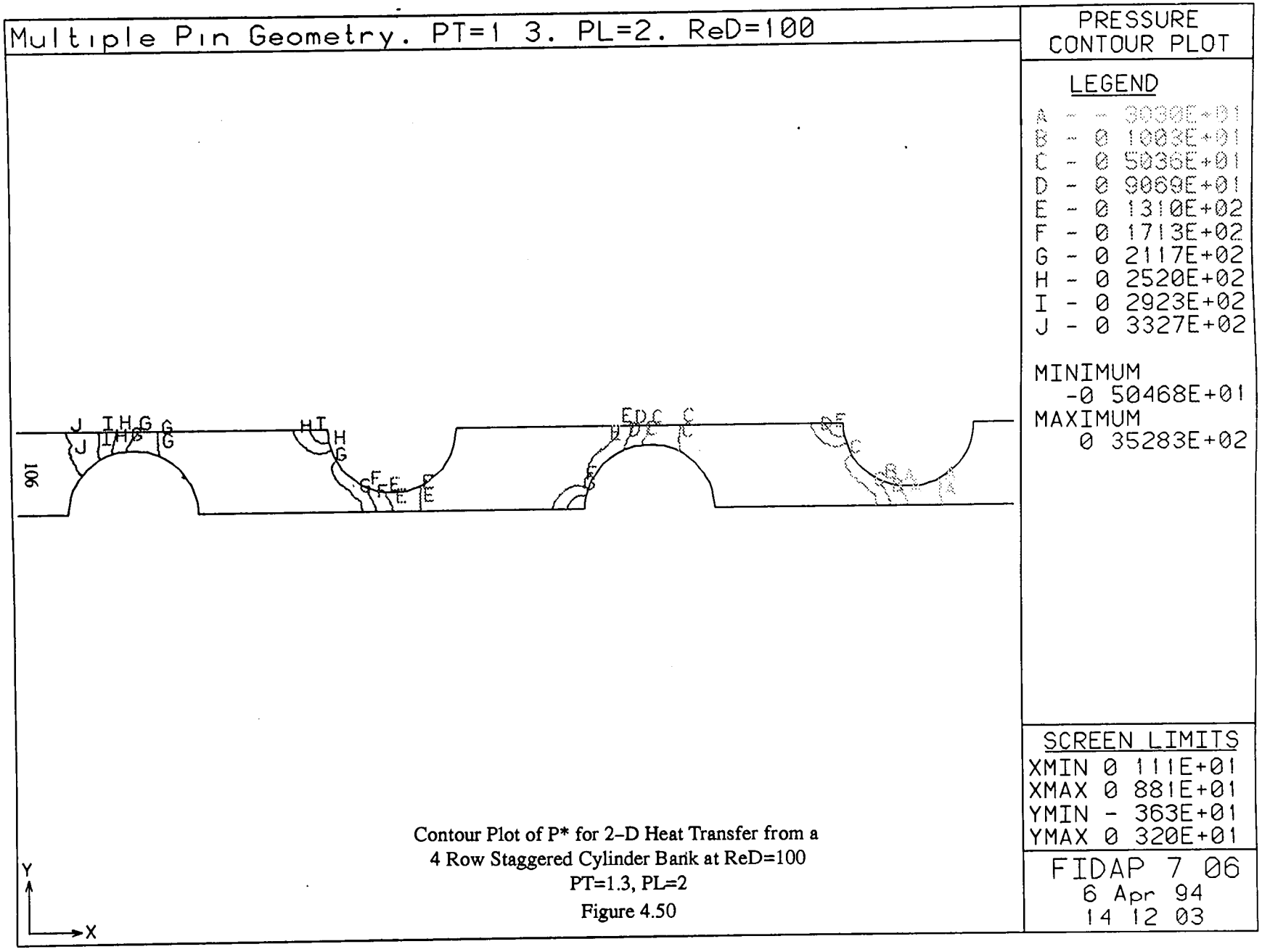

Contour Plot of P* for 2-D Heat Transfer from a
4 Row Staggered Cylinder Bank at ReD=100
PT=1.3, PL=2
Figure 4.50

Table 4.3–Comparison of Predicted Pressure Drops and Nusselt Numbers for a Bank of Heated Cylinders (N=4, P_T=2, P_L=2)

Re_D	Nu predicted by FIDAP	Nu predicted by eqn. 3.12	Dimensionless pressure drop p^* predicted by FIDAP	Dimensionless pressure drop p^* predicted by eqns. 3.1–3.9	Dimensionless pressure drop p^* predicted by eqns. 3.10–3.11
100	8.46	6.92	4.93	5.87	5.04
150	9.75	8.83	4.81	5.16	4.73
200	10.94	10.49	4.90	4.69	4.52
250	12.09	12.00	4.90	4.39	4.36
300	13.20	13.38	4.98	4.19	4.23
325	13.77	14.04	4.97	4.11	4.18
340	14.10	14.43	4.96	4.07	4.15

Table 4.4–Comparison of Predicted Pressure Drops and Nusselt Numbers for a Bank of Heated Cylinders (N=4, P_T=1.3, P_L=2)

Re	Nu predicted by FIDAP	Nu predicted by eqn. 3.12	Dimensionless pressure drop p^* predicted by FIDAP	Dimensionless pressure drop p^* predicted by eqns. 3.1–3.9	Dimensionless pressure drop p^* predicted by eqns. 3.10–3.11
100	13.56	10.10	34.70	44.64	38.84
150	16.20	12.88	30.42	36.61	36.40
200	18.47	15.31	27.94	32.39	34.77
250	20.48	17.50	26.24	30.17	33.55
275	21.42	18.53	25.36	29.50	33.04
300	22.34	19.53	24.62	29.00	32.58

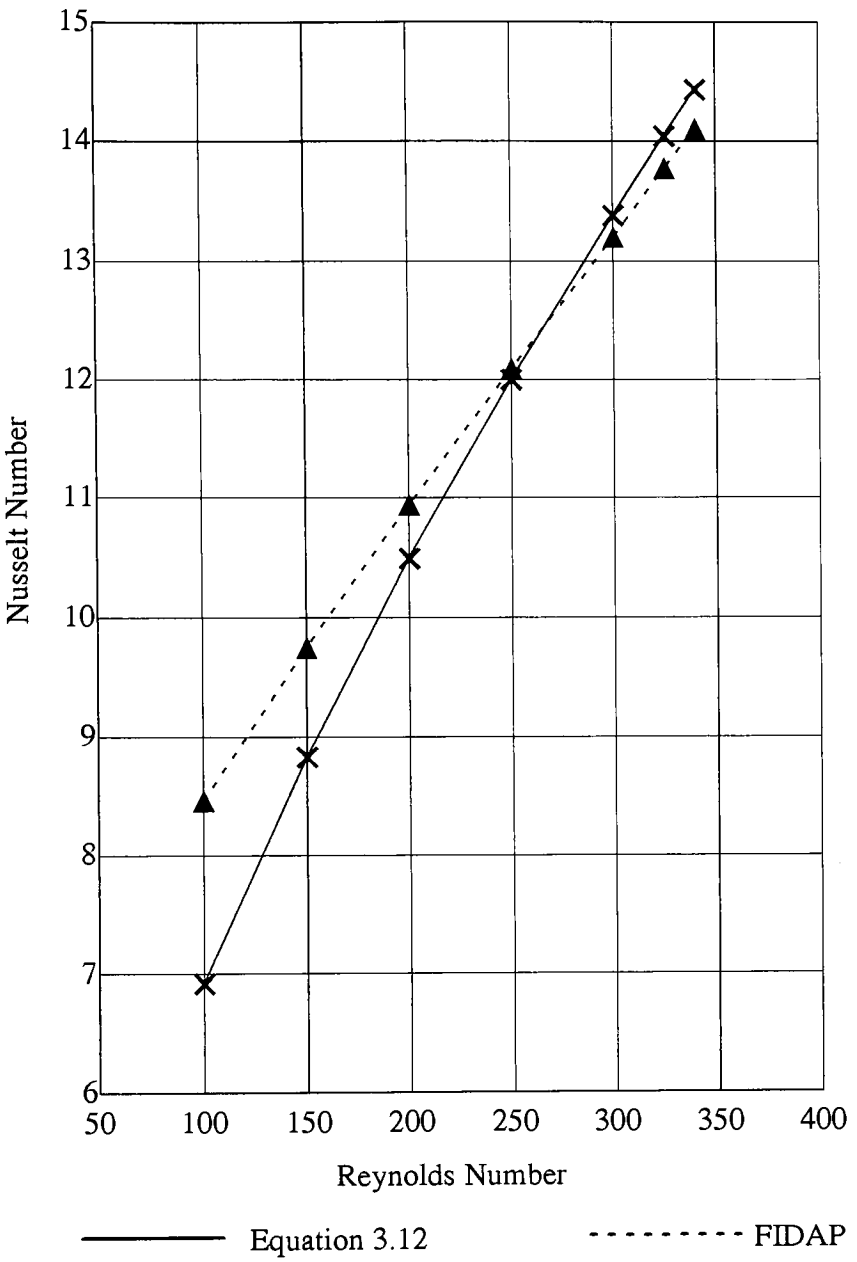

Comparison of FIDAP and
Correlation Predictions of Nusselt
Numbers for a Bank of Heated Cylinders
($N=4$, $P_T=2$, $P_L=2$)

Figure 4.51

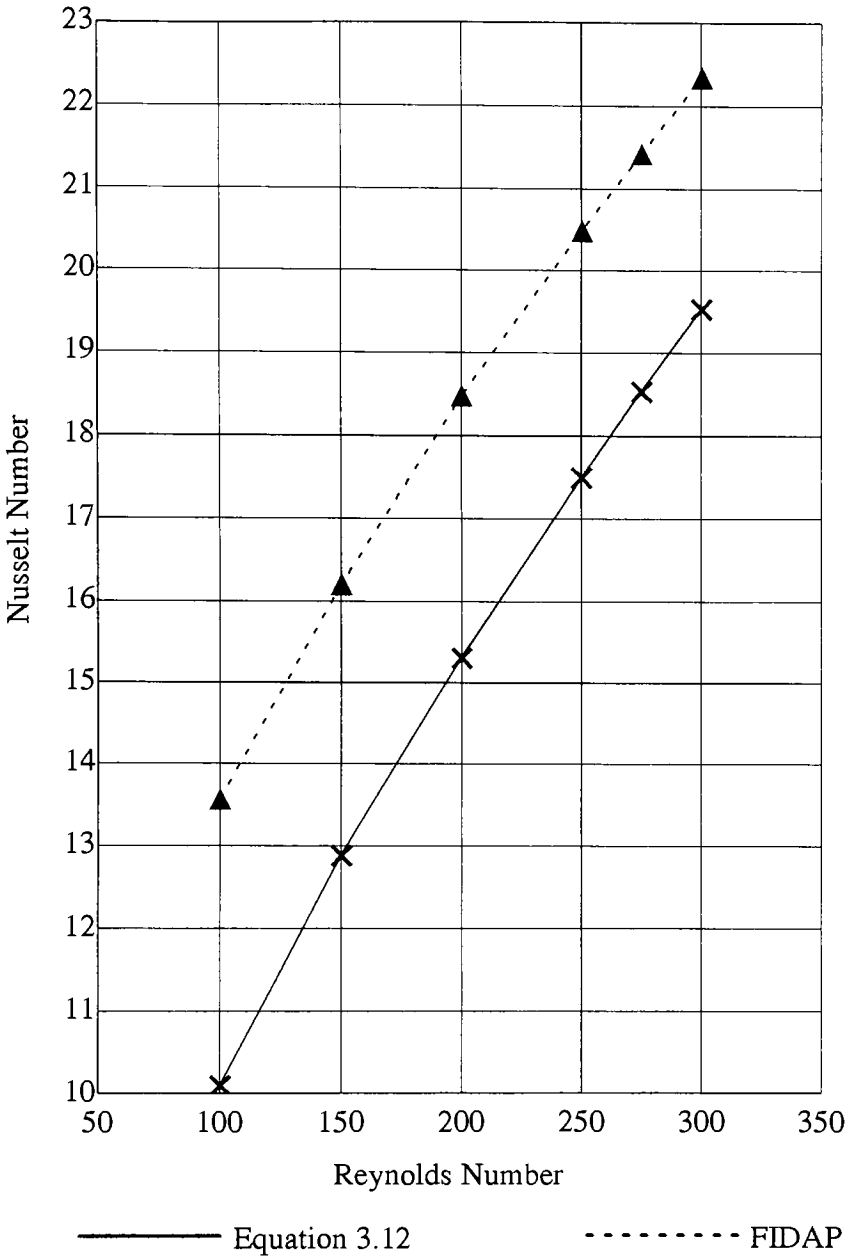

Comparison of FIDAP and
Correlation Predictions of Nusselt
Numbers for a Bank of Heated Cylinders
($N=4$, $P_T=1.3$, $P_L=2$)

Figure 4.52

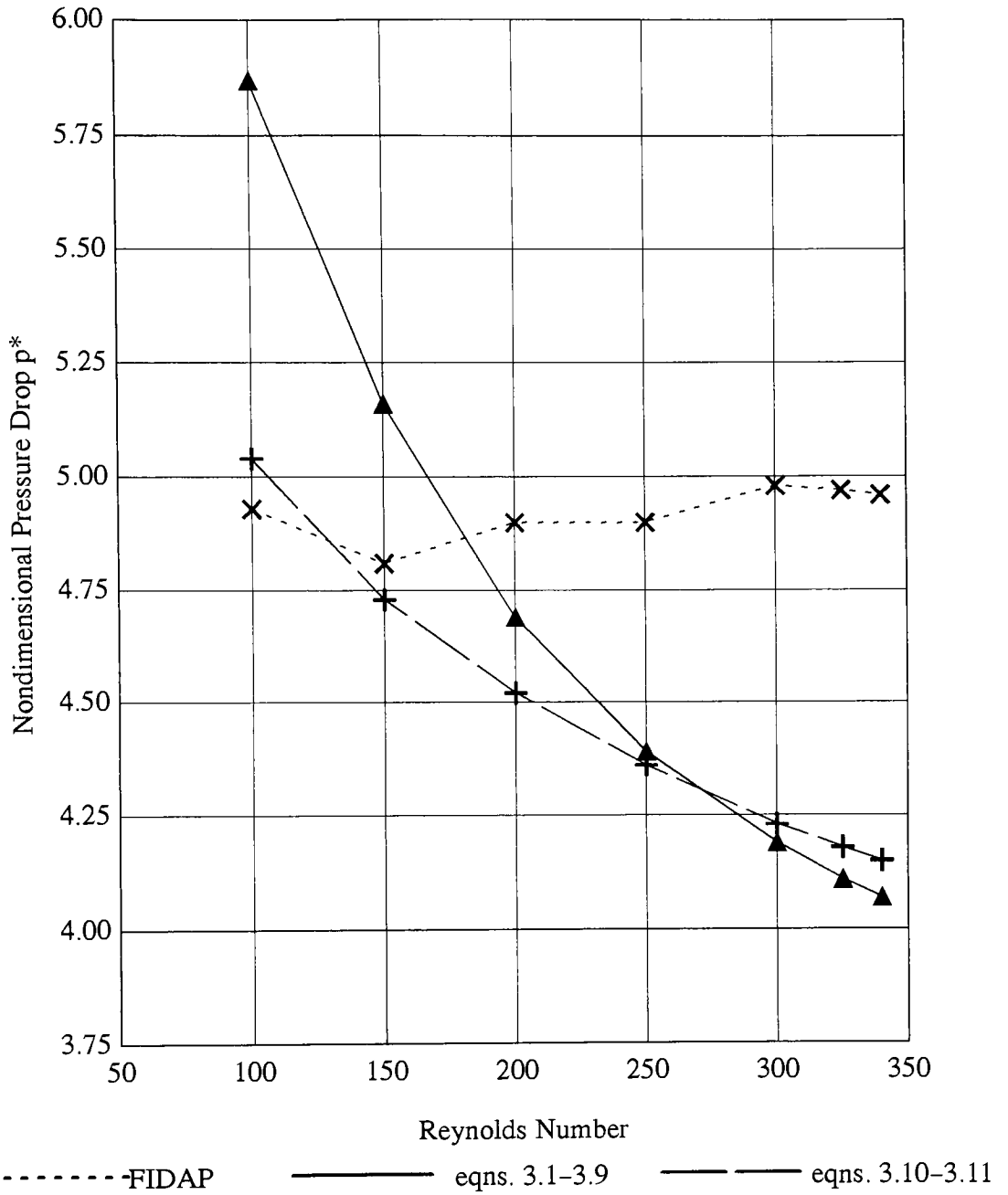

Comparison of Nondimensional Pressure Drop
as Predicted by FIDAP, eqns. 3.1-3.9 and eqns. 3.10-3.11
for N=4, PL=2, PT=2

Figure 4.53

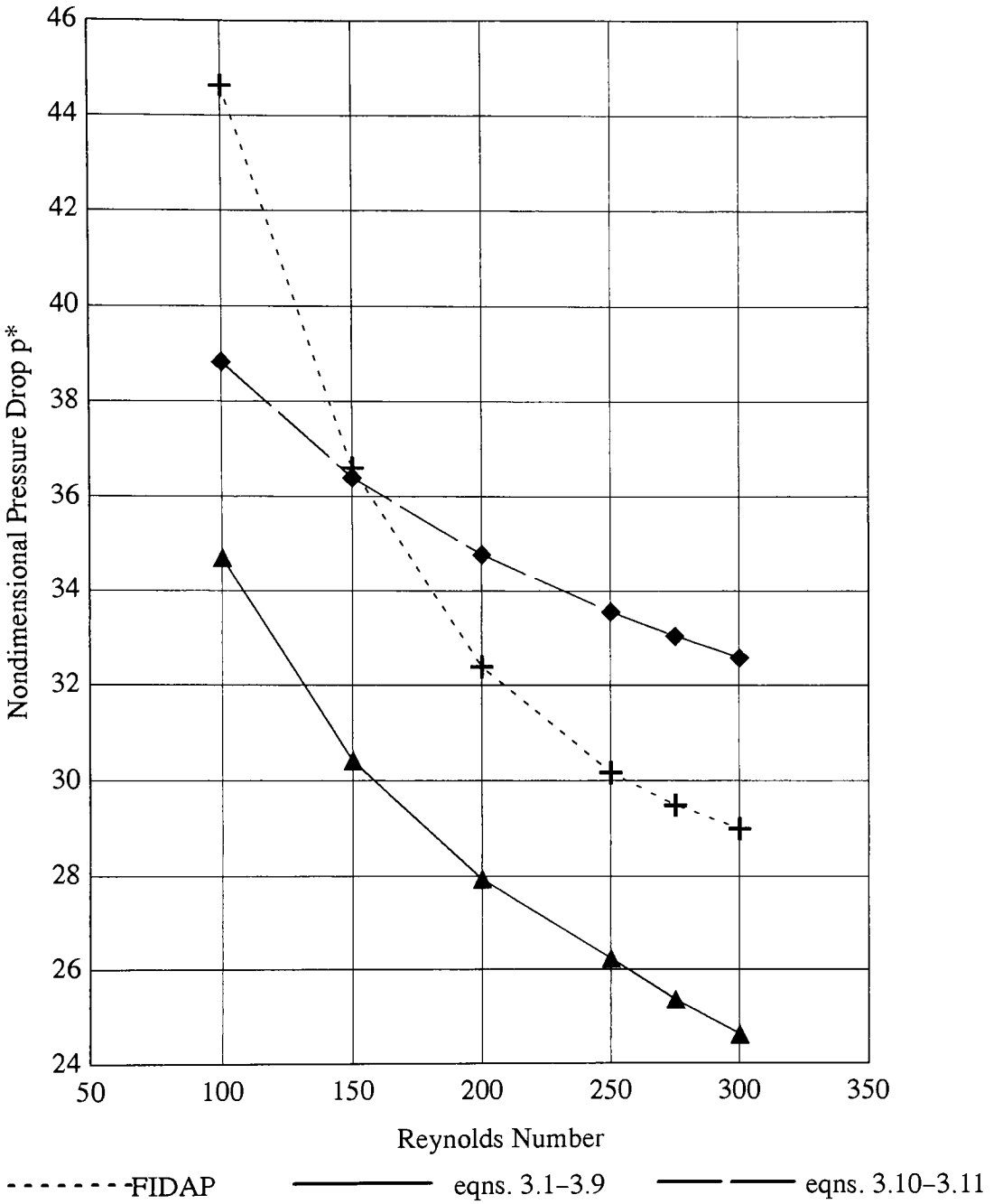

Comparison of Nondimensional Pressure Drop
as Predicted by FIDAP, eqns. 3.1–3.9 and eqns. 3.10–3.11
for N=4, PT=1.3, PL=2

Figure 4.54

of Reynolds number whereas FIDAP results remain fairly flat. For the P_T = 1.3 and P_L = 2 case (Figure 4.12), both correlations and FIDAP exhibit decreasing p* with higher values of Reynolds number.

One of the simplifying assumptions in the all of the FIDAP modeling performed is that flow conditions are laminar everywhere. Free stream turbulence (which is very dependent on experimental setup) is often mentioned in the literature as a possible contributor to correlation–to–correlation differences.

CHAPTER 5

EXPERIMENTAL PROCEDURES AND RESULTS

5.1 Determination of System Fan Performance Curves

The cold side and hot side pin fins of the heat pump in question are supplied air through a ductwork system that significantly alters the raw performance of the fans that move the air. The configuration of this air handling system was described briefly in Section 1.3. It is appropriate to elaborate upon that description at this point because the ductwork/fan system design heavily influenced the way in which the experiments were devised to determine the hot and cold side pressure versus flow curves.

Figures 5.1, 5.2, and 5.3 are diagrams showing the insulated container that the heat pump is meant to cool. The top and bottom sealing/insulating plates have been removed in Figure 5.1 so that the air flow patterns may be better illustrated. The container has two levels. The upper level consists of two concentric annular channels that are hermetically sealed from one another. The two separate flows of cooled air enter this upper level through the cold air exhausts shown in the top view of Figure 5.1. The air from each exhaust splits into two flows, one traveling clockwise around its channel and the other traveling counterclockwise. The two flows meet again at the cold air return, which is situated 180° from the exhaust for both the inner and outer channel. The cold air return is a pathway to a lower level in the container, which is shown in the side and bottom views of Figure 5.2 and 5.3. The air is drawn through the cold air return by a pair of tubeaxial fans, each of which drives the air through either the inner or outer channel exclusively. The fans force the air over the cold side pin fins and then out the cold air exhaust where it once again enters the upper level. Section A–A shown in Figure 5.2 illustrates the cross sectional dimensions of the inner and outer channel with all

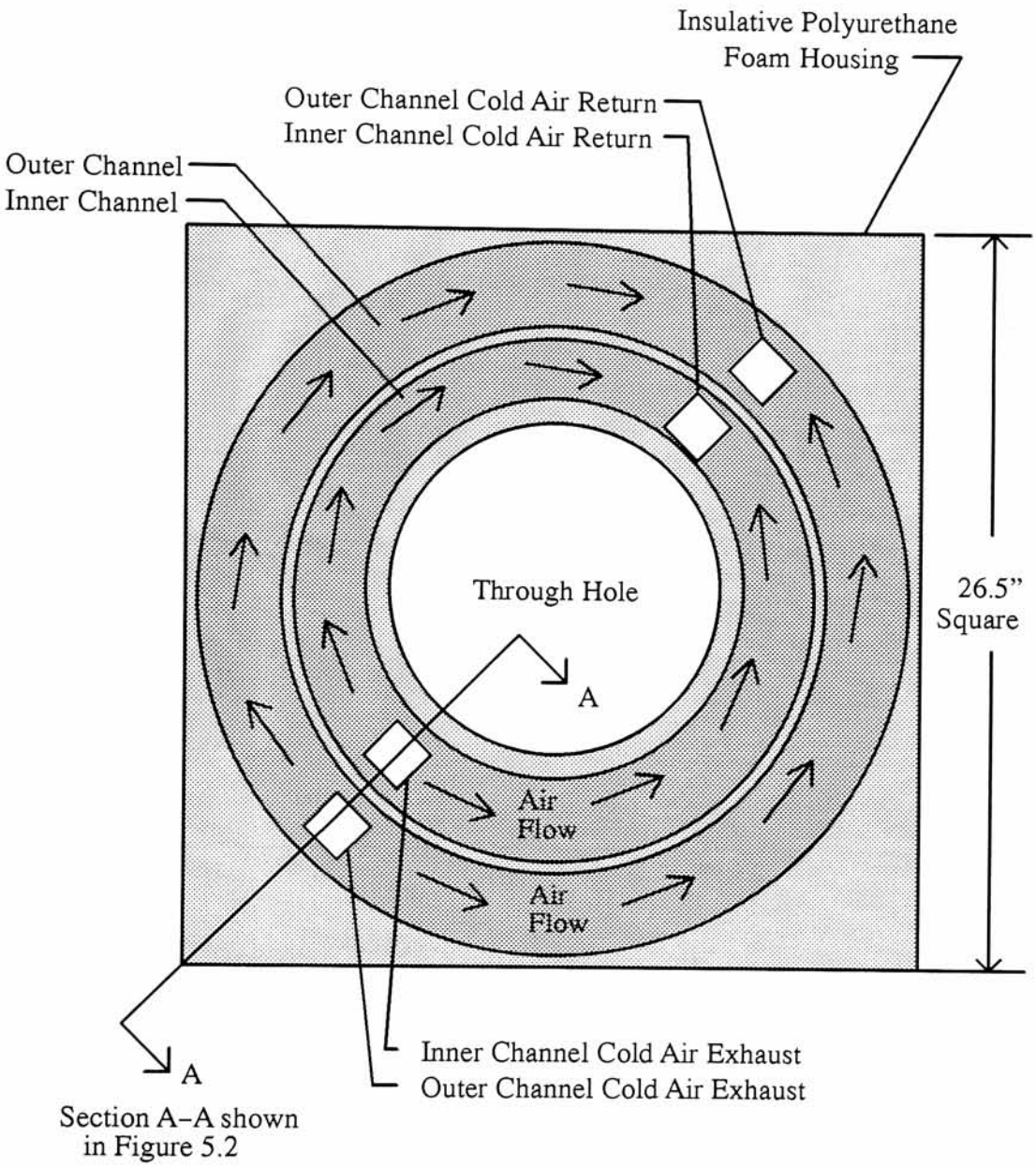

Top View of Insulated Container
Figure 5.1

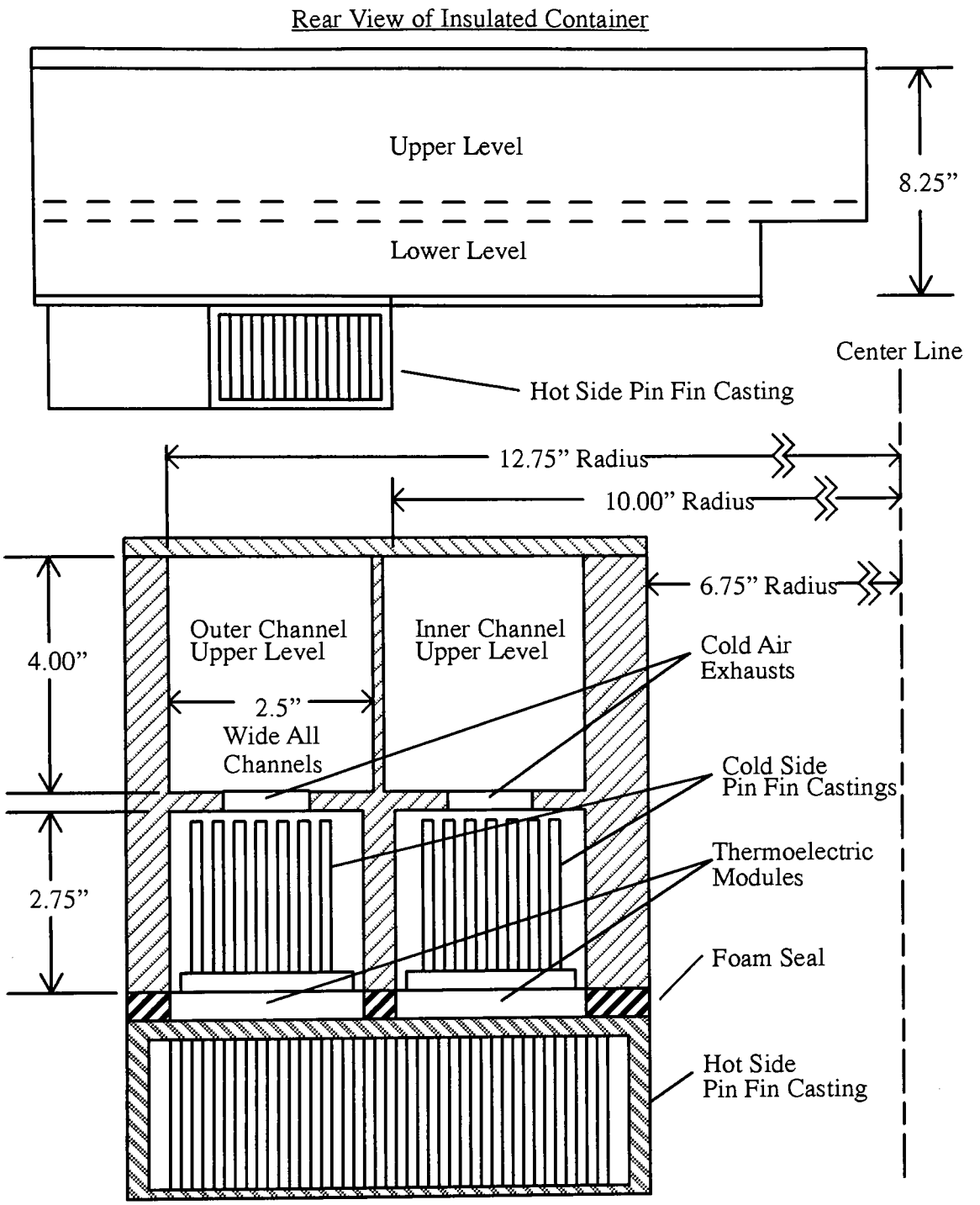

Section A-A shown in
Figure 5.1

Rear and Section View of
Insulated Container
Figure 5.2

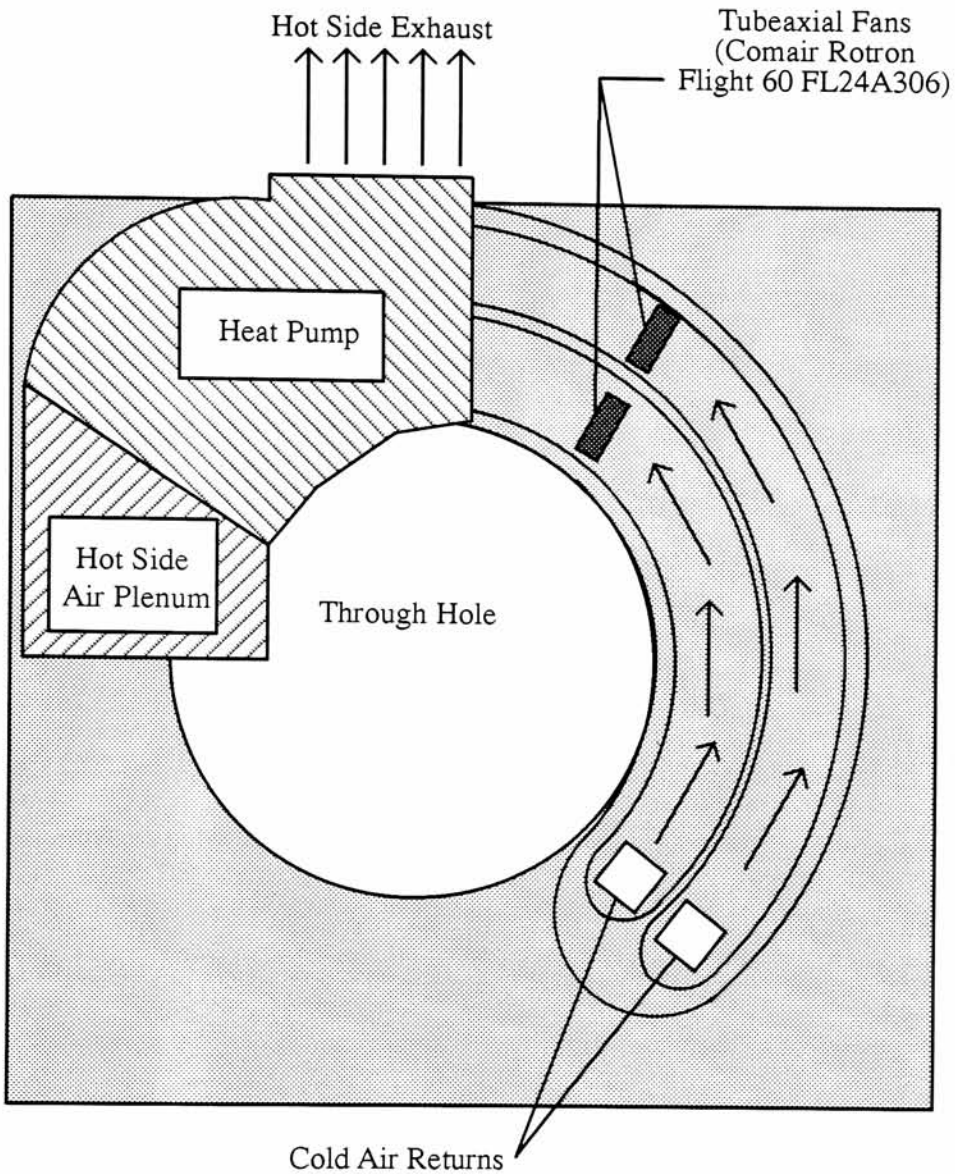

Bottom View of
Insulated Container

Figure 5.3

seals in place.

A plate which replaced the entire heat pump assembly was constructed as a first step in developing a pressure versus flow curve that would be representative of what a variety of cold side pin fin geometries would see. On this plate were provisions for installing choke plates with various impedances to flow which could be introduced into the outer channel. The choke plate was located at the center point of the bank of cold side pin fins which services the outer channel. Two pressure taps were fitted on either side of the choke plate. Three equally spaced holes were drilled into the lower level of the outer ring so that a hot wire anemometer could be introduced into the flow stream to measure air velocity. The hole pattern was located 4" up stream of the fan. Although a greater distance from the fan to this measuring point would have been desirable, this was impractical because of the size of the anemometer probe and the limited space surrounding the insulated container. Only the outer channel was instrumented to make this pressure versus flow determination. Although the path length through the inner channel is somewhat less than that of the outer channel, the same obstructions that result in substantial pressure drops (losses through the cold air exhausts and returns, 90° elbow, and so on) are encountered. It is therefore expected that the impedance characteristics of the inner channel are nearly identical to those of the outer channel. The experimental apparatus is shown in Figure 5.4.

The general experimental procedure followed was to first install a choke plate having a particular impedance and then take a pressure drop reading with the manometer. A total of 9 air velocity readings were then taken (3 positions at each of the 3 holes shown in Figure 5.4). These values were averaged and then multiplied by the cross sectional area of the duct to give the volumetric flow rate. The raw data is displayed in Table 5.1. A plot of the pressure

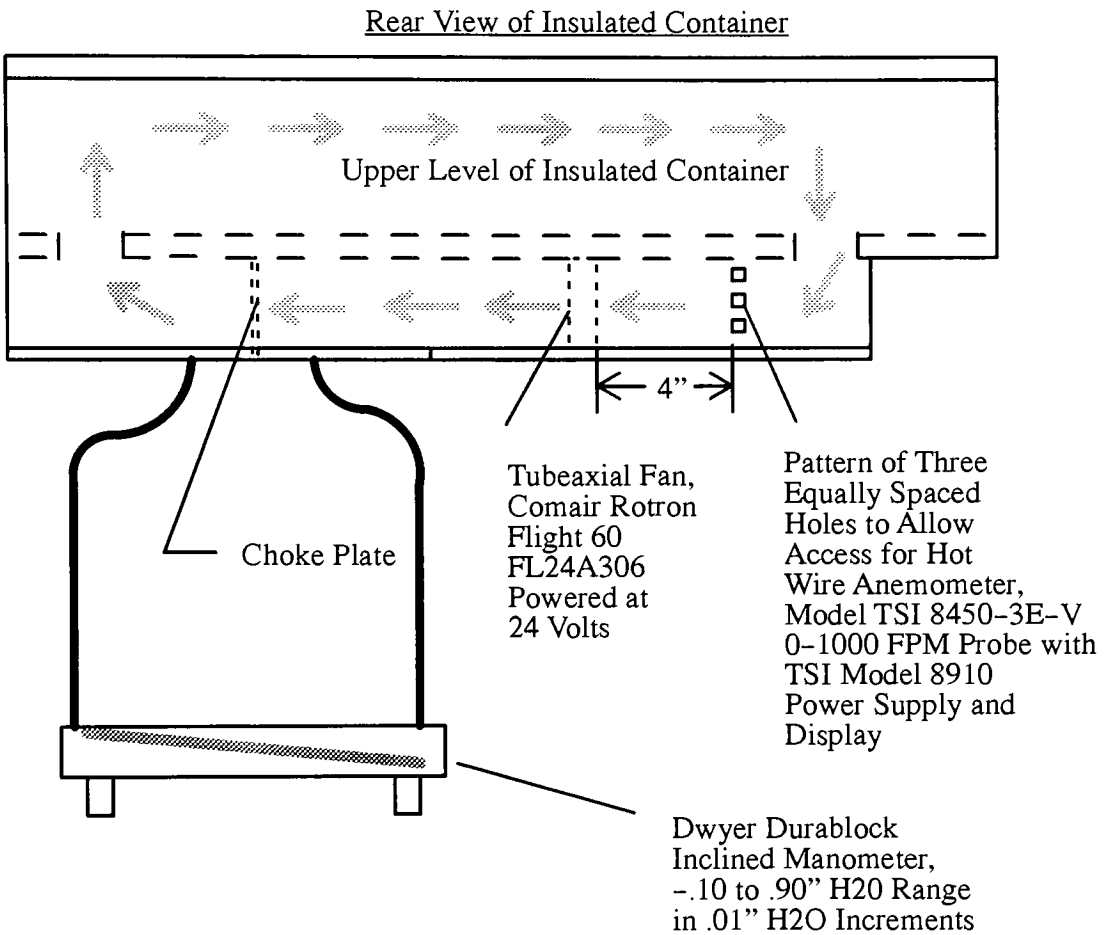

Experimental Apparatus to Measure
Pressure versus Flow Characteristics
of Cold Side Air Delivery System

Figure 5.4

Table 5.1–Pressure Versus Flow Data for Cold Side Air Delivery System	
Pressure Drop in Inches of H_2O	Volumetric Flow Rate in CFM
0.00	11.37
0.02	10.90
0.04	9.66
0.06	6.68
0.08	2.95
0.09	0.08

versus flow curve is shown in Figure 5.5 along with the following correlation which was used in the FORTRAN program COPT.FOR for the determination of fan performance:

$$\Delta P \ ("H_2O) \ = \ .028 * (11.46 - \dot{V})^{.488} \qquad (5.1)$$

ΔP is the pressure drop in inches of water and $\dot{V}$ is the volumetric flow rate in cubic feet per minute.

A similar approach was used to determine the pressure versus flow curves for the hot side air delivery system. Because the side walls of the hot side pin fin casting form part of the ductwork, it was first necessary to remove all the pins from a hot side pin fin casting. A pressure tap was fitted upstream of the hot side casting and a flow straightener was constructed with provisions to accept choke plates having varying amounts of open area. This flow straightener/choke plate assembly was fitted to the exhaust end of the hot side heat exchanger. The experimental apparatus is shown in Figure 5.6. The procedure used to generate data from this apparatus was to install a choke plate with a particular impedance to flow and then take a pressure drop reading with the manometer. Flow velocity readings were then taken at 15 equally spaced points across the exhaust of the flow straightener. These velocity readings were averaged and multiplied by the cross sectional area of the flow straightener to give volumetric flow rate. The raw data from this experiment is presented in Table 5.2. Figure 5.7 is a plot of the data. A point to point interpolation of this data was used in the FORTRAN program HOPT.FOR as part of the iterative process for determining flow rate through the hot side pin fin bank. It is interesting to note that this curve has much more of a linear character than does the cold side system curve. This may be a result of the hot side pin bank being fed through a plenum which also provides air to other areas of the machine (i.e., the flow branches up stream of the hot side heat exchanger). This is illustrated

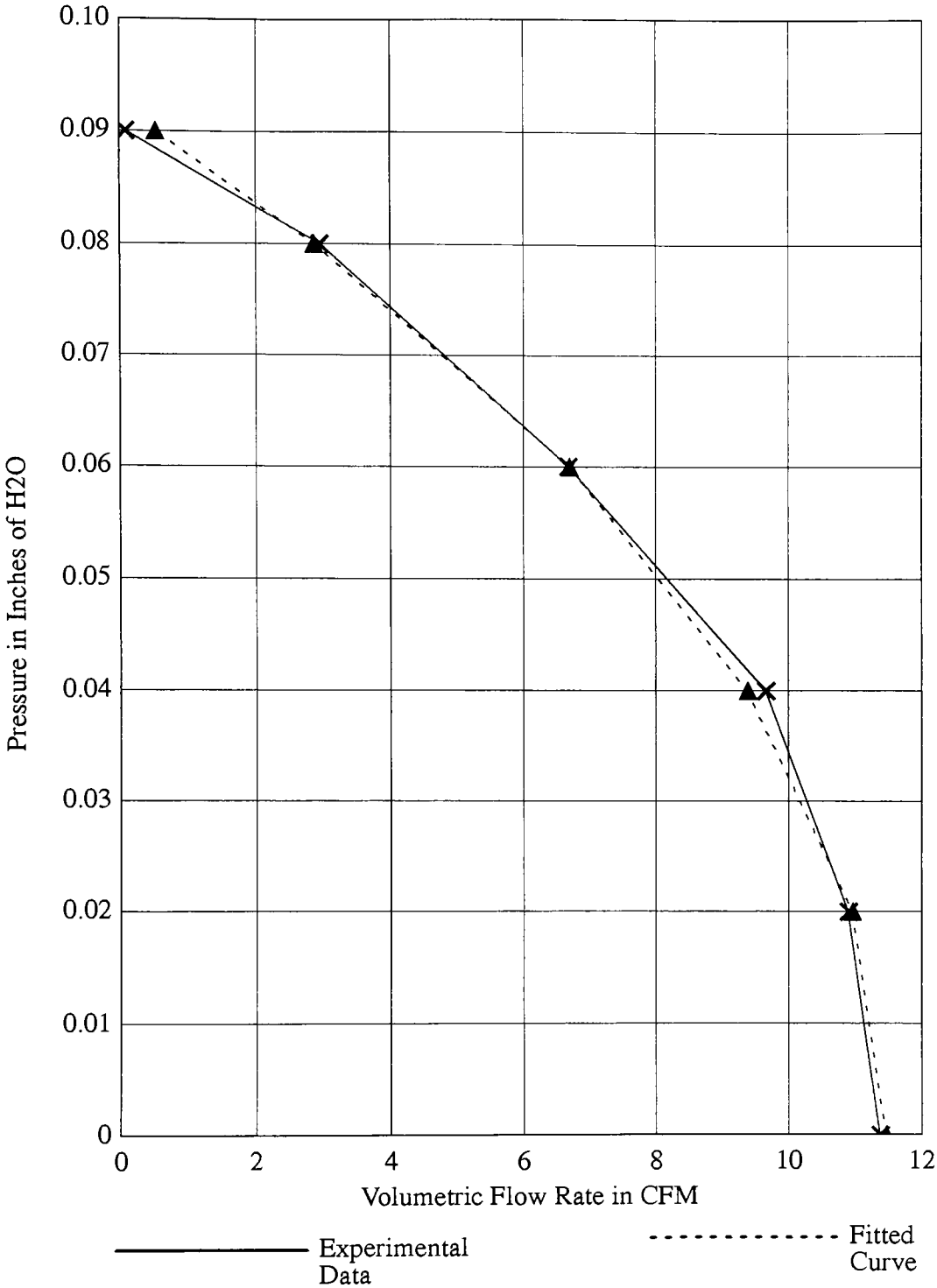

Pressure versus Flow Curve for
Cold Side Air Delivery System

Figure 5.5

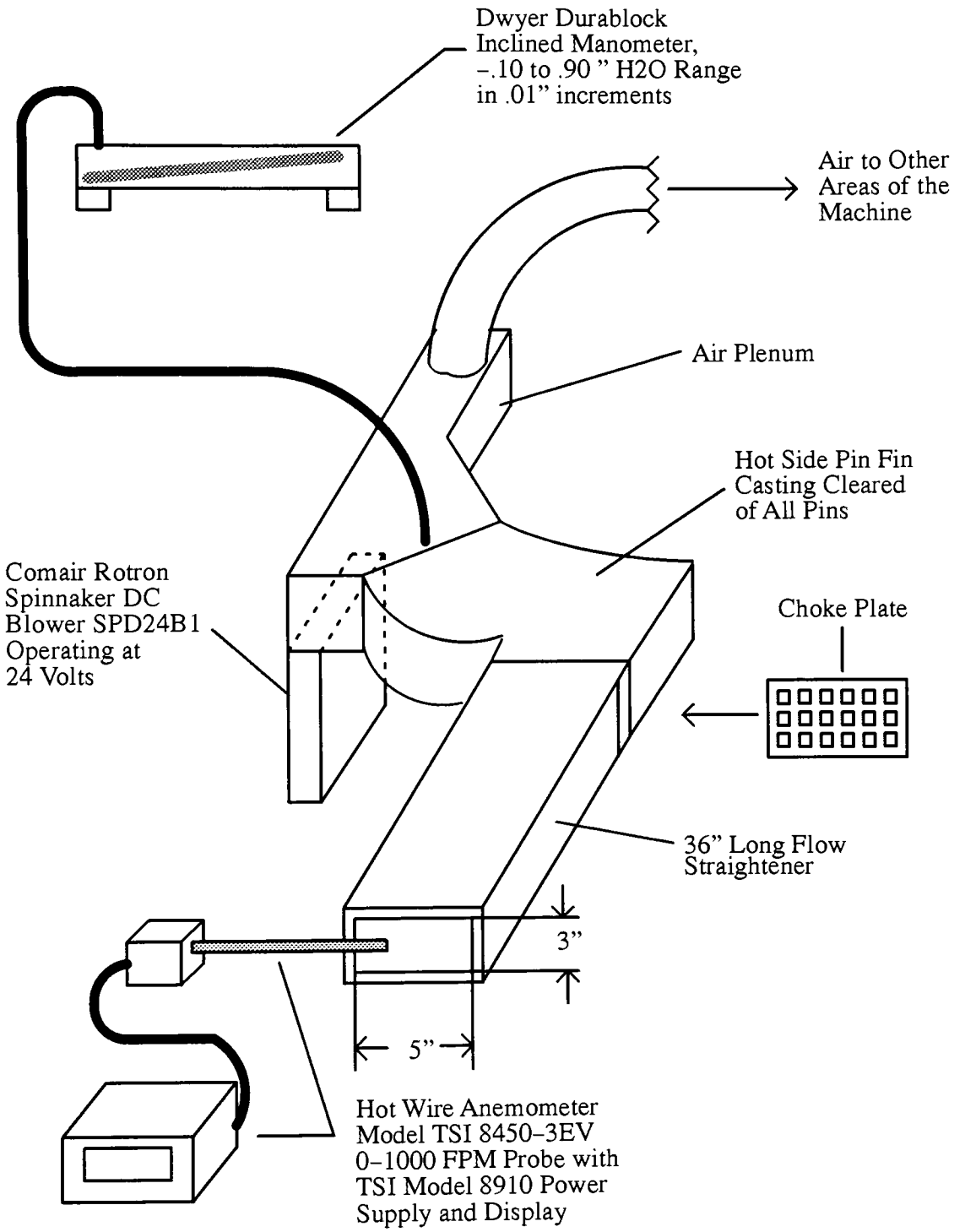

Experimental Apparatus to Measure
Pressure vs. Flow Characteristics of
Hot Side Air Delivery System

Figure 5.6

Table 5.2–Pressure Versus Flow Data for Hot Side Air Delivery System	
Pressure Drop in Inches of H2O	Volumetric Flow Rate in CFM
0.00	26.32
0.09	21.56
0.19	17.87
0.27	16.01
0.41	10.54
0.51	6.74
0.59	3.94
0.67	0.00

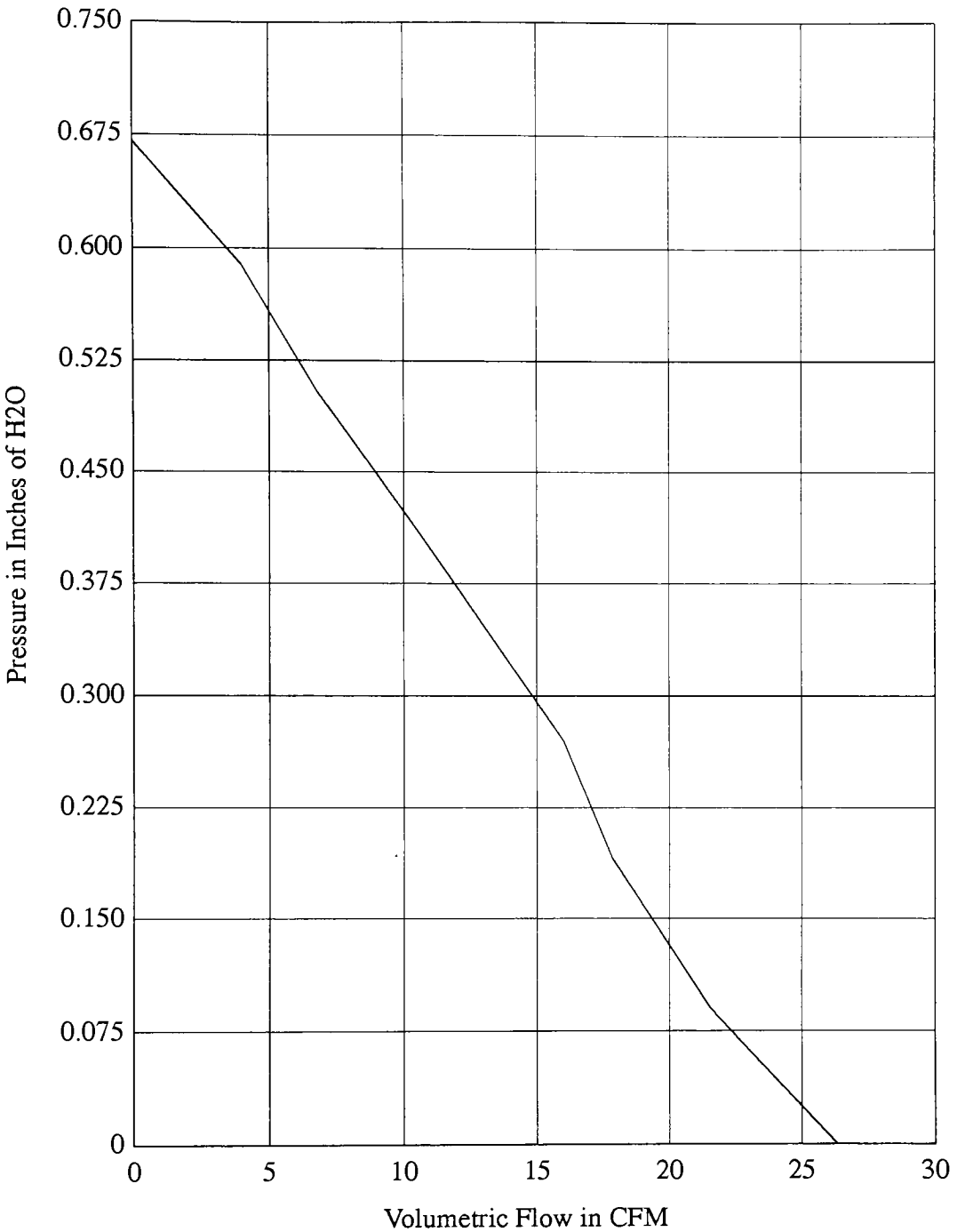

Pressure versus Flow Curve for
Hot Side Air Delivery System

Figure 5.7

in Figure 5.6.

5.2 Determination of System Heat Pump Performance

Experiments were conducted to examine the performance of the heat pump with existing pin bank geometry as a function of volumetric flow rate across the hot and cold side pin fin surfaces and voltage applied to the thermoelectric modules. The performance variables measured in these experiments were pressure drop across the particular pin fin bank in question, heat pumped from the cold side of the heat exchanger, and heat rejected from the hot side of the heat exchanger. A description of the experimental apparatus follows.

Figure 5.8 is an illustration of a device constructed to examine the pressure drop across the cold side pin fin castings as a function of volumetric flow rate. It consists of an 80" long flow straightener having cross sectional dimensions of 2.25" wide by 2.375" tall. A small tubeaxial fan was fitted into one end of the flow straightener. Provisions were make to accommodate different numbers of the cold side heat pin fin casting in the center portion of the flow straightener. These casting fit snugly into the flow straightener. A pressure tap was located 4" up stream of where the castings were located. Volumetric flow rate could be varied by changing the input voltage to the fan. Data was generated by setting the fan voltage to a particular level and noting the pressure drop as indicated by the manometer. Flow velocities were measured at 9 equally spaced points across the exhaust end of the flow straightener. Volumetric flow rate were calculated by averaging the 9 velocity data points and multiplying the result by the cross sectional area of the duct. Table 5.3 contains the data from this experiment. Figures 5.9, 5.10, and 5.11 are plots of the experimental data versus pressure drop results obtained from the two correlations defined in equations 3.1–3.9 and equations 3.10–3.11. Equations 3.10–3.11 offer a better indicator of pressure drop performance of this particular system, especially where larger numbers of pin rows are

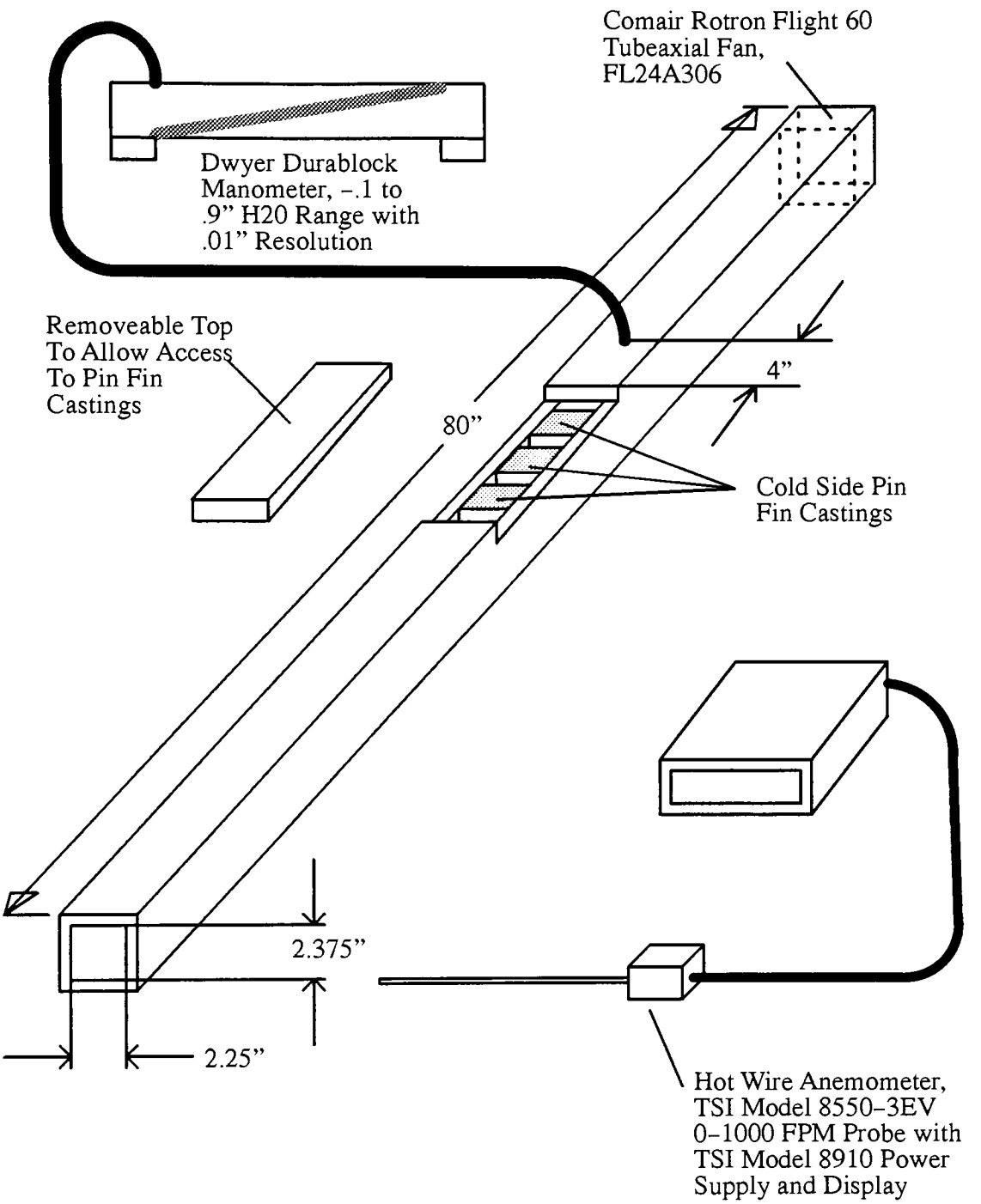

Apparatus to Investigate Pressure Drop Across Cold Side Pin Fin Castings as a Function of Volumetric Flow Rate

Figure 5.8

Table 5.3–Pressure vs. Volumetric Flow Data, Cold Side Pin Fin Castings, Avg. Dia.=3.97 mm, S_T=10.33 mm, S_L=5.49 mm

Volumetric Flow Rate (CFM)	Number of Rows of Pins	$Re_{D,max}$	Measured Pressure Drop, Inches of H20	Calculated Pressure Drop, eqns. 3.1–3.9	Calculated Pressure Drop, eqns. 3.10–3.11
14.60	7	510	.03"	.035"	.030"
11.20	7	718	.06"	.063"	.057"
7.96	7	935	.10"	.102"	.092"
10.93	14	375	.03"	.042"	.034"
8.38	14	537	.06"	.077"	.066"
5.86	14	700	.11"	.122"	.108"
9.69	21	306	.03"	.045"	.035"
7.19	21	461	.06"	.089"	.075"
4.77	21	620	.11"	.148"	.130"

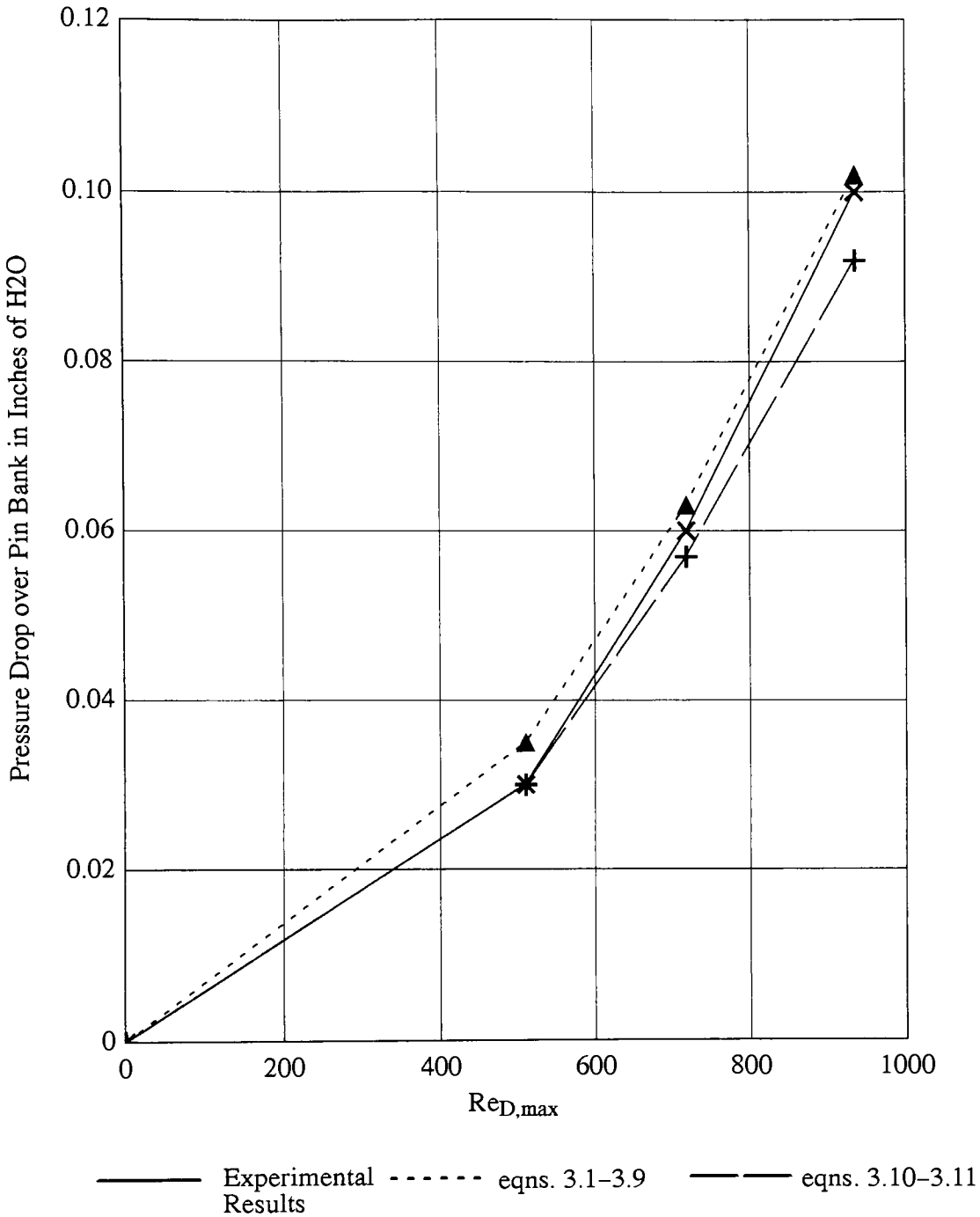

Pressure Drop versus $Re_{D,max}$ for
7 Rows of Pins, Diameter=3.97 mm,
ST=10.33 mm, SL=5.49mm

Figure 5.9

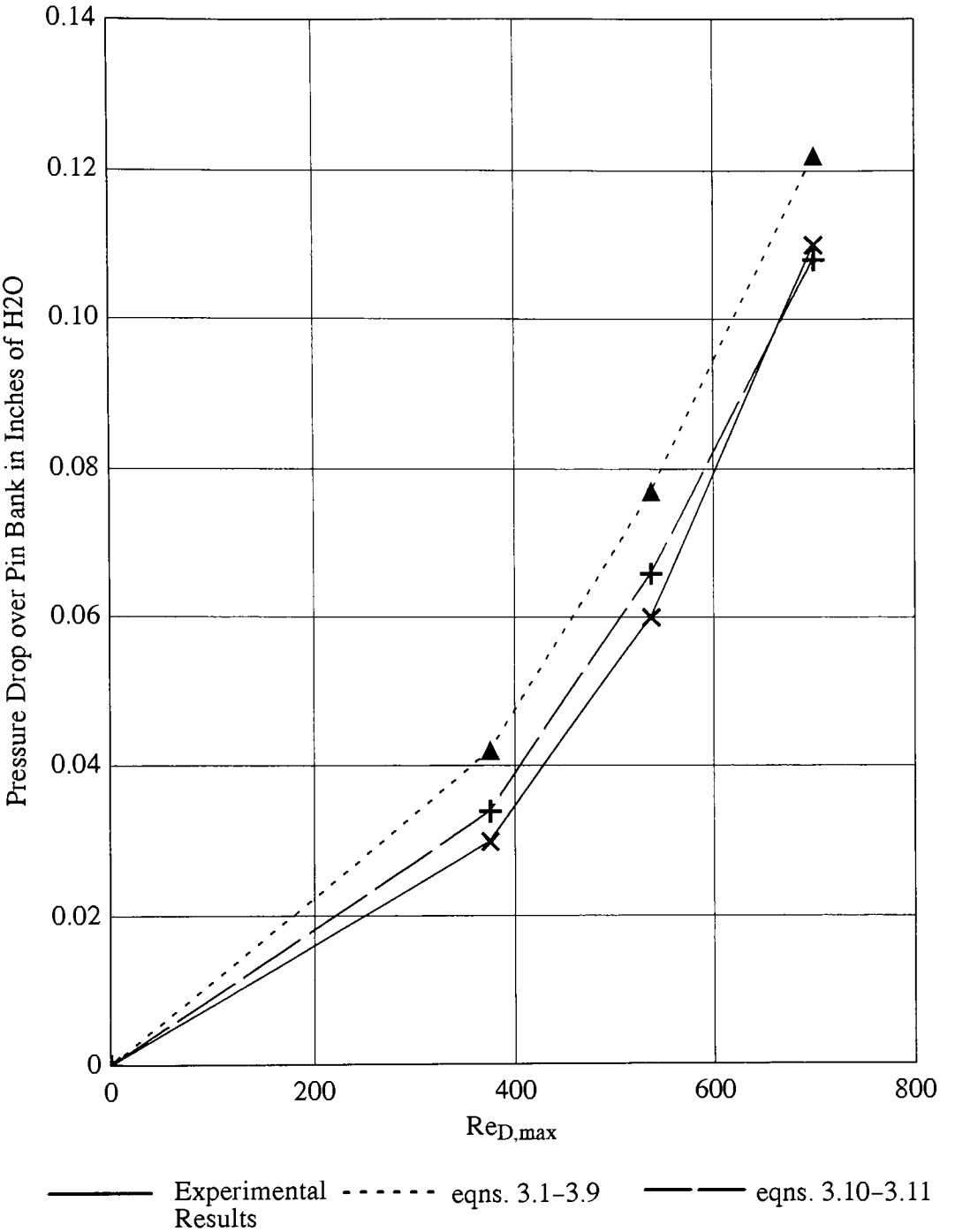

Pressure Drop versus $Re_{D,max}$ for
14 Rows of Pins, Diameter=3.97 mm
ST=10.33 mm, SL=5.49mm

Figure 5.10

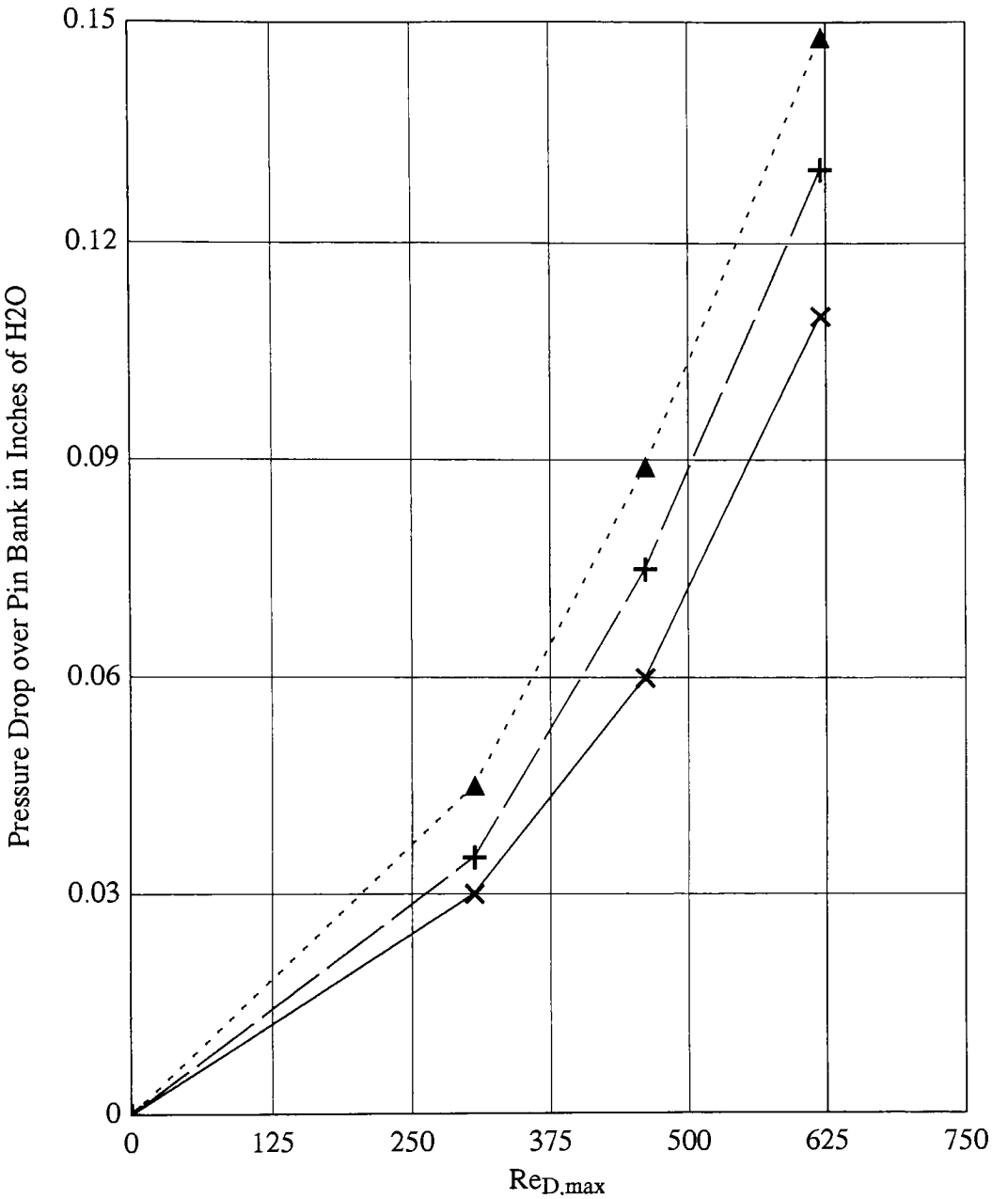

Pressure Drop versus $Re_{D,max}$ for
21 Rows of Pins, Diameter=3.97 mm
ST=10.33 mm, SL=5.49mm

Figure 5.11

concerned and at higher values of Reynolds number. In particular, equations 3.10–3.11 disagree with measured results by only 18.2% with N = 21 rows of pins and $Re_{D,max}$ = 620. On the other hand, equations 3.1–3.9 disagree with measured results by 34.5% under the same conditions. One particular distinction of the pin fin castings is the 2° per side taper that allows the parts to be plaster cast. This may account for some of the error as the correlations under examination were developed for straight cylinders. Equations 3.10–3.11 were used in the FORTRAN program COPT.FOR to predict pressure drop across the cold side pin fins because of the superior performance over equations 3.1–3.9 that were seen in these tests.

A final series of tests were conducted on a complete heat pump system that were meant to exercise the actual hardware and the FORTRAN models through a wide range of input parameters. Figure 5.12 is a diagram of an experimental apparatus devised to allow volumetric flow rate on both the hot and cold sides to be varied as well as the input voltage to the thermoelectric modules. Room air was used for the intake for both the hot and cold sides of the heat pump. Thermocouples were imbedded in the hot and cold side casting associated with each thermoelectric module. Additional thermocouples were available to measure the air intake and exhaust temperatures from the hot side and both the inner and outer channel banks of cold side pin fins. The pressure drop across the hot side pin fin casting was measured using an inclined manometer. From these basic measurements, heat pumped from the hot and cold side (Q_H and Q_C) was calculated. Care was taken to insulate the bottom and side walls of the hot side casting with a low density foam to minimize any error resulting from free convection heat loss from the heated side walls. The ductwork over the cold side pin fins received similar treatment. This was fabricated out of .25" thick expanded polystyrene foam core board and covered with an additional .5" thick layer of low density polyurethane foam.

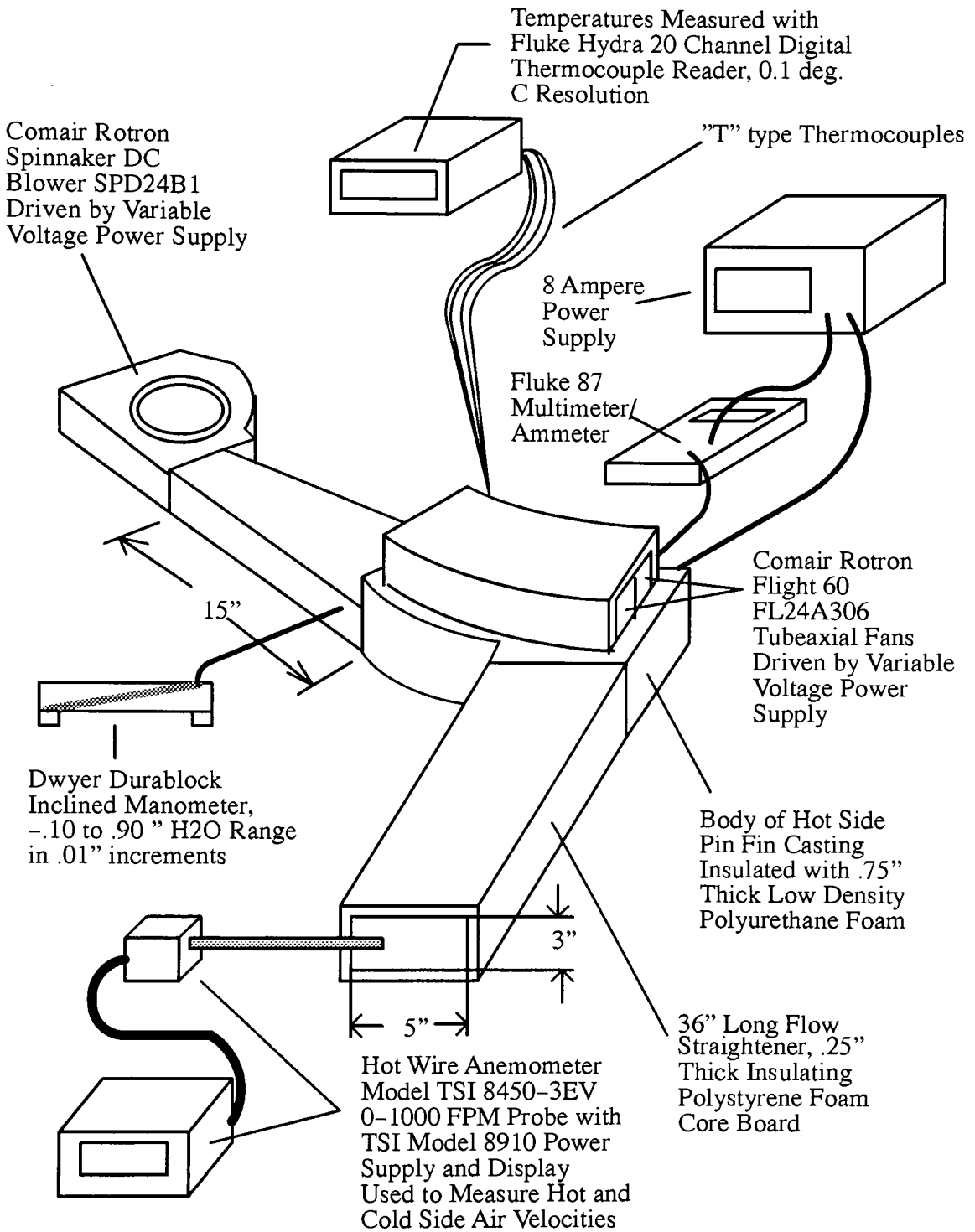

Experimental Apparatus to Measure Pressure versus Flow Characteristics of Hot Side Air Delivery System
Figure 5.12

A description of the procedure followed to collect data from the apparatus shown in Figure 5.12 follows. The power supplies running the hot side blower and the two tubeaxial fans delivering air to the cold side pin fins were set to particular voltage levels. Next, the power supply driving the thermoelectric modules was set to drive at a particular current level. Approximately 45 minutes was then allowed for the entire system to reach steady state operating conditions. Temperature readings for each of the 6 cold side pin fin bases were then taken along with the corresponding temperature readings of the hot side pin fin base directly beneath each of the thermoelectric modules. Voltage drop measurements were taken right at the thermoelectric modules to avoid any potential drop occurring over electrical connectors. Finally, air velocity and air temperature measurements were taken using the hot wire anemometer and the thermocouple reader. It was realized early on that significant temperature gradients existed across the two cold side exhausts and the single hot side exhaust. Matters were complicated by the fact that the room temperature of the lab in which the experiments were conducted would often drift by 1 °C or more during the time period in which the measurements were taken. To remedy this problem, at every position that a measurement of air velocity was taken, an air temperature measurement was taken along with a measurement of the air intake temperature of the duct in question. An average temperature drop or rise of the exhaust air stream in question was then calculated by

$$\Delta T_{avg.} = (1/\Sigma V_i) * \Sigma(V_i (T_{i,ex} - T_{i,amb})) \qquad (5.2)$$

where V_i is the air velocity at a particular position in the duct, $T_{i,ex}$ is the exhaust temperature at that same position, and $T_{i,amb}$ is the ambient temperature of the duct intake at that point in time. 9 measurements of velocity and temperature rise were taken for the hot side air stream at equally spaced increments across the duct to determine average temperature rise

of the air stream. 9 measurements of velocity and temperature drop were taken for each of the 2 cold side air streams, also at equally spaced increments across the duct.

A total of 9 experiments were conducted using the test apparatus shown in Figure 5.12. The settings of the hot side volumetric flow rate, cold side volumetric flow rate, and current variables associated with the 9 experiments are given in Table 5.4. Test 1 was used not only to gain some experience with the test apparatus, but to establish the performance of the unit under design conditions of flow and voltage. Tests 2 through 9 were meant to exercise the apparatus through high and low values of hot side volumetric flow, cold side volumetric flow, and thermoelectric current. Table 5.5 provides a summary of the reduced data from these experiments. The raw data from these runs is contained in Appendix D. Figure 5.13 shows the location of thermoelectric module positions 1 through 6 that is referred to in the Appendix D data. Q_C and Q_H (also presented in Table 5.5) have been calculated from the temperature drop or rise, the air density, and the volumetric flow rate. It is important to note that the air velocity readings given by the hot wire anemometer were in terms of feet per minute of air velocity at 72 °F and sea level conditions. Thus, the air density value used for all calculations was taken to be that at 72 °F and sea level.

5.3 Comparison of Experimental and Analytical Results

Table 5.5 also compares the results from the 9 systems test experiments with results obtained from running the HOPT.FOR, COPT.FOR, and HP.FOR simulations. Since the experiments involved adjusting fan voltages until a desired levels of volumetric flow were achieved over the various heat exchange surfaces, HOPT.FOR and COPT.FOR were modified to accept as input a given volumetric flow rate, and then allowed calculate the thermal resistance of the pin fin geometry in question. These two programs normally

Table 5.4–Variable Settings of 9 Systems Tests				
Test Number	Inner Cold Side Fan Voltage	Outer Cold Side Fan Voltage	Hot Side Fan Voltage	Thermoelectric Current Draw (Amps)
1	20.50	20.50	10.96	3.55
2	28.00	28.00	17.50	4.00
3	28.00	28.00	17.50	1.61
4	12.50	12.50	17.50	4.00
5	12.50	12.50	17.50	1.60
6	28.00	28.00	7.00	3.75
7	28.00	28.00	7.00	1.60
8	12.00	12.00	7.00	3.75
9	12.00	12.00	7.00	1.60

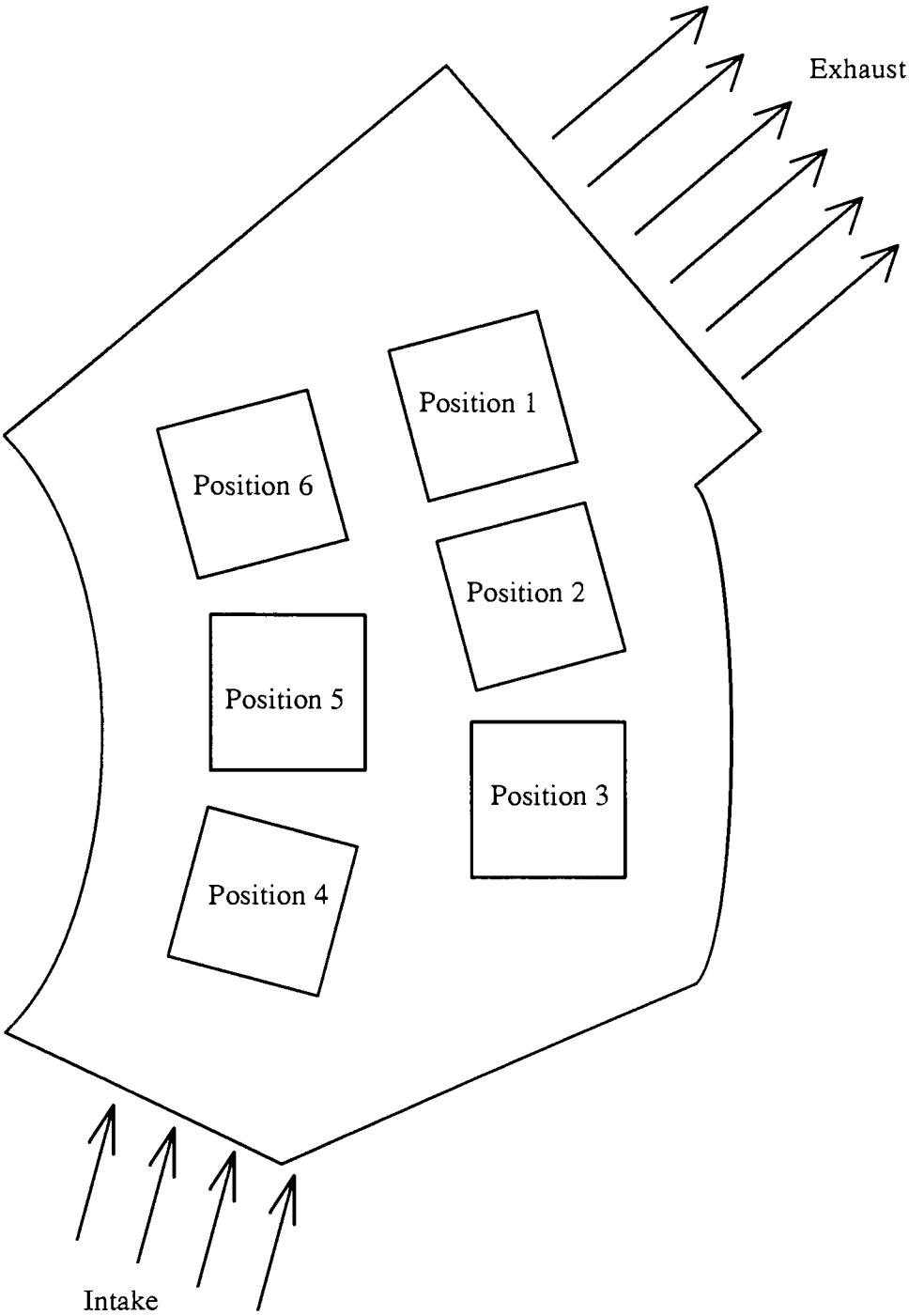

Top View of Hot Side Heat Exchanger Showing
Thermoelectric Positions 1 Through 6

Figure 5.13

Table 5.5–Summary of Measured Results versus Results Predicted by COPT.FOR, HOPT.FOR, and HP.FOR

			Test 1	Test 2	Test 3	Test 4
Test Conditions	CFM Cold Outer		7.06	8.34	8.41	3.98
	CFM Cold Inner		8.13	10.62	9.73	4.67
	CFM Hot		19.72	34.07	34.18	34.18
	ΔP_{hot} Inches H_2O		.09	.24	.26	.25
	Avg. Amb. Temp. (C)		21.33	25.97	25.24	21.47
	Voltage Drop		43.28	48.74	19.14	48.00
Measured and Predicted Parameters	Current Draw, Amps	Measured	3.55	4.01	1.61	4.00
		Predicted	3.37	3.83	1.58	3.86
		Error	-5.07%	-4.49%	-1.86%	-3.50%
	Hot Side Wtd. Temp. C	Measured	46.26	48.32	32.10	42.93
		Predicted	46.28	48.81	31.84	42.77
		Error	0.02	0.49	-0.36	-0.27
	Cold Side Wtd. Temp. C	Measured	12.56	15.19	18.45	7.34
		Predicted	13.26	16.38	18.69	8.36
		Error	0.70	1.19	0.24	1.02
	Q_C, Watts	Measured	51.55	65.45	41.66	50.05
		Predicted	46.33	63.10	42.01	49.98
		Error	-10.13%	-3.59%	0.84%	-0.14%
	Q_H, Watts	Measured	193.65	252.11	76.87	237.13
		Predicted	192.34	249.59	72.34	235.25
		Error	-0.68%	-1.00%	-5.89%	-0.79%

Table 5.5 (continued)

			Test 5	Test 6	Test 7	Test 8	Test 9
Test Conditions	CFM Cold Outer		3.98	8.41	8.41	3.08	3.08
	CFM Cold Inner		4.67	9.73	9.73	3.83	3.83
	CFM Hot		34.18	10.46	10.46	10.46	10.46
	ΔP_{hot} Inches H_2O		.25	.03	.03	.03	.03
	Avg. Amb. Temp.		21.21	24.10	23.02	20.94	22.40
	Voltage Drop		18.91	50.67	19.87	49.92	20.08
Measured andPredicted Parameters	Current Draw, Amps	Measured	1.60	3.75	1.60	3.75	1.60
		Predicted	1.58	3.53	1.56	3.55	1.57
		Error	-1.25%	-5.87%	-2.50%	-5.33%	-1.88%
	Hot Side Wtd. Temp. C	Measured	27.05	64.10	35.34	60.28	33.47
		Predicted	27.02	66.27	35.74	61.41	34.98
		Error	-.03	2.17	0.40	1.13	0.49
	Cold Side Wtd. Temp. C	Measured	11.60	21.12	19.17	15.94	15.07
		Predicted	12.22	20.62	18.38	15.48	14.87
		Error	0.62	-0.50	-0.79	-0.46	-0.20
	Q_C, Watts	Measured	35.34	21.77	27.56	18.87	23.04
		Predicted	34.33	22.34	29.87	17.47	23.99
		Error	-2.86%	2.62%	8.38%	-7.42%	4.12%
	Q_H, Watts	Measured	65.33	191.45	58.06	191.43	54.55
		Predicted	64.23	201.31	60.86	194.87	55.53
		Error	-1.68%	5.15%	4.82%	1.80%	1.80%

calculate flow rate based on fan curve data and pressure drop correlation calculations. The average percent error in the predicted versus measured values of Q_C was 4.45% over all the runs with Test 1 having the worst error of -10.13%. The average percent error in the predicted versus measured values of Q_H was 2.62% with Test 3 having the worst error of -5.89%. These results were obtained by evaluating the predicted versus experimental results over a wide range of hot and cold side thermal contact resistance values (R_{IH} and R_{IC}). Values of R_{IC} = .025 °C/W and a variable quantity

$$R_{IH} = (.1 - .002 * (T_h - T_{base})) \tag{5.5}$$

(where R_{IH} is given in °C/W and T_h and T_{base} are the thermoelectric hot side and the heat exchanger base temperatures respectively) were chosen for all runs of HP.FOR. These values were selected because they seemed to offer the best agreement between experimental and analytical results when examining the composite picture of temperatures and heat flows over all 9 tests.

An analysis of experimental error is contained in Appendix E. Some indication of how well a given test went can be obtained from the error term given by the "Examination of energy balance" entry at the bottom of each data sheet contained in Appendix E. From an energy balance perspective, the heat rejected from the hot side should equal the sum of the heat absorbed at the cold side plus the I^2R losses of the thermoelectric modules (within the limits of uncertainty given by the experimental methods and instrumentation). That is,

$$Q_H = Q_C + I * \Sigma\Delta V \tag{5.3}$$

where $\Sigma\Delta V$ is the sum of the voltage drops over all of the thermoelectric modules. An inequality condition in equation 5.3 is an indication of experimental error. The percent error as expressed by

$$\% \text{ error} = 100 * (Q_H - (Q_C + I * \Sigma\Delta V))/Q_H \quad (5.4)$$

had an average absolute value of 4.36% over all 9 experiments runs.

The analysis of Appendix E takes into consideration sources of error arising from the stated uncertainties in the temperature and flow instrumentation used in the experiment as well as uncertainty in cross sectional dimensions of the flow straighteners used. With the exception of Test 6 and Test 8, equation 5.3 holds within the calculated limits of uncertainty given for each test in Appendix E. The Test 6 analysis leaves approximately 8 W unaccounted for and the Test 8 analysis leaves approximately 4 W unaccounted for. These situations may be explained by the hot side heat sink possibly having heat losses to areas other than the air stream passing through the heat sink. Even though thermal insulation was wrapped around the body of the hot side heat sink, there still may have been an measurable loss of heat by conduction to the lab bench and to the ambient air via convection. In both Test 6 and Test 8, the measured heat flux at the hot side exhaust was less than the sum of the heat pumped from the cold side plus the resistive heating of the thermoelectric modules. Test 6 and Test 8 also registered the highest hot side heat sink temperatures with respect to ambient in comparison to the other tests, which would drive greater heat losses. A final supporting argument can be made by examining the predicted versus measured hot side heat sink temperatures associated with these two tests. The predicted temperature hot side heat sink base temperature of Test 6 was 2.17 °C greater than the measured temperature, and the Test 8 predicted hot side heat sink base temperature was 1.13 °C greater than the measured temperature. The error in hot side heat sink base predicted versus measured temperature was less than 0.5 °C on all other tests. This implies that the experimentally derived hot side base temperatures may have been closer to the analytically derived values if extraneous heat losses could have been better controlled.

Predicted values of heat pumped from the cold side agreed within the limits of experimental uncertainty captured in Appendix E with the exception of Test 1. In this instance, the predicted heat flow was 10.13% lower than the measured value. The error analysis accounts for only 3.74 W out of the 5.22 W difference between experimental and predicted heat flow. One possible explanation for this discrepancy is that there was considerable drift in the ambient temperature during the course of Test 1. Although the experimental methodology described in Section 5.2 attempted to remove the effects of fluctuating ambient temperature, the heat capacity of the heat pump system contributes a delay component to the temperature response, so the method is not perfect. This source of error is not included in the Appendix E analysis. The accuracy of the Nusselt number correlation used in the analytical model could be another source of experimental versus predicted heat flows as could some of the basic assumptions that went into the model, such as utilizing a weighted average temperature to define the base temperature of an entire pin bank. Finally, there was no available information regarding the absolute accuracy of the physical constants used to describe the performance of the thermoelectric modules in the heat pump assembly. Errors in the Seebeck, conductance, or resistivity coefficients could contribute to experimental/analytical differences.

5.4 Heat Sink Distortion and Contact Resistance

Perhaps the most striking aspect of the findings of Section 5.3 was the relatively large value of thermal contact resistance at the pin fin/thermoelectric module interface for both the hot and cold sides (R_{IH} and R_{IC}) that had to be used in the analytical model to match analytical and experimental results. The surfaces of the pin fin castings meant to interface to the thermoelectric modules were specified to be flat to within .025 mm (.001 inches) per

the recommendations of the thermoelectric module vendor. Therefore, in a worst cast situation, a thermal grease film thickness of approximately .025 mm might be found to exist between the pin fins and the thermoelectric modules. Thermal resistance of a planar geometry of uniform thickness t may be calculated by

$$R_{th} = \varrho * t/A \tag{5.6}$$

where ϱ is the thermal resistivity and A is the area of the substance in question. The surface area of the six thermoelectric modules used in the heat pump is 12.47 in^2, or .00805 m^2. Using a value of 1.4 °C-m/W for the thermal resistivity of a typical thermal grease, the thermal contact resistance of the hot or cold side pin fin/thermoelectric module interface should be on the order of

$$R_{th} = (1.4\ °C*m/W)*.000025\ m/.00805\ m^2 = .0043\ °C/W \tag{5.7}$$

Equation 5.5 predicts values of at least .060 °C/W over the temperature ranges examined in the 9 systems tests and R_{IC} was taken to be .025 °C/W. The .025 °C/W figure is 5.8 times larger than the predicted worst case value of .0043 °C/W. The .060 °C/W figure is almost 14 times as large as the predicted worst case contact resistance. More importantly, these values constitute a very large percentage of the total thermal resistance seen by the thermoelectric modules and have a strong negative impact on total system performance.

A possible explanation of the high thermal contact resistances was provided by the examination of a heat pump unit that was undergoing some tests to evaluate the use of a dry thermal interface compound (a pliable, silicon based film) rather than a thermal grease. An examination of the machined surface of several of the cold side heat sinks immediately following disassembly of a unit revealed a contact pattern left by the dry interface material. There appeared to be some transfer of the interface material to the machined surface of the

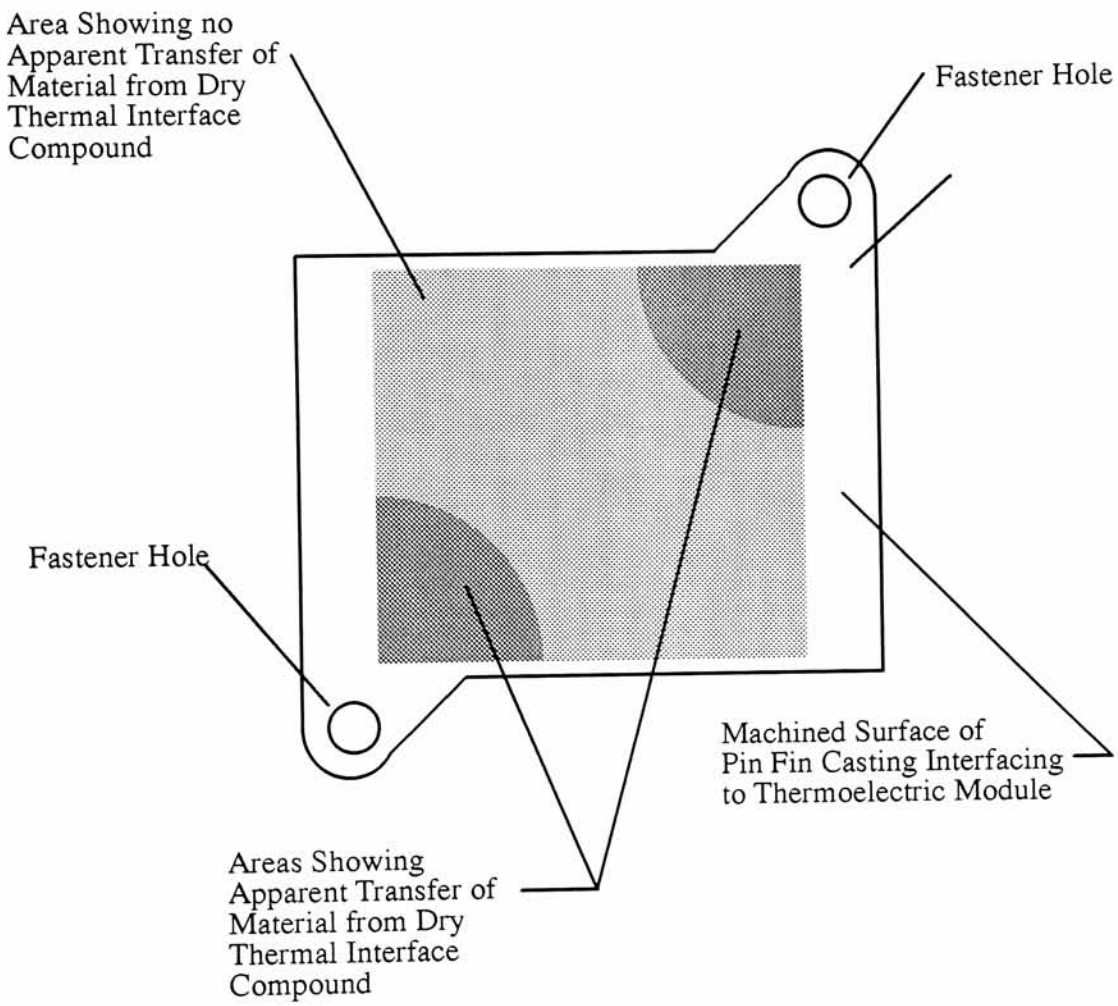

Observations of Patterns Left by Dry Thermal Interface Material on Cold Side Heat Sink

Figure 5.14

heat sinks in the corners where the fasteners clamped the assembly together. The central part of the heat sinks did not show any indication of material transfer. Figure 5.12 illustrates these observations. The heat sinks were then inspected for flatness and found to be within the .025 mm (.001") flatness specification recommended by the thermoelectric manufacturer. These facts suggested that the heat sinks were bowing under the forces exerted by the assembly fasteners, perhaps resulting in a high thermal resistance air pocket in the center portion of the heat sink.

An experiment was performed to verify the idea that a significant amount of heat sink distortion was occurring. The approach was to use pressure measurement film to obtain an indication of contact pressure between the hot and cold side heat sinks and the thermoelectric modules. This film is a thin sheet of polymeric material which has been coated with a microencapsulated dye. The application of pressure to the film causes the microcapsules to rupture, resulting in the appearance of color. A given level of color density can be related to a level of pressure. In this case, the film was used in a qualitative fashion, with the presence of color an indicator of intimate contact and the absence of color an indicator of very low pressure or perhaps even a gap condition. A sheet of Fuji Prescale Film ® in the "Ultra Super Low" pressure sensitivity range (2 to 6 kg_f/cm^2) was obtained. Pieces of this film were placed on the hot and cold sides of a thermoelectric module and assembled to the hot and cold side pin fins. The fasteners joining the components were torqued to the 15 oz-in value specified by the assembly procedures employed to build this unit. After 5 minutes, the unit was disassembled and the pressure measurement film examined. Regions of very high color density were found in the corners of the film closest to the fasteners, indicating intimate contact. The central regions of the film had no color density present. This fact, along with the abrupt change in color (i.e. no gradient) between the two regions indicates that an air gap

probably exists in the center portion of the thermoelectric/heat sink interface in the assembled condition. Figure 5.13 shows several paired examples of the pressure film which was obtained by this method.

Examination of several sets of these films revealed that only 10% to 20% of the area of the thermoelectric appears to be in direct contact with the heat sink. Since air has a significantly higher thermal resistance than the thermal grease does, the air gap acts as a very large resistance in parallel with the relatively low resistance offered by the thermal grease. In such parallel path situations, the smaller resistance dominates. If equation 5.7 is recalculated to reflect the fact that only about 15% of the heat sink area appears to be in direct contact with the thermoelectric, the following value of thermal resistance is obtained:

$$R_{th} = (1.4\ ^\circ C*m/W)*.000025\ m/(.15*.00805\ m^{2)} = .029\ ^\circ C/W \qquad (5.8)$$

This agrees quite well with the values of R_{IC} (.025 °C/W) and R_{IH} (ranging from about .065 °C/W to .09 °C/W) that were selected to obtained agreement between the analytical and experimental results.

Example 1

Hot Side Cold Side

Example 2

Hot Side Cold Side

Example 3

Hot Side Cold Side

Examples of Pressure Sensitive Films Used
to Determine the Presence of Air Gaps at
Heat Sink/Thermoelectric Interfaces

Figure 5.15

CHAPTER 6

OPTIMIZATION OF HEAT PUMP SYSTEM TO ACHIEVE MAXIMUM COOLING CAPACITY

6.1 General Approach

The heat pump parameters to be considered as variables in this study are the pin diameter, longitudinal stagger, transverse stagger, and pin height of the pin fin castings, the voltage applied to the thermoelectric modules, the number of thermoelectric thermocouple junctions present, the geometry factor of the thermoelectric modules, and the thermal contact resistance of the thermoelectric module/pin fin interface. The effects of employing different fans to deliver air to the pin fin banks was not considered, although various pressure versus flow curves could easily be implemented into HOPT.FOR or COPT.FOR. Regardless of the specifics of the thermoelectric modules and the applied voltage level, the best system performance is realized only when the thermal resistance of both the hot and cold side pin fin surfaces has been minimized. Therefore, a parameter study of pin diameter, spacing, and height of both the hot and cold side pin fins may be undertaken as a first task with the goal of minimizing the thermal resistance. Once the optimum pin bank geometries are defined, a study of voltage input and thermoelectric parameters with the goal of maximizing Q_C may be undertaken with the minimized thermal resistances of the hot and cold side taken as known quantities. Consideration of the effects of the thermal junction resistance of the heat exchange surface/thermoelectric module interface can be considered at this point as well.

6.2 Minimizing the Thermal Resistance of the Pin Fins

A three level full factorial run of the programs COPT.FOR and HOPT.FOR was performed considering pin diameter, longitudinal stagger, transverse stagger, and pin height

as variables. Table 6.1 gives the minimum, mid-level, and maximum parameter values chosen for this exercise. Minimum pin diameters and pin heights were selected based on a knowledge of the capabilities of the plaster casting process used to fabricate the heat sinks. Care was taken in choosing the parameters values so that no combination would result in conditions of pin-to-pin interferences. For instance, the maximum pin diameter may be combined with any stagger configuration without concern of creating an interference condition (both COPT.FOR and HOPT.FOR will flag interference conditions, however). Table 6.2 is a listing of the 81 cases considered for all possible combinations of the above variables and the model response. Each row corresponds to a given run of HOPT.FOR. The last 3 columns in the Table 6.2 are HOPT.FOR output data.

A minimum thermal resistance value of 0.106 °C/W for the hot side pin fin bank was achieved at a pin diameter of 3.5 mm, a pin height of 63 mm, S_T = 10 mm, and S_L = 5 mm (case 7 in Table 6.2) and for a pin diameter of 4.0 mm, a pin height of 63 mm, S_T = 10 mm, and S_L = 5 mm (case 8 in Table 6.2). An examination of Table 6.2 shows that with this combination of variables, the performance of the heat sink is relatively insensitive to parameter variation. For instance, increasing the pin diameter from 3.5 mm to 4.5 mm only changes the thermal resistance from 0.106 °C/W to 0.108 °C/W . Increasing the transverse stagger from 10 mm to 14 mm only increases the thermal resistance results by about 3%. Changes in longitudinal stagger have small influences on the final result as well. The data indicates that increasing pin height generally improves thermal performance given any combination of the other variables. In this situation, manufacturability concerns may dictate the selection of the largest pin diameters and stagger distances possible to make the casting process more robust.

Table 6.1–Minimum, Mid–level, and Maximum Parameter Values Selected for 3 Level Full Factorial Exercise of HOPT.FOR and COPT.FOR

	Parameter	Minimum	Mid–level	Maximum
Hot Side	Pin Diameter, mm	3.5	4.0	4.5
	Longitudinal Stagger, mm	5.0	7.0	9.0
	Transverse Stagger, mm	10.0	14.0	18.0
	Pin Height, mm	43.0	53.0	63.0
Cold Side	Pin Diameter, mm	3.5	4.0	4.5
	Longitudinal Stagger, mm	4.5	5.5	6.5
	Transverse Stagger, mm	7.0	10.0	13.0
	Pin Height, mm	43.0	53.0	63.0

Table 6.2–Three Level Full Factorial Study of Pin Diameter, Pin Height, Transverse Stagger, and Longitudinal Stagger Using HOPT.FOR

Case Number	Pin Dia. (mm)	Pin Height (mm)	Transverse Stagger (mm)	Longitudinal Stagger (mm)	Pressure Drop (inches H_2O)	Thermal Resistance (°C/W)	Re_{max}
1	3.5	43	10	5	.252	.117	470
2	4.0	43	10	5	.285	.119	550
3	4.5	43	10	5	.324	.129	648
4	3.5	53	10	5	.198	.111	408
5	4.0	53	10	5	.231	.111	485
6	4.5	53	10	5	.279	.115	594
7	3.5	63	10	5	.164	.106	365
8	4.0	63	10	5	.189	.106	430
9	4.5	63	10	5	.233	.108	534
10	3.5	43	14	5	.165	.121	476
11	4.0	43	14	5	.219	.121	554
12	4.5	43	14	5	.271	.122	653
13	3.5	53	14	5	.128	.115	450
14	4.0	53	14	5	.172	.114	483
15	4.5	53	14	5	.215	.114	570
16	3.5	63	14	5	.101	.112	366
17	4.0	63	14	5	.141	.109	432
18	4.5	63	14	5	.177	.109	508
19	3.5	43	18	5	.070	.120	554
20	4.0	43	18	5	.142	.122	593
21	4.5	43	18	5	.194	.123	657
22	3.5	53	18	5	.044	.116	476
23	4.0	53	18	5	.107	.116	513
24	4.5	53	18	5	.153	.115	576
25	3.5	63	18	5	.028	.115	415
26	4.0	63	18	5	.082	.113	453
27	4.5	63	18	5	.123	.111	512

Table 6.2 (continued)

Case Number	Pin Dia. (mm)	Pin Height (mm)	Transverse Stagger (mm)	Longitudinal Stagger (mm)	Pressure Drop (inches H_2O)	Thermal Resistance (°C/W)	Re_{max}
28	3.5	43	10	7	.183	.124	515
29	4.0	43	10	7	.214	.120	611
30	4.5	43	10	7	.246	.119	720
31	3.5	53	10	7	.145	.117	450
32	4.0	53	10	7	.169	.113	533
33	4.5	53	10	7	.191	.112	626
34	3.5	63	10	7	.118	.114	399
35	4.0	63	10	7	.138	.109	475
36	4.5	63	10	7	.159	.106	561
37	3.5	43	14	7	.117	.136	507
38	4.0	43	14	7	.148	.130	574
39	4.5	43	14	7	.172	.126	649
40	3.5	53	14	7	.087	.132	434
41	4.0	53	14	7	.114	.125	496
42	4.5	53	14	7	.135	.119	566
43	3.5	63	14	7	.069	.130	382
44	4.0	63	14	7	.090	.122	435
45	4.5	63	14	7	.108	.116	499
46	3.5	43	18	7	.044	.147	551
47	4.0	43	18	7	.090	.142	586
48	4.5	43	18	7	.121	.137	647
49	3.5	53	18	7	.026	.144	464
50	4.0	53	18	7	.066	.137	504
51	4.5	53	18	7	.091	.131	555
52	3.5	63	18	7	.015	.144	400
53	4.0	63	18	7	.049	.135	440
54	4.5	63	18	7	.072	.128	487

Table 6.2 (continued)

Case Number	Pin Dia. (mm)	Pin Height (mm)	Transverse Stagger (mm)	Longitudinal Stagger (mm)	Pressure Drop (inches H_2O)	Thermal Resistance (°C/W)	Re_{max}
55	3.5	43	10	9	.150	.134	550
56	4.0	43	10	9	.175	.128	649
57	4.5	43	10	9	.201	.124	762
58	3.5	53	10	9	.116	.129	476
59	4.0	53	10	9	.137	.121	567
60	4.5	53	10	9	.158	.116	668
61	3.5	63	10	9	.092	.126	417
62	4.0	63	10	9	.110	.117	501
63	4.5	63	10	9	.128	.112	595
64	3.5	43	14	9	.092	.156	529
65	4.0	43	14	9	.119	.146	606
66	4.5	43	14	9	.140	.138	691
67	3.5	53	14	9	.069	.152	454
68	4.0	53	14	9	.089	.141	518
69	4.5	53	14	9	.107	.132	592
70	3.5	63	14	9	.053	.150	396
71	4.0	63	14	9	.071	.138	456
72	4.5	63	14	9	.085	.129	522
73	3.5	43	18	9	.034	.171	563
74	4.0	43	18	9	.072	.161	612
75	4.5	43	18	9	.097	.153	675
76	3.5	53	18	9	.199	.169	471
77	4.0	53	18	9	.051	.157	520
78	4.5	53	18	9	.072	.147	578
79	3.5	63	18	9	.012	.170	403
80	4.0	63	18	9	.038	.155	451
81	4.5	63	18	9	.056	.144	505

Table 6.3 contains the 81 runs of COPT.FOR. A minimum thermal resistance value of 0.357 °C/W was achieved with a pin diameter of 4.5 mm, a pin height of 63 mm, S_T = 10 mm, and S_L = 5.5 mm. The data indicates that the thermal performance of this heat sink is rather sensitive to changes in S_T and pin height with this selection of variables. For example, changing S_T from 10 mm to 7 mm while holding all other parameters constant increases the thermal resistance to 0.468 °C/W. Modest sensitivity to changes in pin diameter and S_L is observed. Changing pin diameter from 4.5 mm to 4.0 mm while holding all other parameters constant only increases the thermal resistance to 0.365 °C/W. Changing S_L from 5.5 mm to 6.5 mm increases the thermal resistance to 0.376 °C/W. Recall that these figures are the thermal resistances for either the inner or outer bank of cold side pins. The optimum thermal resistance of both the inner and outer banks of pins taken as a system using the 0.357 °C/W minimum would be two such resistances considered in parallel, giving a result of 0.1785 °C/W.

6.3 Determination of Optimal Voltages and Thermoelectric Module Parameters

The thermal resistances determined by the optimization study of Section 6.2 were used as input to HP.FOR to model the entire heat pump system in an effort to maximize the heat pumping capacity. Studies include examination of the effects of the number of thermoelectric thermocouple junctions present in the system, the geometry factor of the modules, and the operating voltage of the system. To stay within the confines of off-the-shelf product offered by the manufacturer, 3 standard offerings of geometry factor (G = .12, .17, and .28) were examined. Similar constraints were exercised when examining the effects of the number of thermoelectric thermocouple junctions (N) present in the system. The model was only exercised for standard offerings of N with the additional stipulation that equal numbers of thermocouple junctions must be placed on the inner and outer rings. The

Table 6.3–Three Level Full Factorial Study of Pin Diameter, Pin Height, Transverse Stagger, and Longitudinal Stagger Using COPT.FOR

Case Number	Pin Diameter (mm)	Pin Height (mm)	Transverse Stagger (mm)	Longitudinal Stagger (mm)	Pressure Drop (inches H_2O)	Thermal Resistance (C/W)	Re_{max}
1	3.5	43	7	4.5	.075	.487	384
2	4.0	43	7	4.5	.079	.554	387
3	4.5	43	7	4.5	.082	.702	418
4	3.5	53	7	4.5	.072	.417	338
5	4.0	53	7	4.5	.080	.584	410
6	4.5	53	7	4.5	.075	.466	378
7	3.5	63	7	4.5	.068	.371	328
8	4.0	63	7	4.5	.072	.407	370
9	4.5	63	7	4.5	.077	.503	404
10	3.5	43	10	4.5	.069	.451	362
11	4.0	43	10	4.5	.072	.467	420
12	4.5	43	10	4.5	.076	.517	476
13	3.5	53	10	4.5	.063	.517	346
14	4.0	53	10	4.5	.068	.404	405
15	4.5	53	10	4.5	.073	.439	463
16	3.5	63	10	4.5	.058	.369	330
17	4.0	63	10	4.5	.063	.366	390
18	4.5	63	10	4.5	.069	.389	451
19	3.5	43	13	4.5	.066	.483	369
20	4.0	43	13	4.5	.069	.472	430
21	4.5	43	13	4.5	.072	.481	491
22	3.5	53	13	4.5	.061	.433	351
23	4.0	53	13	4.5	.064	.417	412
24	4.5	53	13	4.5	.068	.416	474
25	3.5	63	13	4.5	.055	.405	333
26	4.0	63	13	4.5	.059	.382	394
27	4.5	63	13	4.5	.063	.376	457

Table 6.3 (continued)

Case Number	Pin Diameter (mm)	Pin Height (mm)	Transverse Stagger (mm)	Longitudinal Stagger (mm)	Pressure Drop (inches H_2O)	Thermal Resistance (C/W)	Re_{max}
28	3.5	43	7	5.5	.074	.482	370
29	4.0	43	7	5.5	.078	.536	413
30	4.5	43	7	5.5	.081	.643	445
31	3.5	53	7	5.5	.070	.417	359
32	4.0	53	7	5.5	.074	.454	403
33	4.5	53	7	5.5	.078	.540	437
34	3.5	63	7	5.5	.066	.374	347
35	4.0	63	7	5.5	.071	.401	393
36	4.5	63	7	5.5	.075	.468	429
37	3.5	43	10	5.5	.067	.463	383
38	4.0	43	10	5.5	.069	.450	439
39	4.5	43	10	5.5	.071	.454	493
40	3.5	53	10	5.5	.061	.414	365
41	4.0	53	10	5.5	.063	.397	420
42	4.5	53	10	5.5	.066	.394	475
43	3.5	63	10	5.5	.055	.385	346
44	4.0	63	10	5.5	.058	.365	401
45	4.5	63	10	5.5	.062	.357	456
46	3.5	43	13	5.5	.062	.493	383
47	4.0	43	13	5.5	.064	.462	442
48	4.5	43	13	5.5	.067	.454	507
49	3.5	53	13	5.5	.056	.448	361
50	4.0	53	13	5.5	.058	.415	418
51	4.5	53	13	5.5	.062	.400	483
52	3.5	63	13	5.5	.050	.423	339
53	4.0	63	13	5.5	.052	.388	395
54	4.5	63	13	5.5	.056	.369	460

Table 6.3 (continued)

Case Number	Pin Diameter (mm)	Pin Height (mm)	Transverse Stagger (mm)	Longitudinal Stagger (mm)	Pressure Drop (inches H_2O)	Thermal Resistance (C/W)	Re_{max}
55	3.5	43	7	6.5	.073	.488	398
56	4.0	43	7	6.5	.076	.525	445
57	4.5	43	7	6.5	.080	.613	481
58	3.5	53	7	6.5	.068	.425	384
59	4.0	53	7	6.5	.072	.450	433
60	4.5	53	7	6.5	.077	.522	471
61	3.5	63	7	6.5	.064	.386	370
62	4.0	63	7	6.5	.069	.401	421
63	4.5	63	7	6.5	.074	.457	461
64	3.5	43	10	6.5	.064	.497	409
65	4.0	43	10	6.5	.067	.476	470
66	4.5	43	10	6.5	.069	.469	529
67	3.5	53	10	6.5	.058	.450	387
68	4.0	53	10	6.5	.061	.424	448
69	4.5	53	10	6.5	.064	.412	507
70	3.5	63	10	6.5	.052	.422	365
71	4.0	63	10	6.5	.056	.392	425
72	4.5	63	10	6.5	.059	.376	484
73	3.5	43	13	6.5	.060	.536	408
74	4.0	43	13	6.5	.062	.496	472
75	4.5	43	13	6.5	.064	.470	535
76	3.5	53	13	6.5	.053	.493	382
77	4.0	53	13	6.5	.055	.450	443
78	4.5	53	13	6.5	.057	.422	505
79	3.5	63	13	6.5	.047	.469	356
80	4.0	63	13	6.5	.049	.424	415
81	4.5	63	13	6.5	.051	.392	476

effect of reducing thermal contact resistances between the thermoelectric module and the pin bases on both the hot and cold sides was also considered. The experimentally determined contact resistances (R_{IC} = 0.025 °C/W and R_{IH} given by equation 5.5) were used for one set of studies and values corresponding to a .001" thick layer of thermal grease with no air space ($R_{IH} = R_{IC}$ = 0 .0043 °C/W given by equation 5.7) were used for a second set of studies. It was assumed for these studies that the contact resistance given by equation 5.5 could go no lower than 0.06 °C/W. There was no data collected in the Chapter 5 experiments that indicated how this resistance would behave with temperature drops much greater than about 20 C between the hot side pin base and the hot side thermoelectric module surface. To be conservative, 0.06 °C/W was chosen as a lower limit.

Tables 6.4 through 6.9 contain the raw data from these modeling efforts. Dashes appear in the data where Q_C goes below zero or the maximum current rating of the geometry factor being considered is exceeded. Tables 6.4 through 6.6 show performance as a function of input voltage, geometry factor and number of thermoelectric thermocouple junctions present for the experimentally determined hot and cold side contact resistances. With these factors, it was found that the maximum heat pumped is 66.62 W at 36 volts with a system having 426 thermocouple junctions and a geometry factor of 0.17. This represents about a 29% performance improvement over the stock system examined in Test 1 of Chapter 5 where Q_C =51.55 W. These values were obtained using the optimized values of thermal contact resistance for the hot and cold side pin fins (R_H = 0.106 °C/W and R_C = 0.1785 °C/W) determined in the previous section. Figures 6.1 through 6.3 are the plots of these results. All of the curves indicate that for a given combination of number of thermocouple junctions and geometry factor, the system performance is relatively flat over a range of about +/- 4 volts when operating near maximum Q_C.

Table 6.4–Predicted Q_C versus Applied Voltage for Heat Pump System Having G=.12, R_{PH}=.106 °C/W, R_{PC}=.1785 °C/W, R_{IC}=.025 °C/W, and R_{IH} Given by equation 5.5 for Various N Using HP.FOR

Voltage	Q_C in Watts N=426	Q_C in Watts N=538	Q_C in Watts N=650	Q_C in Watts N=762
0	0	0	0	0
4	12.72	11.19	9.97	8.99
8	23.92	21.21	19.01	17.20
12	33.63	30.11	27.14	24.65
16	41.91	37.90	34.38	31.36
20	48.81	44.64	40.77	37.36
24	54.41	50.37	46.33	42.66
28	58.77	55.13	51.11	47.29
32	61.94	58.97	55.13	51.29
36	63.99	61.93	58.43	54.68
40	64.99	64.05	61.04	57.48
44	64.98	65.38	62.99	59.72
48	64.03	65.96	64.32	61.42
52	62.18	65.81	65.05	62.61
56	59.03	64.97	65.20	63.31
60	54.70	63.48	64.80	63.53
64	49.57	60.79	63.88	63.31
68	43.68	57.22	62.45	62.65
72	-	53.03	59.80	61.57
76	-	48.25	56.55	59.93
80	-	42.91	52.81	57.25
84	-	37.04	48.60	54.13
88	-	30.65	43.93	50.61
92	-	23.77	38.83	46.70
96	-	-	33.30	42.41
100	-	-	27.37	37.75
104	-	-	21.04	32.74

Table 6.4 (continued)

Voltage	Q_C in Watts N=426	Q_C in Watts N=538	Q_C in Watts N=650	Q_C in Watts N=762
108	–	–	14.32	27.39
112	–	–	7.23	21.70
116	–	–	–	15.68
120	–	–	–	9.34
124	–	–	–	2.68

Table 6.5–Predicted Q_C versus Applied Voltage for Heat Pump System Having G=.17, R_{PH}=.106 °C/W, R_{PC}=.1785 °C/W, R_{IC}=.025 °C/W, and R_{IH} Given by equation 5.5 for Various N Using HP.FOR

Voltage	Q_C in Watts N=426	Q_C in Watts N=538	Q_C in Watts N=650	Q_C in Watts N=762
0	0	0	0	0
4	14.50	12.50	10.98	9.79
8	26.97	23.46	20.72	18.53
12	37.5	32.92	29.24	26.25
16	46.19	40.96	36.60	33.00
20	53.13	47.65	42.86	38.80
24	58.45	53.05	48.06	43.72
28	62.23	57.26	52.28	47.79
32	64.59	60.34	55.55	51.06
36	66.62	62.35	57.95	53.57
40	65.39	63.37	59.52	55.37
44	63.99	63.45	60.30	56.49
48	60.96	62.65	60.34	56.97
52	56.19	61.00	59.68	56.84
56	50.34	57.73	58.35	56.14
60	43.49	53.30	56.29	54.89
64	35.69	48.06	52.59	53.12
68	27.00	42.04	48.21	50.29
72	17.44	35.30	43.19	46.41
76	7.06	27.86	37.56	41.97
80	–	19.74	31.34	37.02
84	–	10.97	24.55	31.56
88	–	1.56	17.22	25.61
92	–	–	9.35	19.19
96	–	–	0.96	12.32
100	–	–	–	4.99

Table 6.6–Predicted Q_C versus Applied Voltage for Heat Pump System Having G=.28, R_{PH}=.106 °C/W, R_{PC}=.1785 °C/W, R_{IC}=.025 °C/W, and R_{IH} Given by equation 5.5 for Various N Using HP.FOR

Voltage	Q_C in Watts N=294	Q_C in Watts N=338	Q_C in Watts N=382	Q_C in Watts N=426
0	0	0	0	0
4	21.12	19.33	17.82	16.51
8	37.62	34.72	32.19	29.97
12	49.85	46.44	43.35	40.57
16	58.19	54.80	51.55	48.53
20	63.04	60.13	57.07	54.08
24	64.73	62.71	60.15	57.44
28	63.59	62.80	61.02	58.80
32	59.04	60.64	59.88	58.34
36	50.86	54.91	56.65	56.21
40	40.29	46.61	50.00	51.62
44	27.53	36.31	41.51	44.51
48	16.09	24.17	31.34	35.83
52	5.76	10.29	19.57	25.69
56	–	–	6.30	14.16
60	–	–	–	1.30

Table 6.7–Predicted Q_C versus Applied Voltage for Heat Pump System Having G=.12, R_{PH}=.106 °C/W, R_{PC}=.1785 °C/W, R_{IC}=.0043 °C/W, and R_{IH}=.0043 °C/W for Various N Using HP.FOR

Voltage	Q_C in Watts N=426	Q_C in Watts N=538	Q_C in Watts N=650	Q_C in Watts N=762
0	0	0	0	0
4	15.26	13.68	12.38	11.30
8	28.98	26.20	23.84	21.84
12	41.14	37.55	34.37	31.62
16	51.75	47.72	43.97	40.63
20	60.82	56.73	52.64	48.87
24	68.39	64.60	60.39	56.35
28	74.50	71.34	67.24	63.08
32	79.19	76.98	73.20	69.07
36	82.53	81.55	78.29	74.34
40	84.56	85.09	82.54	78.89
44	85.35	87.65	85.97	82.76
48	84.97	89.25	88.61	85.95
52	83.48	89.94	90.49	88.49
56	80.95	89.77	91.63	90.40
60	77.44	88.77	92.08	91.71
64	–	87.00	91.85	92.43
68	–	84.47	90.98	92.58
72	–	81.25	89.50	92.20
76	–	77.36	87.43	91.30
80	–	72.86	84.80	89.90
84	–	–	81.64	88.03
88	–	–	77.97	85.70
92	–	–	73.81	82.93
96	–	–	69.19	79.94
100	–	–	64.11	76.14
104	–	–	58.61	72.16
108	–	–	–	67.80

Table 6.7 (continued)

Voltage	Q_C in Watts N=426	Q_C in Watts N=538	Q_C in Watts N=650	Q_C in Watts N=762
112	–	–	–	63.07
116	–	–	–	58.00
120	–	–	–	52.60
124	–	–	–	46.86
128	–	–	–	40.80

Table 6.8–Predicted Q_C versus Applied Voltage for Heat Pump System Having G=.17, R_{PH}=.106 °C/W, R_{PC}=.1785 °C/W, R_{IC}=.0043 °C/W, and R_{IH}=.0043 °C/W for Various N Using HP.FOR

Voltage	Q_C in Watts N=426	Q_C in Watts N=538	Q_C in Watts N=650	Q_C in Watts N=762
0	0	0	0	0
4	17.97	15.78	14.06	12.67
8	33.90	30.04	26.91	24.34
12	47.78	42.75	38.53	35.00
16	59.64	53.93	48.93	44.65
20	69.50	63.60	58.12	53.30
24	77.44	71.79	66.13	60.96
28	83.51	78.54	72.96	67.65
32	87.80	83.89	78.67	73.40
36	90.41	87.91	83.28	78.21
40	91.42	90.66	86.84	82.14
44	90.95	92.19	89.39	85.20
48	89.10	92.58	90.97	87.43
52	85.92	91.89	91.63	88.87
56	81.53	90.17	91.42	89.55
60	76.01	87.49	90.37	89.50
64	69.44	83.91	88.54	88.75
68	61.86	79.46	85.96	87.35
72	–	74.21	82.67	85.31
76	–	68.19	78.71	82.68
80	–	61.44	74.10	79.46
84	–	54.00	68.88	75.70
88	–	45.89	63.07	71.42
92	–	37.15	56.70	66.63
96	–	–	49.79	61.35
100	–	–	42.36	55.61
104	–	–	34.42	49.41
108	–	–	25.98	42.78

Table 6.8 (continued)

Voltage	Q_C in Watts N=426	Q_C in Watts N=538	Q_C in Watts N=650	Q_C in Watts N=762
112	-	-	17.07	35.72
116	-	-	7.68	28.24
120	-		-	20.35
124	-	-	-	12.06
128	-	-	-	3.38

Table 6.9–Predicted Q_C versus Applied Voltage for Heat Pump System Having G=.28, R_{PH}=.106 °C/W, R_{PC}=.1785 °C/W, R_{IC}=.0043 °C/W, and R_{IH}=.0043 °C/W for Various N Using HP.FOR

Voltage	Q_C in Watts N=294	Q_C in Watts N=338	Q_C in Watts N=382	Q_C in Watts N=426
0	0	0	0	0
4	26.69	24.70	22.97	21.45
8	48.64	45.40	42.49	39.89
12	65.89	62.12	58.58	55.32
16	78.60	74.98	71.32	67.79
20	87.03	84.15	80.83	77.41
24	91.47	89.86	87.30	84.32
28	92.27	92.38	90.93	88.67
32	89.77	91.96	91.92	90.65
36	84.30	88.87	90.50	90.42
40	76.86	83.35	86.86	88.16
44	69.79	75.61	81.20	84.03
48	62.66	66.92	73.67	78.18
52	55.48	59.25	64.42	70.72
56	48.23	51.51	54.36	61.79
60	40.91	43.70	46.11	51.46
64	33.52	35.80	37.78	39.82
68	26.04	27.81	29.35	30.70
72	18.48	19.73	20.83	21.78
76	10.82	11.56	12.20	12.76
80	3.07	3.28	3.46	3.62

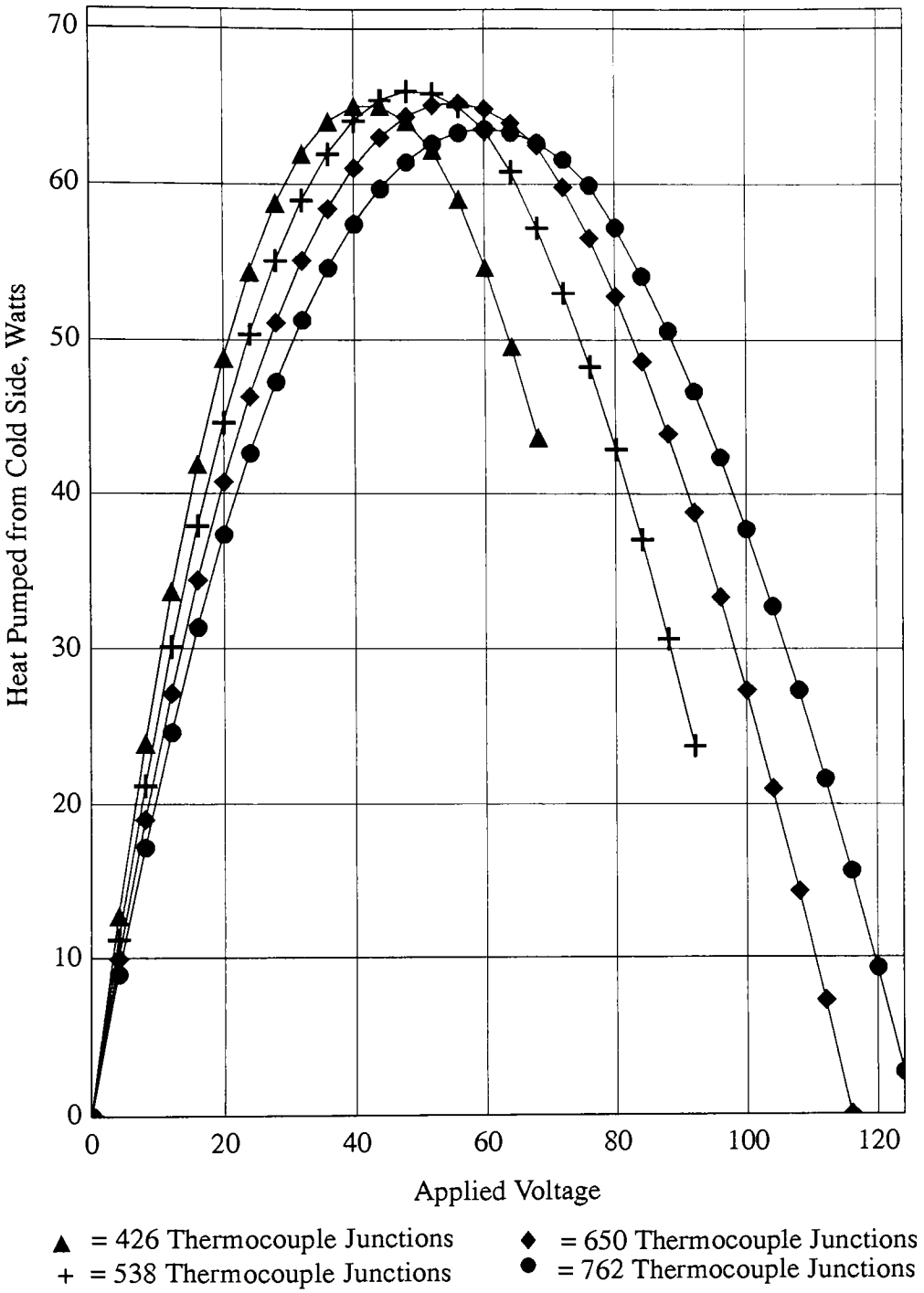

Q_C versus Applied Voltage for Heat Pump System Having G=.12, R_{PH}=.106 °C/W, R_{PC}=.1785 °C/W, R_{IC}=.025 °C/W, and R_{IH} given by equation 5.5 for various N

Figure 6.1

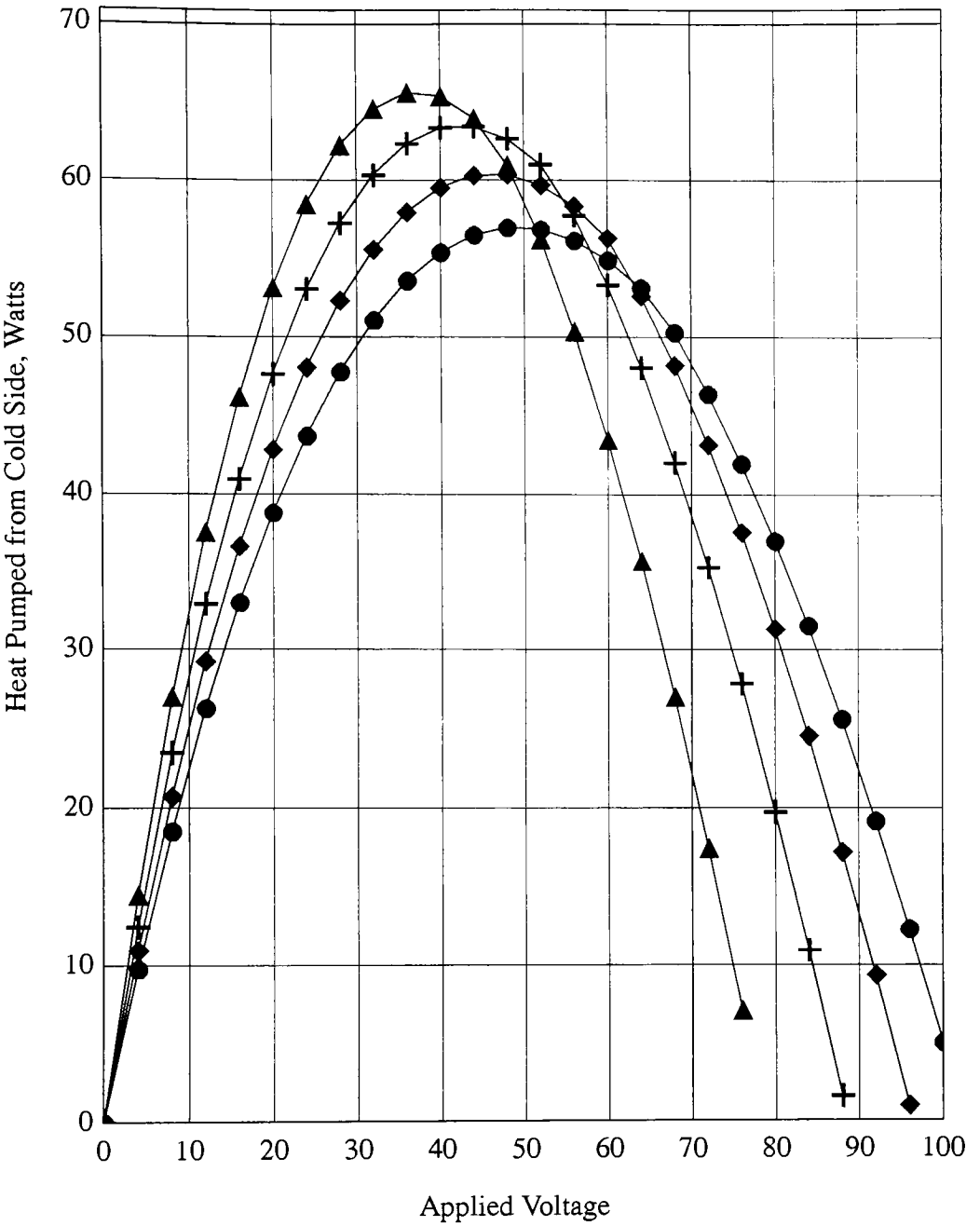

Q_C versus Applied Voltage for Heat Pump System Having G=.17, R_{PH}=.106 °C/W, R_{PC}=.1785 °C/W, R_{IC}=.025 °C/W, and R_{IH} given by equation 5.5 for various N

Figure 6.2

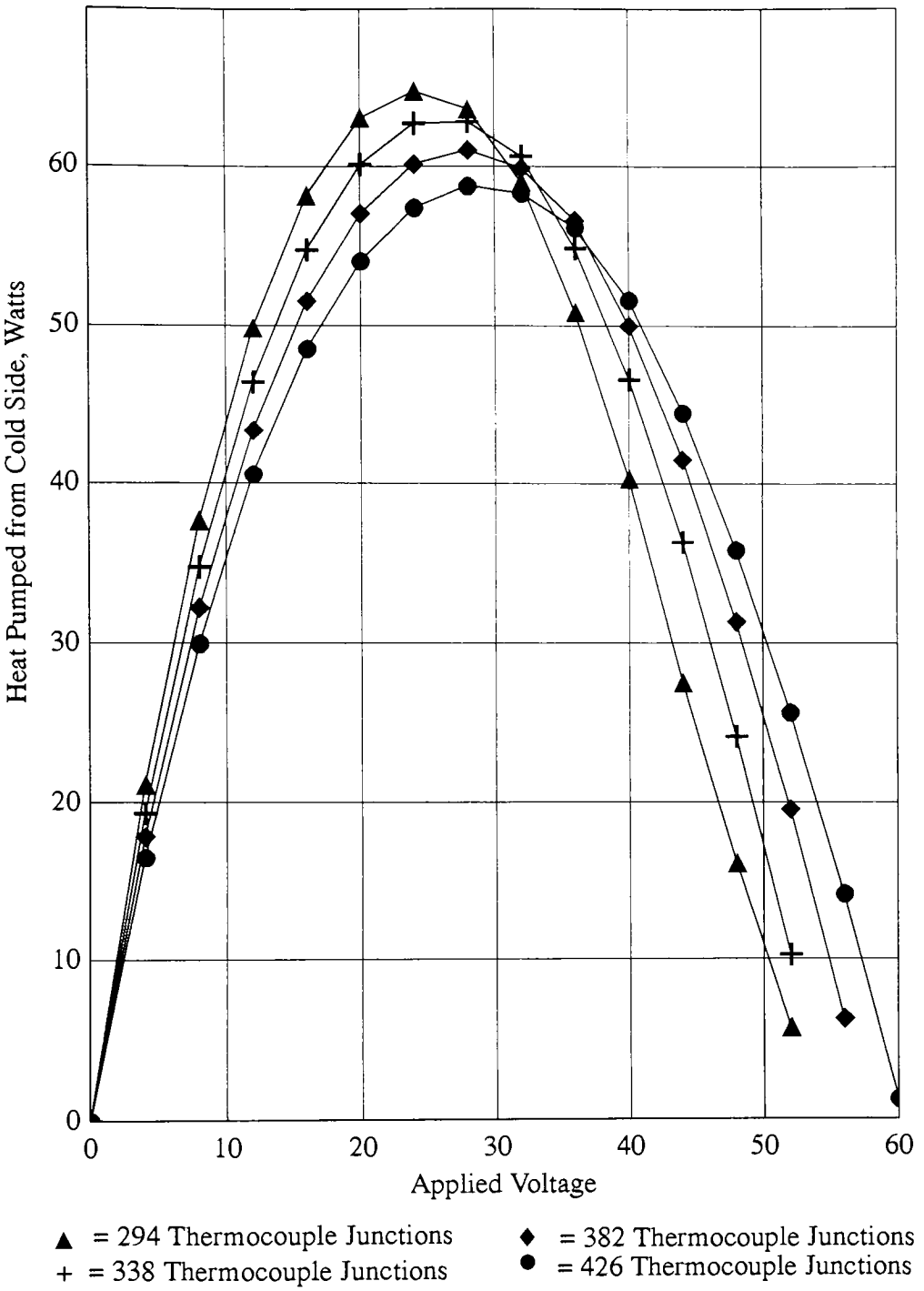

Q_C versus Applied Voltage for Heat Pump System Having G=.28, R_{PH}=.106 °C/W, R_{PC}=.1785 °C/W, R_{IC}=.025 °C/W, and R_{IH} given by equation 5.5 for various N

Figure 6.3

Very dramatic performance improvements are apparent in the data contained in Tables 6.7 through 6.9 where thermal contact resistance between the thermoelectric module and the hot and cold side pin bases was modified to reflect the presence of a .001" thick layer of thermal grease with no air gaps present. Q_C values of 92.58 W were obtained for a system operating at 68 volts having G = .12 and N = 762 as well as for a system operating at 48 volts having G = .17 and N = 538. This is an improvement of about 79% over the stock performance value of 51.74 W. Figures 6.4 through 6.6 show the families of performance curves for these various configurations. Again, performance peaks are relatively flat over a +/- 4 volt range. Figure 6.9 is a family of curves showing the system response with respect to various geometry factors while holding the number of thermocouple junctions (N = 426) constant with the improved thermal contact resistance parameters.

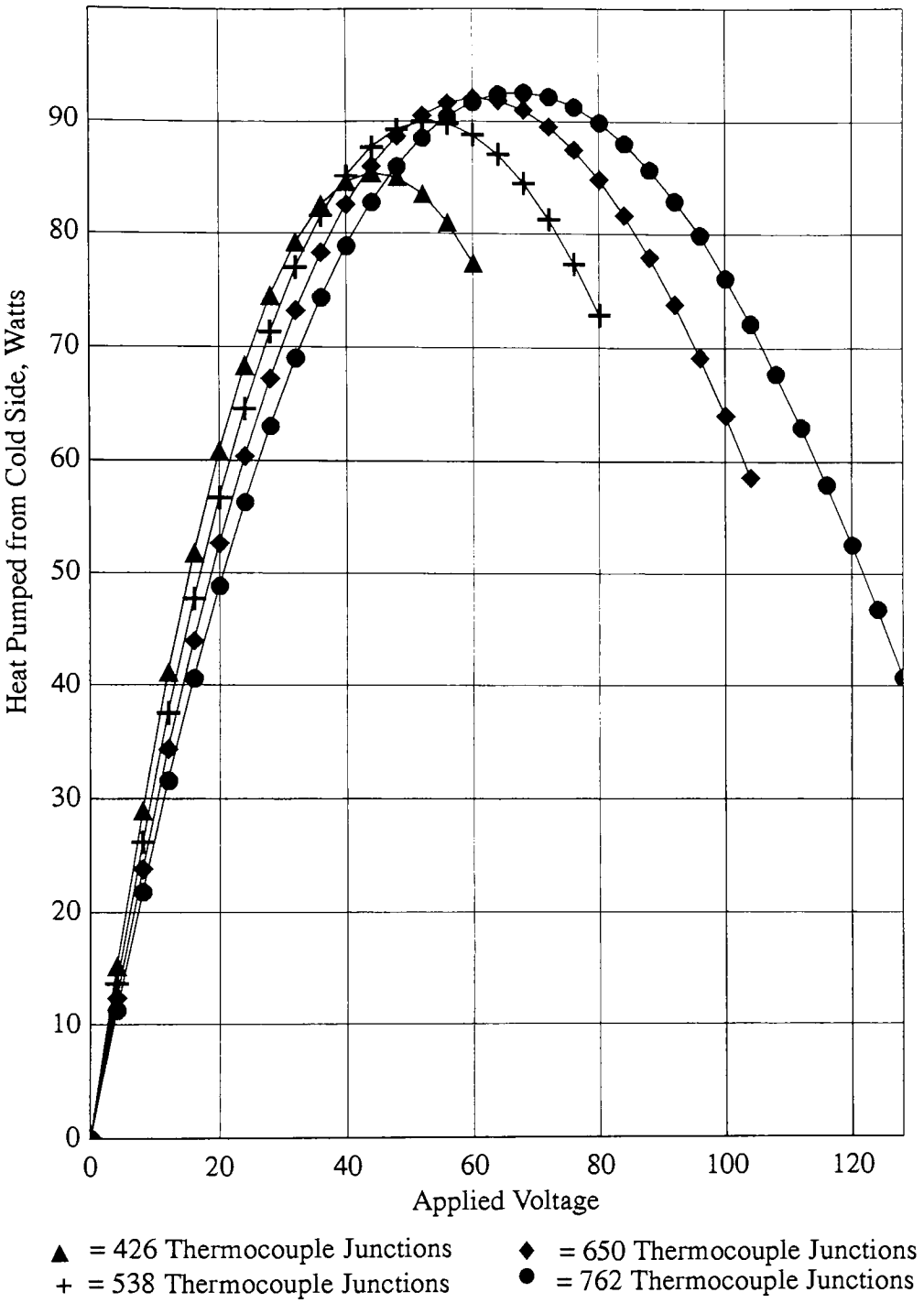

Q_C versus Applied Voltage for Heat Pump System Having G=.12, R_{PH}=.106 °C/W, R_{PC}=.1785 °C/W, R_{IC}=.0043 °C/W, and R_{IH} =.0043 °C/W for various N

Figure 6.4

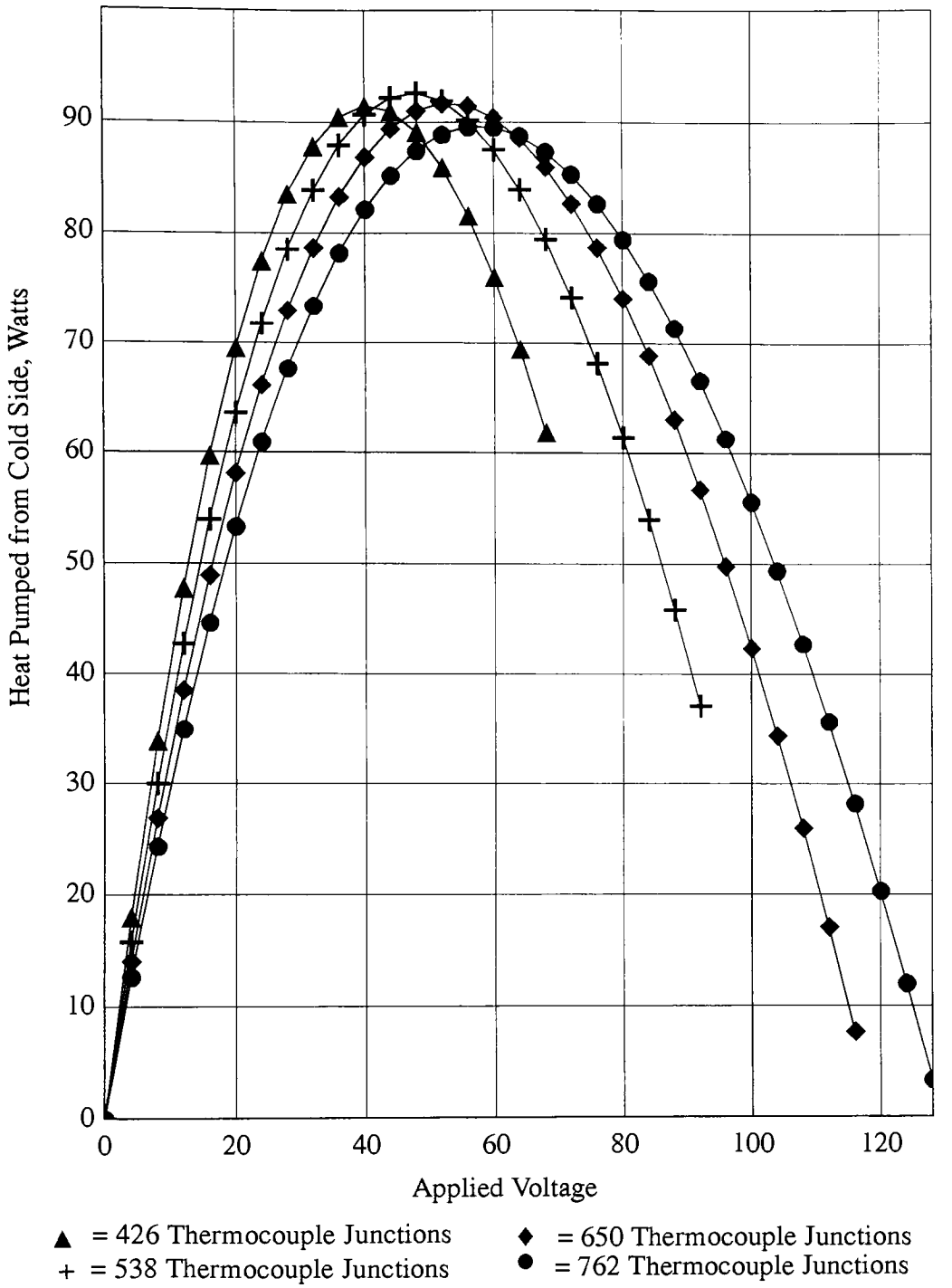

Q_C versus Applied Voltage for Heat Pump System Having G=.17, R_{PH}=.106 °C/W, R_{PC}=.1785 °C/W, R_{IC}=.0043 °C/W, and R_{IH} =.0043 °C/W for various N

Figure 6.5

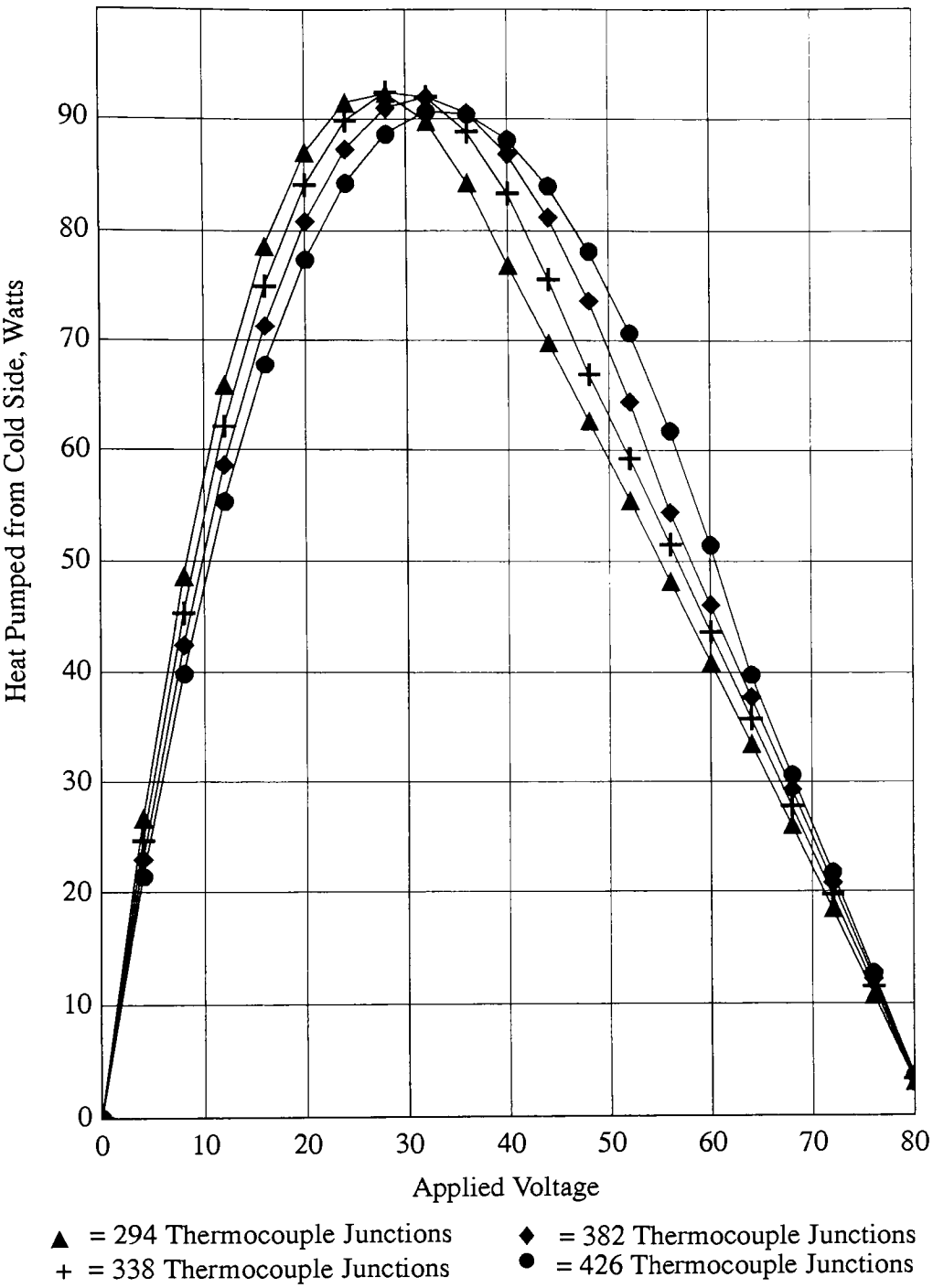

Q_C versus Applied Voltage for Heat Pump System Having G=.17, R_{PH}=.106 °C/W, R_{PC}=.1785 °C/W, R_{IC}=.0043 °C/W, and R_{IH} =.0043 °C/W for various N

Figure 6.6

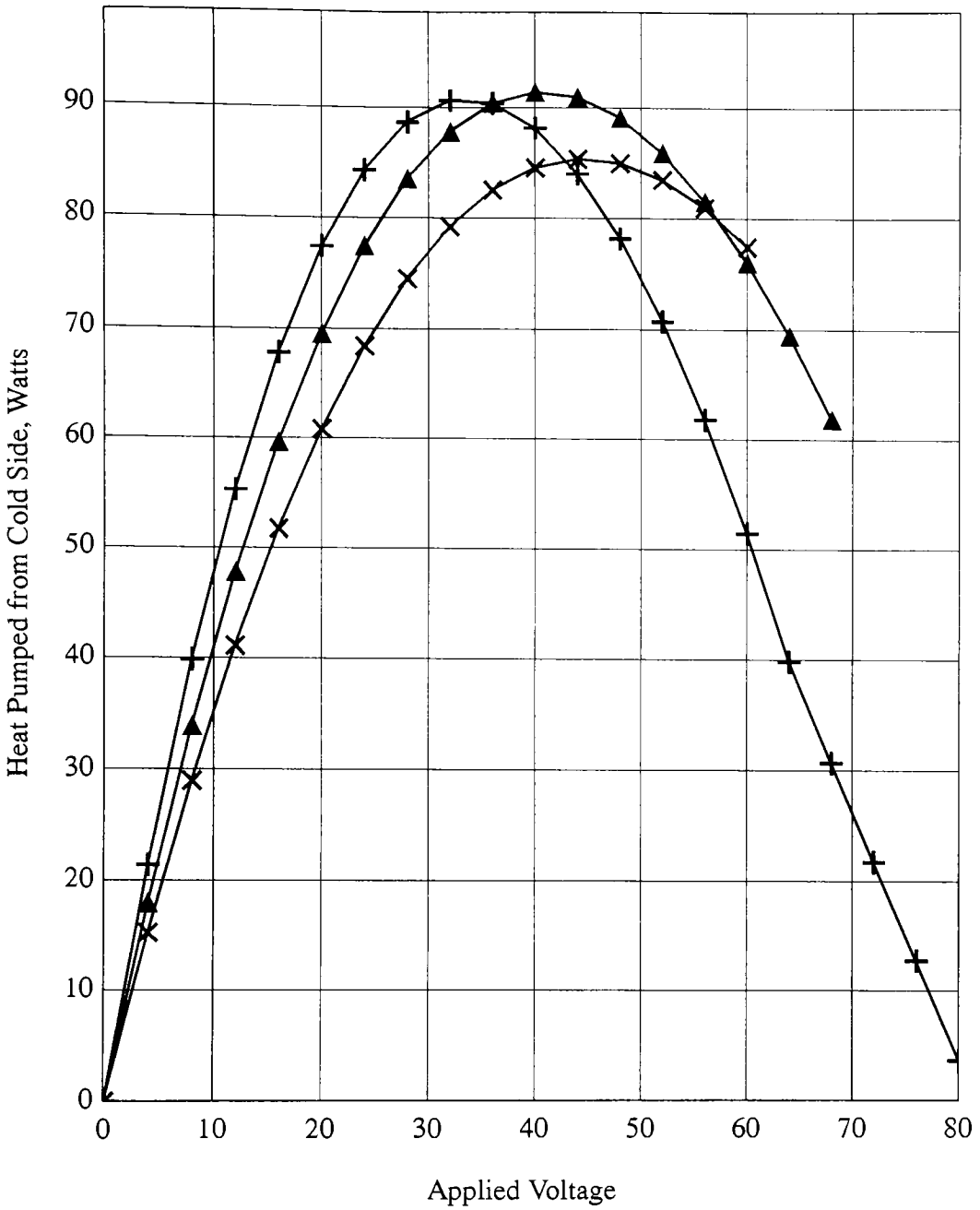

Q_C versus Applied Voltage for Heat Pump System Having N=426, R_{PH}=.106 °C/W, R_{PC}=.1785 °C/W, R_{IC}=.0043 °C/W, and R_{IH} =.0043 °C/W for various G

Figure 6.7

CHAPTER 7

CONCLUSIONS AND RECOMMENDATIONS

7.1 Conclusion

A model has been presented that describes the steady state operation of a thermoelectric heat pump having staggered cylindrical pin fin heat exchange surfaces in forced air cross flow conditions for both the hot and cold sides. The model consists of two main algorithms, one that predicts the thermal resistance of staggered pin fin banks in cross flow, and a second that uses the predicted thermal resistances of the hot and cold side to compute the performance of a thermoelectric module. Specifics of pin and pin bank geometry, pin bank material properties, temperature dependent fluid properties, the characteristics and number of thermoelectric modules used in the heat pump, the pressure versus flow characteristics for the air delivery systems being used for the hot and cold sides, and the input voltage to the system are variable inputs. Heat pumped at both the hot and cold sides, pin base temperatures, exhaust temperature and flow rates, and current draw of the system are predicted quantities.

The pin fin thermal resistance prediction algorithm was developed from correlations describing the heat transfer and pressure drop characteristics of staggered cylinder banks in cross flow. An iterative process for calculating the thermal resistance from the correlation equations is developed and presented in Chapter 3 because the equations cannot be solved in a closed form manner. A comparison of the pressure drop and heat transfer correlations against a FIDAP numerical model for two specific stagger configurations is presented in Chapter 4. Agreement of the heat transfer predictions of the two methods was found to be good, within about 10% over the range of Reynolds numbers investigated. The pressure drop

predictions did not agree as well, differing by as much as 25%.

The thermoelectric module algorithm was developed from performance equations provided by the manufacturer of the devices. Again, these equations cannot be solved in a closed form manner. An algorithm consisting of two coupled iterative processes to solve for the device current and heat pumped from the cold side was developed in Chapter 3.

The performance of the model was compared with temperature and heat transfer data collected from a series of 9 experiments performed on a heat pump fixture. Once empirically determined values for thermal contact resistance at the pin fin base/thermoelectric model interface were established, the results from the experiment and the model were found to agree quite well. The empirically determined thermal contact resistances did not, however, match the level of performance expected from the layer of thermal grease present at the interface. Further investigation into this matter revealed that an air gap existed over a portion of the pin base/thermoelectric module interface which was a result of heat sink bowing induced by the location and force exerted by the assembly fasteners. Additional calculations showed that the empirically determined thermal contact resistance values were reasonable given the presence of this air gap.

The model was used in an effort to maximize the heat pumping capacity of the test fixture unit given the constraints of staying with the existing hot and cold side pin base areas and the existing air delivery system. Two cases were examined, the first being the performance of system with the experimentally determined thermal contact resistances, and the second being the performance of the system with the elimination of the pin base bowing situation and the resulting air gap. The result of these activities was a pin bank configuration and operating voltage giving a predicted 29% increase in heat pumping capacity of the heat

pump system without the elimination of the pin base bowing situation. A 79% increase was predicted by the model with the improved pin bank configuration and new operating voltage when the pin base bowing was eliminated along with the air gap.

7.2 Recommendations for Future Work

There is a very small body of information to draw from with respect to the heat transfer characteristics and pressure drop across staggered pin fin banks at low values of Reynolds number. Only one heat transfer correlation and two pressure drop correlations for staggered banks of heated cylinders in cross flow was discovered in the literature search. The original work in this area dates back a few studies performed in the 1930's and 1940's. A recommendation for future work would be a basic study of these characteristics of pin banks at low Reynolds numbers.

The model presented in this paper was not integrated in the sense that a single computer program could be used to determine the performance of a heat pump system. A single program that could automatically run COPT.FOR, HOPT.FOR, and HP.FOR and match node temperatures would be much easier to use and result in significant time savings to the user.

The transient thermal case was not considered in this work. Depending on the heat pump application, transient behavior may be an important parameter. A more sophisticated model could be developed to examine this.

Correlations for in-line pin banks and fin-type heat exchange surfaces could be incorporated into the model to create a more versatile design tool.

APPENDIX A

SAMPLE MELCOR THERMOELECTRIC MODULE DATA SHEET

MELCOR
Materials Electronic Products Corp.
994 Spruce St., Trenton, NJ 08648 USA
Telephone (609) 393-4178/TELEX 843314
FAX (609) 393-9461

SOLID STATE COOLING WITH THERMOELECTRICS

Thermoelectric (Peltier) Heat Pump Module Specifications

Thermocouples constructed of N & P elements of highest grade bismuth telluride in form of oriented polycrystalline ingots. Ingot ends soldered to copper bus bars interfaced with ceramic plates, affording good mechanical integrity, high dielectric strength and thermal conduction. Temperature range, −150°C to +80°C. Solid state construction. Both hot and cold faces lapped flat, TYPE L. Both faces metallized and tinned, TYPE TT. Hybrid, hot face tinned, cold face lapped, TYPE TL.

	Catalog Number	I Max Amps	Hot Face Th = 25°C Q Max Watts	V Max Volts	ΔT Max °C	Universal Multipliers N No. of Couples	G Geometry Factor	G x N	Dimensions, mm A	B	C	D[5]
CP SERIES	CP 1.0- 7-06L	3.0	1.4	0.85	67	7	0.080	0.42	8	8		3.6
	CP 1.0- 17-06L	3.0	3.4	2.06	67	17	0.060	1.02	12	12		3.6
	CP 1.0- 31-06L	3.0	6.3	3.75	67	31	0.060	1.86	15	15		3.6
	CP 1.0- 63-06L	3.0	12.7	7.62	67	63	0.060	3.78	15	30		3.6
	CP 1.0- 71-06L	3.0	14.4	8.60	67	71	0.080	4.26	23	23		3.6
	CP 1.0-127-06L	3.0	25.7	15.4	67	127	0.060	7.62	30	30		3.6
	CP 1.0- 7-05L	3.9	1.8	0.85	67	7	0.078	0.55	8	8		3.2
	CP 1.0- 17-05L	3.9	4.5	2.06	67	17	0.078	1.33	12	12		3.2
	CP 1.0- 31-05L	3.9	8.2	3.75	67	31	0.078	2.42	15	15		3.2
	CP 1.0- 63-05L	3.9	16.6	7.62	67	63	0.078	4.91	15	30		3.2
	CP 1.0- 71-05L	3.9	18.7	8.60	67	71	0.078	5.54	23	23		3.2
	CP 1.0-127-05L	3.9	33.4	15.4	67	127	0.078	9.90	30	30		3.2
	CP 1.4-127-10L(1)	3.9	33.4	15.4	70	127	0.078	9.90	40	40		4.7
	CP 1.4- 3-06L	6.0	1.2	0.36	67	3	0.12	0.36	5	10		3.8
	CP 1.4- 7-06L	6.0	2.8	0.85	67	7	0.12	0.84	10	10		3.8
	CP 1.4- 11-06L	6.0	4.4	1.33	67	11	0.12	1.32	10	15		3.8
	CP 1.4- 17-06L	8.0	6.9	2.06	67	17	0.12	2.04	15	15		3.8
	CP 1.4- 31-06L	6.0	12.5	3.75	67	31	0.12	3.72	20	20		3.8
	CP 1.4- 35-06L	6.0	14.2	4.24	67	35	0.12	4.20	15	30		3.8
	CP 1.4- 71-06L	6.0	28.7	8.60	67	71	0.12	8.52	30	30		3.8
	CP 1.4-127-06L	6.0	51.4	15.4	67	127	0.12	15.24	40	40		3.8
	CP 1.4- 3-045L	8.5	1.6	0.36	65	3	0.17	0.51	5	10		3.3
	CP 1.4- 7-045L	8.5	3.8	0.65	65	7	0.17	1.19	10	10		3.3
	CP 1.4- 11-045L	8.5	5.6	1.33	65	11	0.17	1.87	10	15		3.3
	CP 1.4- 17-045L	8.5	9.2	2.06	65	17	0.17	2.89	15	15		3.3
	CP 1.4- 31-045L	8.5	16.8	3.75	65	31	0.17	5.27	20	20		3.3
	CP 1.4- 35-045L	8.5	19.0	4.24	65	35	0.17	5.95	15	30		3.3
	CP 1.4- 71-045L	8.5	38.5	8.60	65	71	0.17	12.07	30	30		3.3
	CP 1.4-127-045L	8.5	68.8	15.4	65	127	0.17	21.60	40	40		3.3
	CP 2 - 71-10L(1)	9.0	43.1	8.60	70	71	0.18	12.78	44	44		5.6
	CP 2 - 3-06L	14.0	2.8	0.36	67	3	0.28	0.84	8	15		4.6
	CP 2 - 7-06L	14.0	6.6	0.65	67	7	0.28	1.96	15	15		4.6
	CP 2 - 15-06L	14.0	14.2	1.82	67	15	0.28	4.20	15	30		4.6
	CP 2 - 17-06L	14.0	16.0	2.06	67	17	0.28	4.76	22	22		4.6
	CP 2 - 31-06L	14.0	29.3	3.75	67	31	0.28	6.86	30	30		4.6
	CP 2 - 49-06L	14.0	46.2	5.93	67	49	0.28	13.72	36	36		4.6
	CP 2 - 71-06L	14.0	67.0	8.60	67	71	0.28	19.88	44	44		4.6
	CP 2.8- 32-06L	24.0	51.8	3.87	67	32	0.48	15.36	40	40		5.0
	CP 5 - 31-10L	39.0	81.5	3.75	70	31	0.78	24.18	55	55		5.8
	CP 5 - 31-06L	60.0	125.	3.75	67	31	1.20	37.20	55	55		4.9
FC SERIES	FC 0.45- 4-05L	0.8	0.22	0.48	67	4	0.016	0.06	1.8	3.4	3.4	2.4
	FC 0.45- 8-05L	0.8	0.43	0.97	67	8	0.015	0.13	3.4	3.4	5.0	2.4
	FC 0.45-12-05L	0.8	0.65	1.45	67	12	0.015	0.19	3.4	5.0	5.0	2.4
	FC 0.45-18-05L	0.8	0.97	2.18	67	18	0.016	0.29	5.0	5.0	6.6	2.4
	FC 0.45-32-05L	0.8	1.72	3.87	67	32	0.016	0.51	6.6	6.6	8.3	2.4
	FC 0.45-66-05L	0.8	3.56	7.96	67	66	0.016	1.06	9.9	9.1	11.5	2.4
	FC 0.6- 4-06L	1.2	0.32	0.48	67	4	0.024	0.10	2.2	4.2	4.2	2.7
	FC 0.6- 8-06L	1.2	0.65	0.97	67	8	0.024	0.19	4.2	4.2	6.2	2.7
	FC 0.6- 12-06L	1.2	0.97	1.45	67	12	0.024	0.29	4.2	6.2	6.2	2.7
	FC 0.6- 18-06L	1.2	1.46	2.18	67	18	0.024	0.43	6.2	6.2	8.3	2.7
	FC 0.6- 32-06L	1.2	2.59	3.87	67	32	0.024	0.77	8.3	8.3	10.3	2.7
	FC 0.6- 66-06L	1.2	5.34	7.98	67	66	0.024	1.58	12.3	11.3	14.4	2.7
	FC 0.6- 4-05L	1.5	0.40	0.48	67	4	0.030	0.12	2.2	4.2	4.2	2.4
	FC 0.6- 8-05L	1.5	0.81	0.97	67	8	0.030	0.24	4.2	4.2	6.2	2.4
	FC 0.6- 12-05L	1.5	1.21	1.45	67	12	0.030	0.36	4.2	6.2	6.2	2.4
	FC 0.6- 18-05L	1.5	1.82	2.18	67	18	0.030	0.54	6.2	6.2	8.3	2.4
	FC 0.6- 32-05L	1.5	3.23	3.87	67	32	0.030	0.96	8.3	8.3	10.3	2.4
	FC 0.6- 66-05L	1.5	6.67	7.88	67	66	0.030	1.96	12.3	11.3	14.4	2.4
	FC 0.7- 4-05L	2.0	0.54	0.48	67	4	0.040	0.18	2.4	4.7	4.7	2.4
	FC 0.7- 8-05L	2.0	1.06	0.97	67	8	0.040	0.32	4.7	4.7	7.0	2.4
	FC 0.7- 12-05L	2.0	1.62	1.45	67	12	0.040	0.48	4.7	7.0	7.0	2.4
	FC 0.7- 18-05L	2.0	2.43	2.18	67	16	0.040	0.72	7.0	7.0	9.3	2.4
	FC 0.7- 32-05L	2.0	4.31	3.87	67	32	0.040	1.28	9.3	9.3	11.6	2.4

DIMENSIONS

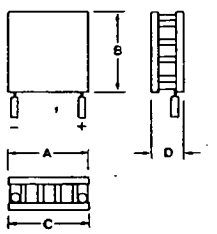

CP Series
FC Series — Option One[2][4]

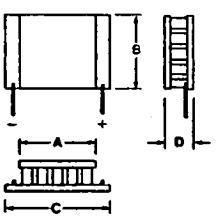

FC Series — Standard

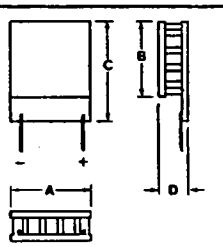

FC Series — Option Two[3]

Notes:

(1) Shown in largest size. Also available in all smaller sizes listed in group that follows.

(2) Option 1: Disregard Dim.C from table. Use Dim.C = Dim.A

(3) Option 2: Dim.C = Dim.B + 1.7 mm (FC 0.45); + 2.1 mm (FC 0.6); + 2.3 mm (FC 0.7)

(4) Option 1: Each size listed contains one less thermocouple, "N." Decrease N, GXN, Q and V accordingly.

(5) Thickness (D,mm) for Type L only.

WIRE STANDARDS

Module Type	Wire Gauge (AWG)	Length (mm/in.)	Insulation
FC 0.45-ALL	32 (SOLID)	50/2.0	None
FC 0.6-ALL	30 (SOLID)	50/2.0	None
FC 0.7-ALL	30 (SOLID)	50/2.0	None
CP 1.0-ALL	24 (STRANDED)	114/4.5	PVC
CP 1.4-ALL	22 (STRANDED)	114/4.5	PVC

Module Type	Wire Gauge (AWG)	Length (mm/in.)	Insulation
CP 2-ALL	18 (STRANDED)	114/4.5	PVC
CP 2.8-ALL	16 (STRANDED)	114/4.5	PVC
CP 5-XX-10	14 (STRANDED)	114/4.5	PVC
CP 5-XX-06	12 (STRANDED)	114/4.5	PVC

APPENDIX B

LISTING OF HOPT.FOR

```
*******************************************************************************
*
*                                  HOPT.FOR
*     PROGRAM TO COMPUTE THERMAL RESISTANCE OF HOT SIDE HEAT SINKS
*
*                              VARIABLE DESCRIPTIONS
*
*    TIN=TEMPERATURE OF INTAKE AIR IN DEGREES C
*    TPIN=TEMPERATURE OF BASE OF PIN IN DEGREES C
*    TOUT=TEMPERATURE OF EXHAUST AIR IN DEGREES C
*    PD=DIAMETER OF BASE OF PIN IN mm
*    PDAVG=AVERAGE DIAMETER OF PIN IN mm
*    ST=TRANSVERSE PITCH OF PIN ARRAY IN mm
*    SL=LONGITUDINAL PITCH OF PIN ARRAY IN mm
*    SD=SQRT(SL**2+ST**2)
*    N=NUMBER OF ROWS OF PINS ON A SINGLE HEAT SINK
*    N1=NUMBER OF PINS IN THE FIRST ROW OF A HEAT SINK
*    N2=NUMBER OF PINS IN THE SECOND ROW OF A HEAT SINK
*    NPINS=TOTAL NUMBER OF PINS ON A SINGLE HEAT SINK
*    NTOT=TOTAL NUMBER OF PINS ON A SINGLE HEAT SINK
*    MU=VISCOSITY OF AIR IN N*S/M**2
*    RHO=DENSITY OF AIR IN KG/M**3
*    KAL=CONDUCTIVITY OF ALUMINUM IN W/M*K
*    K=CONDUCTIVITY OF AIR IN W/M*K
*    CP=HEAT CAPACITY OF AIR IN J/KG*K
*    PR=PRANDTL NUMBER OF AIR
*    W=WIDTH OF HEAT SINK IN mm
*    L=LENGTH OF HEAT SINK IN mm
*    PARAM=(ST+PDAVG)/2
*    FLOWMAX=MAXIMUM VALUE OF FLOW RATE IN CFM USED FOR AN ITERATION
*    FLOWMIN=MINIMUM VALUE OF FLOW RATE IN CFM USED FOR AN ITERATION
*    FLOWBAR=(FLOWMAX+FLOWMIN)/2
*    MAX=MULTIPLICATION FACTOR FOR UINFINITY TO GIVE UMAX
*    UMAX=MAX*UINFINITY
*    UINFINITY=FLUID VELOCITY IN M/S AT INFINITY
*    TLOW=MINIMUM VALUE OF EXHAUST AIR IN DEG. C USED FOR AN ITERATION PASS
*    THIGH=MAXIMUM VALUE OF EXHAUST AIR IN DEG. C USED FOR AN ITERATION PASS
*    DTAVG=LOG MEAN TEMPERATURE DIFFERENCE IN DEG.C
*    EFF=EFFICIENCY OF PIN
*    C=CORRELATION COEFFICIENT TO COMPUTE NUSSELT NUMBER
*    M=CORRELATION COEFFICIENT TO COMPUTE NUSSELT NUMBER
*    NU=NUSSELT NUMBER
*    F=CORRELATION COEFFICIENT TO COMPUTE PRESSURE DROP ACROSS PIN FIN BANK
*    CHI=CORRELATION COEFF. TO COMPUTE PRESSURE DROP ACROSS PIN FIN BANK
*    PT=ST/PDAVG
*    PL=SL/PDAVG
*    DP=CALCULATED PRESSURE DROP ACROSS PIN FIN BANK IN Pa
*    PF=PRESSURE OUTPUT OF FAN AT A GIVEN CFM IN INCHES OF H20
*    QC=HEAT TRANSFER OF PIN FIN BANK IN WATTS CALCULATED FROM NUSSELT #
*   QM=HEAT TRANSFER OF PIN FIN BANK IN WATTS CALCULATED FROM ENERGY BALANCE
```

```
*     LOOP=ITERATION LOOP COUNTER
*     CF=CORRECTION FACTOR TO USE FOR BANKS OF PINS WITH <20 ROWS
*     MM=VARIABLE USED TO CALCULATED PIN EFFICIENCY
*     PRW=PRANDTL NUMBER AT THE WALL OF THE PIN
*     A,A1,A2,B=DUMMY VARIABLES USED IN INTERPOLATION PROCESS FOR F AND CHI
*************************************************************************
      REAL TIN,TPIN,TOUT,PD,PDAVG,SD,ST,SL,N,MU,RHO,UMAX,HP
      REAL N1,N2,W,L,NPINS,PARAM,MAX,FLOWMIN,FLOWMAX
      REAL FLOWBAR,UINFIN,CP,K,PR,F,DP,PF,C,M,QC,QM,CF,TOL,PRW
      REAL DTAVG,NU,PT,PL,CHI,MM,EFF,KAL,THIGH,TLOW,LOOP,A,B,A1,A2
      OPEN(UNIT=20,FILE='HOPT.OUT',STATUS='UNKNOWN')
      CHI=0
*************************************************************************
*     DATA INPUT
*************************************************************************
      TOL=0
5     PRINT *,'INPUT THE TEMPERATURE OF THE INPUT FLOW IN DEG. C:'
      READ *,TIN
      THIGH=TIN
      PRINT *,'INPUT THE BASE TEMPERATURE OF THE PINS IN DEG. C:'
      READ *,TPIN
      TLOW=TPIN
      PDAVG=3.96875
      PRINT *,'THE DESIGN AVERAGE DIAMETER OF A PIN IS',PDAVG,'mm'
      PRINT *,'ENTER NEW VALUE FOR AVERAGE PIN DIAMETER IN mm:'
      READ *,PDAVG
      HP=53.086
      PRINT *,'THE DESIGN PIN HEIGHT IS',HP,'mm'
      PRINT *,'ENTER NEW VALUE FOR PIN HEIGHT IN mm:'
      READ *,H
*     CALCULATE THE DIAMETER OF THE BASE OF THE PIN CONSIDERING 2 DEGREES
*     OF DRAFT PER SIDE FOR CASTING PROCESS
      PD=PDAVG+(HP/2)*2*.01495215
      ST=13.9374
      PRINT *,'THE DESIGN VALUE OF ST IS',ST,'mm'
      PRINT *,'ENTER NEW VALUE FOR ST IN mm:'
      READ *,ST
      SL=6.9687
      PRINT *,'THE DESIGN VALUE OF SL IS',SL,'mm'
      PRINT *,'ENTER NEW VALUE FOR SL IN mm:'
      READ *,SL
      SD=SQRT(SL*SL+.25*ST*ST)
      PRINT *,' '
      PRINT *,'THE SIZE OF THE HOT SIDE HEAT SINK BASE IS'
      PRINT *,'ASSUMED TO BE 139.14mm BY 255.04mm LONG'
      PRINT *,' '
*************************************************************************
CHECK FOR PIN-TO-PIN INTERFERENCES
*************************************************************************
      IF((SL**2+.25*ST**2).LT.(PD**2)) THEN
        PRINT *,'GEOMETRY ERROR DETECTED'
```

```
      GOTO 1001
    END IF
    IF (ST.LT.PD) THEN
      PRINT *,'GEOMETRY ERROR DETECTED'
      GOTO 1001
    END IF
*******************************************************************************
*   CALCULATE THE NUMBER OF PINS IN THE FIRST ROW
*******************************************************************************
    W=130.64
    N1=REAL(INT(W/ST))
    IF(((N1*ST)+PD).LT.W) THEN
      N1=N1+1
    ELSE
      N1=N1
    END IF
*******************************************************************************
*   CALCULATE THE NUMBER OF PINS IN THE SECOND ROW
*******************************************************************************
    N2=REAL(INT((W-.5*ST)/ST))
    IF(((N2*ST)+PD).LT.(W-.5*ST)) THEN
      N2=N2+1
    ELSE
      N2=N2
    END IF
*******************************************************************************
*   CALCULATE THE NUMBER OF ROWS OF PINS ON A SINGLE HEAT SINK BASE
*******************************************************************************
    L=255.04
    N=REAL(INT(L/SL))
    IF(((N*SL)+PD).LT.L) THEN
      N=N+1
    ELSE
      N=N
    END IF
*******************************************************************************
*   CALCULATE THE CORRECTION FACTOR IF NUMBER OF ROWS N
*   IS <20
*******************************************************************************
    IF (N.LT.20) THEN
      CF=1-EXP(-(N+5)*.3)
    ELSE
      CF=1
    END IF
*******************************************************************************
*   CALCULATE THE TOTAL NUMBER OF PINS ON A SINGLE HEAT SINK BASE
*******************************************************************************
    IF (N1.EQ.N2) THEN
      NPINS=N1*N
    ELSE
      IF(MOD(N,2.0).EQ.0) THEN
```

```
        NPINS=(N1+N2)*N/2
      ELSE
        NPINS=(N1+N2)*((N-1)/2)+N1
      END IF
    END IF
*************************************************************************
*   CALCULATION OF Umax=U*MAX, EQN. 3.2
*************************************************************************
    PARAM=(ST+PDAVG)/2
    IF (PARAM.LT.SD) THEN
      MAX=(ST)/(ST-PDAVG)
    ELSE
      MAX=(ST)/(2*(SD-PDAVG
    END IF
*************************************************************************
*   INITIALIZE THE SYSTEM FOR ITERATION
*   SOLVE FOR PRESSURE DROP CORRESPONDING TO ASSUMED FLOW RATE
*************************************************************************
    LOOP=1
*************************************************************************
*   PROVIDE INITIAL ESTIMATE OF TOUT AND DTAVG FOR ITERATION PROCESS
*************************************************************************
    TOUT=(THIGH+TLOW)/2
    DTAVG=TOUT-TIN
*************************************************************************
*   CALCULATE PROPERTIES OF AIR AT TEMPERATURE=DTAVG VIA INTERPOLATION--
*   FROM TABLE A.4, "FUNDAMENTALS OF HEAT TRANSFER", INCROPERA & DEWITT
*   [1981]
*************************************************************************
10  IF ((TIN+273).LT.300) THEN
      RHO=((TIN+273-250)/50)*(1.1614-1.3947)+1.3937
      MU=((TIN+273-250)/50)*(184.6E-7-159.6E-7)+159.6E-7
      CP=((TIN+273-250)/50)*(1007-1006)+1006
      K=((TIN+273-250)/50)*(26.3E-3-22.3E-3)+22.3E-3
      PR=((TIN+273-250)/50)*(.707-.72)+.72
    ELSE
      RHO=((TIN+273-300)/50)*(1.995-1.1614)+1.1614
      MU=((TIN+273-300)/50)*(208.2E-7-184.6E-7)+184.6E-7
      CP=((TIN+273-300)/50)*(1009-1007)+1007
      K=((TIN+273-300)/50)*(29.9E-3-26.3E-3)+26.3E-3
      PR=((TIN+273-300)/50)*(.7-.707)+.707
    END IF
    IF ((TPIN+273).LT.300) THEN
      PRW=((TPIN+273-250)/50)*(.707-.72)+.72
    ELSE
      PRW=((TPIN+273-300)/50)*(.7-.707)+.707
    END IF
*************************************************************************
*   BEGIN ITERATION PROCESS TO SOLVE FOR FLOW AND PRESSURE IN SYSTEM
*************************************************************************
    FLOWMIN=0
```

```
      FLOWMAX=26.32
      FLOWBAR=(FLOWMIN+FLOWMAX)/2
100   UMAX=FLOWBAR*MAX*(4.7195E-4)*(1000**2)/(HP*W)
      REMAX=RHO*UMAX*PDAVG*.001/MU
      PL=SL/PDAVG
      PT=ST/PDAVG
*******************************************************************************
*    CALCULATE VALUE FOR FRICTION FACTOR f FROM EQNS. 3.6-3.9
*******************************************************************************
      IF ((PT.GT.1.25) .AND. (PT.LT.1.5)) THEN
        A=1.8-(1.8-.96)*(PT-1.25)/(.25)
        B=.78-(.78-.57)*(PT-1.25)/(.25)
        A1=2.692-(2.692-1.557)*(REMAX-100)/100
        A2=1.462-(1.462-.9844)*(REMAX-100)/100
        F=A1-(A1-A2)*(PT-1.25)/(.25)
      END IF
      IF ((PT.GT.1.5) .AND. (PT.LT.2)) THEN
        A=.96-(.96-.6)*(PT-1.5)/(.5)
        B=.57-(.57-.475)*(PT-1.5)/(.5)
        A1=1.462-(1.462-.9844)*(REMAX-100)/100
        A2=1-(1-.734)*(REMAX-100)/100
        F=A1-(A1-A2)*(PT-1.5)/(.5)
      END IF
      IF (PT.GE.2) THEN
        A=.6-(.6-.46)*(PT-2)/(.5)
        B=.475-(.475-.415)*(PT-2)/(.5)
        A1=1.0-(1.0-.734)*(REMAX-100)/100
        A2=.801-(.801-.61358)*(REMAX-100)/100
        F=A1-(A1-A2)*(PT-2)/(.5)
      END IF
      IF(REMAX .LT.200) THEN
        GOTO 110
      ELSE
        F=A*EXP(-.0042*REMAX)+B
      END IF
*******************************************************************************
*    CALCULATE CHI FROM EQN. 3.5
*******************************************************************************
110   IF((PT/PL) .LT. 1.17) THEN
        CHI=1
      END IF
      IF((PT/PL).GE. 1.17) THEN
        CHI=(-.0006556*REMAX+1.2655)*LOG10((PT/PL)-.17)+1
      END IF
      DP=N*CHI*.5*RHO*UMAX*UMAX*F*.004015
      CALL PRESFAN(FLOWBAR,PF)
      IF(ABS(FLOWMAX-FLOWMIN).LT..0001) THEN
        GOTO 999
      END IF
      IF(DP.GT.PF) THEN
        FLOWMAX=FLOWBAR
```

```
      FLOWBAR=(FLOWMAX+FLOWMIN)/2
      GOTO 100
    ELSE
      FLOWMIN=FLOWBAR
      FLOWBAR=(FLOWMAX+FLOWMIN)/2
      GOTO 100
    END IF
*************************************************************************
*    CALCULATE AVERAGE NUSSELT NUMBER WITH EQN. 3.12
*************************************************************************
999  IF (ST.LT.(2*SL)) THEN
260     C=.35*(ST/SL)**.2
      M=.6
    ELSE
      C=.4
      M=.6
    END IF
    NU=CF*C*(REMAX**M)*(PR**.36)*(PR/PRW)**.25
*************************************************************************
*    CALCULATE Q WITH EQN. 3.13
*************************************************************************
    QM=FLOWBAR*.00047195*CP*RHO*(TOUT-TIN)
    DTAVG=((TPIN-TIN)-(TPIN-TOUT))/LOG((TPIN-TIN)/(TPIN-TOUT))
*************************************************************************
*    CALCULATE FIN EFFICIENCY EFF FOR A CYLINDRICAL PIN
*    MATERIAL IS 356T-6 ALUMINUM
*************************************************************************
    KAL=159.2
    MM=2*SQRT(NU*K*1000*1000/(KAL*PDAVG**2))
    EFF=(TANH(MM*HP/1000))/(.001*MM*HP)
    QC=(NU*K*1000/PDAVG)*NPINS*3.14159*(PDAVG/1000)*(HP/1000)*DTAVG
    QCACT=QC*EFF
    AREA=NPINS*HP*3.14159*PDAVG
    IF(ABS(QM-QCACT).LT..01) THEN
      GOTO 1000
    ELSE
      IF(QM.GT.QCACT) THEN
        TLOW=TOUT
        TOUT=.5*(TOUT+THIGH)
        LOOP=LOOP+1
        GOTO 10
      ELSE
        THIGH=TOUT
        TOUT=.5*(TOUT+TLOW)
        LOOP=LOOP+1
        GOTO 10
      END IF
    END IF
1000  PRINT *,'THE VALUE OF REMAX = ',REMAX
    PRINT *,'THE VALUE OF PT/PL = ',PT/PL
    PRINT *,'THE VALUE OF PT = ',PT
```

```
      PRINT *,'THE VALUE OF TOUT = ',TOUT, 'DEG. C'
      PRINT *,'THE VALUE OF Q = ',QM,'WATTS'
      PRINT *,'THE VOLUMETRIC FLOW RATE = ',FLOWBAR,'CFM'
      PRINT *,'THE PRESSURE DROP = ',DP,'"H20'
      PRINT *,'THE NUMBER OF ROWS OF PINS = ',N
      PRINT *,'THE NUMBER OF PINS IN THE FIRST ROW = ',N1
      PRINT *,'THE HEAT SINK TH. RES. = ',(TIN-TPIN)/QM,'DEG. C/WATT'
      PRINT *,'THE PIN AREA = ',AREA,'SQ. MM'
      WRITE(20,*) 'EFF=',EFF
      WRITE(20,*) 'TIN=',TIN,'DEG. C'
      WRITE(20,*) 'TOUT=',TOUT,'DEG. C'
      WRITE(20,*) 'TPIN=',TPIN,'DEG. C'
      WRITE(20,*) 'FLOWBAR=',FLOWBAR,'CFM'
      WRITE(20,*) 'CP=',CP,'J/KG*K'
      WRITE(20,*) 'MU=',MU,'N*SEC/M^2'
      WRITE(20,*) 'K=',K,'W/M*K'
      WRITE(20,*) 'RHO=',RHO,'KG/M^3'
      WRITE(20,*) 'LOG MEAN TEMP. DIFF=',DTAVG,'DEG. C'
      WRITE(20,*) 'QM=',QM,'WATTS'
      WRITE(20,*) 'QCACT=',QCACT,'WATTS'
      WRITE(20,*) 'NUSSELT #=',NU
      WRITE(20,*) 'REMAX=',REMAX
      WRITE(20,*) 'SL=',SL,'MM'
      WRITE(20,*) 'ST=',ST,'MM'
      WRITE(20,*) 'SD=',SD,'MM'
      WRITE(20,*) 'N=',N
      WRITE(20,*) 'NUMBER OF PINS IN FIRST ROW=',N1
      WRITE(20,*) 'NUMBER OF PINS IN SECOND ROW=',N2
      WRITE(20,*) 'TOTAL NUMBER OF PINS=',NPINS
      WRITE(20,*) 'PRESSURE CALCULATED FROM CORRELATION=',DP,'"H20'
      WRITE(20,*) 'PRESSURE CALCULATED FROM FAN CURVE=',PF,'"H20'
      WRITE(20,*) 'UINFIN=',UINFIN,'M/S'
      WRITE(20,*) 'UMAX=',UMAX,'M/S'
      WRITE(20,*) 'PIN BASE DIAMETER=',PDAVG,'MM'
      WRITE(20,*) 'AVG. PIN DIAMETER=',PDAVG,'MM'
      WRITE(20,*) 'HEIGHT OF PIN=',HP,'MM'
      WRITE(20,*) 'W=',W,'MM'
      WRITE(20,*) 'CHI=',CHI
      WRITE(20,*) 'F=',F
      WRITE(20,*) 'MAX=',MAX
      WRITE(20,*) 'PT=',PT
      WRITE(20,*) 'C=',C
      WRITE(20,*) 'M=',M
      WRITE(20,*) 'PRANDTL # =',PR
      WRITE(20,*) 'CORRECTION FACTOR=',CF
      WRITE(20,*) 'PIN AREA=',AREA,'MM'
      CLOSE(UNIT=20)
 1001 STOP
      END
```

```
*************************************************************************
*    SUBROUTINE TO RETURN PRESSURE FOR A GIVEN FLOW RATE FOR SYSTEM FAN
*************************************************************************
      SUBROUTINE PRESFAN(X,Y)
      REAL X,Y
      Y=.02545593*(-X+26.32)
      END
```

APPENDIX C

LISTING OF HP.FOR

```
************************************************************************
                          HP.FOR
        PROGRAM TO SOLVE SYSTEM OF EQUATIONS DESCRIBING
          A THERMOELECTRIC HEAT PUMP FOR HEAT FLOW
             THROUGH THE COLD SIDE HEAT SINK
                  VIA BISECTION METHOD
************************************************************************
*              DESCRIPTION OF VARIABLES
*   IQMIN==LOWER VALUE OF CURRENT USED IN BISECTION METHOD (AMPS)
*   IQMAX==UPPER VALUE OF CURRENT USED IN BISECTION METHOD (AMPS)
*   IBAR==AVERABE OF IMIN AND IMAX USED IN BISECTION METHOD (AMPS)
*   QMIN==LOWER VALUE ESTIMATE OF HEAT PUMPED AT COLD SIDE (WATTS)
*   QMAX==UPPER VALUE ESTIMATE OF HEAT PUMPED AT COLD SIDE (WATTS)
*   QBAR==AVERAGE OF QMIN AND QMAX (WATTS)
*   RH==THERMAL RESISTANCE OF HOT SIDE HEAT SINK (K/WATT)
*   RC==THERMAL RESISTANCE OF COLD SIDE HEAT SINK (K/WATT)
*   V=APPLIED VOLTAGE TO THERMOELECTRIC HEAT PUMP (VOLTS)
*   TH==TEMPERATURE OF HOT SIDE OF THERMOELECTRIC MODULE (K)
*   TC==TEMPERATURE OF COLD SIDE OF THERMOELECTRIC MODULE (K)
*   TBAR==AVERAGE TEMPERATURE OF THERMOELECTRIC MODULE (K)
*   A==SEEBECK COEFFICIENT OF THERMOELECTRIC MODULE (VOLTS/K)
*   A0==SEEBECK CONSTANT COEFFICIENT (VOLTS/K)
*   A1==SEEBECK LINEAR COEFFICIENT (VOLTS/K**2)
*   A3==SEEBECK QUADRATIC COEFFICIENT (VOLTS/K**3)
*   K==THERMAL CONDUCTIVITY OF THERMOELECTRIC MODULE (W/CM*K)
*   K0==THERMAL CONDUCTIVITY CONSTANT COEFFICIENT (W/CM*K)
*   K1==THERMAL CONDUCTIVITY LINEAR COEFFICIENT (W/CM*K**2)
*   K2==THERMAL CONDUCTIVITY QUADRATIC COEFFICIENT (W/CM*K**3)
*   R==RESISTIVITY OF THERMOELECTRIC DEVICE (OHM*CM)
*   R0==RESISTIVITY CONSTANT COEFFICIENT (OHM*CM)
*   R1==RESISTIVITY LINEAR COEFFICIENT (OHM*CM/K)
*   R2==RESISTIVITY QUADRATIC COEFFICIENT (OHM*CM/K**2)
*   N==NUMBER OF THERMOELECTRIC THERMOCOUPLES IN HEAT PUMP ASSEMBLY
*   G==THERMOELECTRIC GEOMETRY FACTOR (AREA/LENGTH OF ELEMENT, CM)
*   Q==HEAT PUMPED AT COLD SURFACE (WATTS)
*   RIBAR==RESIDUAL CALCULATED FOR IBAR TO REESTIMATE CURRENT (AMPS)
*   IQBAR==CALCULATED CURRENT FOR Q=QBAR (AMPS)
*   AQBAR==CALCULATED VALUE FOR SEEBECK COEFFICIENT AT Q=QBAR (V/K)
*   TCQBAR==MODULE COLD SIDE TEMPERATURE CALCULATED FOR Q=QBAR (K)
*   DTQBAR==TEMPERATURE DIFFERENCE ACROSS DEVICE CALCULATED FOR Q=QBAR (K)
*   QR==CALCULATED RESIDUAL OF HEAT PUMPED TO REESTIMATE Q (WATTS)
*   QRBAR==CALCULATED RESIDUAL FOR QBAR (WATTS)
************************************************************************
    REAL IMIN,IMAX,QMIN,QMAX,IBAR,QBAR,RH,RC,V,TH,TC,DT,TBAR
    REAL A,A0,A1,A2,R,R0,R1,R2,G,N,Q
    REAL IQBAR,AQBAR,TCQBAR,DTQBAR
    REAL RIBAR,QRBAR
    INTEGER OLOOP,ILOOP
************************************************************************
    INITIALIZATION OF VARIABLES
************************************************************************
```

```
      OPEN(UNIT=20,FILE='HP.OUT',STATUS='UNKNOWN')
      OLOOP=0
      ILOOP=0
      QMIN=0
      QMAX=200
      QBAR=(QMIN+QMAX)/2
      PRINT *,'INPUT VALUE FOR THERMOELECTRIC HEAT PUMP VOLTAGE:'
      READ *,V
      PRINT *,'INPUT VALUE FOR AMBIENT TEMPERATURE IN DEG. C:'
      READ *,TAMB
      TAMB=TAMB+273
      PRINT *,'INPUT VALUE FOR HOT SIDE HEAT SINK RESISTANCE IN C/WATT:'
      READ *,RH
      PRINT *,'INPUT VALUE FOR COLD SIDE HEAT SINK RES. IN C/WATT:'
      READ *,RC
      PRINT *,'INPUT VALUE FOR THERMOELECTRIC MODULE GEOMETRY FACTOR:'
      READ *,G
      PRINT *,'INPUT VALUE FOR NUMBER OF THERMOCOUPLE JUNCTIONS'
      PRINT *,'IN HEAT PUMP ASSEMBLY:'
      READ *,N
*******************************************************************************
      DEFINE THERMOELECTRIC MODULE TEMPERATURE DEPENDENT
      PARAMETERS BASED  ON MELCOR DATA, EQNS. 3.32-3.35
*******************************************************************************
      A0=22224
      A1=930.6
      A2=-.9905
      R0=-5112
      R1=163.4
      R2=.6279
*******************************************************************************
      BEGIN BISECTION METHOD ROUTINE TO CALCULATE
      CURRENT FOR AN INITIAL ESTIMATE OF Q
*******************************************************************************
1     IMIN=0
      IMAX=12
      Q=QBAR
5     ILOOP=ILOOP+1
      IBAR=(IMIN+IMAX)/2
      TH=TAMB+(V*IBAR+Q)*RH
      TC=TAMB-Q*RC
       DT=TH-TC
       TBAR=(TH+TC)/2
       A=(A0+A1*TBAR+A2*TBAR**2)*1E-9
       R=(R0+R1*TBAR+R2*TBAR**2)*1E-8
       RIBAR=IBAR-((V/(2*N))-A*DT)*G/R
       IF(RIBAR.LT.0) THEN
          IMIN=IBAR
      ELSE
         IMAX=IBAR
      END IF
```

```
      IF((IMAX-IMIN).LT. .000001) THEN
        GOTO 100
      ELSE
        GOTO 5
      END IF
  100 IQBAR=IBAR
      AQBAR=A
      TCQBAR=TC
      RQBAR=R
      DTQBAR=DT
      TBQBAR=TBAR
*******************************************************************************
*     BEGIN BISECTION METHOD TO CALCULATE Q
*******************************************************************************
      CALL QRES(QBAR,N,AQBAR,IQBAR,TCQBAR,RQBAR,G,TBQBAR,DTQBAR,QRBAR)
      IF(QRBAR .GT. 0) THEN
        QMAX=QBAR
        QBAR=(QMAX+QMIN)/2
      ELSE
        QMIN=QBAR
        QBAR=(QMAX+QMIN)/2
      END IF
      IF((QMAX-QMIN) .LT. .0001) THEN
        GOTO 200
      ELSE
        OLOOP=OLOOP+1
        WRITE(20,*),'OUTER LOOP COUNT = ',OLOOP
        WRITE(20,*),'INNER LOOP COUNT = ',ILOOP
        ILOOP=0
        GOTO 1
      END IF
  200 PRINT *,'HEAT PUMPED FROM COLD SIDE = ',QBAR,' WATTS'
      PRINT *,'HEAT PUMPED FROM HOT SIDE = ',QBAR+IBAR*V,' WATTS'
      PRINT *,'DEVICE CURRENT DRAW = ',IQBAR,' AMPS'
      PRINT *,'SEEBECK COEFF. = ',AQBAR,' V/K'
      PRINT *,'RESISTIVITY = ',R,' OHMS/CM'
      PRINT *,'TCOLD = ',TCQBAR-273,' DEG. C'
      PRINT *,'THOT = ',TCQBAR+DTQBAR-273,' DEG. C'
      PRINT *,'AVERAGE DEVICE TEMPERATURE = ',TBQBAR-273,' DEG. C'
      PRINT *,'THOT-TCOLD = ',DTQBAR,' DEG. C'
      PRINT *,'RHOT = ',RH,' C/W'
      PRINT *,'RCOLD = ',RC,' C/W'
      PRINT *,'DRIVING VOLTAGE = ',V,' VOLTS'
 1000 STOP
      END
*******************************************************************************
*     SUBROUTINE TO CALCULATE RESIDUAL OF Q
*******************************************************************************
      SUBROUTINE QRES(Q,N,A,I,TC,R,G,TB,DT,QR)
      REAL,Q,N,A,I,TC,R,G,TB,DT,QR,K
      K=(62605-277.7*TB+.4131*TB**2)*1E-6
```

```
QR=Q-2*N*(A*I*TC-I*I*R/(2*G)-K*DT*G)
END
```

APPENDIX D

SYSTEMS TEST RAW DATA

System Test 1 Data

Test conditions:

Inner cold side fan voltage:	20.5 volts
Outer cold side fan voltage:	20.5 volts
Hot side fan voltage:	10.96 volts
System current draw:	3.55 amps

Temperatures and voltage drops associated with each thermoelectric module:
(Note: Refer to Figure 5.5 for locations of thermoelectrics).

Thermoelectric Number	Number of Semiconductor Junctions (N)	Voltage Drop (volts)	Hot side heat sink base temperature (C)	Cold side heat sink base temperature (C)
1	127	7.76	48.3	13.9
2	127	8.12	47.4	11.7
3	71	5.68	41.2	10.6
4	71	5.50	42.6	11.2
5	127	7.73	45.4	11.8
6	127	8.49	48.8	14.7
	Total Num. Junctions=650	Total Voltage Drop =43.28 v	Weighted Avg. Temp. = 46.26	Weighted Avg. Temp. = 12.56

Note: Weighted Avg. Temp.= $\langle \sum N_i * T_i \rangle \div$(Total Number of Junctions) where N_i and T_i are the number of junctions and temperature of the thermoelectric module in question.

Hot side velocity profiles measured at outlet of flow straightener:

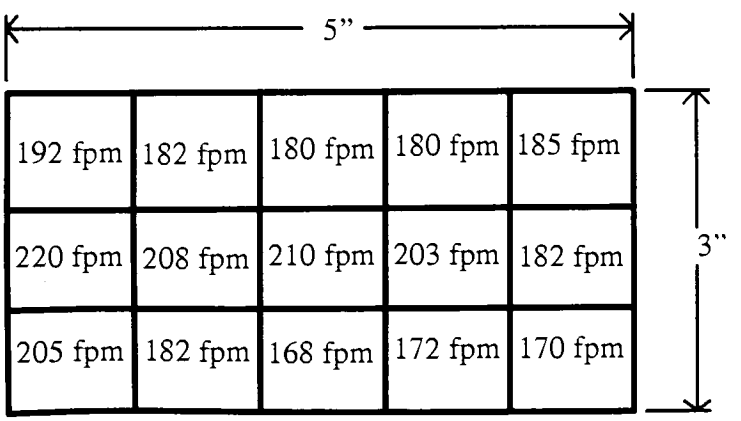

Notes: -Above cells are 1" x 1" square

Volumetric flow rate based on profiles on left is 19.72 CFM

Calculated by:

$\dot{V} = A * \frac{1}{n}(\Sigma V_i)$

where A = duct cross sectional area, n= number of cells, Vi=velocity measurement of a given cell

Pressure drop across hot side = .09" H_2O

System Test 1 Data (continued)

Hot side velocities and temperatures measured right at heat exchanger exhaust

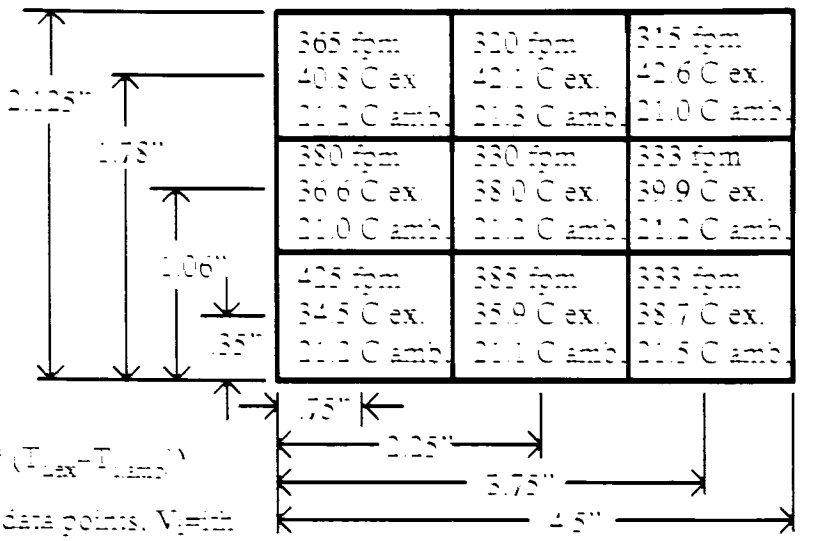

Hot side temperature rise = 17.39 C

Calculated by:

$$\Delta T = \frac{\dot{}}{\Sigma V_i} * \Sigma (V_i * (T_{i\,ex} - T_{i\,amb}))$$

where n = number of data points, V_i=ith velocity data point, $T_{i\,ex}$ = ith exhaust temperature, and $T_{i\,amb}$=ambient temperature at time $T_{i\,ex}$ was collected

Note: ex.=exhaust
amb.=ambient

Cold side velocities and temperatures for outer rung

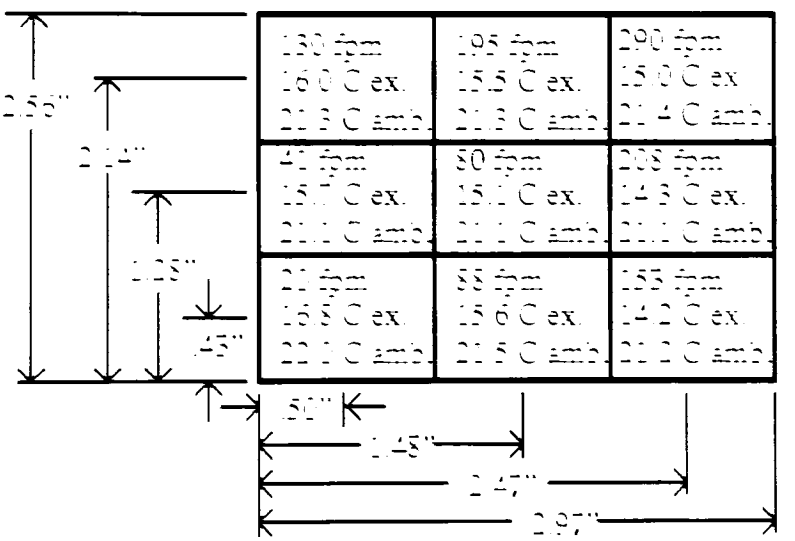

Notes:
1. ex.=exhaust
2. amb.=ambient

Outer cold side temperature drop = 6.21 C

Calculated by:

$$\Delta T = \frac{\dot{}}{\Sigma V_i} * \Sigma (V_i * (T_{i\,ex} - T_{i\,amb}))$$

where n = number of data points, V_i=ith velocity data point, $T_{i\,ex}$ = ith exhaust temperature, and $T_{i\,amb}$=ambient temperature at time $T_{i\,ex}$ was collected

Volumetric flow rate based on velocity profiles above is 7.06 CFM

Calculated by: $\dot{V} = A * \frac{\dot{}}{n} \Sigma V_i$

where A= duct cross sectional area, n=number of data points, V_i is the velocity at a given point

System Test 1 Data (continued)

Cold side velocities and temperatures for inner ring:

Notes:
1. ex.=exhaust
2. amb.=ambient

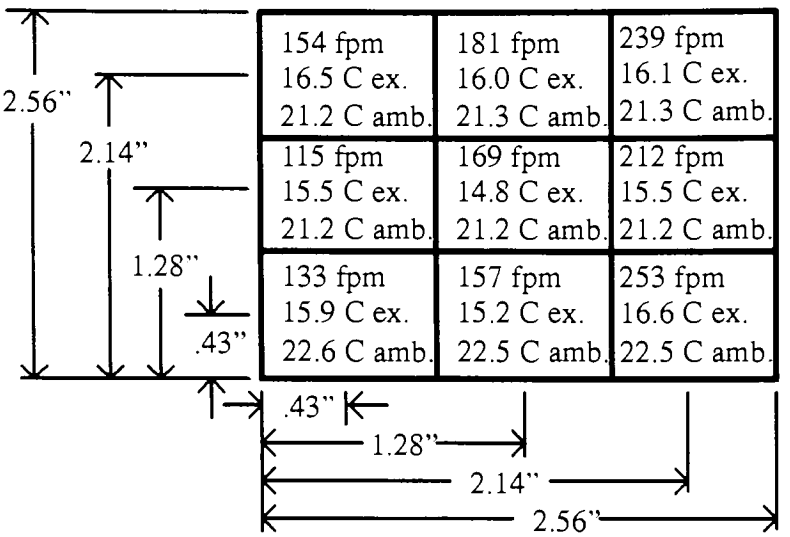

Inner cold side temperature drop = 5.83 C

Calculated by:

$$\Delta T = \frac{1}{\Sigma V_i} * \Sigma \, (V_i * (T_{i,ex} - T_{i,amb}))$$

where n = number of data points, V_i=ith velocity data point, $T_{i,ex}$ = ith exhaust temperature, and $T_{i,amb}$=ambient temperature at time $T_{i,ex}$ was collected

Volumetric flow rate based on velocity profiles above is 8.13 CFM

Calculated by: $\dot{V} = A * \frac{1}{n}(\Sigma V_i)$

where A= duct cross sectional area, n=number of data points, V_i is the velocity at a given point

Calculated parameters:

1. Average ambient temperature during test (average of 9 ambient temperature data points taken for cold side, outer ring) = 21.33 C
2. Heat rejected by hot side heat sink ($\varrho \dot{V} c_p \Delta T$) = 193.65 W
3. Heat rejected by outer cold side heat sink ($\varrho \dot{V} c_p \Delta T$) = 24.77 W
4. Heat rejected by inner cold side heat sink ($\varrho \dot{V} c_p \Delta T$) = 26.77 W
5. Electrical resistive heating ($P = I^2R = I V_{total}$) = 153.64 W
6. Energy balance:

Heat pumped at cold side:	51.54 W (item 3 + item 4)
I^2R heating:	153.64 W (item 5)
	205.18 W vs. 193.65 W measured
Error:	5.95%

System Test 2 Data

Test conditions:

Inner cold side fan voltage: 28.00 volts
Outer cold side fan voltage: 28.00 volts
Hot side fan voltage: 17.50 volts
System current draw: 4.005 amps

Temperatures and voltage drops associated with each thermoelectric module:
(Note: Refer to Figure 5.5 for locations of thermoelectrics).

Thermoelectric Number	Number of Semiconductor Junctions (N)	Voltage Drop (volts)	Hot side heat sink base temperature (C)	Cold side heat sink base temperature (C)
1	127	8.75	50.0	16.0
2	127	9.24	49.5	13.8
3	71	6.40	42.6	13.2
4	71	6.18	44.2	14.8
5	127	8.62	48.2	14.4
6	127	9.55	51.1	17.9
	Total Num. Junctions=650	Total Voltage Drop = 48.74 v	Weighted Avg. Temp. = 48.32	Weighted Avg. Temp. = 15.19

Note: Weighted Avg. Temp.= $\langle \sum N_i * T_i \rangle \div$(Total Number of Junctions) where N_i and T_i are the number of junctions and temperature of the thermoelectric module in question.

Hot side velocity profiles measured at outlet of flow straightener:

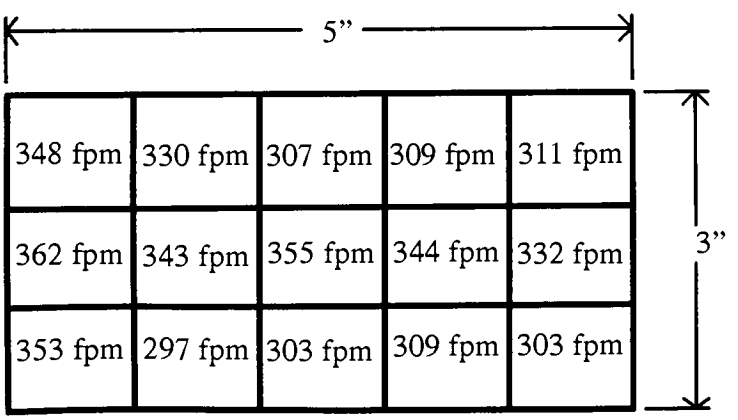

Notes: -Above cells are 1" x 1" square

Volumetric flow rate based on profiles on left is 34.07 CFM

Calculated by:

$$\dot{V} = A * \frac{1}{n}(\Sigma V_i)$$

where A = duct cross sectional area, n= number of cells, Vi=velocity measurement of a given cell

Pressure drop across hot side = .24" H_2O

System Test 2 Data (continued)

Hot side velocities and temperatures **measured right at heat exchanger exhaust**:

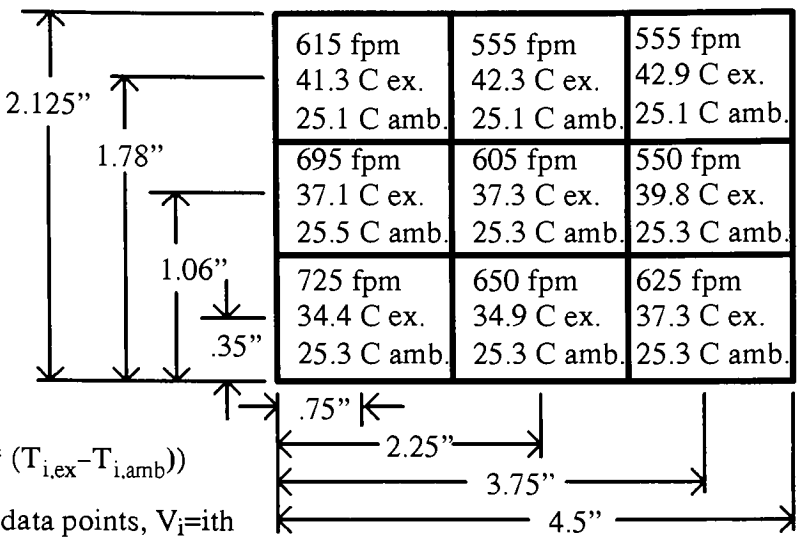

Hot side temperature rise = 13.10 C

Calculated by:

$$\Delta T = \frac{1}{\Sigma V_i} * \Sigma \ (V_i * (T_{i,ex} - T_{i,amb}))$$

where n = number of data points, V_i=ith velocity data point, $T_{i,ex}$ = ith exhaust temperature, and $T_{i,amb}$=ambient temperature at time $T_{i,ex}$ was collected

Note: ex.=exhaust
amb.=ambient

Cold side velocities and temperatures for outer ring:

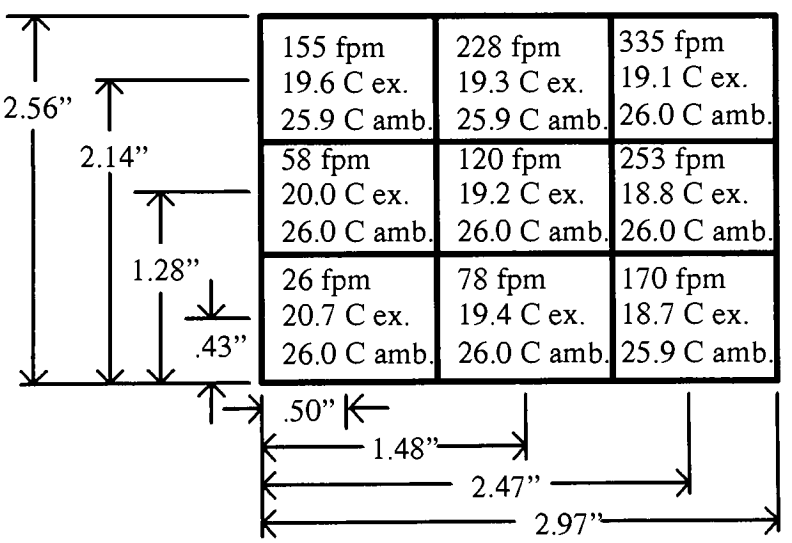

Notes:
1. ex.=exhaust
2. amb.=ambient

Outer cold side temperature drop = 6.78 C

Calculated by:

$$\Delta T = \frac{1}{\Sigma V_i} * \Sigma \ (V_i * (T_{i,ex} - T_{i,amb}))$$

where n = number of data points, V_i=ith velocity data point, $T_{i,ex}$ = ith exhaust temperature, and $T_{i,amb}$=ambient temperature at time $T_{i,ex}$ was collected

Volumetric flow rate based on velocity profiles above is 8.34 CFM

Calculated by: $\dot{V} = A * \frac{1}{n}(\Sigma V_i)$

where A= duct cross sectional area, n=number of data points, V_i is the velocity at a given point

System Test 2 Data (continued)

Cold side velocities and temperatures for inner ring:

Notes:
1. ex.=exhaust
2. amb.=ambient

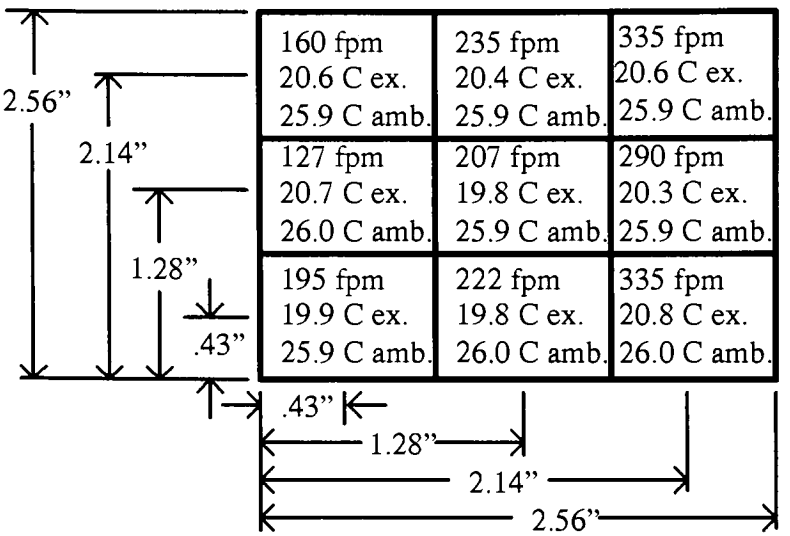

Inner cold side temperature drop = 5.59 C

Calculated by:

$$\Delta T = \frac{1}{\Sigma V_i} * \Sigma \left(V_i * (T_{i,ex} - T_{i,amb})\right)$$

where n = number of data points, V_i=ith velocity data point, $T_{i,ex}$ = ith exhaust temperature, and $T_{i,amb}$=ambient temperature at time $T_{i,ex}$ was collected

Volumetric flow rate based on velocity profiles above is 10.62 CFM

Calculated by: $\dot{V} = A * \frac{1}{n}(\Sigma V_i)$

where A= duct cross sectional area, n=number of data points, V_i is the velocity at a given point

Calculated parameters:

7. Average ambient temperature during test (average of 9 ambient temperature data points taken for cold side, outer ring) = 25.97 C

8. Heat rejected by hot side heat sink ($\varrho \dot{V} c_p \Delta T$) = 252.11 W

9. Heat rejected by outer cold side heat sink ($\varrho \dot{V} c_p \Delta T$) = 31.95 W

10. Heat rejected by inner cold side heat sink ($\varrho \dot{V} c_p \Delta T$) = 33.50 W

11. Electrical resistive heating ($P = I^2R = I V_{total}$) = 195.20 W

12. Energy balance:
    Heat pumped at cold side: 65.45 W (item 3 + item 4)
    I^2R heating: 195.20 W (item 5)
    260.65 W vs. 252.11 W measured

    Error: 3.39 %

System Test 3 Data

Test conditions:

Inner cold side fan voltage: 28.00 volts
Outer cold side fan voltage: 28.00 volts
Hot side fan voltage: 17.52 volts
System current draw: 1.611 amps

Temperatures and voltage drops associated with each thermoelectric module:
(Note: Refer to Figure 5.5 for locations of thermoelectrics).

Thermoelectric Number	Number of Semiconductor Junctions (N)	Voltage Drop (volts)	Hot side heat sink base temperature (C)	Cold side heat sink base temperature (C)
1	127	3.34	32.7	19.1
2	127	3.69	32.6	17.6
3	71	2.46	30.1	17.4
4	71	2.40	30.9	18.4
5	127	3.34	31.9	18.0
6	127	3.91	33.0	19.7
	Total Num. Junctions=650	Total Voltage Drop = 19.14 v	Weighted Avg. Temp. = 32.10	Weighted Avg. Temp. = 18.45

Note: Weighted Avg. Temp.= $\langle \sum N_i * T_i \rangle \div$(Total Number of Junctions) where N_i and T_i are the number of junctions and temperature of the thermoelectric module in question.

Hot side velocity profiles measured at outlet of flow straightener:

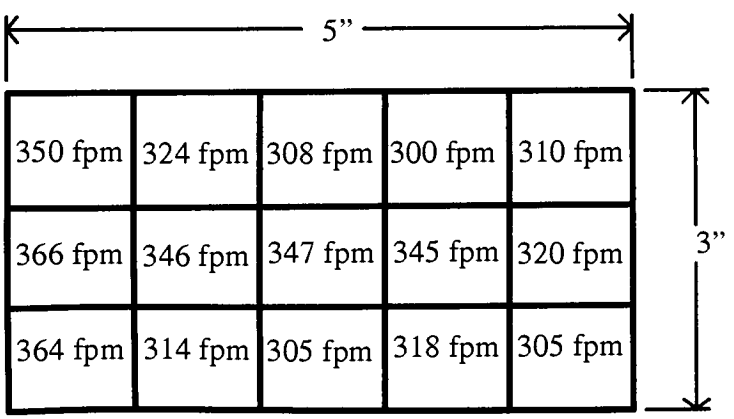

Notes: -Above cells are 1" x 1" square

Volumetric flow rate based on profiles on left is 34.18 CFM

Calculated by:

$$\dot{V} = A * \frac{1}{n}(\Sigma V_i)$$

where A = duct cross sectional area, n= number of cells, Vi=velocity measurement of a given cell

Pressure drop across hot side = .26" H_2O

System Test 3 Data (continued)

Hot side velocities and temperatures **measured right at heat exchanger exhaust**:

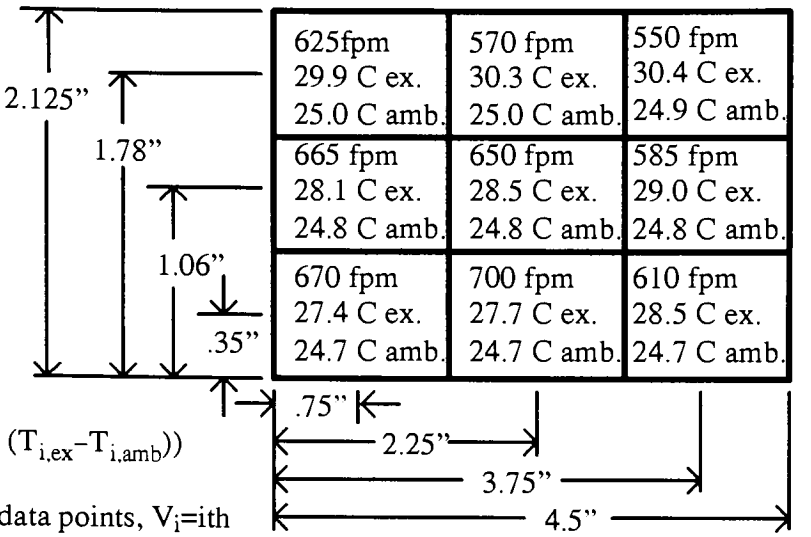

Hot side temperature rise = 3.98 C

Calculated by:

$$\Delta T = \frac{1}{\Sigma V_i} * \Sigma \ (V_i * (T_{i,ex} - T_{i,amb}))$$

where n = number of data points, V_i=ith velocity data point, $T_{i,ex}$ = ith exhaust temperature, and $T_{i,amb}$=ambient temperature at time $T_{i,ex}$ was collected

Note: ex.=exhaust
amb.=ambient

Cold side velocities and temperatures for outer ring:

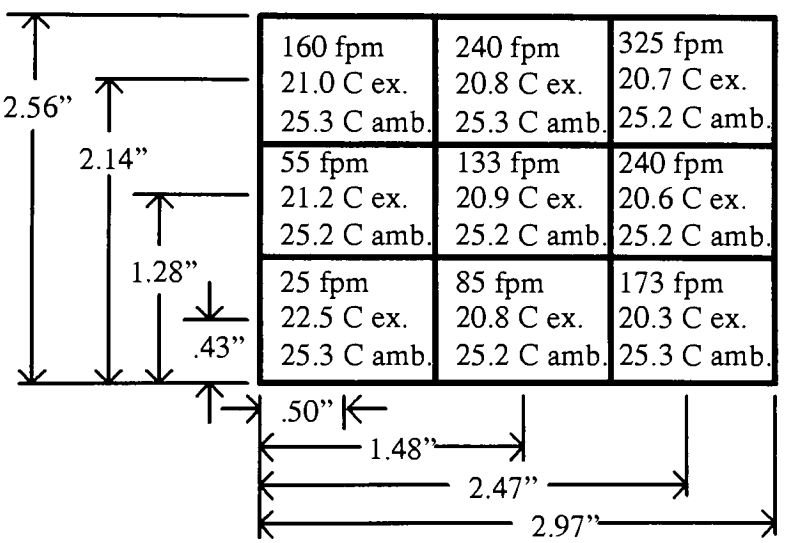

Notes:
1. ex.=exhaust
2. amb.=ambient

Outer cold side temperature drop = 4.48 C

Calculated by:

$$\Delta T = \frac{1}{\Sigma V_i} * \Sigma \ (V_i * (T_{i,ex} - T_{i,amb}))$$

where n = number of data points, V_i=ith velocity data point, $T_{i,ex}$ = ith exhaust temperature, and $T_{i,amb}$=ambient temperature at time $T_{i,ex}$ was collected

Volumetric flow rate based on velocity profiles above is 8.41 CFM

Calculated by: $\dot{V} = A * \frac{1}{n}(\Sigma V_i)$

where A= duct cross sectional area, n=number of data points, V_i is the velocity at a given point

System Test 3 Data (continued)

Cold side velocities and temperatures for inner ring:

Notes:
1. ex.=exhaust
2. amb.=ambient

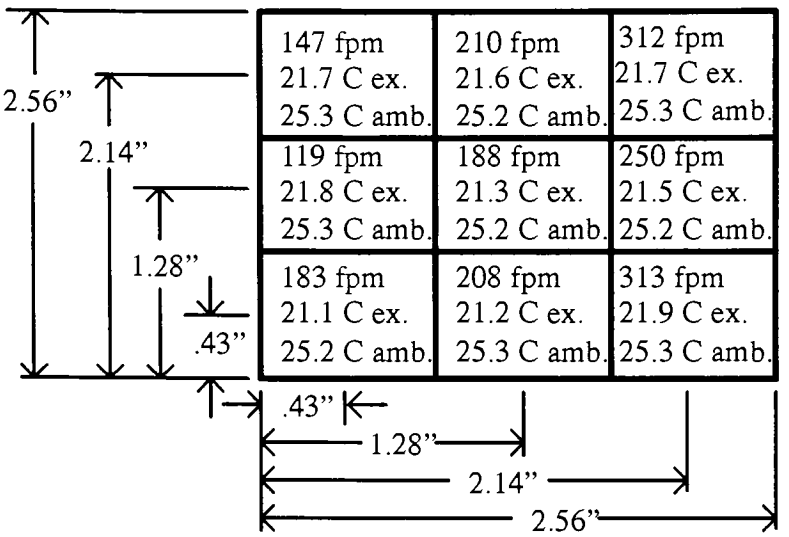

Inner cold side temperature drop = 3.70 C

Calculated by:

$$\Delta T = \frac{1}{\Sigma V_i} * \Sigma \left(V_i * (T_{i,ex} - T_{i,amb})\right)$$

where n = number of data points, V_i=ith velocity data point, $T_{i,ex}$ = ith exhaust temperature, and $T_{i,amb}$=ambient temperature at time $T_{i,ex}$ was collected

Volumetric flow rate based on velocity profiles above is 9.73 CFM

Calculated by: $\dot{V} = A * \frac{1}{n}(\Sigma V_i)$

where A= duct cross sectional area, n=number of data points, V_i is the velocity at a given point

Calculated parameters:

13. Average ambient temperature during test (average of 9 ambient temperature data points taken for cold side, outer ring) = 25.24 C

14. Heat rejected by hot side heat sink ($\varrho \dot{V} c_p \Delta T$) = 76.87 W

15. Heat rejected by outer cold side heat sink ($\varrho \dot{V} c_p \Delta T$) = 21.30 W

16. Heat rejected by inner cold side heat sink ($\varrho \dot{V} c_p \Delta T$) = 20.36 W

17. Electrical resistive heating ($P = I^2R = I V_{total}$) = 30.83 W

18. Energy balance:
    Heat pumped at cold side: 41.66 W (item 3 + item 4)
    I^2R heating: 30.83 W (item 5)
    72.49 W vs. 76.87 W measured

    Error: -5.70 %

System Test 4 Data

Test conditions:

Inner cold side fan voltage: 12.50 volts
Outer cold side fan voltage: 12.50 volts
Hot side fan voltage: 17.50 volts
System current draw: 4.005 amps

Temperatures and voltage drops associated with each thermoelectric module:
(Note: Refer to Figure 5.5 for locations of thermoelectrics).

Thermoelectric Number	Number of Semiconductor Junctions (N)	Voltage Drop (volts)	Hot side heat sink base temperature (C)	Cold side heat sink base temperature (C)
1	127	8.60	44.6	8.6
2	127	9.11	44.0	6.0
3	71	6.28	37.3	4.9
4	71	6.09	38.9	5.8
5	127	8.54	42.8	6.4
6	127	9.38	45.7	10.6
	Total Num. Junctions=650	Total Voltage Drop = 48.00 v	Weighted Avg. Temp. = 42.93	Weighted Avg. Temp. = 7.34

Note: Weighted Avg. Temp.= $\langle \sum N_i * T_i \rangle \div$(Total Number of Junctions) where N_i and T_i are the number of junctions and temperature of the thermoelectric module in question.

Hot side velocity profiles measured at outlet of flow straightener:

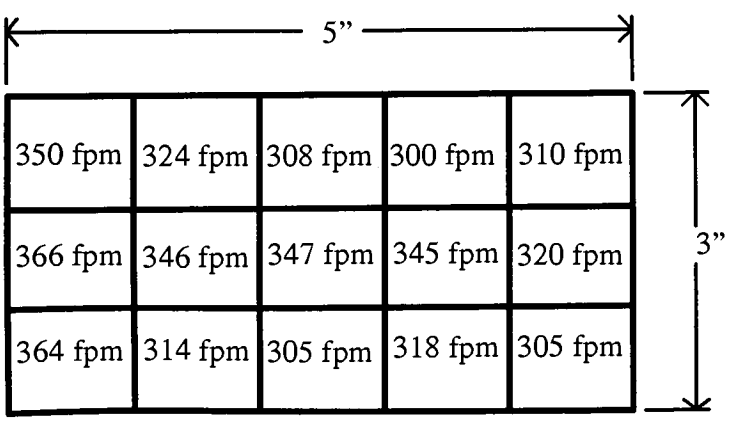

Notes: -Above cells are 1" x 1" square

Volumetric flow rate based on profiles on left is 34.18 CFM

Calculated by:

$$\dot{V} = A * \frac{1}{n}(\Sigma V_i)$$

where A = duct cross sectional area, n= number of cells, Vi=velocity measurement of a given cell

Pressure drop across hot side = .25" H_2O

System Test 4 Data (continued)

Hot side velocities and temperatures **measured right at heat exchanger exhaust**:

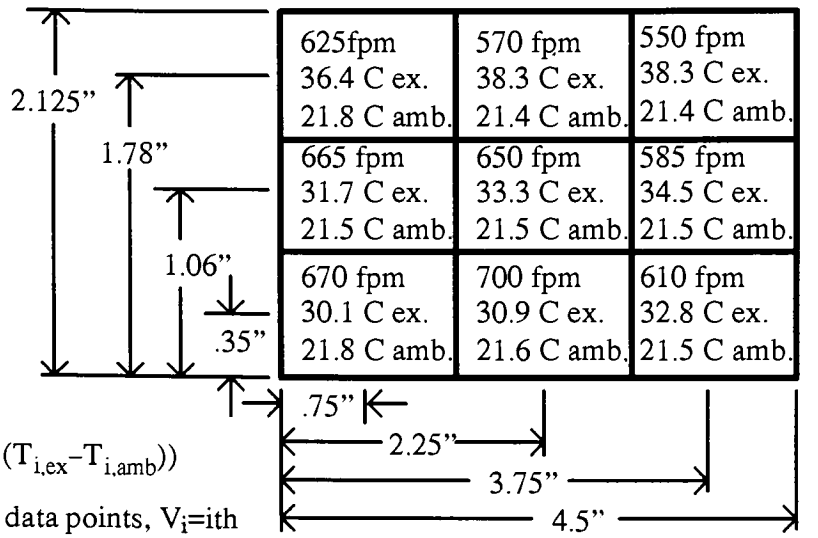

Hot side temperature rise = 12.28 C

Calculated by:

$$\Delta T = \frac{1}{\Sigma V_i} * \Sigma \ (V_i * (T_{i,ex} - T_{i,amb}))$$

where n = number of data points, V_i=ith velocity data point, $T_{i,ex}$ = ith exhaust temperature, and $T_{i,amb}$=ambient temperature at time $T_{i,ex}$ was collected

Note: ex.=exhaust
amb.=ambient

Cold side velocities and temperatures for outer ring:

Notes:
1. ex.=exhaust
2. amb.=ambient

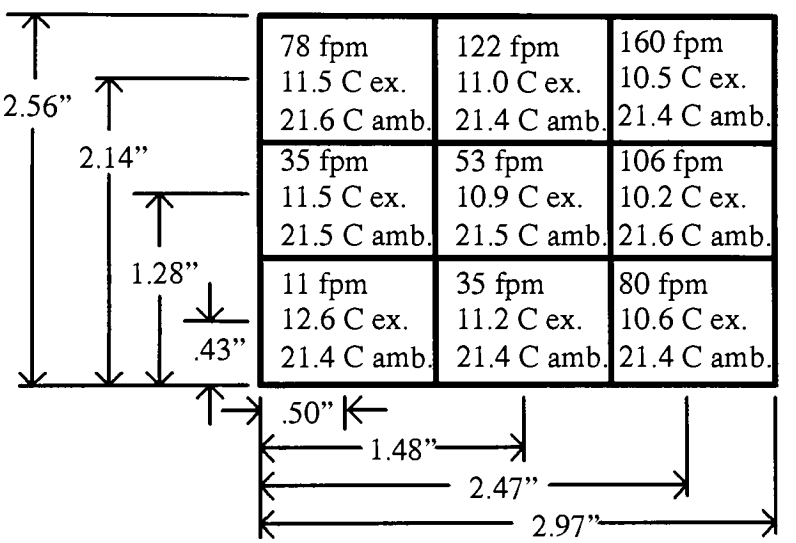

Outer cold side temperature drop = 10.65 C

Calculated by:

$$\Delta T = \frac{1}{\Sigma V_i} * \Sigma \ (V_i * (T_{i,ex} - T_{i,amb}))$$

where n = number of data points, V_i=ith velocity data point, $T_{i,ex}$ = ith exhaust temperature, and $T_{i,amb}$=ambient temperature at time $T_{i,ex}$ was collected

Volumetric flow rate based on velocity profiles above is 3.98 CFM

Calculated by: $\dot{V} = A * \frac{1}{n}(\Sigma V_i)$

where A= duct cross sectional area, n=number of data points, V_i is the velocity at a given point

System Test 4 Data (continued)

Cold side velocities and temperatures for inner ring:

Notes:
1. ex.=exhaust
2. amb.=ambient

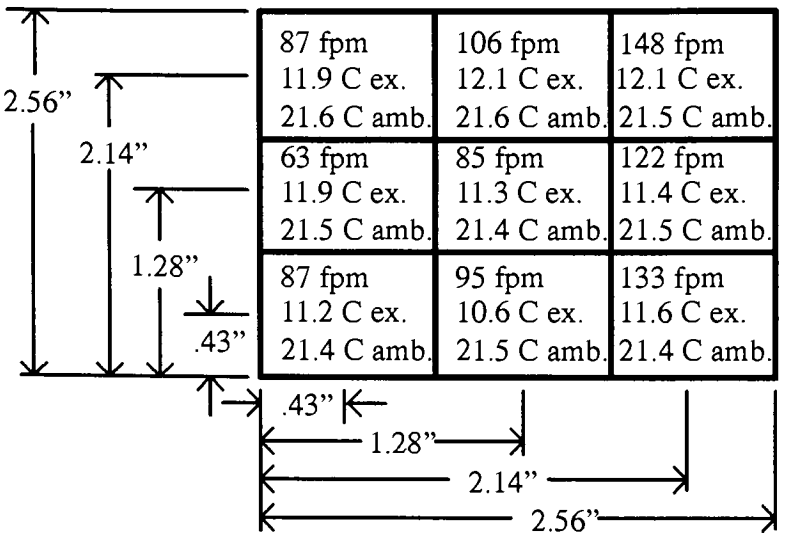

Inner cold side temperature drop = 9.90 C

Calculated by:

$$\Delta T = \frac{1}{\Sigma V_i} * \Sigma \left(V_i * (T_{i,ex} - T_{i,amb})\right)$$

where n = number of data points, V_i=ith velocity data point, $T_{i,ex}$ = ith exhaust temperature, and $T_{i,amb}$=ambient temperature at time $T_{i,ex}$ was collected

Volumetric flow rate based on velocity profiles above is 4.67 CFM

Calculated by: $\dot{V} = A * \frac{1}{n}(\Sigma V_i)$

where A= duct cross sectional area, n=number of data points, V_i is the velocity at a given point

Calculated parameters:

19. Average ambient temperature during test (average of 9 ambient temperature data points taken for cold side, outer ring) = 21.47 C

20. Heat rejected by hot side heat sink ($\varrho \dot{V} c_p \Delta T$) = 237.13 W

21. Heat rejected by outer cold side heat sink ($\varrho \dot{V} c_p \Delta T$) = 23.95 W

22. Heat rejected by inner cold side heat sink ($\varrho \dot{V} c_p \Delta T$) = 26.10 W

23. Electrical resistive heating ($P = I^2R = I V_{total}$) = 192.24 W

24. Energy balance:
    Heat pumped at cold side: 50.05 W (item 3 + item 4)
    I^2R heating: 192.24 W (item 5)
    242.29 W vs. 237.13 W measured

    Error: 2.18 %

System Test 5 Data

Test conditions:

Inner cold side fan voltage: 12.50 volts
Outer cold side fan voltage: 12.50 volts
Hot side fan voltage: 17.50 volts
System current draw: 1.60 amps

Temperatures and voltage drops associated with each thermoelectric module:
(Note: Refer to Figure 5.5 for locations of thermoelectrics).

Thermoelectric Number	Number of Semiconductor Junctions (N)	Voltage Drop (volts)	Hot side heat sink base temperature (C)	Cold side heat sink base temperature (C)
1	127	3.31	27.7	13.0
2	127	3.68	27.4	10.4
3	71	2.48	25.0	9.4
4	71	2.36	25.9	10.4
5	127	3.29	26.9	11.1
6	127	3.79	28.0	13.8
	Total Num. Junctions=650	Total Voltage Drop = 18.91 v	Weighted Avg. Temp. = 27.05	Weighted Avg. Temp. = 11.60

Note: Weighted Avg. Temp.= $\langle \sum N_i * T_i \rangle \div$(Total Number of Junctions) where N_i and T_i are the number of junctions and temperature of the thermoelectric module in question.

Hot side velocity profiles measured at outlet of flow straightener:

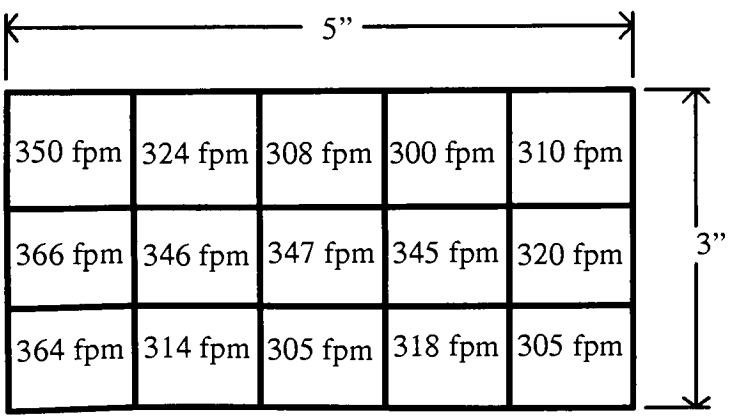

Notes: -Above cells are 1" x 1" square

Volumetric flow rate based on profiles on left is 34.18 CFM

Calculated by:

$$\dot{V} = A * \frac{1}{n}(\Sigma V_i)$$

where A = duct cross sectional area, n= number of cells, Vi=velocity measurement of a given cell

Pressure drop across hot side = .25" H_2O

System Test 5 Data (continued)

Hot side velocities and temperatures **measured right at heat exchanger exhaust**:

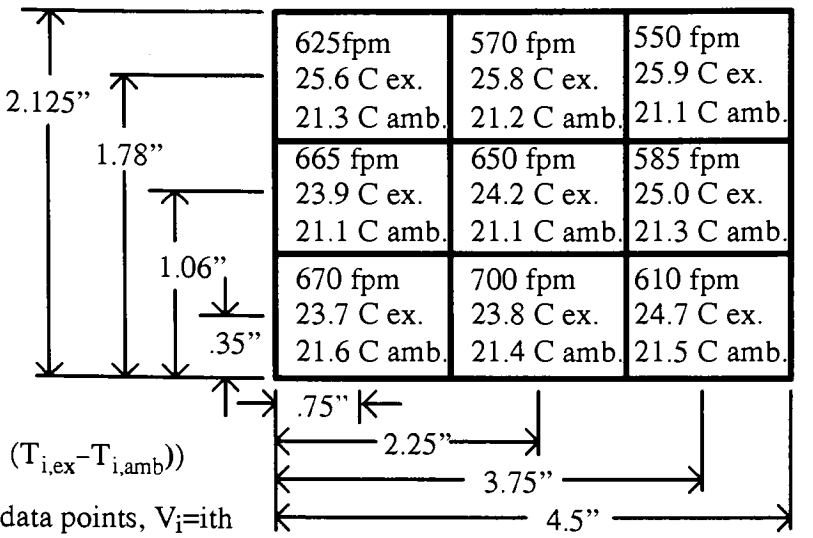

Hot side temperature rise = 3.38 C

Calculated by:

$$\Delta T = \frac{1}{\Sigma V_i} * \Sigma \ (V_i * (T_{i,ex} - T_{i,amb}))$$

where n = number of data points, V_i=ith velocity data point, $T_{i,ex}$ = ith exhaust temperature, and $T_{i,amb}$=ambient temperature at time $T_{i,ex}$ was collected

Note: ex.=exhaust
amb.=ambient

Cold side velocities and temperatures for outer ring:

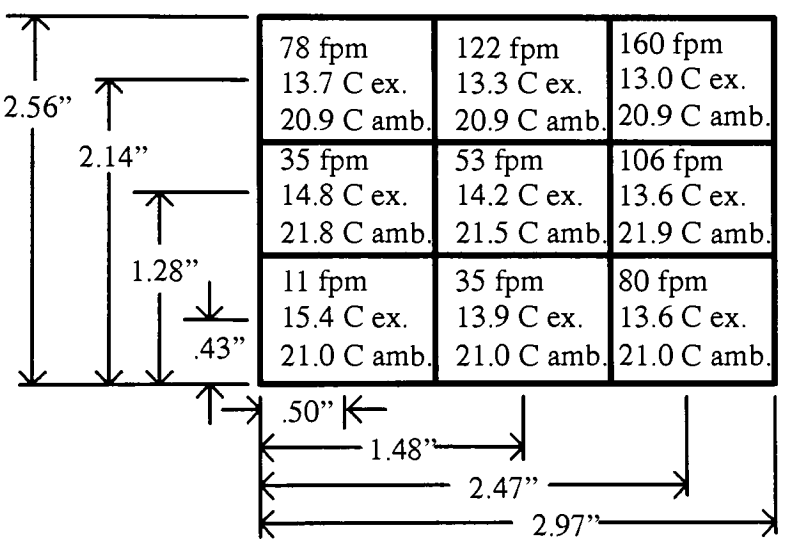

Notes:
1. ex.=exhaust
2. amb.=ambient

Outer cold side temperature drop = 7.60 C

Calculated by:

$$\Delta T = \frac{1}{\Sigma V_i} * \Sigma \ (V_i * (T_{i,ex} - T_{i,amb}))$$

where n = number of data points, V_i=ith velocity data point, $T_{i,ex}$ = ith exhaust temperature, and $T_{i,amb}$=ambient temperature at time $T_{i,ex}$ was collected

Volumetric flow rate based on velocity profiles above is 3.98 CFM

Calculated by: $\dot{V} = A * \frac{1}{n}(\Sigma V_i)$

where A= duct cross sectional area, n=number of data points, V_i is the velocity at a given point

System Test 5 Data (continued)

Cold side velocities and temperatures for inner ring:

Notes:
1. ex.=exhaust
2. amb.=ambient

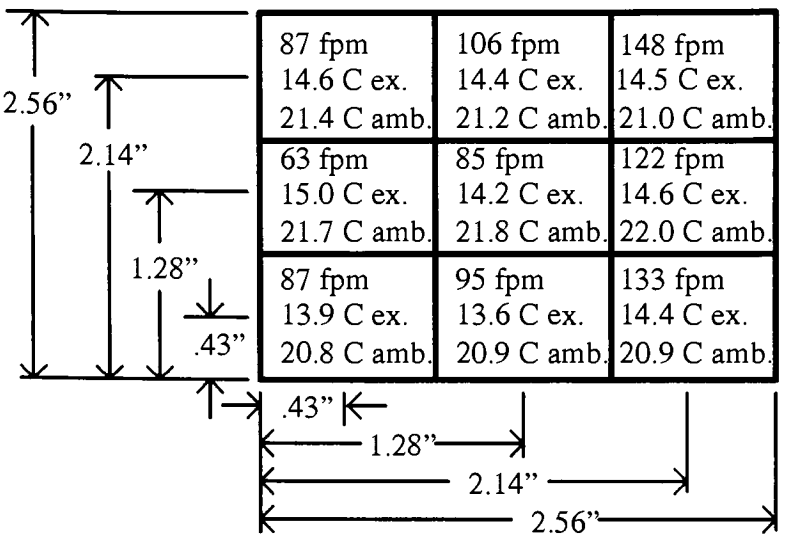

Inner cold side temperature drop = 6.92 C

Calculated by:

$$\Delta T = \frac{1}{\Sigma V_i} * \Sigma \left(V_i * (T_{i,ex} - T_{i,amb})\right)$$

where n = number of data points, V_i=ith velocity data point, $T_{i,ex}$ = ith exhaust temperature, and $T_{i,amb}$=ambient temperature at time $T_{i,ex}$ was collected

Volumetric flow rate based on velocity profiles above is 4.67 CFM

Calculated by: $\dot{V} = A * \frac{1}{n}(\Sigma V_i)$

where A= duct cross sectional area, n=number of data points, V_i is the velocity at a given point

Calculated parameters:

25. Average ambient temperature during test (average of 9 ambient temperature data points taken for cold side, outer ring) = 21.21 C

26. Heat rejected by hot side heat sink ($\varrho \dot{V} c_p \Delta T$) = 65.33 W

27. Heat rejected by outer cold side heat sink ($\varrho \dot{V} c_p \Delta T$) = 17.10 W

28. Heat rejected by inner cold side heat sink ($\varrho \dot{V} c_p \Delta T$) = 18.24 W

29. Electrical resistive heating ($P = I^2R = I V_{total}$) = 30.26 W

30. Energy balance:
    Heat pumped at cold side: 35.34 W (item 3 + item 4)
    I^2R heating: 30.26 W (item 5)
    65.60 W vs. 65.33 W measured

    Error: 0.41 %

System Test 6 Data

Test conditions:

Inner cold side fan voltage: 28.00 volts
Outer cold side fan voltage: 28.00 volts
Hot side fan voltage: 7.00 volts
System current draw: 3.75 amps

Temperatures and voltage drops associated with each thermoelectric module:
(Note: Refer to Figure 5.5 for locations of thermoelectrics).

Thermoelectric Number	Number of Semiconductor Junctions (N)	Voltage Drop (volts)	Hot side heat sink base temperature (C)	Cold side heat sink base temperature (C)
1	127	9.19	67.2	21.6
2	127	9.57	65.9	20.9
3	71	6.54	57.0	18.9
4	71	6.35	58.3	19.7
5	127	9.01	63.1	20.8
6	127	10.01	67.4	23.2
	Total Num. Junctions=650	Total Voltage Drop = 50.67 v	Weighted Avg. Temp. = 64.10	Weighted Avg. Temp. = 21.12

Note: Weighted Avg. Temp.= $\langle \sum N_i * T_i \rangle \div$(Total Number of Junctions) where N_i and T_i are the number of junctions and temperature of the thermoelectric module in question.

Hot side velocity profiles measured at outlet of flow straightener:

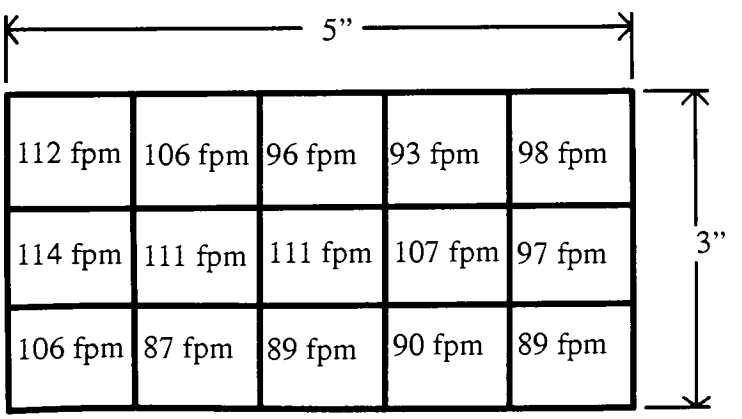

Notes: -Above cells are 1" x 1" square

Volumetric flow rate based on profiles on left is 10.46 CFM

Calculated by:

$$\dot{V} = A * \frac{1}{n}(\Sigma V_i)$$

where A = duct cross sectional area, n= number of cells, Vi=velocity measurement of a given cell

Pressure drop across hot side = .03" H_2O

System Test 6 Data (continued)

Hot side velocities and temperatures **measured right at heat exchanger exhaust**:

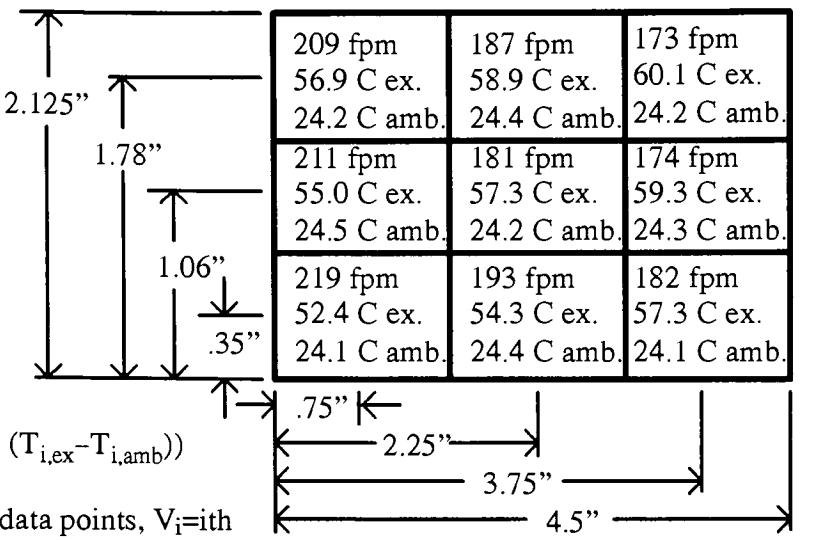

Hot side temperature rise = 32.40 C

Calculated by:

$$\Delta T = \frac{1}{\Sigma V_i} * \Sigma \ (V_i * (T_{i,ex} - T_{i,amb}))$$

where n = number of data points, V_i=ith velocity data point, $T_{i,ex}$ = ith exhaust temperature, and $T_{i,amb}$=ambient temperature at time $T_{i,ex}$ was collected

Note: ex.=exhaust
amb.=ambient

Cold side velocities and temperatures for outer ring:

Notes:
1. ex.=exhaust
2. amb.=ambient

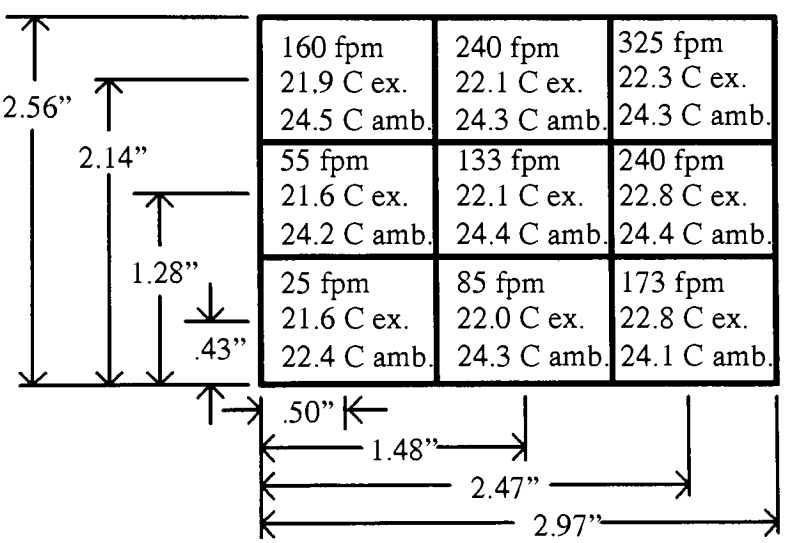

Outer cold side temperature drop = 2.00 C

Calculated by:

$$\Delta T = \frac{1}{\Sigma V_i} * \Sigma \ (V_i * (T_{i,ex} - T_{i,amb}))$$

where n = number of data points, V_i=ith velocity data point, $T_{i,ex}$ = ith exhaust temperature, and $T_{i,amb}$=ambient temperature at time $T_{i,ex}$ was collected

Volumetric flow rate based on velocity profiles above is 8.41 CFM

Calculated by: $\dot{V} = A * \frac{1}{n}(\Sigma V_i)$

where A= duct cross sectional area, n=number of data points, V_i is the velocity at a given point

System Test 6 Data (continued)

Cold side velocities and temperatures for inner ring:

Notes:
1. ex.=exhaust
2. amb.=ambient

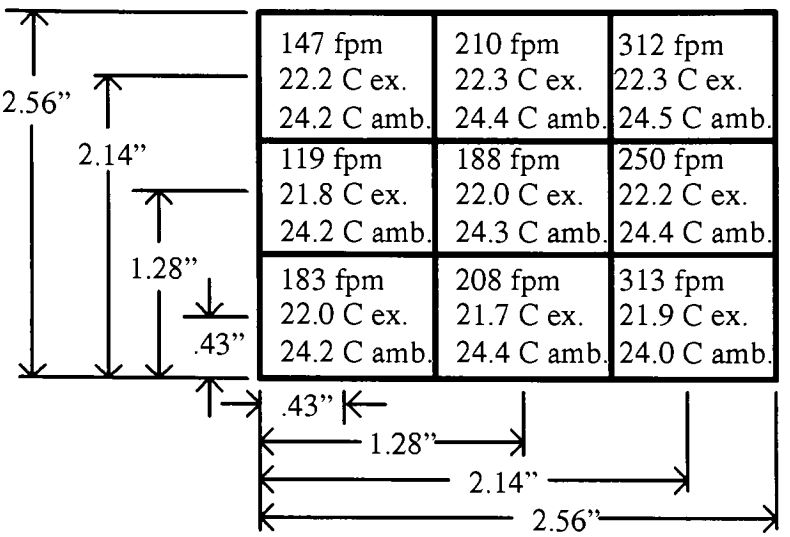

Inner cold side temperature drop = 2.23 C

Calculated by:

$$\Delta T = \frac{1}{\Sigma V_i} * \Sigma \left(V_i * (T_{i,ex} - T_{i,amb})\right)$$

where n = number of data points, V_i=ith velocity data point, $T_{i,ex}$ = ith exhaust temperature, and $T_{i,amb}$=ambient temperature at time $T_{i,ex}$ was collected

Volumetric flow rate based on velocity profiles above is 9.73 CFM

Calculated by: $\dot{V} = A * \frac{1}{n}(\Sigma V_i)$

where A= duct cross sectional area, n=number of data points, V_i is the velocity at a given point

Calculated parameters:

31. Average ambient temperature during test (average of 9 ambient temperature data points taken for cold side, outer ring) = 24.10 C

32. Heat rejected by hot side heat sink ($\varrho \dot{V} c_p \Delta T$) = 191.45 W

33. Heat rejected by outer cold side heat sink ($\varrho \dot{V} c_p \Delta T$) = 9.49 W

34. Heat rejected by inner cold side heat sink ($\varrho \dot{V} c_p \Delta T$) = 12.28 W

35. Electrical resistive heating ($P = I^2R = I V_{total}$) = 190.01 W

36. Energy balance:
    Heat pumped at cold side: 21.77 W (item 3 + item 4)
    I^2R heating: 190.01 W (item 5)
    211.78 W vs. 191.45 W measured

    Error: 10.62 %

System Test 7 Data

Test conditions:

Inner cold side fan voltage: 28.00 volts
Outer cold side fan voltage: 28.00 volts
Hot side fan voltage: 7.00 volts
System current draw: 1.600 amps

Temperatures and voltage drops associated with each thermoelectric module:
(Note: Refer to Figure 5.5 for locations of thermoelectrics).

Thermoelectric Number	Number of Semiconductor Junctions (N)	Voltage Drop (volts)	Hot side heat sink base temperature (C)	Cold side heat sink base temperature (C)
1	127	3.50	36.2	19.6
2	127	3.83	36.0	18.4
3	71	2.56	32.9	17.8
4	71	2.47	33.6	18.9
5	127	3.48	35.0	19.0
6	127	4.03	36.5	20.6
	Total Num. Junctions=650	Total Voltage Drop = 19.87 v	Weighted Avg. Temp. = 35.34	Weighted Avg. Temp. = 19.17

Note: Weighted Avg. Temp.= $\langle \sum N_i * T_i \rangle \div$(Total Number of Junctions) where N_i and T_i are the number of junctions and temperature of the thermoelectric module in question.

Hot side velocity profiles measured at outlet of flow straightener:

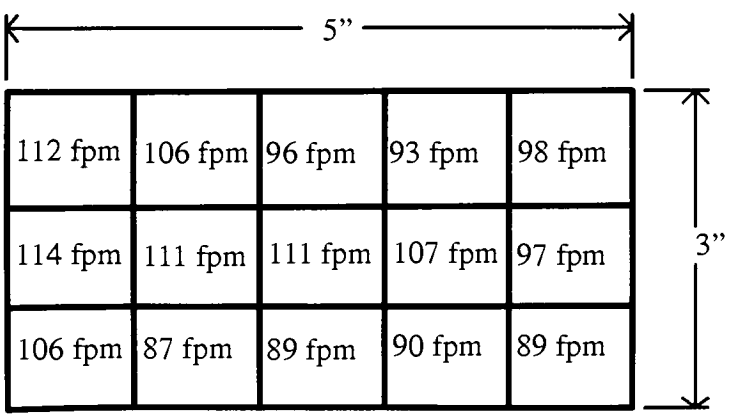

Notes: -Above cells are 1" x 1" square

Volumetric flow rate based on profiles on left is 10.46 CFM

Calculated by:

$$\dot{V} = A * \frac{1}{n}(\Sigma V_i)$$

where A = duct cross sectional area, n= number of cells, Vi=velocity measurement of a given cell

Pressure drop across hot side = .03" H_2O

System Test 7 Data (continued)

Hot side velocities and temperatures **measured right at heat exchanger exhaust**:

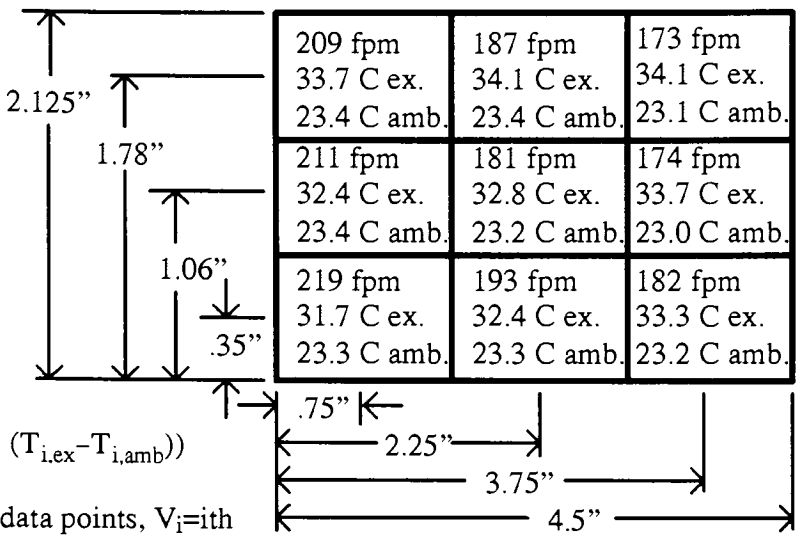

Hot side temperature rise = 9.83 C

Calculated by:

$$\Delta T = \frac{1}{\Sigma V_i} * \Sigma \ (V_i * (T_{i,ex} - T_{i,amb}))$$

where n = number of data points, V_i=ith velocity data point, $T_{i,ex}$ = ith exhaust temperature, and $T_{i,amb}$=ambient temperature at time $T_{i,ex}$ was collected

Note: ex.=exhaust
amb.=ambient

Cold side velocities and temperatures for outer ring:

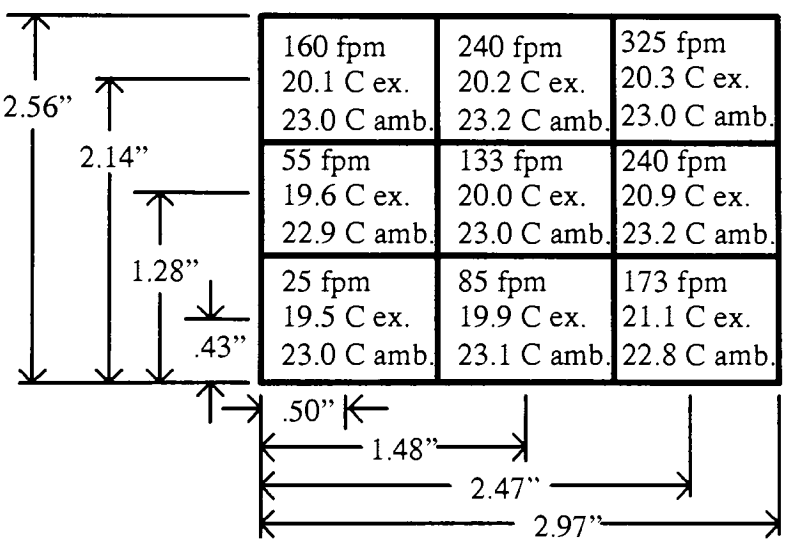

Notes:
1. ex.=exhaust
2. amb.=ambient

Outer cold side temperature drop = 2.68 C

Calculated by:

$$\Delta T = \frac{1}{\Sigma V_i} * \Sigma \ (V_i * (T_{i,ex} - T_{i,amb}))$$

where n = number of data points, V_i=ith velocity data point, $T_{i,ex}$ = ith exhaust temperature, and $T_{i,amb}$=ambient temperature at time $T_{i,ex}$ was collected

Volumetric flow rate based on velocity profiles above is 8.41 CFM

Calculated by: $\dot{V} = A * \frac{1}{n}(\Sigma V_i)$

where A= duct cross sectional area, n=number of data points, V_i is the velocity at a given point

System Test 7 Data (continued)

Cold side velocities and temperatures for inner ring:

Notes:
1. ex.=exhaust
2. amb.=ambient

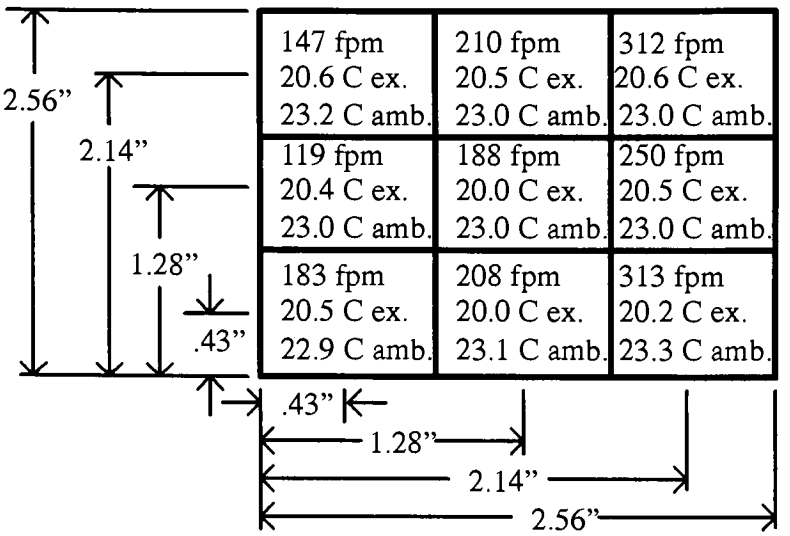

Inner cold side temperature drop = 2.70 C

Calculated by:

$$\Delta T = \frac{1}{\Sigma V_i} * \Sigma \left(V_i * (T_{i,ex} - T_{i,amb})\right)$$

where n = number of data points, V_i=ith velocity data point, $T_{i,ex}$ = ith exhaust temperature, and $T_{i,amb}$=ambient temperature at time $T_{i,ex}$ was collected

Volumetric flow rate based on velocity profiles above is 9.73 CFM

Calculated by: $\dot{V} = A * \frac{1}{n}(\Sigma V_i)$

where A= duct cross sectional area, n=number of data points, V_i is the velocity at a given point

Calculated parameters:

37. Average ambient temperature during test (average of 9 ambient temperature data points taken for cold side, outer ring) = 23.02 C

38. Heat rejected by hot side heat sink ($\varrho \dot{V} c_p \Delta T$) = 58.06 W

39. Heat rejected by outer cold side heat sink ($\varrho \dot{V} c_p \Delta T$) = 12.73 W

40. Heat rejected by inner cold side heat sink ($\varrho \dot{V} c_p \Delta T$) = 14.83 W

41. Electrical resistive heating ($P = I^2R = I V_{total}$) = 31.79 W

42. Energy balance:
    Heat pumped at cold side: 27.56 W (item 3 + item 4)
    I^2R heating: 31.79 W (item 5)
    59.35 W vs. 58.06 W measured

    Error: 2.22 %

System Test 8 Data

Test conditions:

Inner cold side fan voltage: 12.00 volts
Outer cold side fan voltage: 12.00 volts
Hot side fan voltage: 7.00 volts
System current draw: 3.75 amps

Temperatures and voltage drops associated with each thermoelectric module:
(Note: Refer to Figure 5.5 for locations of thermoelectrics).

Thermoelectric Number	Number of Semiconductor Junctions (N)	Voltage Drop (volts)	Hot side heat sink base temperature (C)	Cold side heat sink base temperature (C)
1	127	9.02	63.5	17.4
2	127	9.47	62.0	16.1
3	71	6.42	52.9	12.6
4	71	6.28	54.1	12.6
5	127	8.92	59.4	15.3
6	127	9.81	63.8	18.7
	Total Num. Junctions=650	Total Voltage Drop = 49.92 v	Weighted Avg. Temp. = 60.28	Weighted Avg. Temp. = 15.94

Note: Weighted Avg. Temp.= $\langle \sum N_i * T_i \rangle \div$(Total Number of Junctions) where N_i and T_i are the number of junctions and temperature of the thermoelectric module in question.

Hot side velocity profiles measured at outlet of flow straightener:

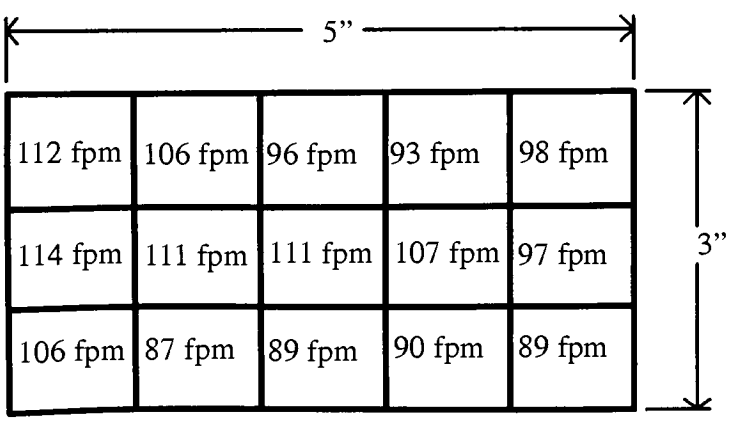

Notes: -Above cells are 1" x 1" square

Volumetric flow rate based on profiles on left is 10.46 CFM

Calculated by:

$$\dot{V} = A * \frac{1}{n}(\Sigma V_i)$$

where A = duct cross sectional area, n= number of cells, Vi=velocity measurement of a given cell

Pressure drop across hot side = .03" H_2O

System Test 8 Data (continued)

Hot side velocities and temperatures **measured right at heat exchanger exhaust**:

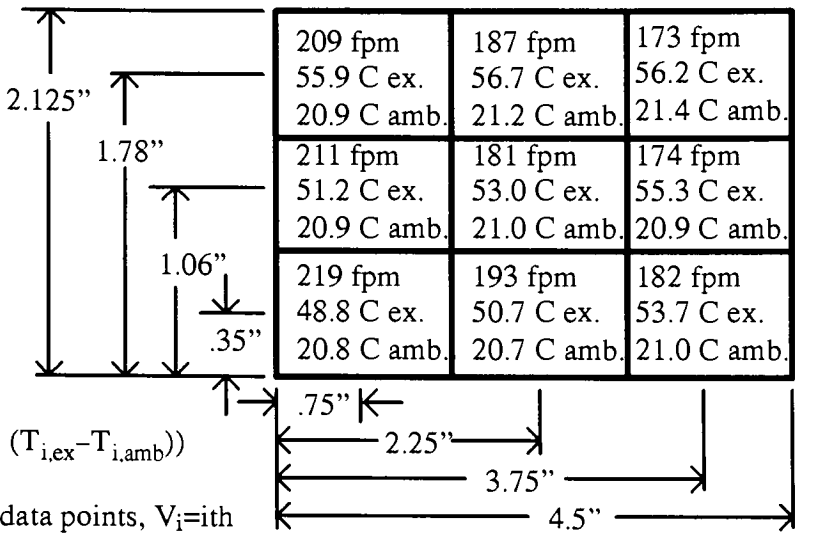

Hot side temperature rise = 32.40 C

Calculated by:

$$\Delta T = \frac{1}{\Sigma V_i} * \Sigma \ (V_i * (T_{i,ex} - T_{i,amb}))$$

where n = number of data points, V_i=ith velocity data point, $T_{i,ex}$ = ith exhaust temperature, and $T_{i,amb}$=ambient temperature at time $T_{i,ex}$ was collected

Note: ex.=exhaust
amb.=ambient

Cold side velocities and temperatures for outer ring:

Notes:
1. ex.=exhaust
2. amb.=ambient

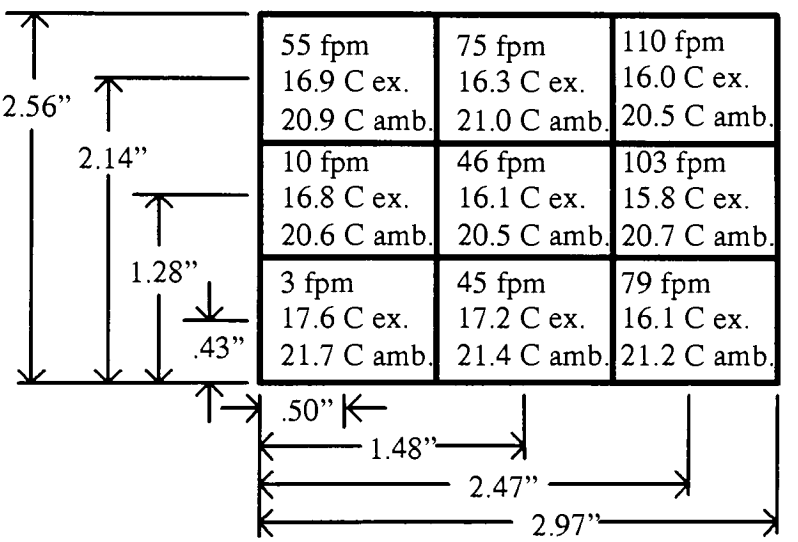

Outer cold side temperature drop = 4.59 C

Calculated by:

$$\Delta T = \frac{1}{\Sigma V_i} * \Sigma \ (V_i * (T_{i,ex} - T_{i,amb}))$$

where n = number of data points, V_i=ith velocity data point, $T_{i,ex}$ = ith exhaust temperature, and $T_{i,amb}$=ambient temperature at time $T_{i,ex}$ was collected

Volumetric flow rate based on velocity profiles above is 3.08 CFM

Calculated by: $\dot{V} = A * \frac{1}{n}(\Sigma V_i)$

where A= duct cross sectional area, n=number of data points, V_i is the velocity at a given point

System Test 8 Data (continued)

Cold side velocities and temperatures for inner ring:

Notes:
1. ex.=exhaust
2. amb.=ambient

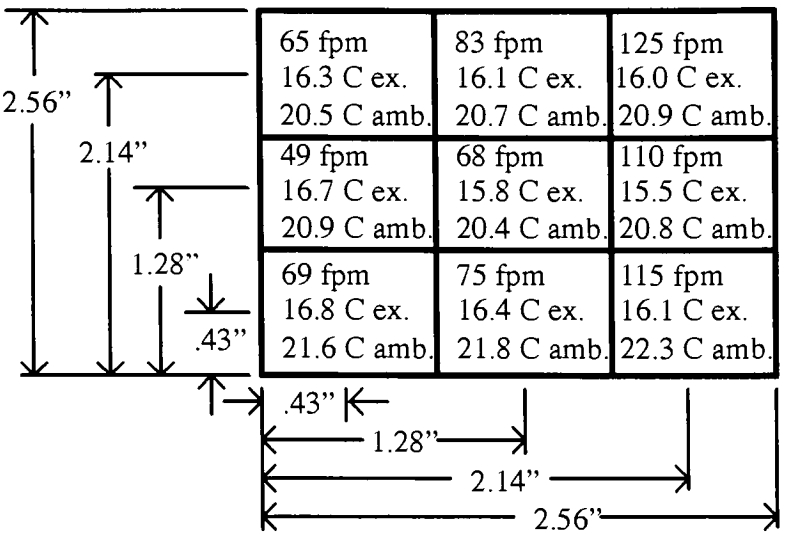

Inner cold side temperature drop = 5.03 C

Calculated by:

$$\Delta T = \frac{1}{\Sigma V_i} * \Sigma \ (V_i * (T_{i,ex} - T_{i,amb}))$$

where n = number of data points, V_i=ith velocity data point, $T_{i,ex}$ = ith exhaust temperature, and $T_{i,amb}$=ambient temperature at time $T_{i,ex}$ was collected

Volumetric flow rate based on velocity profiles above is 3.83 CFM

Calculated by: $\dot{V} = A * \frac{1}{n}(\Sigma V_i)$

where A= duct cross sectional area, n=number of data points, V_i is the velocity at a given point

Calculated parameters:

43. Average ambient temperature during test (average of 9 ambient temperature data points taken for cold side, outer ring) = 20.94 C

44. Heat rejected by hot side heat sink ($\varrho \dot{V} c_p \Delta T$) = 191.43 W

45. Heat rejected by outer cold side heat sink ($\varrho \dot{V} c_p \Delta T$) = 8.00 W

46. Heat rejected by inner cold side heat sink ($\varrho \dot{V} c_p \Delta T$) = 10.87 W

47. Electrical resistive heating ($P = I^2R = I V_{total}$) = 187.20 W

48. Energy balance:
    Heat pumped at cold side: 18.87 W (item 3 + item 4)
    I^2R heating: 187.20 W (item 5)
    206.07 W vs. 191.43 W measured

    Error: 7.65 %

System Test 9 Data

Test conditions:

Inner cold side fan voltage: 12.00 volts
Outer cold side fan voltage: 12.00 volts
Hot side fan voltage: 7.00 volts
System current draw: 1.60 amps

Temperatures and voltage drops associated with each thermoelectric module:
(Note: Refer to Figure 5.5 for locations of thermoelectrics).

Thermoelectric Number	Number of Semiconductor Junctions (N)	Voltage Drop (volts)	Hot side heat sink base temperature (C)	Cold side heat sink base temperature (C)
1	127	3.49	34.4	16.3
2	127	3.84	34.0	14.4
3	71	2.59	30.8	12.7
4	71	2.53	31.8	13.5
5	127	3.54	33.2	14.7
6	127	4.09	34.7	17.1
	Total Num. Junctions=650	Total Voltage Drop = 20.08 v	Weighted Avg. Temp. = 33.47	Weighted Avg. Temp. = 15.07

Note: Weighted Avg. Temp.= $\langle \sum N_i * T_i \rangle \div$(Total Number of Junctions) where N_i and T_i are the number of junctions and temperature of the thermoelectric module in question.

Hot side velocity profiles measured at outlet of flow straightener:

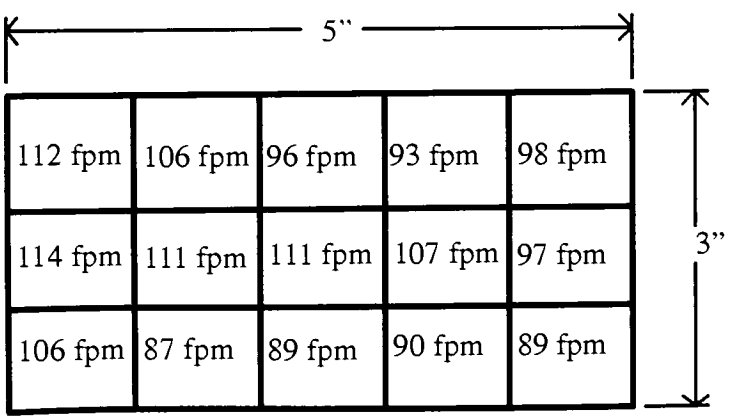

Notes: -Above cells are 1" x 1" square

Volumetric flow rate based on profiles on left is 10.46 CFM

Calculated by:

$$\dot{V} = A * \frac{1}{n}(\Sigma V_i)$$

where A = duct cross sectional area, n= number of cells, Vi=velocity measurement of a given cell

Pressure drop across hot side = .03" H_2O

System Test 9 Data (continued)

Hot side velocities and temperatures **measured right at heat exchanger exhaust**:

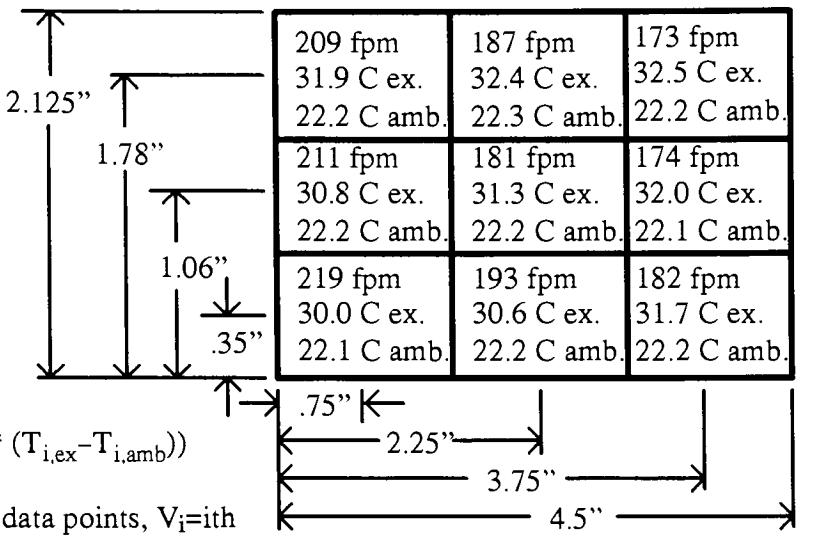

Hot side temperature rise = 9.23 C

Calculated by:

$$\Delta T = \frac{1}{\Sigma V_i} * \Sigma \ (V_i * (T_{i,ex} - T_{i,amb}))$$

where n = number of data points, V_i=ith velocity data point, $T_{i,ex}$ = ith exhaust temperature, and $T_{i,amb}$=ambient temperature at time $T_{i,ex}$ was collected

Note: ex.=exhaust
amb.=ambient

Cold side velocities and temperatures for outer ring:

Notes:
1. ex.=exhaust
2. amb.=ambient

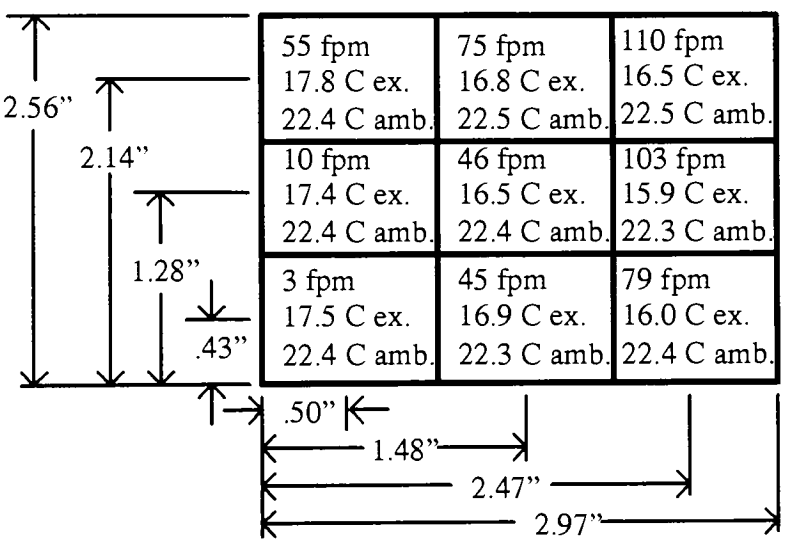

Outer cold side temperature drop = 5.86 C

Calculated by:

$$\Delta T = \frac{1}{\Sigma V_i} * \Sigma \ (V_i * (T_{i,ex} - T_{i,amb}))$$

where n = number of data points, V_i=ith velocity data point, $T_{i,ex}$ = ith exhaust temperature, and $T_{i,amb}$=ambient temperature at time $T_{i,ex}$ was collected

Volumetric flow rate based on velocity profiles above is 3.08 CFM

Calculated by: $\dot{V} = A * \frac{1}{n}(\Sigma V_i)$

where A= duct cross sectional area, n=number of data points, V_i is the velocity at a given point

System Test 9 Data (continued)

Cold side velocities and temperatures for inner ring:

Notes:
1. ex.=exhaust
2. amb.=ambient

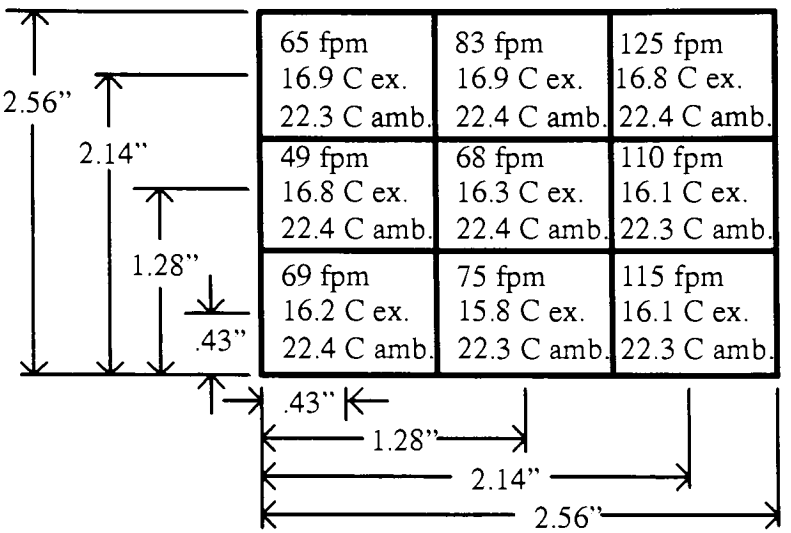

Inner cold side temperature drop = 5.94 C

Calculated by:

$$\Delta T = \frac{1}{\Sigma V_i} * \Sigma \, (V_i * (T_{i,ex} - T_{i,amb}))$$

where n = number of data points, V_i=ith velocity data point, $T_{i,ex}$ = ith exhaust temperature, and $T_{i,amb}$=ambient temperature at time $T_{i,ex}$ was collected

Volumetric flow rate based on velocity profiles above is 3.83 CFM

Calculated by: $\dot{V} = A * \frac{1}{n}(\Sigma V_i)$

where A= duct cross sectional area, n=number of data points, V_i is the velocity at a given point

Calculated parameters:

49. Average ambient temperature during test (average of 9 ambient temperature data points taken for cold side, outer ring) = 22.40 C

50. Heat rejected by hot side heat sink ($\varrho \dot{V} c_p \Delta T$) = 54.55 W

51. Heat rejected by outer cold side heat sink ($\varrho \dot{V} c_p \Delta T$) = 10.21 W

52. Heat rejected by inner cold side heat sink ($\varrho \dot{V} c_p \Delta T$) = 12.84 W

53. Electrical resistive heating ($P = I^2R = I V_{total}$) = 32.13 W

54. Energy balance:
    Heat pumped at cold side: 23.05 W (item 3 + item 4)
    I^2R heating: 32.13 W (item 5)
    55.18 W vs. 54.55 W measured

    Error: 1.15 %

APPENDIX E

ERROR ANALYSIS

Analysis of Error

The following is a listing of equations used to compute the various derived quantities that were used as heat pump performance indices in this paper. An expression for the uncertainty in each of the derived quantities is also presented.

Experimental

1. Total voltage drop across the thermoelectric modules of the heat pump:

$$E = \Sigma E_i$$

$$dE = \Sigma dE_i$$

2. Volumetric air flow through a duct:

$$\dot{V} = w_d * h_d * \frac{1}{n}(\Sigma V_i)$$

$$d\dot{V} = dw_d * h_d * \frac{1}{n}(\Sigma V_i) + w_d * dh_d * \frac{1}{n}(\Sigma V_i) + w_d * h_d * \frac{1}{n}(d\Sigma V_i)$$

3. Electrical power:

$$P = I * E$$

$$dP = dI * E + I * dE$$

4. The temperature rise or drop of an air stream traveling over a heat exchange surface (equation 5.2):

$$\Delta T_{avg} = \frac{1}{(\Sigma V_i)} * \Sigma[\ V_i * (T_{i,ex} - T_{i,amb})]$$

$$d\Delta T_{avg} = -\frac{\Sigma dV_i}{(\Sigma V_i)^2} * \Sigma[\ V_i * (T_{i,ex} - T_{i,amb})] + \frac{1}{(\Sigma V_i)} * \Sigma[\ dV_i * (T_{i,ex} - T_{i,amb})] + \frac{1}{(\Sigma V_i)} * \Sigma[\ V_i * (dT_{i,ex} - dT_{i,amb})]$$

5. Power dissipated by an air stream traveling over a heat exchange surface (assumes $d\varrho$ and dc_p are zero because $d\Delta T$ is small):

$$P = \varrho * c_p * \dot{V} * \Delta T_{avg}$$

$$dP = \varrho * c_p * d\dot{V} * \Delta T_{avg} + \varrho * c_p * \dot{V} * d\Delta T_{avg}$$

System Test 1 Error Analysis
Experimental

Parameter	Nominal Value	d(Parameter)
E	43.28 V	0.06 V
I	3.55 A	0.0271 A
P	153.64 W	1.59 W
$w_{d,\ hot}$	0.4170 ft	0.0027 ft
$h_{d,\ hot}$	0.2500 ft	0.0027 ft
$\dot{V}_{hot}$	19.72 CFM	0.63 CFM
$w_{d,\ cold,outer}$	0.2480 ft	0.0027 ft
$h_{d,cold,outer}$	0.2130 ft	0.0027 ft
$\dot{V}_{cold,\ outer}$	7.06 CFM	0.27 CFM
$w_{d,\ cold,inner}$	0.213 ft	0.0027 ft
$h_{d,cold,inner}$	0.213 ft	0.0027 ft
$\dot{V}_{cold,\ inner}$	8.13 CFM	0.33 CFM
$\varrho_{air,\ 70°F}$	1.1889 kg/m^3	0.0 kg/m^3
$c_{p\ air,\ 70°F}$	1006.88 J/kg-K	0.0 J/kg-K
Temp. rise, hot side air	17.39 C	0.20 C
Heat rejected, hot side	193.65 W	8.44 W
Temp. drop, cold side air, outer	6.21 C	0.20 C
Heat pumped, cold side, outer	24.77 W	1.75 W
Temp. drop, cold side air, inner	5.83 C	0.20 C
Heat pumped, cold side, inner	26.77 W	1.99 W
Wtd. avg. temp., hot side	46.26 C	0.10 C
Wtd. avg. temp., cold side	12.56 C	0.10 C

Examination of energy balance:

Heat pumped at hot side, measured: 193.65 W +/- 8.44 W
Heat pumped at cold side plus I*V: 205.19 W+/- 5.34 W

System Test 2 Error Analysis
Experimental

Parameter	Nominal Value	d(Parameter)
E	48.74 V	0.06 V
I	4.005 A	0.028 A
P	195.20 W	1.85 W
$w_{d,\ hot}$	0.4170 ft	0.0027 ft
$h_{d,\ hot}$	0.2500 ft	0.0027 ft
$\dot{V}_{hot}$	34.18 CFM	1.10 CFM
$w_{d,\ cold,outer}$	0.2480 ft	0.0027 ft
$h_{d,cold,outer}$	0.2130 ft	0.0027 ft
$\dot{V}_{cold,\ outer}$	8.34 CFM	0.32 CFM
$w_{d,\ cold,inner}$	0.213 ft	0.0027 ft
$h_{d,cold,inner}$	0.213 ft	0.0027 ft
$\dot{V}_{cold,\ inner}$	10.62 CFM	0.43 CFM
$\varrho_{air,\ 70°F}$	1.1889 kg/m^3	0.0 kg/m^3
$c_{p\ air,\ 70°F}$	1006.88 J/kg-K	0.0 J/kg-K
Temp. rise, hot side air	13.10 C	0.20 C
Heat rejected, hot side	252.11 W	11.94 W
Temp. drop, cold side air, outer	6.78 C	0.20 C
Heat pumped, cold side, outer	31.95 W	2.17 W
Temp. drop, cold side air, inner	5.59 C	0.20 C
Heat pumped, cold side, inner	33.50 W	2.54 W
Wtd. avg. temp., hot side	48.32 C	0.10 C
Wtd. avg. temp., cold side	15.19 C	0.10 C
Examination of energy balance: Heat pumped at hot side, measured: 252.11 W +/- 11.94 W Heat pumped at cold side plus I*V: 260.66 W+/- 6.55 W		

System Test 3 Error Analysis
Experimental

Parameter	Nominal Value	d(Parameter)
E	19.14 V	0.06 V
I	1.611 A	0.005 A
P	30.84 W	0.20 W
$w_{d,\ hot}$	0.4170 ft	0.0027 ft
$h_{d,\ hot}$	0.2500 ft	0.0027 ft
$\dot{V}_{hot}$	34.18 CFM	1.10 CFM
$w_{d,\ cold,outer}$	0.2480 ft	0.0027 ft
$h_{d,cold,outer}$	0.2130 ft	0.0027 ft
$\dot{V}_{cold,\ outer}$	8.41 CFM	0.322 CFM
$w_{d,\ cold,inner}$	0.213 ft	0.0027 ft
$h_{d,cold,inner}$	0.213 ft	0.0027 ft
$\dot{V}_{cold,\ inner}$	9.73 CFM	0.39 CFM
$\varrho_{air,\ 70°F}$	1.1889 kg/m^3	0.0 kg/m^3
$c_{p\ air,\ 70°F}$	1006.88 J/kg-K	0.0 J/kg-K
Temp. rise, hot side air	3.98 C	0.20 C
Heat rejected, hot side	76.87 W	6.33 W
Temp. drop, cold side air, outer	4.48 C	0.20 C
Heat pumped, cold side, outer	21.30 W	1.77 W
Temp. drop, cold side air, inner	3.70 C	0.20 C
Heat pumped, cold side, inner	20.36 W	1.92 W
Wtd. avg. temp., hot side	32.10 C	0.10 C
Wtd. avg. temp., cold side	18.45 C	0.10 C
Examination of energy balance: Heat pumped at hot side, measured: 76.76 W +/- 6.33 W Heat pumped at cold side plus I*V: 72.48 W+/- 3.88 W		

System Test 4 Error Analysis
Experimental

Parameter	Nominal Value	d(Parameter)
E	48.00 V	0.06 V
I	4.005 A	0.028 A
P	192.24 W	1.83 W
$w_{d,\ hot}$	0.4170 ft	0.0027 ft
$h_{d,\ hot}$	0.2500 ft	0.0027 ft
$\dot{V}_{hot}$	34.18 CFM	1.10 CFM
$w_{d,\ cold,outer}$	0.2480 ft	0.0027 ft
$h_{d,cold,outer}$	0.2130 ft	0.0027 ft
$\dot{V}_{cold,\ outer}$	3.98 CFM	0.15 CFM
$w_{d,\ cold,inner}$	0.213 ft	0.0027 ft
$h_{d,cold,inner}$	0.213 ft	0.0027 ft
$\dot{V}_{cold,\ inner}$	4.67 CFM	0.19 CFM
$\varrho_{air,\ 70°F}$	1.1889 kg/m^3	0.0 kg/m^3
$c_{p\ air,\ 70°F}$	1006.88 J/kg-K	0.0 J/kg-K
Temp. rise, hot side air	10.65 C	0.20 C
Heat rejected, hot side	237.13 W	11.47 W
Temp. drop, cold side air, outer	10.65 C	0.20 C
Heat pumped, cold side, outer	23.95 W	1.37 W
Temp. drop, cold side air, inner	9.90 C	0.20 C
Heat pumped, cold side, inner	26.10 W	1.57 W
Wtd. avg. temp., hot side	42.93 C	0.10 C
Wtd. avg. temp., cold side	7.34 C	0.10 C

Examination of energy balance:

Heat pumped at hot side, measured: 237.13 W +/- 11.47 W
Heat pumped at cold side plus I*V: 242.29 W+/- 4.77 W

System Test 5 Error Analysis
Experimental

Parameter	Nominal Value	d(Parameter)
E	18.19 V	0.06 V
I	1.600 A	0.005 A
P	30.26 W	0.19 W
$w_{d,\ hot}$	0.4170 ft	0.0027 ft
$h_{d,\ hot}$	0.2500 ft	0.0027 ft
$\dot{V}_{hot}$	34.18 CFM	1.10 CFM
$w_{d,\ cold,outer}$	0.2480 ft	0.0027 ft
$h_{d,cold,outer}$	0.2130 ft	0.0027 ft
$\dot{V}_{cold,\ outer}$	3.98 CFM	0.15 CFM
$w_{d,\ cold,inner}$	0.2130 ft	0.00267 ft
$h_{d,cold,inner}$	0.2130 ft	0.00267 ft
$\dot{V}_{cold,\ inner}$	4.67 CFM	0.19 CFM
$\varrho_{air,\ 70°F}$	1.1889 kg/m^3	0.0 kg/m^3
$c_{p\ air,\ 70°F}$	1006.88 J/kg-K	0.0 J/kg-K
Temp. rise, hot side air	3.38 C	0.2 C
Heat rejected, hot side	65.33 W	5.96 W
Temp. drop, cold side air, outer	7.60 C	0.2 C
Heat pumped, cold side, outer	17.10 W	1.11 W
Temp. drop, cold side air, inner	6.92 C	0.2 C
Heat pumped, cold side, inner	18.24 W	1.26 W
Wtd. avg. temp., hot side	27.05 C	0.1 C
Wtd. avg. temp., cold side	11.60 C	0.1 C
Examination of energy balance: Heat pumped at hot side, measured: 65.33 W +/- 5.96 W Heat pumped at cold side plus I*V: 65.59 W+/- 2.56 W		

System Test 6 Error Analysis
Experimental

Parameter	Nominal Value	d(Parameter)
E	50.67 V	0.06 V
I	3.750 A	0.028 A
P	190.01 W	1.84 W
$w_{d,\ hot}$	0.4170 ft	0.0027 ft
$h_{d,\ hot}$	0.2500 ft	0.0027 ft
$\dot{V}_{hot}$	10.46 CFM	0.34 CFM
$w_{d,\ cold,outer}$	0.2480 ft	0.0027 ft
$h_{d,cold,outer}$	0.2130 ft	0.0027 ft
$\dot{V}_{cold,\ outer}$	8.41 CFM	0.32 CFM
$w_{d,\ cold,inner}$	0.2130 ft	0.00267 ft
$h_{d,cold,inner}$	0.2130 ft	0.00267 ft
$\dot{V}_{cold,\ inner}$	9.73 CFM	0.39 CFM
$\varrho_{air,\ 70°F}$	1.1889 kg/m^3	0.0 kg/m^3
$c_{p\ air,\ 70°F}$	1006.88 J/kg-K	0.0 J/kg-K
Temp. rise, hot side air	32.40 C	0.2 C
Heat rejected, hot side	191.45 W	7.32 W
Temp. drop, cold side air, outer	2.00 C	0.2 C
Heat pumped, cold side, outer	9.49 W	1.31 W
Temp. drop, cold side air, inner	2.23 C	0.2 C
Heat pumped, cold side, inner	12.28 W	1.59 W
Wtd. avg. temp., hot side	64.10 C	0.1 C
Wtd. avg. temp., cold side	21.11 C	0.1 C

Examination of energy balance:

Heat pumped at hot side, measured: 191.45 W +/- 7.32 W
Heat pumped at cold side plus I*V: 211.78 W+/- 4.75 W

System Test 7 Error Analysis
Experimental

Parameter	Nominal Value	d(Parameter)
E	19.87 V	0.06 V
I	1.600 A	0.005 A
P	31.79 W	0.20 W
$w_{d,\ hot}$	0.4170 ft	0.0027 ft
$h_{d,\ hot}$	0.2500 ft	0.0027 ft
$\dot{V}_{hot}$	10.46 CFM	0.34 CFM
$w_{d,\ cold,outer}$	0.2480 ft	0.0027 ft
$h_{d,cold,outer}$	0.2130 ft	0.0027 ft
$\dot{V}_{cold,\ outer}$	8.41 CFM	0.32 CFM
$w_{d,\ cold,inner}$	0.2130 ft	0.00267 ft
$h_{d,cold,inner}$	0.2130 ft	0.00267 ft
$\dot{V}_{cold,\ inner}$	9.73 CFM	0.39 CFM
$\varrho_{air,\ 70°F}$	1.1889 kg/m^3	0.0 kg/m^3
$c_{p\ air,\ 70°F}$	1006.88 J/kg-K	0.0 J/kg-K
Temp. rise, hot side air	9.83 C	0.2 C
Heat rejected, hot side	58.06 W	3.04 W
Temp. drop, cold side air, outer	2.68 C	0.2 C
Heat pumped, cold side, outer	12.73 W	1.44 W
Temp. drop, cold side air, inner	2.70 C	0.2 C
Heat pumped, cold side, inner	14.83 W	1.69 W
Wtd. avg. temp., hot side	35.34 C	0.1 C
Wtd. avg. temp., cold side	19.17 C	0.1 C
Examination of energy balance: Heat pumped at hot side, measured: 58.06 W +/- 3.04 W Heat pumped at cold side plus I*V: 59.36 W+/- 3.33 W		

System Test 8 Error Analysis
Experimental

Parameter	Nominal Value	d(Parameter)
E	49.92 V	0.06 V
I	3.750 A	0.028 A
P	187.20 W	1.82 W
$w_{d,\ hot}$	0.4170 ft	0.0027 ft
$h_{d,\ hot}$	0.2500 ft	0.0027 ft
$\dot{V}_{hot}$	10.46 CFM	0.34 CFM
$w_{d,\ cold,outer}$	0.2480 ft	0.0027 ft
$h_{d,cold,outer}$	0.2130 ft	0.0027 ft
$\dot{V}_{cold,\ outer}$	3.08 CFM	0.12 CFM
$w_{d,\ cold,inner}$	0.2130 ft	0.00267 ft
$h_{d,cold,inner}$	0.2130 ft	0.00267 ft
$\dot{V}_{cold,\ inner}$	3.83 CFM	0.15 CFM
$\varrho_{air,\ 70°F}$	1.1889 kg/m^3	0.0 kg/m^3
$c_{p\ air,\ 70°F}$	1006.88 J/kg-K	0.0 J/kg-K
Temp. rise, hot side air	32.40 C	0.2 C
Heat rejected, hot side	191.43 W	7.32 W
Temp. drop, cold side air, outer	4.59 C	0.2 C
Heat pumped, cold side, outer	8.00 W	0.65 W
Temp. drop, cold side air, inner	5.03 C	0.2 C
Heat pumped, cold side, inner	10.87 W	0.87 W
Wtd. avg. temp., hot side	60.28 C	0.1 C
Wtd. avg. temp., cold side	15.94 C	0.1 C

Examination of energy balance:

Heat pumped at hot side, measured: 191.43 W +/- 7.32 W
Heat pumped at cold side plus I*V: 206.07 W+/- 3.35 W

System Test 9 Error Analysis
Experimental

Parameter	Nominal Value	d(Parameter)
E	20.08 V	0.06 V
I	1.600 A	0.005 A
P	32.13 W	0.20 W
$w_{d,\ hot}$	0.4170 ft	0.0027 ft
$h_{d,\ hot}$	0.2500 ft	0.0027 ft
$\dot{V}_{hot}$	10.46 CFM	0.34 CFM
$w_{d,\ cold,outer}$	0.2480 ft	0.0027 ft
$h_{d,cold,outer}$	0.2130 ft	0.0027 ft
$\dot{V}_{cold,\ outer}$	3.08 CFM	0.12 CFM
$w_{d,\ cold,inner}$	0.2130 ft	0.00267 ft
$h_{d,cold,inner}$	0.2130 ft	0.00267 ft
$\dot{V}_{cold,\ inner}$	3.83 CFM	0.15 CFM
$\varrho_{air,\ 70°F}$	1.1889 kg/m^3	0.0 kg/m^3
$c_{p\ air,\ 70°F}$	1006.88 J/kg-K	0.0 J/kg-K
Temp. rise, hot side air	9.23 C	0.2 C
Heat rejected, hot side	54.55 W	2.93 W
Temp. drop, cold side air, outer	5.86 C	0.2 C
Heat pumped, cold side, outer	10.21 W	0.74 W
Temp. drop, cold side air, inner	5.94 C	0.2 C
Heat pumped, cold side, inner	12.84 W	0.95 W
Wtd. avg. temp., hot side	33.47 C	0.1 C
Wtd. avg. temp., cold side	15.07 C	0.1 C

Examination of energy balance:

Heat pumped at hot side, measured: 54.55 W +/- 2.93 W
Heat pumped at cold side plus I*V: 55.17 W+/- 1.89 W

BIBLIOGRAPHY

1. Churchill, S. W. and Bernstein, M. (1977) "A Correlating Equation for Forced Convection From Gasses and Liquids to a Circular Cylinder in Crossflow" *Transactions of the ASME* v 99, pp 300-305.

2. Bergelin, O. P., Brown, G. A., Hull, H. L. and Sullivan, F. W. (1950) "Heat Transfer and Fluid Friction During Viscous Flow Across Banks of Tubes-III" *Transactions of the ASME* v 72, pp 881-888.

3. Bergelin, O. P., Brown, G. A., and Doberstein, S. C. (1952) "Heat Transfer and Fluid Friction During Flow Across Banks of Tubes-IV" *Transactions of the ASME* v 74, pp 953-960.

4. Bermeister, Louis (1983) *Convective Heat Transfer* John Wiley & Sons, NY.

5. Eckert, R. R. G. and Soehngren, E. (1952) "Distribution of Heat Transfer Coefficients Around Circular Cylinders in Crossflow at Reynolds Numbers from 20 to 550" *Transaction of the ASME* v 74, pp 343-347.

6. Fand, R. M. and Keswani, K. K. (1972) "A Continuous Correlation Equation for Heat Transfer From Cylinders to Air in Crossflow For Reynolds Numbers From 10^{-2} to 2 x 10^{5}" *International Journal of Heat and Mass Transfer* v 15, pp 559-561.

7. Fox, Robert W. and McDonald, Alan T. (1978) *Introduction to Fluid Mechanics* John Wiley & Sons, New York.

8. Frank, L. E. (1993) "Optimization Techniques for Thermoelectric (Peltier) Counter-Flow Heat Exchangers" Paper Presented at 1993 ASME Conference.

9. Guyer, Eric C. ed. (1989) *Handbook of Applied Thermal Design* McGraw-Hill, New York, NY.

10. Hilpert, R (1933) "Wärmeabgabe Von Geheizten Drähten und Rohren im Luftstrom" *Forsch. Geb. Ingenieurw* v 4, pp 215-224.

11. Incropera, Frank P. and DeWitt, David P. (1981) *Fundamentals of Heat Transfer* John Wiley & Sons, New York, NY.

12. Jacob, M. (1938) "Heat Transfer and Flow Resistance in Cross Flow of Gasses over Tube Banks" *Transactions of the ASME* v 60, p 384.

13. Kays, W. M. and London, A. L. (1984) *Compact Heat Exchangers* McGraw-Hill, New York, NY.

14. Krall, K.M, and Eckert, E. R. C. (1973) "Local Heat Transfer Around a Cylinder at Low Reynolds number" *Journal of Heat Transfer* v 95, pp 273-275.

15. Materials Electronic Products Corp. (MELCOR) "Device Performance Formulae" 1 page facsimile from MELCOR received 21Jan93.

16. Meyers, Glen E. (1987) *Analytical Methods in Conduction Heat Transfer* Genium Publishing Corp., Schenectady, NY.

17. Morgan, Vincent T. (1975) "The Overall Convective Heat Transfer From Smooth Circular Cylinders" *Advances in Heat Transfer* v 11, pp 199-263.

18. Nunn, Robert H. (1989) *Intermediate Fluid Mechanics* Hemisphere Publishing Corp., New York.

19. Omohundro, G. A., Bergelin, O. P. and Colburn, A. P. (1949) "Heat Transfer and Fluid Friction During Viscous Flow Across Banks of Tubes" *Transactions of the ASME* v 71, pp 27-34.

20. Sparrow, E. M. and Ramsey, J. W. (1978) "Heat Transfer and Pressure Drop For a Staggered Wall-Attached Array of Cylinders with Tip Clearance" *International Journal of Heat and Mass Transfer* v 21, pp 1369-1377.

21. Sparrow, E. M., Ramsey, J. W., and Altemani, C. A. C. (1980) "Experiments on In-Line Pin Fin Arrays and Performance Comparisons with Staggered Arrays" *Transactions of the ASME* v 102, pp 44-50.

22. Threlkeld, J. L. (1970) *Thermal Environmental Engineering* Prentice-Hall Inc., Englewood Cliffs, NJ.

23. Wylie, R. G., and Lalas, T. (1973) "The Measurement of Heat Transfer Coefficients Using Psychrometric Wet Elements" *Proc. Australas. Conf. Heat Mass Transfer, 1st, Melbourne* Section 4.2, pp 19-24.

24. Zukauskas, A. (1972) "Heat Transfer From Tubes in Crossflow" *Advances in Heat Transfer* v 8, pp 93-160.